Macrocyclic Bisphosphonates for PET-Diagnosis and Endoradiotherapy of Bone Metastases

Dissertation

Zur Erlangung des Grades

“Doktor der Naturwissenschaften“

im Promotionsfach Chemie

am Fachbereich Chemie, Pharmazie und Geowissenschaften

der Johannes Gutenberg-Universität Mainz

Marian Meckel

geb. in Diez

Mainz 2014

Dekan: Univ.-Prof. Dr. Holger Frey

1. Berichterstatter: [redacted]
2. Berichterstatter: [redacted]
3. Berichterstatter: [redacted]

Tag der mündlichen Prüfung: 20.10.2014

In Loving Memory Of

[redacted]

I hereby declare that I wrote the dissertation submitted without any unauthorized external assistance and used only sources acknowledged in the work. All textual passages which are appropriated verbatim or paraphrased from published and unpublished texts as well as all information obtained from oral sources are duly indicated and listed in accordance with bibliographical rules. In carrying out this research, I complied with the rules of standard scientific practice as formulated in the statutes of Johannes Gutenberg-University Mainz to insure standard scientific practice.

Mainz, 2014

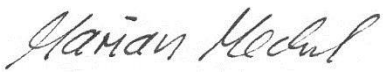

Abstract

Prostate and breast cancer are high rated in the numbers of cancer cases worldwide. The serious consequence of this disease is the metastatic spread of the cancer into the bones. It is associated with severe bone pain, spinal cord compression, skeletal fractures and a metabolic hypercalceamie. Finally, the symptoms reduce the patients quality of life dramatically.

Radiopharmaceuticals play a key role in the assessment and therapy of this disease. Conjugates of macrocyclic chelates and bone affine bisphosphonates are an appropriate means, as so called *theranostics*, to unite diagnosis and therapy in one molecule. In this connection the generator based PET-nuclide ^{68}Ga(III) and the therapy nuclide ^{177}Lu(III) showed promising first results with BPAMD in initial patient studies. For both trivalent radiometals, new derivatives were successful synthesized deduced by further developments of the BPAMD lead structure with enhanced pharmacological properties. These novel compounds, based on the modern osteoporosis drugs pamidronate and zoledronate, distinguished by an increased bone affinity and a superior target to background ratio. In addition it was also succeeded to develop a derivative of longer blood retention, which finally resulted in an enhanced bioavailability of the tracer. This class of bisphosphonate enables an increased tumor to healthy bone ratio, which might end up in an improved therapeutic success. One of these novel macrocyclic bisphosphonates, [^{68}Ga]NO2AP^{BP} showed superior results in the animal testing and was therefore chosen for an initial clinical phase 0 and I trials. Within this study the compound was able to underline its high diagnostic efficiency in combination with ^{68}Ga-PET. The first series of tests in 12 patients revealed a similar compliance in the detection capability of skeletal metastases as the gold standard ^{18}F-fluoride. Moreover in selected metastatic foci a higher uptake of the bisphosphonate could be obtained.

The promising results indicate that in future the macrocyclic bisphosphonate concept may play a key role in the management of skeletal metastases in nuclear medicine.

Kurzzusammenfassung

Die Fallzahlen von Prostata- und Brustkrebs nehmen aktuell die Spitzenplätze bei Krebserkrankungen weltweit ein. Eine schwerwiegende Folge dieser Erkrankung stellen Metastasierungen in das Knochengewebe dar, welche zu einer dramatischen Verschlechterung des Allgemeinzustandes und der Lebensqualität des Patienten führen. Die Symptome sind gekennzeichnet durch enorme Schmerzen in Kombination mit osteoblastischen und osteolytischen Knochenveränderungen, bis hin zu Frakturen und spinalen Kompressionssyndromen, sowie einer metabolischen Hypercalcaemie.

Bei der Diagnose und Therapie nehmen verschiedene Radiopharmaka eine Schlüsselrolle ein. Konjugate aus makrozyklischen Chelatoren und knochenaffinen Bisphosphonaten stellen ein geeignetes Mittel dar als so genannte *Theranostika*, die Diagnose und Therapie in einem Molekül vereinen. Hierbei konnten mit dem Generator basierenden PET-Nuklid ^{68}Ga(III) und dem Therapienuklid ^{177}Lu(III) erste Erfolge mit der Verbindung BPAMD am Patienten erzielt werden. Im Rahmen der vorliegenden Arbeit ist es gelungen, die pharmakologischen Eigenschaften der BPAMD-Leitstruktur weiter zu optimieren und neue Derivate erfolgreich zu synthetisieren. Diese zeichneten sich durch eine erhöhte Knochenaffinität und eines besseren ´target to background´ Verhältnisses aus. Im Zuge der Derivatisierung ist es außerdem gelungen, erfolgreich eine Substanz darzustellen, welche über eine gesteigerte Blutretention verfügt und die letztendlich die Bioverfügbarkeit des Tracers erhöhte. Verbindungen solchen Typs können zu einem besseren Tumor zu gesundem Knochen Verhältnis beitragen und eventuell einen höheren Therapieerfolg erzielen. Eines dieser neuen vielversprechenden Bisphosphonate, [^{68}Ga]NO2AP^{BP} konnte innerhalb einer klinischen Phase 0 bzw. I sein großes Potential als Diagnostikum zur Erfassung von Skelettmetastasen unter Beweis stellen. Innerhalb einer Testreihe mit 12 Patienten wurde eine hohe diagnostische Übereinstimmung mit dem Goldstandard ^{18}F-Fluorid erreicht. In ausgesuchten Metastasen konnte sogar eine höhere Tracer-Aufnahme erzielt werden.

In Zukunft können makrozyklische Bisphosphonate eine wichtige Rolle bei der palliativen Schmerztherapie von Knochenmetastasen einnehmen.

Contents

1. Introduction

Cancer is one of the leading causes of death, beside diseases of the heart and the vascular system [1]. Actually more than 32.6 million people worldwide suffering from that diseases and it must be assumed that the rate of cancer cases increases in the next decades, based on the further aging population [1,2]. Particularly in the industrialized and developing countries spreading cases of malignant diseases will be a challenging burden for their societies [2].

The type of human cancer is various and more than 100 different forms are known today [3]. In Germany, the most cases are attributed to only some major types of malignant tumors inflicting selected tissues, such as the lung and the intestine [4], and gender characteristic diseases, like prostate and breast cancer, are the leading group with around 25-30 % of all new cancer cases [4]. The World Health Organization expects that close to the half of all cancer cases could have been prevented by a better lifestyle, healthier environmental influences and a better medical care [2]. The consumption of tobacco and an unhealthy diet is one of the main risk factors to become a malignant disease in the developed countries. The second cause is based on environmental pollution, whereas air contamination is the major threat. Additionally, infections such as hepatitis viruses or human papilloma viruses are important factors [5,6,7]. On the other hand, the origin of most cancer cases is not definable or unavoidable, like the genetical preferences for the development of tumorous tissue [4].

Besides the avoiding of the risk factors, the fight against the acute tumor diseases is an urgent challenge in medicine. The therapy of cancer differs in the type of the malignant tissue and includes the removal of neoplasms by surgery, chemotherapy and external beam radiation [8]. Recently, new methods come into clinical practice, like the targeted cancer therapies utilizing ´matching bullets´, such as antibodies and the peptide receptor radionuclide therapy (PRRT), as well as new pharmaceutical and radiation concepts [8,9,10]. Today, in the developed countries the mean 5-year survival rate is between 50 to 60 %, whereby large distinctions in the morbidity of different tumor types exist, which varies from a 5-year survival rate of less than 10 % for pancreatic cancer to more than 90 % for the melanoma of the skin [2,4]. The main factor which influences the success of the cancer treatment is the

diagnosis in an early stage of diseases. Regular cancer check-ups, an informed population and the overall resources of the public health system show here an important criterion for the clinical prediction of cancer patients. In contrary, the mean 5-year survival rate in the rest of the world is only between 30 to 40 % and many patients in the developing countries diagnosed in late stages of their diseases without no prospect of any cure of their suffering [1,2].

The consequences for patients living with and dying from cancer are severe and reduce the quality of life drastically. These consequences include mostly serious pain and physical and psychological suffering. Palliative care, which comes more and more into the focus of medical welfare, is an urgent humanitarian need to relief patients and their families from these sufferings. On the contrary, patients with an improved quality of life show longer survival tendencies [2,11]. Malignant tumors inflict in their late stages several tissues and lead to various symptoms.

One major complication is the spread of cancer from the primary tumor tissue to other organs [12]. By penetrating the walls of blood and lymphatic vessels, single tumor cells are able to circulate in the body and can thus invade healthy tissues to generate new tumor lesions. The organ preferences of metastases depend on the type of the primary tumor, but statistically lymphnotes, the lungs, the liver and the brain are frequently affected [13,14]. Another organ, where tumor cell invasion occurs at a high percentage, with severe complications inflicting the patients quality of life, are the bones [14].

1.1. Bone Metastases

In the year 1889, Stephen Paget summarized the results of the necropsies of breast cancer victims in *The Lancet* [13]. He reported that the bones are most frequently inflicted by breast tumor metastases, furthermore he postulated his *seed and soil* theory of secondary cancer growths. Since other primary tumors did not show these statistical high preference for the skeleton, Paget concluded that circulating cancer cells originating from a certain tissue (the seed) only colonize in specific organs of the body (the soil), where the microenvironment is convenient for the type of tumor. Additional autopsy studies revealed that not only breast cancer enhances the risk of developing secondary tumor growths in the bone, but rather prostate and lung cancer are likewise the main causes. It was found, that close to 85 % of patients dying on breast, prostate or lung cancer suffering from osseous metastases [15]. The results showed further that the cancer does not spread randomly over the skeleton, quite the opposite is the case and the metastases are located predominantly in the spine, pelvis and the ribs at an early stage. Later on the skull, the scapula, the femur and the sternum are involved. Usually patients develop not only one metastatic site, but rather multiple lesions [15].

The growths of secondary cancer in bone have fatal consequences and it is associated with a higher morbidity and mortality. The most harmful effect is the severe multiple pain syndrome, which decreases the patients quality of life dramatically. The further progress of the diseases is characterized by bone fractions and spinal cord, as well as nerve root compressions [16]. A common metabolic complication is the hypercalcemia, which induces acute renal failures and cardiac arrhythmias leading to death at last [17].

The genesis of these symptoms has its origin in the disorder of the well balanced bone remodelling, mediated by the tumor cell invasion. The healthy bone underlies a continuous degradation and reconstruction of the mature mineral compartment and the rate of bone replacement averages 10 % of the skeleton per year. The bone turnover is executed by two types of cells associated on the bone matrix, which are known as the osteoblasts and the osteoclasts.

The osteoblasts mineralizing the bone with hydroxyl apatite (HAP), which is a hard inorganic salt of the chemical formula $Ca_{10}(PO_4)_5(OH)_2$, attributing the skeleton its solid strength. About 50-60 % of the human bone consists of this material, embedded with few amounts of different counter ions like Mg^{2+} and Cl^-, while the remaining proteins, mainly collagen, preserve the elasticity to prevent an easy splintering of the bone [18]. The bones function further as the hugest reservoir of Ca^{2+} and phosphate in the human body. A sketch of the cells and the mechanism involved in the bone remodelling is depicted in figure 1. The osteoblasts originate from mesenchymal stem cells (MSC) and are located usually on the bone surface. During the formation of new bone tissue some osteoblasts were implanted inside the bone and develop further to osteocytes, which are known to have a very long lifespan and are rather sparsely active, but sensitive to the mechanical bone stress. The remaining osteoblasts develop in their inactive state to so called lining cells, which cover the bone surface and protect it with a cell layer [19]. Recruitment of the osteoblasts takes place by signaling pathways including high serum Ca^{2+} levels, growth factors and cytokines [20].

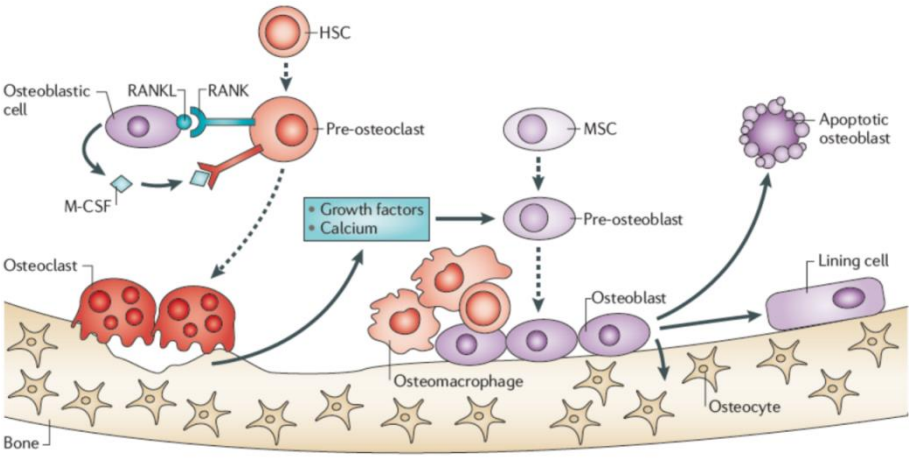

Figure 1. Overview of cells and signaling pathways involved in the bone remodelling. Osteoblasts develop from mesenchymal stem cells (MSC), osteoclasts from haematopoietic stem cells (HSC). The osteoblasts synthesize the bone proteins, mostly collagen and depose calcium and phosphate minerals in the bone matrix. Implemented osteoblasts develop to osteocytes, remained surface osteoblast to lining cells. Osteoclast recruitment is mediated by RANK/L and M-CSF (K. N. Weilbaecher et al. [19]).

The counterpart of the osteoblasts are the osteoclasts, which degrade the bone by the secretion of acids and collagenases. Osteoclasts are large multinucleated cells and can have

huge dimensions especially around tumor lesions. The bone remodeling is complexely organized and several organs like the kidneys and the parathyroid glands are involved as well as a feedback mechanism between the osteoblasts and the osteoclasts, controlling their activity. The recruitment of the osteoclasts is mediated by RANK/L (receptor activator of nuclear factor κβ ligand), which is expressed on the surface of osteoblasts and M-CSF (macrophage-colony stimulating factor), secreted also by osteoblasts. The release of growth factors embedded in the bone matrix and the increase of Ca^{2+} levels by bone degradation of the osteoclasts, stimulates the osteoblast activity again to form new bone material. Finally, high osteoblast activity stimulates the osteoclast formation and vice versa [19,20]. This fine-tuned balance is manipulated in the one or the other direction, as required. The factors influencing the osteoblast and osteoclast balance are signaling pathways by mechanical stimulation, by hormones of the kidneys (calcitriol) and the parathyroid (PTH, parathyroid hormone) as well as by local inflammatory occurrences [20,21].

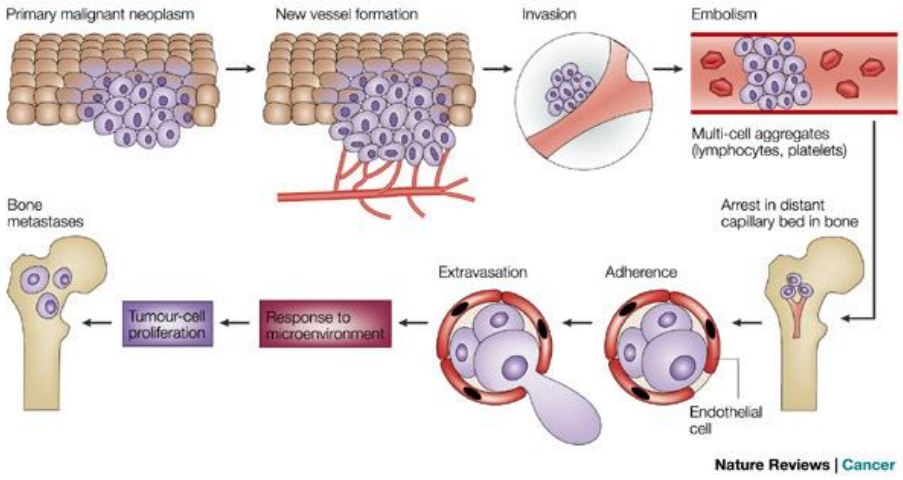

Figure 2. Steps in the tumor cell invasion to the bone. Tumor cell penetration of blood vessels releases malignant cells in the circulation, which get trapped in the bone marrow. Extravasation of the tumor cells trough the endothelium is followed by tumor growth in response to the favorable bone microenvironment [17].

The formation of secondary cancer growths in the bone can be described in six steps (see figure 2), starting with the penetration of blood and lymphatic vessels by tumor cells. In the second step tumor cells are released in the circulatory system and only a minority of less than

0.01 % of them are able to form metastases in general [22]. It is yet in the discussion if the tumor cells adhere in the bone preferably by a vascular niche which is permeable for tumor cells or if the tumor cells allocate randomly over the body and only the special bone microenvironment allows a tumor cell survival [15]. In the next step the bone placed tumor cells secret growth factors, cytokines and chemokines, which finally interrupt the RANK/RANKL communication between the osteoblasts and osteoclasts [23]. This interruption can be attributed to the secretion of the parathyroid hormone-related peptide (PTHrP) and interleukins (IL-8, IL-11) by the tumor cells, which increases the osteoclast activity. In turn the enhanced osteoclast activity, releases Ca^{2+} and matrix-embedded growth factors like TGF-β (tumor growth factor) and IGF (insulin like growth factor), stimulating the tumor growth. This feed-back mechanism of tumor growth and bone response is depicted in figure 3 and is so called as the *vicious circle* [23].

Despite an overall enhanced activity of osteoblasts and osteoclasts, the disturbance of the bone cell balance in the lesions caused by metastases can have preferentially an osteolytic or osteoblastic character. It could be the case, that the stimulation of one of these two bone modelling cells is more intense affected and the tumor lesion tends more or less to the one or the other trend. It is also known, that breast cancer metastases cause predominantly osteolytic lesions, while prostate cancer derived lesions tend to form osteoblastic metastases. However, in the most cases the lesions have a mixed character of osteolytic and osteoblastic sites or both types can be found in affected patients [17].

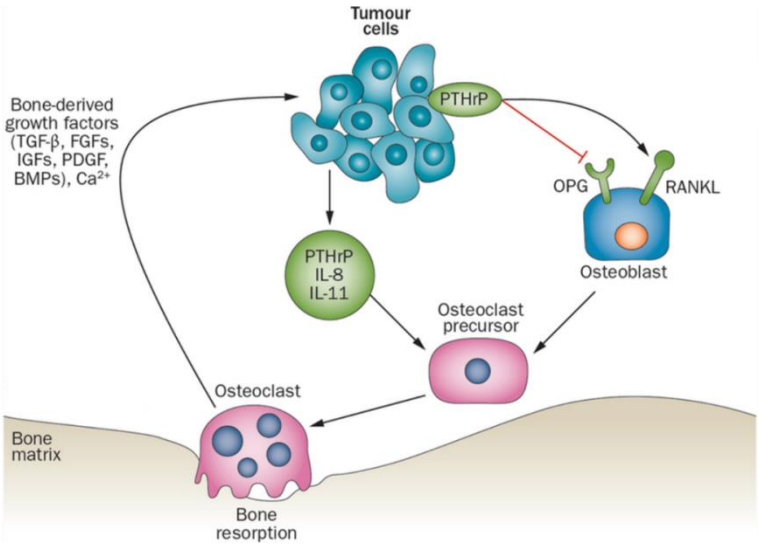

Figure 3. Illustration of the biochemical pathways and cells involved in the *vicious circle* of bone metastases. The tumor secrets signaling molecules like PTHrP (parathyroid hormone-related peptide) and IL-8/11 (interleukin-8/11) which recruits osteoclast activity. Furthermore the secretory molecules inhibit the OPG (Osteoprotegerin) receptor of osteobolasts, which prevent in its natural state the activation pathways of osteoclasts by osteoblasts within RANK/L. The enhanced osteoclast activity further releases growth factors and Ca^{2+} from the bone matrix, which again increases tumor cell proliferation (M. Ignatiadis et al. [24]).

Thus, the increased uncontrolled metabolic activity of bone cells on the metastatic lesion benefits the tumor to proliferate and supports the tumor growth deeper in the bone tissue, causing severe bone pain. In the later stage, the bone structure gets fragile and fractures can occur on the lesion sites. Furthermore, the tumor can invade the bone marrow itself and can cause a bone marrow carcinosis. The metabolic effects of bone metastasis are severe and the release of Ca^{2+} can further emerge a hypercalcaemia, which could finally lead to death.

1.2. Diagnosis

Several methods are available for clinicians to diagnose bone metastases. One part are clinical markers related to enhanced bone metabolism. These specific markers can give an access to the rate of bone resorption or formation. Two serum parameters are recently in the discussion, one is the bone specific isoenzyme of the alkaline phosphatase (ALP), released by osteoblasts during the formation of new bone. The other one is the degradation product of type I collagen, which is a cross-linked telopeptide named NTx and CTx and is associated with the bone resorption by the osteoclasts [25]. Especially for prostate cancer related bone metastases, PSA (prostate specific antigen) serum levels are also an important factor. Clinical markers are easy to acquire and relatively cheap in practice, but in case of bone metastases they lack of their ability to localize the metastatic foci. For this reason imaging modalities are common to detect osseous tumor lesions and several techniques are suitable, but with differences in detection specifity, sensitivity and costs. The used techniques are XR (X-ray examination), CT (computed tomography), MRI (magnetic resonance imaging), the so called skeletal scintigraphy (SS) and the SPECT (single photon emission computed tomography) as well as the PET (positron emission tomography) and summarized in table 1, respectively [26].

Table 1. Characteristics of different imaging modalities for the detection of osseous metastases.

imaging modality	anatomic detail	metabolism	extent of image	diagnostic sensitivity	diagnostic specificity
XR[a]	yes	no	regional / whole body	low (44-50%)	n.d.
CT[a]	yes	no	regional	high (71-100%)	n.d.
MRI[a]	yes	no	regional	high (82-100%)	high (73-100%)
SS[a]	no	yes	whole body	varies (62-100%)	varies (78-100%)
SPECT[a]	no	yes	whole body	high (87-92%)	high (91-93%)
PET[b]	no	yes	whole body	very high (94-99%)	very high (97-100%)

[a]Data from Hamaoka et al. [26]. [b]Data for [^{18}F]NaF from Tateishi et al. [27].

XR: X-ray examinations are quite cheap to acquire but a whole body roentgenographic bone survey shows only low performance in specification and sensitivity for the detection of metastatic lesions. The XR exposes differences in bone density, and usually a change in 30 % to 75 % of the bone density according to the initial status has to be triggered by the tumor to ascertain an accurate result. This deduces that tumor lesions can only be detected by XR in a late state of diseases, when distinct pain syndromes are already present. Thus, XR appears to be as an additional method in the diagnosis of bone metastases to obtain some morphological information in addition to other better suited imaging techniques [26].

CT: The computed tomography offers a more detailed anatomic view on the skeletal structure in comparison to the XR and thus enhances the diagnostic sensitivity. It also shows superior results in the examination of the spine, but the technique is limited according to its long time frame to scan different parts of the body, and whole body images are quite not implemented. Despite the high radiation dose delivered to the patient, the CT reveals to be an efficient technique in addition with metabolic imaging modalities like SPECT or PET and combinations of PET and CT devices are recently introduced into clinical practice [26].

MRI: Magnetic resonance images are usually done to visualize soft tissue by the proton relaxation of water molecules. Nevertheless it is suitable to gain worthy anatomic information about the bone and the bone marrow, in particular. The recently developed

diffusion-weighted MRI (DIW) mode shows excellent results in the detection of boney metastases especially in the spinal cord and bones. The drawbacks are the time consuming imaging procedures, assoiated with the problems of obtaining a whole body scan [28].

Skeletal scintigraphy and SPECT: From the above mentioned imaging techniques the skeletal scintigraphy, as well as the single photon emission computed tomography differ basically, not only in their imaging acquisition, but also in their imaging object. While XR, CT and MRI obtain morphological information, the SS and SPECT rather reveal biochemical and metabolic information, respectively. The source of the SS/SPECT imaging is of tracing the γ-emission of radionuclides, which distribute in the human body. The concept of using radioactive indicators to monitor biochemical processes was introduced first by de Hevesy and offered revolutionary insights in chemistry and life [29]. Since metastases tend to increase bone resorption and formation, bone targeting radionuclides respectively radioactive labelled compounds, preferentially accumulate in tumor lesions. First applications of this concept localizing skeletal metastases were published in the late 1950´s. They followed the skeletal distribution of ^{85}Sr and ^{47}Ca by simple external counting [30]. The techniques develop further and scinitigraphic images obtained from ^{87m}Sr and ^{85}Sr are widely used in the late 1960´s to visualize tumor lesions (Figure 4) [31]. By detecting the γ-emission of the radioactive decay, the origin of the radionuclide conversation can be calculated back and high metabolic areas are depicted as so-called *hot spots*.

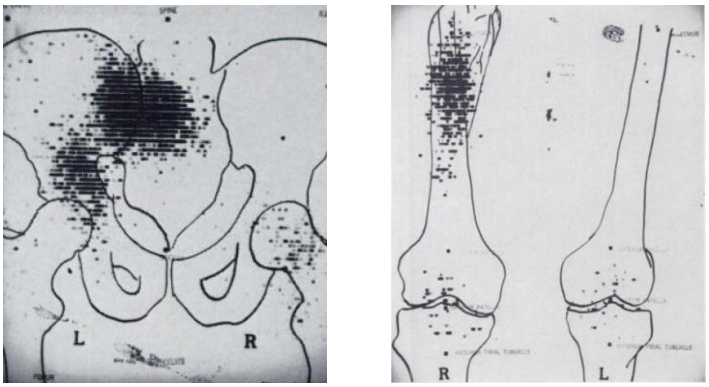

Figure 4. Scinitgraphic images from the pelvis and the femurs, obtained in 1966 by ^{85}Sr to detect skeletal metastases by enhanced bone turnover (G. L. DeNardo et al. [31]).

The evolution of the γ-cameras offered more and more detailed images of the metabolic progress in the bone and the developing technique necessitates better fitted nuclides in terms of half-life and γ-emission yield. The most promising candidate was found to be ^{99m}Tc, which is still today the most commonly used radionuclide in nuclear medicine. ^{99m}Tc has a half-life of 6.01 h combined with a very high γ-emission yield of 86 %. The energy of the γ-rays is 140.5 keV and thus well suited for NaI-scintillators [32]. Technetium-99m is the decay product of ^{99}Mo (EC, $t_{1/2}$ = 66 h) and can be conveniently obtained from a ^{99}Mo/^{99m}Tc generator system. Molybdenum-99 is commonly produced by nuclear fission of ^{235}U in nuclear reactors [32]. Techentium isotopes do not accumulate in the bone, like the isotopes of $^{87m/85}$Sr and ^{47}Ca and therefore they have to be delivered in a complex with a targeting agent to the skeleton [33]. The complexing agents generally used to deliver the ^{99m}Tc to the bone are MDP (methylene diphosphonate), HMDP (hydroxyl methylene diphosphonate) and EHDP (ethyl hydroxyl diphosphonate). These agents are depicted in figure 5 [34].

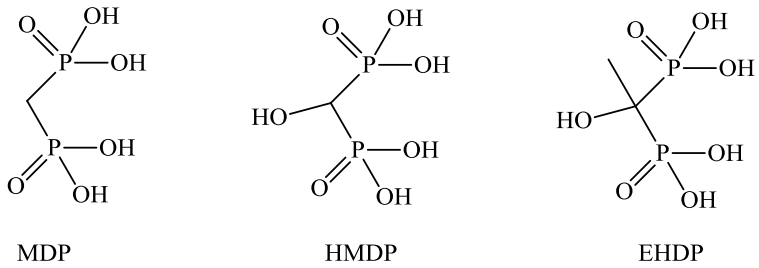

Figure 5. Common ^{99m}Tc-complexing agents for bone scintigraphy.

Images obtained by ^{99m}Tc-phosphonates have been a giant leap in the diagnosis of skeletal related diseases, but first applications were only orientated in planar acquisitions, giving less detailed information about metabolic events compared to 3-dimensional techniques. Nevertheless, the plain skeletal scintigraphy with ^{99m}Tc-phosphonates became the work horse in the detection of osseous metastases. Today, the 3-dimensional whole body SPECT is the most commonly used imaging technique in nuclear medical practice, since it has a high sensitivity and specificity for visualizing areas of high bone turnover. Hence, it is not only indicated to reveal metastatic lesions, but also offers the opportunity for examinations of other skeletal related issues. Compared to the planar skeletal scintigraphy, the 3-dimensional multi-field of view SPECT results in a better image quality, which is clearly visible in figure 6.

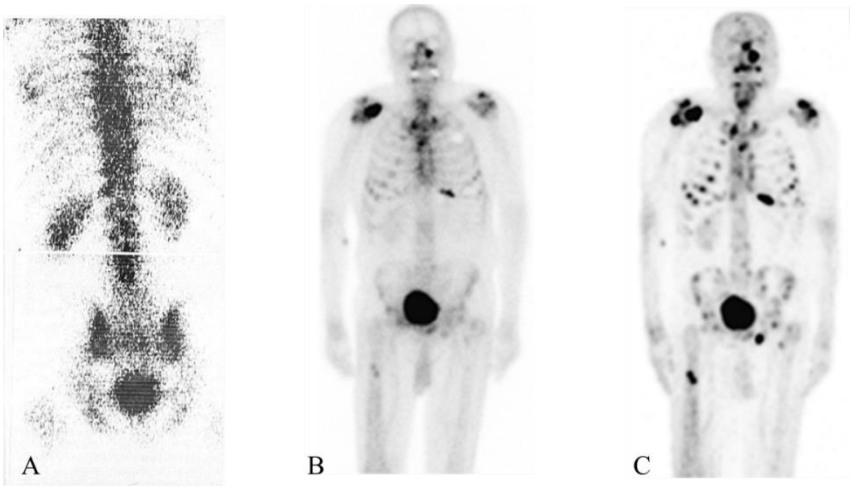

Figure 6. Examples of ^{99m}Tc-diphosphonate images, obtained by different imaging methods. A: ^{99m}Tc-polyphosphate image of a metastatic patient developed with a γ-camera in the mid 1970´s by Malmud et al. [35]. B: Current anterior planar SS developed with [^{99m}Tc]MDP with metastatic foci in the shoulder, sternum, ribs and the skull. C: SPECT image of patient (B) reveals a more detailed finding, with additional lesions countable (E. Even-Sapir et al. [36]).

PET and PET/CT: Similar to SS and SPECT the PET scanner detects the emission of γ-rays and a mainframe calculates back the origin of the radioactive conversation to generate a 3-dimensional image of the tracer concentration in the body. In contrast to the SPECT technique, the PET uses the photons emitted by the electron-positron annihilation. The positron (β^+) is the antiparticle of the electron, it has the same mass and spin but an opposing charge. It was first postulated by Dirac in 1928 until it was discovered by Anderson in 1933 [37,38]. The annihilation can occur in a direct way when a positron hits an electron from the surrounding matter. The electron-positron annihilation results in two photons with a distinct energy of 511 keV, which are emitted in a 180° angle. Instead of direct annihilation, the positron can form an exotic pseudo-atom of short half-life with an electron and annihilation can also occur out of this so called positronium [39]. The PET technique is superior in resolution compared to SPECT, because of the detector system, surrounding the patient, that registers only collinear photons of 511 keV, cf. figure 7. Due to that, single photon events as well as non-linear photon detections are withdrawn from the image calculation.

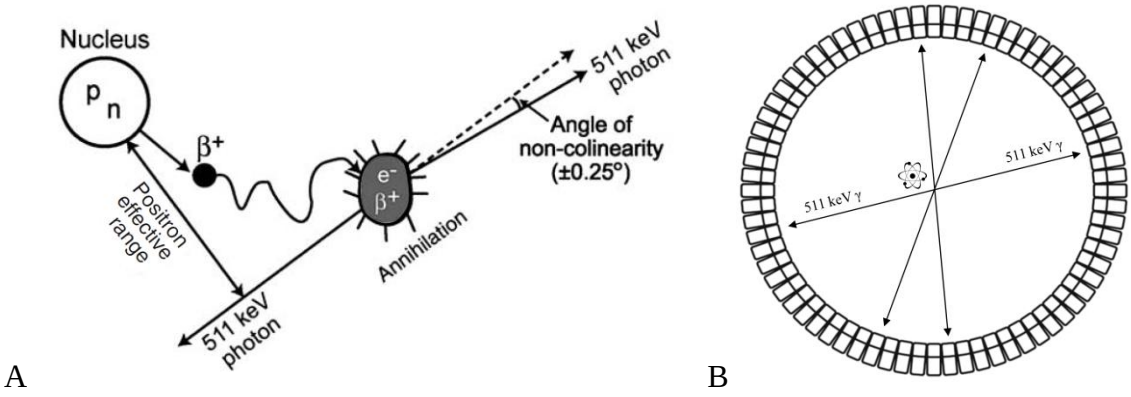

Figure 7. Principles of the photon detection of the PET techniques. A: Emission of the 511 keV annihilation photons in a 180° angle. The distance between the origin of decay and the annihilation event depends on the positron energy, emitted by a proton rich nuclide. B: Sketch of the scintillation detectors surrounding a positron source [39].

The source of the positrons are proton rich nuclides of low atomic number and the nuclear conversion can be described as following:

$$\text{Positron conversion:} \quad p \rightarrow n + \beta^+ + \nu_e$$

A proton in the nucleus is converted to a neutron under the emission of a positron and an electron neutrino. The competitive mechanism is the electron capture (EC) conversation and it occurs statistically higher with the increasing atomic number of the mother nuclide.

$$\text{EC:} \quad p + e^- \rightarrow n + \nu_e$$

Optimal nuclides for PET imaging are thus characterized by having a high β^+ yield and low β^+ energies. Typical PET nuclides are ^{11}C, ^{13}N, ^{15}O, ^{18}F, ^{68}Ga and ^{64}Cu. The cyclotron produced isotope ^{18}F is most widely used. Because of its moderate half-life of 110 min, it could be introduced in several biological active molecules called as tracers, such as [^{18}F]FDG (2-deoxy-2-(^{18}F)fluoro-D-glucose), [^{18}F]F-choline, [^{18}F]FET (O-(2-[^{18}F]fluoroethyl)-L-tyrosine) and [^{18}F]NaF [32].

PET scans of the bone revealing metastatic lesions can be performed with three different ^{18}F-tracers, and thus targeting different biochemical processes. [^{18}F]FDG is the most common used PET radiopharmaceutical in clinical practice and several studies revealed the potential

of [^{18}F]FDG-PET in the assessment of osseous metastases. The accumulation principle of [^{18}F]FDG is based on its structural relationship to natural glucose and thus it is incorporated in high quantities by high metabolic cancer cells. Due to that fact [^{18}F]FDG is a more or less unspecific tracer, it is also used to reveal several types of malignancies including the bone [26,32]. [^{18}F]F-choline shows affinity to prostate cancer cells and was introduced to detect bone metastases derived from prostate carcinoma. However, [^{18}F]F-choline showed insufficient target to background ratios, since other organs tend to accumulate large quantities of choline. Moreover, the application is limited to prostate cancer patients.

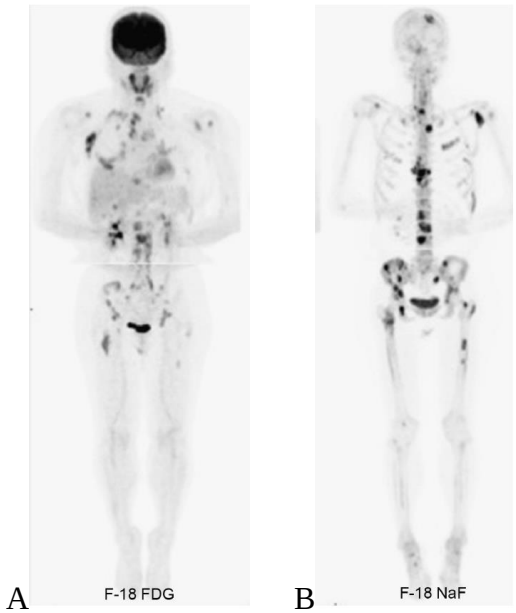

Figure 8. Comparison of PET images of a bone metastatic patient, implemented with [^{18}F]FDG (A) and [^{18}F]NaF [40].

Fluoride ions have a natural affinity to the bone based on their strong binding to hydroxyl apatite. Within the apatite structure ($Ca_{10}(PO_4)_5(OH)_2$), the F^- ions replace with OH^- by anion exchange to form the very stable fluoroapatit $Ca_5(PO_4)_3F$. The use of [^{18}F]NaF for bone scanning was first introduced by Monte Blau in the early 1960´s, but short after approval it was replaced by ^{99m}Tc-bisphosphonates according to its lack of nuclide properties in relation with the SPECT technique [41]. Since the quality of the PET technology overtakes the SPECT in the last decades, [^{18}F]NaF-PET scans offer now the best specificity and sensitivity

to detect skeletal metastases [42]. [^{18}F]NaF-PET shows a superior quality against [^{18}F]FDG and [^{99m}Tc]MDP-SPECT as depicted in figure 8 and figure 9, respectively. Recently, new multimodality imaging techniques combine PET with CT and MRI and thus offer to gain hybrid images of anatomical and metabolical information. The accurate physiological localization of the PET-tracers enrichment in the human body, strengthen the diagnostic impact of the single imaging technique. Recently, the best results in the detection of bone metastases are provided by PET/CT [43,44].

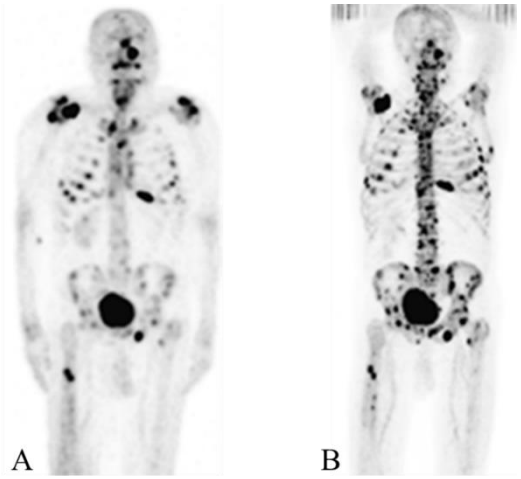

Figure 9. Comparison of images of a bone metastatic patient, obtained from [^{99m}Tc]MDP SPECT (A) and [^{18}F]NaF PET. The PET scan offers a more detailed view on the skeletal related metastases [36].

Recently developed compounds like ^{68}Ga-HBED-CC-PSMA and BPAMD ((4-{[bis-(phosphonomethyl))carbamoyl]methyl}-7,10-bis(carboxymethyl)-1,4,7,10-tetraaza-cyclododec-1-yl) acetic acid) provide new opportunities in the assessment of bone metastases. BPAMD offers not only a high qualitative imaging, but also a therapy option [45]. BPAMD is a conjugate of a chelator moiety to a specific bone targeting molecule and hence it can be labelled with the metal PET nuclide ^{68}Ga(III). ^{68}Ga(III) has a half-life of 67.7 min and it provides β^+-particles of a maximum energy of 1.9 MeV with a β^+-branching of 89 %. ^{68}Ga(III) can be obtained conveniently by a generator system from a ^{68}Ge source [46]. The chelator-based concept of radiopharmaceuticals offers the chance of using various nuclides, which includes SPECT, PET and therapy applications. Instead of PSMA, BPAMD

can be used to detect bone lesions indifferently, whether it is from prostate, breast or any other type of cancer origin and it can be truly function as a carrier of therapeutic nuclides, such as ^{177}Lu(III). Therefore BPAMD can be used for diagnostic imaging and therapy and it can be thus called as a *theranostic* agent [47].

1.3. Therapy

Tumor metastases are generally difficult to treat and once spread to the bones, they are close to be incurable. The most treatments aim at the reduction of the follow up effects, like the hyper calcaemia, or the prevention of pathological fractures. Pain relief by analgetics needs the most attention, since this symptom is vigorously dominant and it reduces the patients quality of life dramatically [48].

Nevertheless, there are several treatment possibilities dealing with skeletal metastases. Single lesions might be removed surgically or treated by external radiation. Unfortunately, most patients suffer from metastases inflicting multiple sites in the skeleton and therefore a more systemic treatment is necessary. The application of the new cytostatic agent docetaxel showed promising results, but seemed not to influence the emerge of skeletal related events [49]. In case of bone metastases derived from prostate or breast cancer origin, androgen receptor targeting drugs or tumor specific antibodies like trastuzumab may delay the progress of the disease [49, 50]. Other drugs aim on the interruption of the vicious circle of the tumor cells and the bone micro environment. For this reason they reduce the onset of skeletal related events and bone pain and they also may increase the overall survival rate. This interruption can be initiated at different steps of the complicate way of tumor and bone cell interaction. The monoclonal antibody denosumab is an inhibitor of RANK and thus prevents the recruitment of osteoclasts, which is an important factor in the bone metastases formation. Denosumab reduces the occurrences of skeletal related events but showed not to enhance the overall survival rate [51]. There are several other new compounds and concepts in preclinical and clinical trials targeting different mechanistic parts of tumor cell invasion to the bone.

Some may become an important role in the treatment in future, but nevertheless the strongest focus in the management of bone metastases are of palliative care. Today, the common treatment of bone metastases are based on bisphosphonates and of targeted radionuclide therapy.

Bisphosphonates (BPs): In the management of bone metastases the administration of BPs is an integral part of the treatment today. BPs have effects on the bone turnover and therefore in different ways on bone metastases. Their chemical structure is derived from natural pyrophosphate. Important derivatives are shown in chart 1.

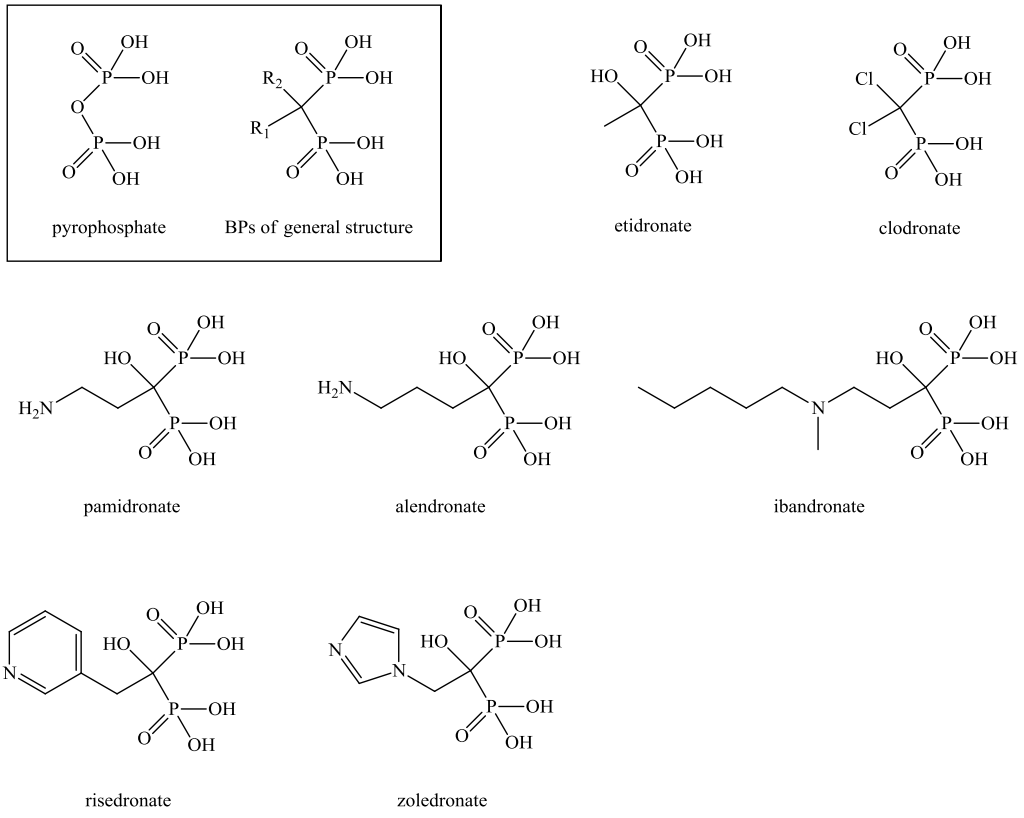

Chart 1. Overview of therapeutic bisphosphonates derived from pyrophosphate (box). In the BP structure the P-O-P bond is replaced by a P-C-P bond, which is considerable stable against hydrolysis in contrast to the phosphate ester of pyrophosphate. The evolution of BPs started with the chloro-compound clodronate and the hydroxy-BP etidronate. Further developments leaded to the more powerful N-hydroxy-BPs pamidronate, alendronate and ibandronate. The recently most effective compounds are the nitrogen containing hetero aromats risedronate and zoledronate [52].

BPs have a unique affinity to apatite, due to the high complexation ability of calcium, and thus they exlusively accumulate on the bone. The common indication for a BP treatment is osteoporosis, but also other bone related diseases are predestinated [53]. Their mechanism of action is the inhibition of the bone resorption induced by osteoclasts, which can be described as following. During the bone resorption process the osteoclasts incorporate the BPs, that are concentrated in the mineralic bone compartment. Once the BPs are in the osteoclast, they induce the apoptosis, which leads to a decreased osteoclast activity on the bone. In turn, the decreased bone resorption reduces the release of growth factors embedded in the bone matrix and thus have antiproliferating effects on the tumor. In addition, the tumor is not able to growth deeper in the solid bone, without the assistance of the bone remodelling cells.

The apoptosis can be introduced in two ways. Since BPs function as pyrophosphate mimetics, it can be taken by enzyms as a substrate for phosphorylation reactions. Phosphorylation is an important mechanism for energy transfer and activation of biochemical compound, intermediates and proteins in the organism. Usually the step of energy release to initiate a chemical reaction at biochemical levels can be obtained by pyrophosphate hydrolysis. As a result of the very stabel P-C-P bond of bisphosphonates, the hydrolysis cannot occurre and the phosphorylated intermediate will be the endpoint of an initial reaction cascade. As a consequence, the apoptosis is initiated in the cell. The second mechanism is the function as an inhibtior of the farnesyl pyrophophosphate synthase (FPPS). The enzym is involved in the mevalonate pathway. It represents the main biochemical route for the production of farnesylated and geranyl-geranylated membrane proteins in the cell. A decrease in these proteins leads strongly to apoptosis [55,56].

The therapeutic efficencies of BPs depend on two factors. The first one is the tendency of bone binding and depence on the complexation abilities to calcium within apatite. This affinity increases from simple α-H-BP to α-OH-BP. The OH-group between the bisphosphonate moiety function as an additional donor. It is arranged similar like the OH^- is placed in apatite. Nitrogen-containing BPs are not only stronger in binding to the bone surface by a hydrogen bridge, but also by their enhanced capability to inhibit the FPPS. Within these criteria, zoledronic acid shows the best FPPS inhibition and the best affinity to hydroxyl apatite as well, and it is therefore the most potent BP of all [56,57]. BP treatment is

now a common part in the treatment of bone metastases, they delay the occurrence of skeletal related events and thus showed improvements of the analgesia score [57,58].

Bone targeted radiotherapy: The usage of radioisotopes for bone pain palliation shows excellent results in terms of pain relief and thus enhances the patients quality of life. Moreover, endoradiotherapy (ERT) treatment of bone metastases indicates a decrease in bone and tumor markers and seems to enhance the overall longer survival rate. The therapeutic effect is based on a synergy of an increased skeletal accumulation of bone targeting agents on the metastatic foci and the nearby energy deposit of β^-- or α-particle irradiation [59]. According to the natural bone accumulation of earth alkaline metals and phosphates, the radioisotopes of strontium and phosphorus were first included in clinical applications [60]. ^{32}P-labelled phosphate was used in the early 1950´s to treat bone related diseases, but it showed to have a poor tumor to healthy bone ratio and an intolerable high bone marrow uptake [61,62]. Additionally, ^{32}P has a relatively long half-life of 14.3 d and a high β^- range, based on the high energetic β^--particle emission of E_{max} = 1.7 MeV, which inflicts the radio-sensitive bone marrow with a high fraction of radiation energy [61].

More effective was the calcium mimetic strontium isotope ^{89}Sr in the management of bone pain in the last decades. Many studies were published, which revealed a pain reduction by the administration of 140 MBq $^{89}SrCl_2$ per patient and the compound was finally approved for treatment [59]. The half-life of ^{89}Sr is quite long with 50.5 days. Additionally, the energy of the β^--particles emitted is as high as that of ^{32}P (E_{max} = 1.5 MeV), and thus a palliative $^{89}SrCl_2$ therapy induces similar site effects, which are mainly myelosuppression, and anemia [59, 60]. As a consequence, new therapeutic concepts, based on better fitted radionuclides, came into clinical practice. The development of new tracers focused on isotopes, which reduced the bone marrow toxicity and thus decreased the unpleasant side effects of an ERP for bone pain relief. However, most of these new isotopes like $^{188/186}$Rh or ^{117m}Sn remained only in an preclinical experimental state [63].

Today the most common radionuclide for bone palliation is the lanthanide ^{153}Sm. It has a half-life of 1.9 d and emits β^--particles of a low maximum energy of 0.8 MeV. The nuclide properties of ^{153}Sm offer an effective pain relief combined with a low bone marrow toxicity

and ^{153}Sm is thus now widely used in clinical practice. Despite all the advantages, no indications of a positive effect on the overall survival rate exist [59,64]. The administration of lanthanides like Sm is not that easy like the usage of calcium mimetics. Hence, they do not naturally accumulate on the bone like the earth alkaline isotopes ^{89}Sr and [^{32}P]PO_4^{3-}, a carrier complex is necessary to guide the radio nuclide to the bone. ^{153}Sm is commonly used with the complexing agent EDTMP (ethylenediamine tetra(methylene phosphonic acid)), cf. chart 2. EDTMP delegates the lanthanides to the bone by keeping the uptake low in critical organs like the liver [65]. It is further an open chain chelator, which is able to form complexes with various nuclides including the low energetic β^--emitter ^{177}Lu and the α-particle emitter ^{225}Ac. Unfortunately, EDTMP complexes show the character of having a low kinetical inertness *in vivo* and thus have the tendencies at low EDTMP blood level to dissociate [66,67].

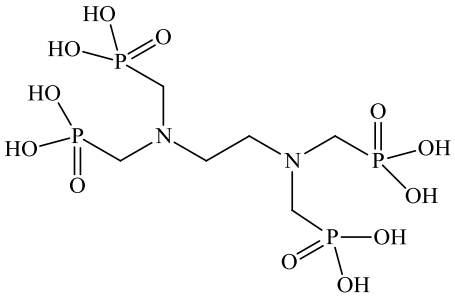

Chart 2. Structure of the open chain chelator EDTMP.

Dissociation of the [*Me]EDTMP complex is characterized by the release of the therapy nuclide in the blood stream and its consequent liver accumulation, which is to avoid, due to the resulting high toxicity. The problem is bypassed by coinjection of a large EDTMP excess, thus keeping the complex stable *in vivo* [67]. The production route of ^{153}Sm starts with a neutron capture reaction of enriched ^{152}Sm targets in a nuclear reactor as described with the following formula [68].

$$^{152}\mathrm{Sm}(n,\gamma)^{153}\mathrm{Sm}$$

It is apparent that the separation of the target nuclide of Sm and the desired therapy nuclide are not able to separate. As a consequence the ^{153}Sm therapy compounds are carrier added

with a high rate of the non-functional ´cold´ ^{152}Sm, thus could lower the therapeutic efficiency. Nevertheless, the results of [^{153}Sm]EDTMP reveal a significant pain relief in metastatic patients in combination with a low toxicity and in line with this [^{153}Sm]EDTMP is actually the most common administered bone targeting agent for palliative care.

Recently new compounds were developed with improved characteristics. One of these compounds is [^{177}Lu]EDTMP. The exchange of the therapy nuclide form ^{153}Sm to ^{177}Lu offers mainly two benefits. The first one is the lower β^--energy of ^{177}Lu compared to ^{153}Sm and therefore ^{177}Lu showed to be more bone marrow protective. It has a half-life of 6.7 d and provides β^--particles of a maximum energy of 0.5 MeV. The second reason concerns to the production route of ^{177}Lu, which could be done in two ways. The standard way is similar to that of ^{153}Sm by neutron capture of enriched ^{176}Lu targets [68].

$$^{176}\mathrm{Lu}(n,\gamma)^{177/177m}\mathrm{Lu}$$

Although the reaction is used worldwide and a new non-carrier added route is preferable, which starts by neutron irradiation of enriched ^{176}Yb targets. The conversation of ^{177}Yb yields ^{177}Lu, free of the metastable ^{177m}Lu. ^{177}Lu is separated by ion exchange methods from the target [69].

$$^{176}\mathrm{Yb}(n,\gamma)^{177}\mathrm{Yb} \rightarrow {}^{177}\mathrm{Lu}$$

[^{177}Lu]EDTMP is under clinical trials in phase II and shows promising results in terms of pain relief and bone marrow toxicity [70,71]. Nevertheless, the exchange of the therapy nuclide does not solve the problem of the low kinetic stability of EDTMP complexes with rare earth elements.

The recently approved α-particle emitter ^{223}Ra is actually the only ERT for bone metastases, which offers a significant longer overall survival rate. ^{223}Ra is administered as the ^{223}Ra-chloride salt in six separate injections over a period of two month. In clinical trial it reveals a significant pain relief, which occurs usually after the second or third therapy cycle. It also shows a mean longer survival rate of 2.8 month against placebo [72]. Radium naturally accumulates in the skeleton based on its chemical analogy to calcium and for that reason it is strongly taken up by bone tumor lesions. The α-particle emission has the character of a very

short range combined with a high linear energy transfer and the energy deposit in the surrounding tissue by α-emission is obviously higher compared to β-emissions in a magnitude. Despite all the benefits the new ^{223}Ra therapy offers, it shows still some disadvantages, among them are significant toxic side effects on the bone marrow and the guts and unsolved problems deduced from the decay chain [73].

Consequently, bone metastases remain a challenging disease to manage. A method for curing patients, who suffer from that plague, is still a claim of medical sciences. New concepts are needed to develop, with properties of improved pharmacokinetics and lower side effects. Multimodal compounds suitable for imaging and therapy, which are so called *theranostics*, offer a great potential in the management of skeletal metastases. Subsequent treatment with a personalized calculated dose in relation to the previously determined patients specific uptake profile provide an evidently improvement and clinicians as well as patients would strongly benefit.

1.4. References

[1] World Health Organization (WHO), GLOBOCAN 2012 (IARC): Estimated Cancer Incidence, Mortality and Prevalence Worldwide in 2012. WHO Press, Geneva, **2012**.

[2] World Health Organization (WHO), Global Action Against Cancer - Updated version 2005, WHO Press, Geneva **2005**.

[3] American Cancer Society, Cancer Facts and Figures 2014. American Cancer Society, Atlanta, **2014**.

[4] Zentrum für Krebsregistrierdaten GEK/D, Krebs in Deutschland 2009/2010, Robert Koch Institut, 9. Ausgabe, Berlin, **2013**.

[5] B. Secretan, K. Straif, R. Baan, Y. Grosse, F. El Ghissassi, V. Bouvard, C. Freeman, L. Galichet, V. Cogliano, A review of human carcinogens - Part E: tobacco, areca nut, alcohol, coal smoke, and salted fish, *The Lancet: Oncology*, **2009**; 10: 1033-1034.

[6] V. Bouvard, R. Baan, K. Straif, Y. Grosse, B. Secretan, F. El Ghissassi, C. Freeman, L. Galichet, V. Cogliano, A review of human carcinogens - Part B: biological agents, *The Lancet: Oncology*, **2009**; 10: 321-322.

[7] M. Tommasino, The human papillomavirus family and its role in carcinogenesis, *Seminars in Cancer Biology*, **2014**; 26:13–21.

[8] A. Urruticoechea, R. Alemany, J. Balart, A. Villanueva, F. Viñals, G. Capellá, Recent Advances in Cancer Therapy: An Overview, *Current Pharmaceutical Design*, **2010**; 16: 3-10.

[9] SM. Bison, MW. Konijnenberg, M. Melis, SE. Pool, MR. Bernsen, JJ. Teunissen, DJ. Kwekkeboom ,M. de Jong, Peptide receptor radionuclide therapy using radiolabeled somatostatin analogs: focus on future developments, *Clin Transl Imaging*, **2014**; 2: 55-66.

[10] W. P. Levin, H. Kooy, J. S. Loeffler, T. F. DeLaney, Proton beam therapy, *British Journal of Cancer*, **2005**; 93: 849–854.

[11] A. Montazeri, Quality of life data as prognostic indicators of survival in cancer patients: an overview of the literature from 1982 to 2008, *Health and Quality of Life Outcomes*, **2009**, 7: 102.

[12] C. A. Klein, The Metastasis Cascade, *Sience*, **2008**, 312, 1785.

[13] S. Paget, The Distribution of Secondary Growths in Cancer of the Breast, *The Lancet*, **1889**; 133: 571-573.

[14] L. Mathot, J. Stenninger, Behavior of seeds and soil in the mechanism of metastasis: A deeper understanding, *Cancer Sci.*, **2012**; 103: 626-631.

[15] O. S. Nielsen, A. J. Munro, I. F. Tannock, Bone Metastases: Pathophysiology and Management Policy, *Journal of Clinical Oncology*, **1991**; 9: 509-524.

[16] R. E. Coleman, Metastatic bone disease: clinical features, pathophysiology and treatment strategies, *Cancer Treatment Reviews*, **2001**; 27: 165–176.

[17] G. R. Mundy, Metastasis to Bone: Causes, Consequences and Therapeutic Opportunities, *Nature Reviews|Cancer*, **2002**; 2: 584-593.

[18] S. V. Dorozhkin, M. Eppl, Die biologische und medizinische Bedeutung von Calciumphosphate, *Angew. Chem.*, **2002**; 114: 3260-3277.

[19] K. N. Weilbaecher, T. A. Guise, L. K. McCauley, Cancer to bone: a fatal attraction, *Nature Reviews|Cancer*, **2011**; 11: 411-425.

[20] H. C. Blair, M. Zaidi, C. L.-H. Huang, L.Sun, The Developmental Basis of Skeletal Cell Differentiation and the Molecular Basis of Major Skeletal Defects, *Biol. Rev.* **2008**; 83: 401–415.

[21] A. G. Robling, P. J. Niziolek, L. A. Baldridge, K. W. Condon, M. R. Allen, I. Alam, S. M. Mantila, J. Gluhak-Heinrich, T. M. Bellido, S. E. Harris, C. H. Turner, Mechanical stimulation of bone in vivo reduces osteocyte expression of Sost/sclerostin, *J. Biol. Chem.,* **2008**; 283: 5866-75.

[22] R. R. Langley, I. J. Fidler, The seed and soil hypothesis revisited - the role of tumor-stroma interactions in metastasis to different organs, *Int. J. Cancer*, **2011**; 128: 2527–2535.

[23] D. Santini, S. Galluzzo, A. Zoccoli, F. Pantano, M.E. Fratto, B. Vincenzia, L. Lombardi, C. Gucciardino, N. Silvestris, E. Riva, S. Rizzo, A. Russo, E. Maiello, G. Colucci, G. Tonini, New molecular targets in bone metastases, *Cancer Treatment Reviews*, **2010**; 36S3: 6–10.

[24] M. Ignatiadis, C. Sotiriou, Luminal breast cancer: from biology to treatment, *Nature Reviews|Clinical Oncology*, **2013**; 10: 494–506.

[25] Q. Huang, X. Ouyang, Biochemical-markers for the diagnosis of bone metastasis: A clinical review, *Cancer Epidemiology*, **2012**; 36: 94–98.

[26] T. Hamaoka, J. E. Madewell, D.A. Podoloff, G. N. Hortobagyi, and N. T. Ueno, Bone Imaging in Metastatic Breast Cancer, *J. Clin. Oncol*., **2004** ; 22: 2942-2953.

[27] U. Tateishi, S. Morita, M. Taguri, K. Shizukuishi, R. Minamimoto, M. Kawaguchi, T. Murano, T. Terauchi, T. Inoue, E. E. Kim, A meta-analysis of ^{18}F-Fluoride positron emission tomography for assessment of metastatic bone tumor, *Ann. Nucl. Med*., **2010**; 24: 523-531.

[28] F. Mosavi, S. Johansson, D. T. Sandberg, I. Turesson, J. Sörensen, H. Ahlström, Whole-Body Diffusion-Weighted MRI Compared With ^{18}F-NaF PET/CT for Detection of Bone Metastases in Patients With High-Risk Prostate Carcinoma, *AJR Am. J. Roentgenol*., **2012**; 199: 1114-20.

[29] H. Levi, George Hevesy and His Concept of Radioactive Indicators - In Retrospect, *Eur. J. Nucl. Med.*, **1976**; 1: 3-10.

[30] G. C. H. Bauer, B. Wendeberg, External counting of Ca-47 and Sr-85 in studies of localized skeletal lesions in man, *J. Bone Joint Surg.*, **1959**; 41B: 558.

[31] G. L. DeNardo, J. A. Volpe, Detection of bone lesions with the Strontium-85 Scintiscan, *J. Nucl. Med*., **1966**; 7: 219-236.

[32] M. J. Welch, C. S. Redvanly, Handbook of Radiopharmaceuticals: radiochemistry and Applications, *John Wiley & Sons, Ltd*, **2003**; ISBN: 0-471-49560-3.

[33] G. Subramanian, J. G. McAfee, A new complex of ^{99m}Tc for skeletal imaging, *Radiology*, **1971**; 99: 192-6.

[34] E. Bombardieri, C. Aktolun, R. P. Baum, A. Bishof-Delaloye, J. Buscombe, J. F. Chatal, L. Maffioli, R. Moncayo, L. Mortelmans, S. N. Reske, Bone scintigraphy: procedure guidelines for tumour imaging, *Eur. J. Nucl. Med. Mol. Imaging*, **2003**; 30: 99–106.

[35] L. S. Malmud, N. D. Charkes, Bone scanning: Principles, Technique and Interpretation, *Clin. Orthop. Relat. Res*., **1975**; 107: 112-22.

[36] E. Even-Sapir, Ur Metser, E. Mishani, G. Lievshitz, H. Lerman, I. Leibovitch, The Detection of Bone Metastases in Patients with High-Risk Prostate Cancer: ^{99m}Tc-MDP Planar Bone Scintigraphy, Single- and Multi-Field-of-View SPECT, ^{18}F-Fluoride PET, and ^{18}F-Fluoride PET/CT, *J. Nucl. Med*., **2006**; 47: 287–297.

[37] P. A. M. Dirac, The Quantum Theory of the Electron, *Proc. R. Soc. Lond. (A)*, **1928**; 117: 610-624.

[38] C. D. Anderson, The Positive Electron, *The Physical Review*, **1933**; 43: 491-49.

[39] G. B. Saha, Basics of PET imaging physics, chemistry and regulations, *Springer Science+Business Media Inc*., NY, **2005**; ISBN: 0-387-21307-4.

[40] W. Langsteger, M. Heinisch, I. Fogelman, The Role of Fluorodeoxyglucose,^{18}F-Dihydroxyphenylalanine, ^{18}F-Choline, and ^{18}F-Fluoride in Bone Imaging with Emphasis on Prostate and Breast, *Semin. Nucl. Med.*, **2006**; 36: 73-92.

[41] M. Blau, W. Nagler, M. A. Bender, Fluorine-18: a new isotope for bone scanning, *J. Nucl. Med.*, **1962**; 3: 332.

[42] A. Iagaru, P. Young, E. Mittra, D. W. Dick, R. Herfkens, S. S. Gambhir, Pilot Prospective Evaluation of ^{99m}Tc-MDP Scintigraphy, ^{18}F -NaF PET/CT, ^{18}F-FDG PET/CT and Whole-Body MRI for Detection of Skeletal Metastases, *Clin. Nucl. Med*., **2013**; 38: 290-296.

[43] Z. Hu, W. Yang, H. Liu, K. Wang, C. Bao, T. Song, J. Wang, J. Tian, From PET/CT to PET/MRI: Advances in Instrumentation and Clinical Applications, *Mol. Pharmaceutics*, **2014**; recently published manuscript.

[44] S.-H. Yoon, K. S. Kim, S. Y. Kang, H. S. Song, K. S. Jo, B. H. Choi, S. J. Lee, J. K. Yoon, Y. S. An, Usefulness of ^{18}F-fluoride PET/CT in Breast Cancer Patients with Osteosclerotic Bone Metastases, *Nucl. Med. Mol. Imaging*, **2013**; 47: 27–35.

[45] A. Afshar-Oromieh, C. M. Zechmann, A. Malcher, M. Eder, M. Eisenhut, H. G. Linhart, T. Holland-Letz, B. A. Hadaschik, F. L. Giesel, J. Debus, U. Haberkorn, Comparison of PET imaging with a ^{68}Ga-labelled PSMA ligand and ^{18}F-choline-based PET/CT for the diagnosis of recurrent prostate cancer, *Eur. J. Nucl. Med. Mol. Imaging*, **2014**; 41: 11–20.

[46] F. Rösch, Past, present and future of ^{68}Ge/^{68}Ga generators, *Appl. Radiat. Isot*., **2013**; 76 : 24–30.

[47] R. P. Baum, H. R. Kulkarni, THERANOSTICS: From Molecular Imaging Using Ga-68 Labeled Tracers and PET/CT to Personalized Radionuclide Therapy – The Bad Berka Experience, *Theranostics*, **2012**; 2: 437-447.

[48] A. Muralidharan, M.T. Smith, Pathobiology and management of prostate cancer-induced bone pain: recent insights and future treatments, *Inflammopharmacology*, **2013**; 21: 339–363.

[49] F. Zustovich, F. Fabiani, Therapeutic opportunities for castration-resistant prostate cancer patients with bone metastases, *Critical Reviews in Oncology/Hematology*, **2014**; 91: 197–209.

[50] N. Niikura, J. Liu, N. Hayashi, S. L. Palla, Y. Tokuda, G. N. Hortobagyi, N. T. Ueno, R. L. Theriault, Treatment Outcome and Prognostic Factors for Patients with Bone-Only Metastases of Breast Cancer: A Single-Institution Retrospective Analysis, *Oncologist*, **2011**; 16: 155–164.

[51] X. Deng, G. He, J. Liu, F. Luo, X. Peng, S. Tang, Z. Gao, Q. Lin, J. M. Keller, T. Yang, E. T. Keller, Recent advances in bone-targeted therapies of metastatic prostate cancer, *Cancer Treatment Reviews*, **2014**; 40: 730–738.

[52] D. Heymann, B. Ory, F. Gouin, J. R. Green, F. Redini, Bisphosphonates: new therapeutic agents for the treatment of bone tumors, *TRENDS in Molecular Medicine*, **2004**; 10: 337-343.

[53] A. Heidenreich, Bisphosphonates in the Management of Metastatic Prostate Cancer, *Oncology*, **2003**; 65: 5–11.

[54] S. E. Papapoulos, Bisphosphonates: how do they work?, *Best Pract. Res. Clin. Endocrinol. Metab*., **2008**; 22: 831–847.

[55] R. G. G. Russell, N. B. Watts, F. H. Ebetino, M. J. Rogers, Mechanisms of action of bisphosphonates: similarities and differences and their potential influence on clinical efficacy, *Osteoporos Int*., **2008**; 19: 733–759.

[56] Z. J. Henneman, G. H. Nancollas, F. H. Ebetino, R. G. G. Russell, R. J. Phipps, Bisphosphonate binding affinity as assessed by inhibition of carbonated apatite dissolution *in vitro*, *J. Biomed. Mater Res. A*, **2008**; 85: 993–1000.

[57] M. Tolia, A. Zygogianni, J. R. Kouvaris, C. Meristoudis, N. Margari, N. Kelekis, V. Kouloulias, The Key Role of Bisphosphonates in the Supportive Care of Cancer Patients, *Anticancer Research*, **2014**; 34: 23-38.

[58] M. Apro, F. Saad, L.Costac, Optimizing Clinical Benefits of Bisphosphonates in Cancer Patients with Bone Metastases, *Oncologist*, **2010**; 15: 1147–1158.

[59] O. Sartor, P. Hoskin, O. S. Bruland, Targeted radio-nuclide therapy of skeletal metastases, *Cancer Treatment Reviews*, **2013**; 39: 18–26.

[60] V. J. Lewington, Targeted radionuclide therapy for bone metastases, *Eur. J. Nucl. Med.*, **1993**; 20: 66-74.

[61] A. Morales, R. C. Burr, A. W. Bruce, The use of radioactive phosphorus to treat bone pain in metastatic carcinoma of the prostate, *Can. Med. Assoc. J.*, **1970**; 103: 372–373.

[62] S. Hertz, Modifying effect of steroid hormone therapy on human neoplastic disease as judged by radioactive phosphorus (P-32), *J. Clin. Invest*.,**1950**; 29: 821.

[63] B. E. Zimmerman, J. T. Cessna, F. J. Schima, The Standardization of the Potential Bone Palliation Radiopharmaceutical ^{117m}Sn(+4)DTPA, *Appl. Radiat. Isot*., **1998**;49: 317-328.

[64] R.A. Holmes, [^{l53}Sm] EDTMP: A Potential Therapy for Bone Cancer Pain, *Semin. Nucl. Med*., **1992**; 12: 41-45.

[65] M. Laznicek, A. Laznickova, F. Budskv, J. Prokop, K. Kopicka, Comparison of Biological Characteristics of EDTMP Complexes with ^{99m}Tc, ^{111}In and ^{153}Sm in Rats, *Appl. Radiat. Isot*., **1994**; 45: 949-953.

[66] F. K. Kálmán, R. Király, E. Brücher, Stability Constants and Dissociation Rates of the EDTMP Complexes of Samarium(III) and Yttrium(III), *Eur. J. Inorg. Chem*., **2008**; 30: 4719–4727.

[67] G. J. Beyer, R. Offord, G. Künzi, Y. Aleksandrova, U. Ravn, S. Jahn, J. Barker, O. Tengblad, M. Lindroos, ISOLDE Collaboration, The Influence of EDTMP-Concentration on the Biodistribution of Radio-Lanthanides and 225-Ac in Tumor-Bearing Mice, *Nucl. Med. Biol*., **1997**; 24: 367-372.

[68] F. Rösch, Radiolanthanides in endoradiotherapy: an overview, *Radiochim. Acta*, **2007** ; 95: 303–311.

[69] N. A. Lebedev, A. F. Novgorodov, R. Misiak, J. Brockmann, F. Rösch, Radiochemical separation of no-carrier-added ^{177}Lu as produced via the ^{176}Yb(n,γ)^{177}Yb→^{177}Lu process, **2000**; 53: 421–425

[70] J. Yuan, C. Liu, X. Liu, Y. Wang, D. Kuai, G. Zhang, J. J. Zaknun, Efficacy and safety of ^{177}Lu-EDTMP in bone metastatic pain palliation in breast cancer and hormone refractory prostate cancer: a phase II study, *Clin Nucl Med*., **2013**; 38: 88-92.

[71] K. K. Agarwal, S. Singla, G. Arora, C. S. Bal, ^{177}Lu-EDTMP for palliation of pain from bone metastases in patients with prostate and breast cancer: a phase II study, *Eur. J. Nucl. Med. Mol. Imaging*, **2014**, recently published data.

[72] P. G. Kluetz, W. Pierce, V. E. Maher, H. Zhang, S. Tang, P. Song, Q. Liu, M. T. Haber, E. E. Leutzinger, A. Al-Hakim, W. Chen, T. Palmby, E. Alebachew, R. Sridhara, A. Ibrahim, R. Justice, R. Pazdur, Radium Ra 223 dichloride injection: U.S. Food and Drug Administration drug approval summary, *Clin. Cancer Res*. **2014**; 20: 9-14.

[73] J. A. Carrasquillo, J. A. O'Donoghue, N. Pandit-Taskar, J. L. Humm, D. E. Rathkopf, S. F. Slovin, M. J. Williamson, K. Lacuna, A. K. Aksnes, S. M. Larson, H. I. Scher, M. J. Morris, Phase I pharmacokinetic and biodistribution study with escalating doses of ^{223}Ra-dichloride in men with castration-resistant metastatic prostate cancer. *Eur. J. Nucl. Med. Mol. Imaging*., **2013**; 40: 1384-93.

2. Objectives and Outlines

The management of bone metastases is a demanding multidisciplinary field, which physicians and patients have to deal with. Despite the medical progress in the last decades, the status of skeletal metastases is still a problematic burden. Imaging modalities are the backbone of metastases diagnosis and the endo-radiotherapy of disseminated bone lesions is well-established in the palliative care. While these keystones have been considered independently from each other in the past, a new concept was successfully developed in the previous work. It is based on a macrocyclic chelate which is combined with a bisphosphonate entity and depicted in figure 2.1 [1]. The new compound can be labelled both with the generator derived metallic PET nuclide ^{68}Ga and the therapy nuclide ^{177}Lu. It thus combines high quality imaging with an adequate therapy option. This *theranostic* concept opens up new possibilities in the treatment and assessment of bone metastases and thus qualifies macrocyclic bisphosphonates as a leap towards personalized medicine. First successful patient studies exhibited the potential of this approach using the proof of principle compound [^{68}Ga/^{177}Lu]BPAMD, cf. figure 2.2 [3,4].

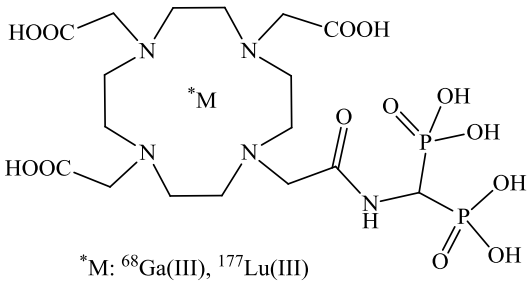

Figure 2.1. Structure of BPAMD (4-{[bis-(phosphonomethyl))carbamoyl]methyl}-7,10-bis(carboxymethyl)-1,4,7,10-tetraazacyclododec-1-yl)acetic acid). The macroyclic bisphosphonate was successfully evaluated by Fellner et al. with the PET nuclide ^{68}Ga(III) and the therapy nuclide ^{177}Lu(III) [4].

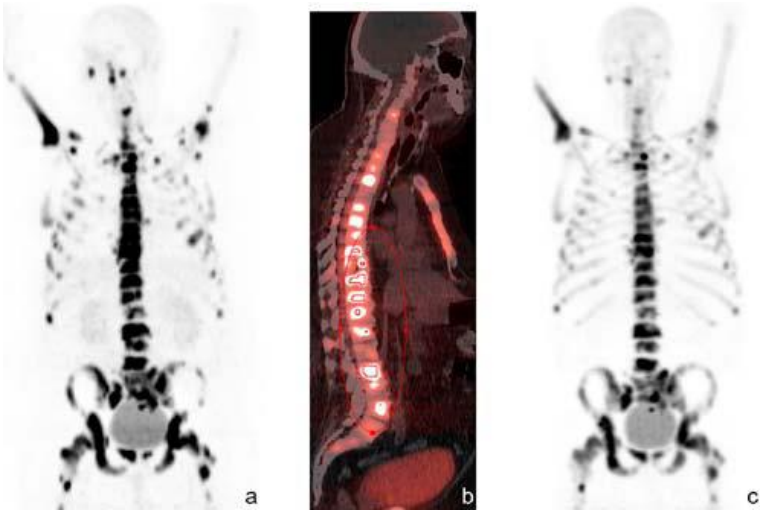

Figure 2.2. First study of [^{68}Ga]BPAMD in a prostate cancer patient. From left to right: Coronal slice, sagittal slice and a coronal [^{18}F]NaF scan for comparison (Fellner et al. [3]).

Despite all achieved success, lots of questions remain unsolved and further improvements are open. The concept has to be proven in clinical practice and hence a routine GMP (good medical practice) application of [^{177}Lu]BPAMD is installed, clinical trials can reveal the treatment potential in cancer patients, suffering from bone metastases. Nevertheless, BPAMD represents one compound of the first generation of macrocyclic bisphosphonates. New derivatives with improved structures concerning the chelate as well as the targeting moiety may enhance the *theranostic* power of this novel concept. The concept can be further developed by modification of the BPAMD lead structure and the used nuclides in five subitems and is illustrated in figure 2.3.

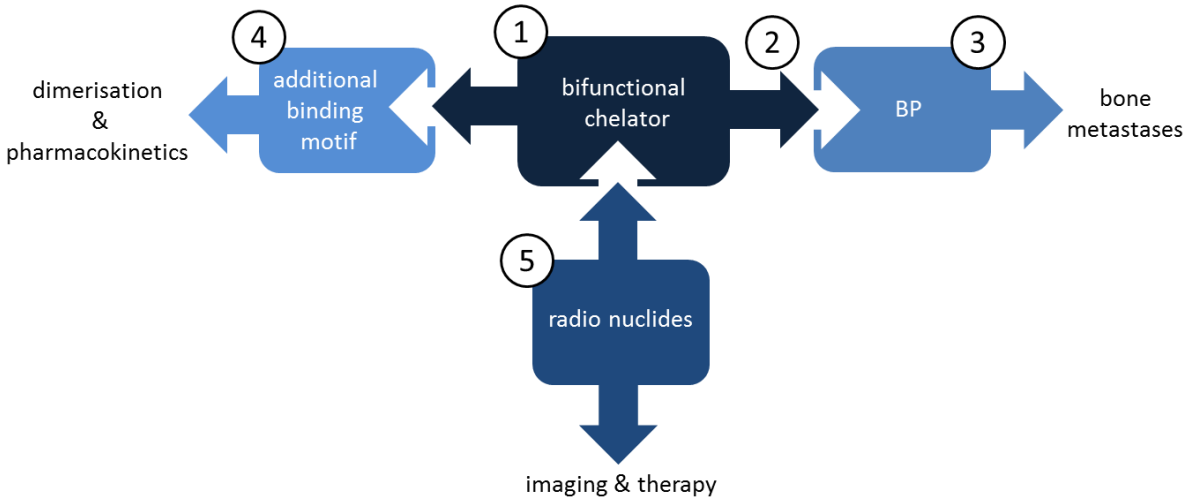

Figure. 2.3. Schematic overview of the BPAMD modification sites based on the bifunctional chelator concept of radiopharmaceutical.

① The bifunctional chelator is the starting point in the evolution of macrocyclic bisphosphonates. New bifunctional chelates were recently developed for a fast and stable complexation of various radionuclides and new tracer designs should take account of that, consequently. The usage of NOTA (1,4,7-triazacyclononane-triacetic acid) and NOTA-derivatives instead of DOTA may enable a convenient Kit-type labelling approach for ^{68}Ga-PET imaging, since this chelator is ideal fitted for Ga-complexation. The chelator DO2A (1,4,7,10-tetraazacyclododecane-1,7-diacetic acid) offer the possibility of further modifications, since it provides an additional functional entity. The DOTA derivative DOTAGA (2-[4,7,10-tris(carboxymethyl)-1,4,7,10-tetracyclododecan-1-yl]pentanedioic acid) contains an auxiliary donor group, which may facilitates the radiometal complexation, with therapeutic lanthanides or actinides.

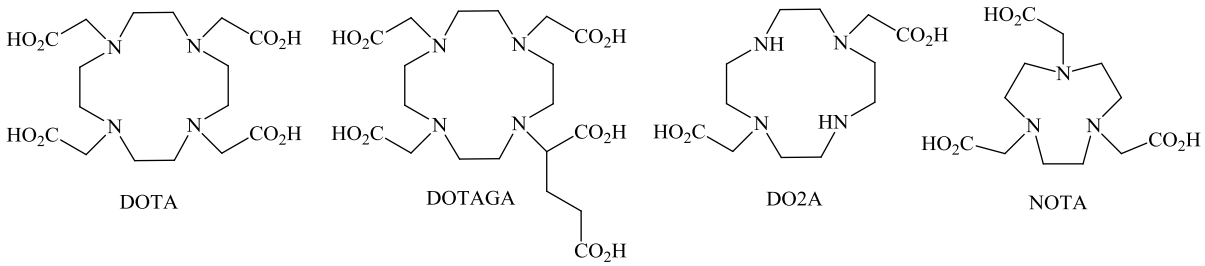

② The common link between the macrocycle and the targeting moiety is an amide bond. The conjugation is relatively stable *in vivo* and easy to obtain. However, the formation occupies one of the carboxylic acid groups and thus reduces the number of donors of the macrocyclic chelate. Recently developed phosphinic acid based linkers enable a very stable connection between the chelator and the targeting vector, but the phosphinic acid acts as an additional complexation group and finally preserves the numbers of donors of the macrocycle in spite of conjugation.

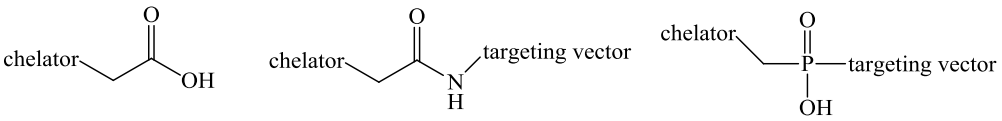

carboxylic acid donor amide conjugation phosphinic acid conjugation

③ During the last decades novel highly potent bone targeting pharmaceuticals like pamidronic and zoledronic acid were developed and became keystones in the management of skeletal related diseases. Structural improvements of bone targeting macrocyclic ligands should thus orientate on the binding motif of these compounds. The substitution of α-H-BP of BPAMD with novel α-OH-BPs and heteroaromatic nitrogen containing α-OH-BPs may increase the affinity of the resulting radiopharmaceutical to the target.

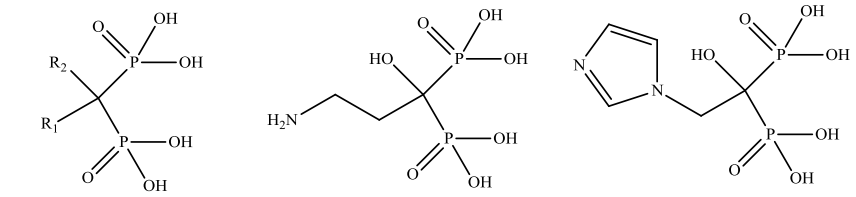

BPs of general structure pamidronate zoledronate

The pamidronate structure contains a primary amine and offers therefore a functional group for a convinient amide coupling to the bifunctional chelate. Contrary to that, the zoledronic acid structure has to be midified first for a subsequent conjugation, since it is missing a coupling site in the original molecule.

④ The additional conjugation site of the DO2A chelator makes it possible to add a further functional group. This could be the identical targeting vector leading to dimerizations, which may enhance the binding characteristics and may result in favorable target to background ratios [5]. Functional groups, which influence the pharmacokinetics of the tracer, such as an ablumin binding motif, can also be added. It is reported that small lipophilic molecules (e.g. **428**-D-Lys-OH) suitable for chemical derivatisation of imaging agents have a high binding affinity to serum albumin [6].

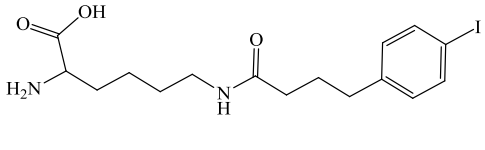

428-D-Lys-OH K_d (albumin) = 3.2 µM

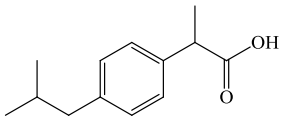

Ibuprofen K_d (albumin) = 1.5 mM

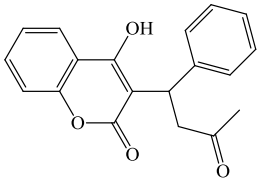

Warfarin K_d (albumin) = 1.4 µM

Beside novel innovative nuclide and targeting vector applications, the focusing on an enhancement of the pharmacokinetics of the macrocyclic bisphosphonates is also a key note. Since bisphosphonates show a fast blood and body clearance, the most of the injected activity is not able to bind on the targeted tissue, thus a modified bisphosphonates with an albumin binding entity may influence the pharmacokinetics in terms of blood and skeletal retention.

⑤ However, improvements of the quantitative structure-activity relationship are only one side of the medal. The bifunctional chelator concept of radiopharmaceuticals, offer the opportunity of choosing various radionuclides, which are suitable fitted for different issues and needs. Beside ^{68}Ga ($t_{1/2}$ = 67.6 min) other positron emitters like ^{64}Cu ($t_{1/2}$ = 12.7 h) or ^{44}Sc ($t_{1/2}$ = 3.9 h) have a promising potential as clinical PET nuclides. A wide range of therapeutic nuclides are available, including α and β^--particle emitters. Indeed the targeted α-particle therapy showed remarkable results in the past and the usage of macoryclic bisphosphonates in combination with the α-particle emitter ^{225}Ac(III) might be pioneering for the future of the *theranostic* bone metastases treatment.

Within this present work novel macrocyclic bisphosphonates are described, representing the next generation of bone *theranostics*, and evaluated in *in vitro* and *in vivo* studies, including first clinical applications. The results are summarized in chapter 3 in individual manuscripts concerning the above outlined aspects and complemented with additional findings.

2.1. References

[1] V. Kubıcek, J. Rudovsky, J . Kotek, P. Hermann, L. Vander Elst, R. N. Muller, Z. I. Kolar, H. T. Wolterbeek, J. A. Peters, I. Lukes, A Bisphosphonate Monoamide Analogue of DOTA: A Potential Agent for Bone Targeting, *J. Am. Chem. Soc*., **2005**; 127: 16477-16485.

[2] F. Rösch, R. P. Baum, Generator-based PET radiopharmaceuticals for molecular imaging of tumours: On the way to THERANOSTICS. *Dalton Trans.*, **2011**; 40/23: 6104-6111.

[3] M. Fellner, R. P. Baum, V. Kubíček, P. Hermann, I. Lukeš , V. Prasad, F. Rösch, PET/CT imaging of osteoblastic bone metastases with ^{68}Ga-bisphosphonates: first human study, *Eur. J. Nucl. Med. Mol. Imaging*, **2010**; 37: 834.

[4] M. Fellner, B. Biesalski, N. Bausbacher, V. Kubícek, P. Hermann, F. Rösch, O. Thews, ^{68}Ga-BPAMD: PET-imaging of bone metastases with a generator based positron emitter, *Nucl. Med. Biol*., **2012**; 39: 993-999.

[5] J. Notni, K. Pohle, J. H. Wester, Be spoilt for choice with radiolabelled RGD peptides: Preclinical evaluation of ^{68}Ga-TRAP(RGD)$_3$, *Nucl. Med. Biol.* **2013**; 40: 33-41.

[6] C. E. Dumelin, S. Trüssel, F. Buller, E. Trachsel, D. Neri, J. Scheuermann, A portable albumin binder from a DNA-encoded chemical library, *Angew. Chem. Int. Ed.* **2008**; 47: 3196-3201.

3. Manuscripts and Supplementary Results

This work is based on the following mansucripts:

3.1 M. Meckel, M. Fellner, N. Thieme, R. Bergmann, V. Kubíček, F. Rösch, In vivo comparison of DOTA based ^{68}Ga-labelled bisphosphonates for bone imaging in non-tumour models *Nucl Med Biol*. **2012**; 40: 823-30.

3.2. M. Meckel, A. Nauth, J. Timpe, K. Zhernosekov, A. D. Puranik, R. P. Baum, F. Rösch, Development of a [^{177}Lu]BPAMD labeling Kit and an automated synthesis module for routine bone targeted endoradiotherapy, *Cancer Biotherapy & Radiopharmaceuticals*, **2014**, recently accepted.

3.3. J. Holub, M. Meckel, V. Kubíček, F. Rösch, P. Hermann, Gallium(III) complexes of NOTA-bis (phosphonate) conjugates as PET radiotracers for bone imaging, *CMMI*, **2014**, ahead of print.

3.4. M. Meckel, N. Bausbacher, B. Biesalski, V. Kubíček, P. Hermann, M. Miederer, F. Rösch, Bone targeting compounds for PET-imaging and radiotherapy: Bisphosphonate-, pamidronate and zoledronate DOTA conjugates, *PLoS One*, in preparation.

3.5. M. Meckel, N. Bausbacher, B. Biesalski, V. Kubíček, P. Hermann, M. Miederer, F. Rösch, A DOTA based bisphosphonate with an albumin binding moiety for delayed body clearance in bone targeting radiotherapy, *Bionconj. Chem.*, **2014**, recently submitted.

3.6. M. Meckel, R. Bergmann, A. Suhl, J. Pietzsch, V. Kubicek, J. Steinbach, P. Hermann, F. Rösch, ^{177}Lu labelled macrocyclic bisphosphonates for targeting disseminated in cancer treatment, *Nucl Med Biol*, in preparation.

3.7.1. Supplementary Results I: *Ex vivo* organ distribution studies of the α-particle emitting calcium mimetic $^{223}RaCl_2$ (Xofigo®) in healthy Wistar rats.

3.7.2. Supplementary Results II: Synthesis and metal chelate stability studies of DOTA bisphosphonates with the α-particle emitter ^{225}Ac(III).

3.1. *In vivo* comparison of DOTA based ^{68}Ga-labelled bisphosphonates for bone imaging in non-tumour model.

In vivo comparison of DOTA based ^{68}Ga-labelled bisphosphonates for bone imaging in non-tumour models

Marian Meckel [1], Marco Fellner [1], Nathalie Thieme [2], Ralf Bergmann [2], Vojtěch Kubíček[3] and Frank Rösch [1]

[1] *Institute of Nuclear Chemistry, Johannes-Gutenberg-University Mainz, Germany*

[2] *Institute of Radiopharmacy, Helmholtz-Zentrum Dresden-Rossendorf, Germany*

[3] *Department of Inorganic Chemistry, Charles University Prague, The Czech Republic.*

Key words

Bone metastases, ^{68}Ga, PET, ^{177}Lu, DOTA, bisphosphonates

Abstract

Bone metastases are a class of cancerous metastases that result from the invasion of a tumor into bone. The solid mass which forms inside the bone is often associated with a constant dull ache and severe spikes in pain, which greatly reduce the quality of life of the patient. Numerous ^{99m}Tc-labeled bisphosphonate functionalised complexes are well established tracers for bone metastases imaging. The objective of this research was to evaluate the pharmacokinetics and behaviour of three DOTA based bisphosphonate functionalised ligands (BPAMD, BPAPD and BPPED), using both ^{68}Ga µ-PET *in vivo* imaging and *ex vivo* biodistribution studies in healthy Wistar rats. The compounds were labelled with ^{68}Ga in high yields using an ammonium acetate buffer, and subsequently purified using a cation exchange resin. High bone uptake values were observed for all ^{68}Ga-labelled bisphosphonates at 60 minutes p.i. The highest uptake was observed for [^{68}Ga]BPPED (2.6±0.3 % ID/g) which compares favourably with that of [^{99m}Tc]MDP (2.7±0.1 ID/g) and [^{18}F]fluoride (2.4±0.2 % ID/g). The ^{68}Ga-labelled DOTA-bisphosphonates showed rapid clearance from the blood and renal system, as well as low binding to soft tissue, resulting in a high bone to blood ratio (9.9 at 60 minutes p.i. for [^{68}Ga]BPPED, for example). Although further studies are required to assess their performance in tumor models, the results obtained suggest that these ligands could be useful both in imaging (^{68}Ga) and therapeutic treatment (^{177}Lu) of bone metastases.

1. Introduction

Together with the lungs and liver, the bones are most frequently affected by metastases. A significant portion (60-80 %) of bone metastases are caused by breast or prostate carcinoma. The formation usually occurs at the early stages of tumour development, however their symptoms are only recognized at later stages [1, 2]. For this reason the none-invasive diagnosis of bone metastases in a premature state, which allows for a profound and timely decision on subsequent therapy, is of great importance to improving the quality of life of the patients. ^{99m}Tc-labelled bisphosphonate functionalised ligands are well established for SPECT/CT imaging of osteoblastic metastases [3]. The resolution and sensitivity of metastases imaging would be significantly enhanced if a positron emitter was to be used instead, of which there are only a few examples. The inherent advantages of PET/CT, over the SPECT/CT, is clearly demonstrated by using [^{18}F]fluoride ([^{18}F]F$^-$) [4]. The images obtained with [^{18}F]F$^-$ are far superior to those obtained using ^{99m}Tc-radiopharmaceuticals. There is considerable interest in ^{68}Ga-labelled complexes as an alternatives to [^{18}F]F$^-$.

Bisphosphonates are known to show high and fast binding to apatite (bone) structures [5]. Commonly used ^{99m}Tc-labelled phosphonates include methylene diphosphonate (MDP), dicarboxypropane diphosphonate (DPD) and hydroxymethylene diphosphonate (HDP). Chemically attaching these bisphosphonates to a positron emitter is of great interest and potential for the *in vivo* imaging of bone metastases using PET/C. Combining the bisphosphonate targeting moieties with the macrocyclic ligand DOTA, an established ligand for use in ^{68}Ga-PET, led to a new generation of radiolabelled bisphosphonates. In addition to the benefits associated with the application of the PET radionuclide, in particular ^{68}Ga, the DOTA-bisphonsphates also have the potential to be used in therapeutic applications. DOTA is known to form complexes, which are stable *in vivo*, with a range of metal cations, and therefore DOTA-bisphosphonates could also be labelled with therapeutic nuclides (such as ^{177}Lu for example). In this way a single DOTA-bisphosphonate structure may have the potential to be used for both imaging and therapy of bone metastases simply by changing the radionuclide incorporated. This is a significant advantage over the [^{18}F]F$^-$, [^{153}Sm]EDMTP and [^{99m}Tc]MDP/[^{153}Sm]EDMTP systems. In general terms, this 2-in-1 "theranostic"

approach has a number of significant advantages (commercially and in practice) and is of considerable commercial interest.

One of the more promising DOTA conjugated bisphosphonates, (4-{[bis-(phosphonomethyl) carbamoyl] methyl}-7,10-bis(carboxymethyl)-1,4,7,10-tetraazacyclo-dodec-1-yl) acetic acid (BPAMD), has already been labelled using ^{68}Ga, to give the PET tracer [^{68}Ga]BPAMD [6]. Very promising initial human studies have been reported for this tracer following evaluation in a patient with extensive bone metastases arising from prostate cancer [7]. In this evaluation [^{68}Ga]BPAMD provided excellent imaging of bone metastases with very high bone to soft tissue ratios and fast clearance (no detectable blood pool and very faint renal activity). PET/CT depicted multiple, intense osteoblastic metastases in the entire skeleton, with a maximum standardised uptake value (SUV_{max}) of 77.1 in the 10th thoracic vertebra and an SUV of 62.1 for vertebra L2. These values are superior to those quantified for the same vertebra, 39.1 and 39.2 respectively, when the PET/CT was performed in the same patient using [^{18}F]F$^-$.

Following the very favourable and promising results obtained with [^{68}Ga]BPAMD, two further DOTA-bisphonates derivatives have been described recently in the search for even better structures [8]. How these derivatives compare to [^{68}Ga]BPAMD has not yet been addressed, and is the subject of the present study. *In vivo* PET/CT studies and systematic biodistribution experiments have been carried out for each of these three ^{68}Ga-labelled DOTA-bisphosphonates. The results obtained for these ^{68}Ga-labelled compounds have been compared with [^{18}F]F$^-$ and [^{99m}Tc]MDP.

2. Materials and Methods

2.1. Generator

Decay of Germanium-68 ($t_{1/2}$ = 270.8 d) provides an easily available source of the PET nuclide Gallium-68 ($t_{1/2}$ = 67.71 min). Germanium-68 is fixed on a solid phase of modified titanium dioxide, and Gallium-68 eluted from the generator with 10 mL 0.1 M HCl. This is

followed by immobilisation of the ^{68}Ga on an acidic cation exchanger. Impurities such as zinc, iron and titanium as well as ^{68}Ge generator breakthrough are removed using a mixture of acetone and hydrochloric acid. Subsequently, ^{68}Ga is quantitatively eluted with 1 M HCl (300 µL) from the cation exchanger. This eluate serves as an ideal low–volume and chemically highly pure source of ^{68}Ga for subsequent labelling [9, 10].

2.2. DOTA-bisphosphonates

The following macrocyclic DOTA based bisphosphonate chelators have been used (see Fig. 1 for their chemical structures): BPAMD (4–{[(bis-phosphonomethyl) carbomoyl]methyl}–7,10–bis–(carboxymethyl)–1,4,7,10-tetraazacyclododec–1–yl)–acetic acid, BPAPD (4–{[(bis–phosphonopropyl)carbomoyl]methyl}–7,10–bis–(carboxymethyl)–1,4,7,10-tetraazacyclododec–1–yl)–acetic acid and BPPED tetraethyl-10-{[(2,2-bis-phosphonoethyl)hydroxyphosphoryl]methyl}-1,4,7,10-tetraazacyclododecane-1,4,7-triacetic acid. According to a different terminology, these ligands are also denoted as DOTAM^{BP}, DOTAP^{BP} and DO3AP^{BP}. The ligands were synthesized following literature procedures [6, 8].

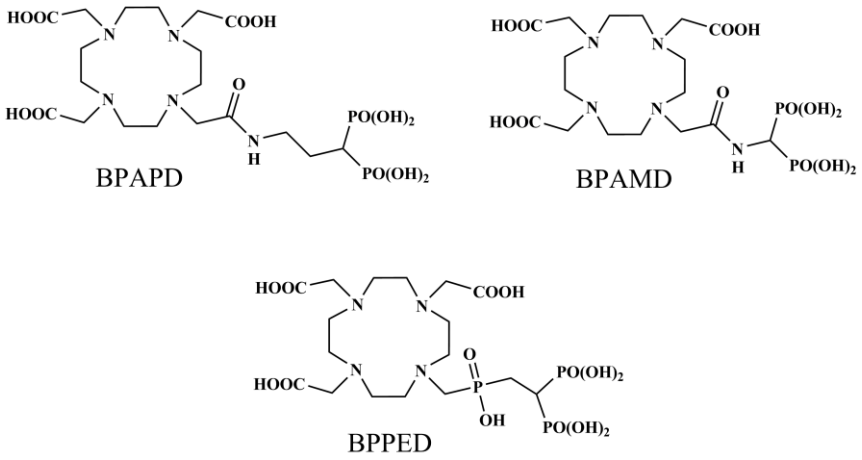

Figure. 1. Structures of the DOTA functionalised bisphosphonate derivatives.

2.3. Labeling

^{68}Ga labeling was performed in an ammonium acetate solution (2 M, 200 µL) by adding 300 µL of processed ^{68}Ga, giving a labeling pH of 3.75. The ligand (30 nmol) was added and the solution shaken in a heating block for 10 min at 100°C. After cooling, the labeled bisphosphonate was separated from un-complexed ^{68}Ga by passing the solution over a strong cation exchange resin (STRATA X-C, Phenomenex). The pH was adjusted to pH = 7 by adding small amounts of a 1 M NaOH solution. The radiochemical yield was determined by radio-TLC (solid phase: SiO_2, 60 F_{254}, Merck) using a mixture of 2 parts A (conc. HCl, acetone, water) and 1 part B (acetylacetone) as the mobile phase. The radioactivity distribution on the TLC plates was determined on a Canberra Packard Instant Imager. The reaction was also monitored via radio-HPLC (SCX-column, solvent: 1 M phosphate buffer, pH=3). The labeled bisphosphonates were obtained in radiochemical purities greater than 95%, after resin purification [11]. No-carrier-added aqueous [^{18}F]F^- was obtained from an IBA CYCLONE 18/9 cyclotron (IBA, Louvain-la-Neuve, Belgium) by irradiation of [^{18}O]H_2O via the ^{18}O(p,n)^{18}F nuclear reaction. [^{18}F]F^- was dissolved in electrolyte injection solution E-153 (Serumwerk Bernburg AG). [^{99m}Tc]$NaTcO_4$ was obtained from a commercial ^{99}Mo/^{99m}Tc-generator (Covidien) and [^{99m}Tc]MDP was produced according to the manufacturer procedure (ROTOP Pharmaka AG).

2.4. Animals, Feeding, Husbandry, and Animal Preparation

The local animal research committee at the Landesdirektion Dresden approved the animal facilities and the experiments according to institutional guidelines and the German animal welfare regulations. The experimental procedure used conforms to the *European Convention for the Protection of Vertebrate Animals used for Experimental and other Scientific Purposes (ETS No. 123)*, to the *Deutsches Tierschutzgesetz*, and to the *Guide for the Care and Use of Laboratory Animals* published by the US National Institutes of Health [DHEW Publication No. (NIH) 82-23, revised 1996, Office of Science and Health Reports, DRR/NIH, Bethesda, MD 20205]. Wistar rats (Wistar Unilever, HsdCpb:WU, Harlan Winkelmann, Borchen, Germany) were housed under standard conditions with free access to food (2016 Teklad

Global 16% Protein Rodent Diet, Harlan Laboratories, Inc., Germany) and tap water. Rats were housed (5 rats per cage) in Uni Protect airflow cabinet (Ehret GmbH Labor- und Pharmatechnik, Schönwalde, Germany) in polysulfone cages (380 x 200 x 590 mm; floor area, 1815 cm^2). The caging had a solid bottom and stainless steel wire lid, andthe cage floor was covered with chipped wood. The cages were changed weekly. Tap water was provided in polycarbonate bottles, changed twice weekly, and refilled once between the cage changes. The room temperature was 22±1°C and relative humidity was 53±6%, but the temperature was 1 to 4°C higher in the airflow cabinets. Artificial lighting was in 12 h light and dark cycles with fluorescent tubes (light color, warm white).

Surgery: Male Wistar-Unilever rats weighing 183±56g (mean ± SD, n=19) were anesthetized using desflurane. The guide value for breathing frequency was 65 breaths/min. Animals were put in the supine position and placed on a heating pad to maintain body temperature. The rats were treated with 100 units/kg heparin (Heparin-Sodium 25.000-ratiopharm, Ratiopharm, Germany) by subcutaneous injection to prevent blood clotting on intravascular catheters. After local anesthesia by injection of Lignocaine 1% (Xylocitin loc, Mibe, Jena, Germany) into the right groin, catheter was introduced into the right femoral artery (0.8 mm Umbilical Vessel Catheter, Tyco Healthcare, Tullamore, Ireland) for blood samples for metabolite analysis, for gas analysis, and arterial blood pressure measurements. A second needle (35 G) catheter in one tail vein was used for administration of the tracers.

2.5. Metabolite analysis

The metabolism of [^{68}Ga]BPAPD, [^{68}Ga]BPAMD, [^{68}Ga]BPPED *in vivo* was analyzed in arterial blood plasma samples. The radiotracer was injected intravenously into anesthetized male Wistar rats. Blood samples from the right femoral artery were taken using the catheter at various time points up to 120 min post injection (p.i.). Plasma was separated by centrifugation (3 min, 11'000 g) followed by precipitation of the plasma proteins with ice-cold methanol (1.5 parts per 1 part plasma) and centrifugation (3 min, 11'000 g). The supernatants were analyzed by TLC on cellulose (Merck KGaA, Darmstadt, Germany) with a mixture of 2 volume parts solution A) H_2O (9 mL), 12 M HCl (0.6 mL), acetone (88 mL),

and one volume part B) acetylacetone. A second TLC system was used to determine free ^{68}Ga with silica TLC-plates (Nano-Sil-20, Macherey-Nagel, Germany) with citrate buffer (0.24 M, pH 4). The metabolite fraction of the arterial blood plasma activity was calculated using the fraction of parent compound by the equation metfrac = 1 - parent fraction. The chemical nature of the radioactive metabolites was not evaluated.

2.6. Biodistribution studies

Biodistribution studies were performed in male Wistar rats. The rats were injected intravenously, each with ~ 10 MBq of the ^{68}Ga-labeled compound in 0.5 mL saline. Specific details are as follows. [^{68}Ga]BPAPD: 63±13 MBq/kg, 123±16 body-weight (BW, g), n=16; [^{68}Ga]BPAMD: 67±7 MBq/kg, 146±14 BW (g), n=16; [^{68}Ga]BPPED: 82±28 MBq/kg, 148±12 BW (g), n=16; [^{99m}Tc]MDP: 1 MBq/kg, 204±5 (g), n=6; [^{18}F]F$^-$: 7.0±0.5 MBq/kg, 183±12 BW (g), n=8. Animals were sacrificed at 5 and 60 min p.i for [^{18}F]F$^-$ and the ^{68}Ga-labeled tracers, and 5 and 120 min for [^{99m}Tc]MDP. Organs and tissues of interest were excised rapidly, weighed, and the radioactivity determined using a Wallac WIZARD automatic gamma counter (PerkinElmer, Germany). The activity of the tissue samples was decay-corrected and calibrated by comparing the counts in the tissue with the counts in aliquots of the injected tracer. Counts of the sample and calibration aliquots were measured in the gamma counter at the same time. The amount of activity in the selected tissues and organs is expressed as a percent of the injected dose per organ (% ID) or activity concentration normalized to the BW as the SUV [(activity per g tissue)/(injected activity) × BW]. Values are quoted as the mean ID % ± standard deviation (SD) of the eight rats per group. The activity associated with the skeleton was calculated using the activity concentration in the femur and the total skeleton weight, calculated using: skeleton weight = 9.66 + 0.0355 × BW [12].

2.7. Small animal PET

In vivo small animal PET imaging in male Wistar rats was carried out under general anesthesia of the rats (induced with 10% and maintained with inhalation of 6.5% desflurane in 30% oxygen/air), with a scan time of 120 min. Rats were immobilized in the supine position, with their medial axis parallel to the axial axis of the scanner (microPET® P4, Siemens Medical Solutions, Knoxville, TN, USA). In the PET experiments 0.5 mL of the tracers ([^{68}Ga]BPAPD: n=2, 341±21 MBq/kg; [^{68}Ga]BPAMD: n=3, 265±30 MBq/kg; [^{68}Ga]BPPED: n=2, 232±75 MBq/kg; [^{18}F]F^{-}: n=1, 77.8 MBq/kg) was administered via a tail vein as an infusion (0.5 mL/min) using a syringe pump (Harvard Apparatus, Holliston, MA, USA) and a needle catheter. Transmission scans and PET acquisition followed, details of which have been published elsewhere [13]. No correction for partial volume effects was applied. The image volume data were converted to Siemens ECAT7 format for further processing, and the image files processed using ROVER software (ABX GmbH, Radeberg, Germany). Masks for defining three-dimensional regions of interest were set and the regions of interest (ROI's) defined by thresholding. ROI time activity curves (TAC) were derived for the subsequent data analysis. The ROI data and TAC were further analyzed using R (R is available as Free Software under the terms of the Free Software Foundation's GNU General Public License in source code form) and specifically developed program packages [14]. SUV's (mL/g) were calculated for the ROI's using the equation: SUV = (activity/mL tissue)/ (injected activity/body weight).

2.8. Small animal SPECT

In vivo small animal SPECT imaging in a male Wistar rat was carried out under general anesthesia (induced with 10% and maintained with inhalation of 6.5% desflurane in 30% oxygen/air) with a scan time of 120 min. The rat was immobilized in the prone position with the medial axis parallel to the axial axis of the SPECT scanner (NanoSPECT, Bioscan Inc., Washington, D.C., USA).The camera was fitted with four nine-pin-hole apertures. The pinhole diameters were 2.5 mm and allow a resolution of ~ 1.6 mm in rat-sized animals. [^{99m}Tc]MDP (0.5 mL, 322 MBq/kg, n=1) was administered via a tail vein as an infusion (0.5

mL/min) using a syringe pump (Harvard Apparatus, Holliston, Ma, USA) and a needle catheter. Data was acquired in a step-and-shoot mode with the bed also stepping to include the complete rat within the field of view. An energy window was used for ^{99m}Tc with a peak at 140 keV. The SPECT acquisitions were reconstructed using InVivoScope 1.37 software (Bioscan) with a voxel size of 0.8 mm, using the ordered subsets expectation maximization iterative reconstruction algorithm with four subsets and six iterations. During reconstruction, high noise suppression was selected to produce smoother and more artifact-free images. The DICOM datasets were converted to ECAT7 format and analyzed as per the small animal PET protocol. The total counts within this volume were then converted to activity using a predetermined calibration factor. The CT acquisition was carried out in a SkyScan 1178 (SkyScan, Belgium) and was reconstructed at standard resolution.

2.9. Statistical analysis

Continuous variables were expressed as the mean ± SD. Normality was assessed using the D'Agostino-Pearson normality test. Groups were compared using the Student t test or the Mann-Whitney U test, as appropriate. All statistical tests were 2-tailed, with a P value of less than 0.05 denoting significance, the symbols represent *P<0.05, **P<0.01, ***P<0.001. All statistical analyses were performed using GraphPad Prism (V5.02 for Windows, GraphPad Software, San Diego California USA, www.graphpad.com).

3. Results

3.1. Radiolabeling

The DOTA conjugated bisphosphonates were labeled with ^{68}Ga, and isolated with high radiochemical purities of 95-98% after purification.

3.2. Biodistribution

The biodistribution data of [^{68}Ga]-DOTA-bisphosphonates, [^{18}F]F$^-$ and [^{99m}Tc]MDP studied in normal Wistar rats are presented in tables 1 and 2. All radiotracers investigated showed a high degree of association with the bone. The detailed analysis of the activity associated with the bones reveals a significantly ($P<0.001$) higher level of [^{68}Ga]BPPED, [^{18}F]F$^-$, and [^{99m}Tc]MDP accumulation compared to [^{68}Ga]BPAMD and [^{68}Ga]BPAPD. This is also evident from the estimation of the total activity in the skeleton for [^{68}Ga]BPAPD (38% ID), [^{68}Ga]BPAMD (31% ID), [^{68}Ga]BPPED (49% ID), [^{18}F]F$^-$ (44% ID), and [^{99m}Tc]MDP (41% ID) at the end of the scan. The tracers showed fast renal elimination and high clearance from the blood, which is presumably a result of their high hydrophilicity.

Table 1. Activity (% ID, mean±SD of n animals) at different ROI's of Wistar rats for [^{68}Ga]BPAMD, [^{68}Ga]BPAPD, [^{68}Ga]BPPED and [^{18}F]F$^-$. Data recorded at 5 min p.i.

	[^{68}Ga]BPAPD			[^{68}Ga]BPAMD			[^{68}Ga]BPPED			[^{18}F]Fluoride		
	5 min			5 min			5 min			5 min		
	mean	SD	n	mean	SD	n	mean	SD	n	mean	SD	n
Brain	0.10	0.04	8.00	0.07	0.01	8.00	0.05	0.01	8.00	0.05	0.05	4.00
Pancreas	0.10	0.03	8.00	0.08	0.01	8.00	0.09	0.02	8.00	0.06	0.01	4.00
Spleen	0.09	0.02	8.00	0.07	0.01	8.00	0.07	0.01	8.00	0.08	0.01	4.00
Adrenals	0.02	0.00	8.00	0.02	0.00	8.00	0.02	0.01	8.00	0.01	0.00	4.00
Kidneys	3.38	0.91	8.00	2.94	1.04	8.00	3.12	0.69	8.00	1.55	0.58	4.00
Heart	0.30	0.06	8.00	0.27	0.06	8.00	0.20	0.03	8.00	0.12	0.00	4.00
Lung	0.73	0.22	8.00	0.61	0.09	8.00	0.53	0.09	8.00	0.30	0.03	4.00
Thymus	0.16	0.04	8.00	0.12	0.02	8.00	0.15	0.04	8.00	0.17	0.02	4.00
Thyroide	0.07	0.01	8.00	0.06	0.01	8.00	0.07	0.02	8.00	0.07	0.01	4.00
Harderian glands	0.08	0.01	8.00	0.08	0.01	8.00	0.06	0.01	8.00	0.04	0.01	4.00
Liver	3.53	0.51	8.00	2.96	0.40	8.00	2.68	0.35	8.00	1.44	0.10	4.00
Femur	1.38	0.20	8.00	1.29	0.09	8.00	1.91	0.13	8.00	1.74	0.14	4.00
Testes	0.53	0.08	8.00	0.47	0.08	8.00	0.53	0.08	8.00	0.24	0.05	4.00
Intestine	2.29	0.25	8.00	1.97	0.18	8.00	2.08	0.22	8.00	1.48	0.18	4.00
Stomach	0.58	0.10	8.00	0.43	0.03	8.00	0.52	0.13	8.00	0.19	0.03	4.00
Skeleton	26.21	3.87	8.00	22.71	3.09	8.00	34.21	3.16	8.00	26.60	2.14	4.00
Urine calculated	14.91	0.94	4.00	8.98	5.90	4.00	10.40	7.53	8.00	7.87	6.78	4.00

Table 2. Activity (% ID, mean±SD of n animals) at different ROI's of Wistar rats for for [^{68}Ga]BPAMD, [^{68}Ga]BPAPD, [^{68}Ga]BPPED, [^{18}F]F$^-$ (60 min p.i.) and [^{99m}Tc]MDP (120 min p.i.).

	[^{68}Ga]BPAPD			[^{68}Ga]BPAMD			[^{68}Ga]BPPED			[^{18}F]Fluoride			[^{99m}Tc]MDP		
	60 min			60 min			60 min			60 min			120 min		
	mean	SD	n	mean	SD	n	mean	SD	n	mean	SD	n	mean	SD	n
Brain	0.05	0.02	8.00	0.04	0.01	8.00	0.03	0.02	8.00	0.01	0.00	4.00	0.01	0.02	6.00
Pancreas	0.05	0.02	8.00	0.10	0.14	8.00	0.08	0.09	8.00	0.03	0.03	4.00	0.01	0.00	6.00
Spleen	0.06	0.02	8.00	0.10	0.09	8.00	0.06	0.03	8.00	0.02	0.04	4.00	0.01	0.00	6.00
Adrenals	0.02	0.01	8.00	0.01	0.01	8.00	0.01	0.00	8.00	0.00	0.00	4.00	0.00	0.00	6.00
Kidneys	0.58	0.08	8.00	0.58	0.03	8.00	0.56	0.34	8.00	0.09	0.01	4.00	0.60	0.03	6.00
Heart	0.14	0.06	8.00	0.12	0.01	8.00	0.07	0.01	8.00	0.01	0.00	4.00	0.01	0.00	6.00
Lung	0.32	0.08	8.00	0.25	0.05	8.00	0.17	0.03	8.00	0.03	0.01	4.00	0.06	0.02	6.00
Thymus	0.11	0.03	8.00	0.08	0.02	8.00	0.05	0.01	8.00	0.02	0.01	4.00	0.01	0.00	6.00
Thyroide	0.04	0.01	8.00	0.03	0.01	8.00	0.03	0.01	8.00	0.04	0.02	4.00	0.02	0.01	6.00
Harderian glands	0.08	0.03	8.00	0.06	0.02	8.00	0.05	0.01	8.00	0.01	0.00	4.00	0.01	0.01	6.00
Liver	1.95	0.45	8.00	2.00	0.37	8.00	1.10	0.23	8.00	0.09	0.02	4.00	0.26	0.03	6.00
Femur	2.09	0.15	8.00	1.68	0.16	8.00	2.58	0.33	8.00	2.71	0.09	4.00	2.36	0.17	6.00
Testes	0.33	0.10	8.00	0.33	0.09	8.00	0.17	0.02	8.00	0.05	0.00	4.00	0.03	0.00	6.00
Intestine	1.93	0.37	6.00	1.76	0.62	8.00	2.56	1.78	8.00	1.13	0.18	4.00	6.57	2.87	6.00
Stomach	1.79	2.61	8.00	0.30	0.14	8.00	2.94	5.85	8.00	0.15	0.20	4.00	1.55	1.61	6.00
Skeleton	38.31	5.01	8.00	30.90	4.14	8.00	48.90	4.82	8.00	43.70	1.93	4.00	41.22	5.61	6.00
Urine calculated	25.93	7.34	8.00	42.20	5.11	8.00	31.90	9.84	8.00	24.30	2.83	4.00	38.10	4.11	6.00

PET Scans were conducted over 60 min p.i. for the [^{68}Ga]-DOTA-bisphosphonates and [^{18}F]F^{-}, and 120 min p.i. for [^{99m}Tc]MDP. The bone to blood ratios determined at the end of the scan were [^{68}Ga]BPAMD 3.4; [^{68}Ga]BPAPD 3.7; [^{68}Ga]BPPED 9.9; [^{18}F]F^{-} 103; [^{99m}Tc]MDP 52.3. The measured urine activity was 26% ID for [^{68}Ga]BPAPD, 42% ID for [^{68}Ga]BPAMD, 49% ID for [^{68}Ga]BPPED, 44% ID for [^{18}F]fluoride, and 41% ID for [^{99m}Tc]MDP at the end of the respective scans. The summed activity in the skeleton and urine was 64% ID for [^{68}Ga]BPAPD, 73% ID for [^{68}Ga]BPAMD, 81% ID for [^{68}Ga]BPPED, 68% ID for [^{18}F]F^{-}, and MDP 79% ID for [^{99m}Tc]. In all cases the activity concentration in the other tissues and organs was very low, and there was no visible activity accumulation observed in the brain or liver

Table 3. Bone to blood ratios and the combined activity associated with the urine and skeleton (% ID, mean±SD of n animals) for [^{68}Ga]BPAMD, [^{68}Ga]BPAPD, [^{68}Ga]BPPED, [^{18}F]F^{-} (at 60 min p.i.) and [^{99m}Tc]MDP (at 120 min p.i.).

compound	bone/blood			sum urine + skeleton (% ID)		
	mean	SD	n	mean	SD	n
[^{68}Ga]BPAMD (60 min)	3.42	0.54	8	64.2	12.4	8
[^{68}Ga]BPAPD (60 min)	3.73	0.68	8	73.1	9.3	8
[^{68}Ga]BPPED (60 min)	9.87	1.24	8	80.9	14.7	8
[^{18}F]F^{-} (60 min)	103.0	9.00	4	68.2	4.8	4
[^{99m}Tc]MDP (120 min)	52.3	15.6	15	79.4	9.7	6

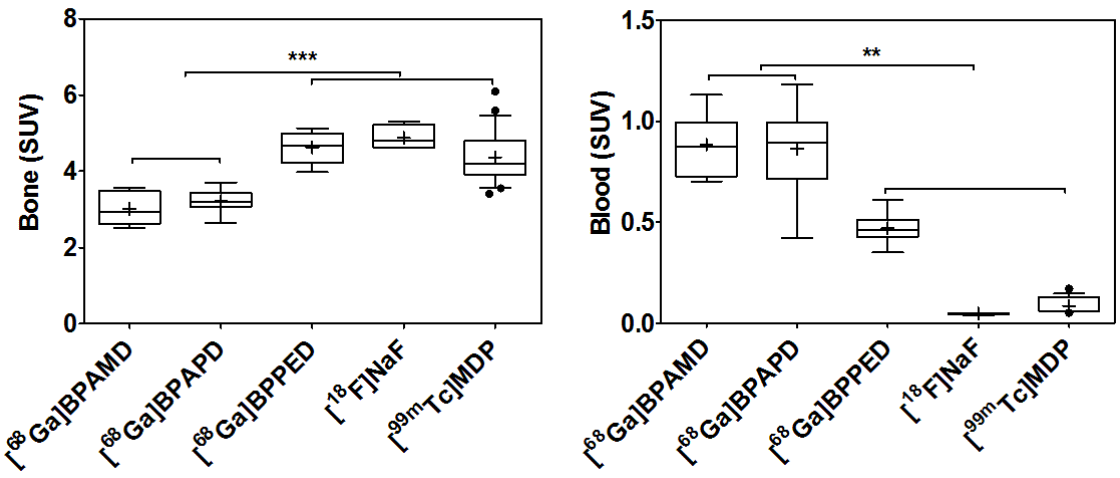

Figure. 2. Comparison of [^{68}Ga]BPAMD, [^{68}Ga]BPAPD, [^{68}Ga]BPPED [^{18}F]NaF and [^{99m}Tc]MDP. The graph on the left represents the SUV of the bone at 60 min p.i., and the right hand side graph represents the SUV of the blood at 60 min p.i.

3.3. Small animal PET

The *in vivo* PET data are summarized in figure 3. [^{68}Ga]BPAMD, [^{68}Ga]BPAPD and [^{68}Ga]BPPED were accumulated fast in the skeleton, reaching a plateau after one hour. The distribution half-lives of the radiotracers in the circulation were between one and two min, which correlates to the blood circulation time in rats. The half-lives of the slow components were 13 min for [^{68}Ga]BPAMD, 19 min for [^{68}Ga]BPAPD and 12 min for [^{68}Ga]BPPED. The measured target to background ratios were equal to the established standards in bone imaging set by [^{18}F]F$^-$ and [^{99m}Tc]MDP (figure 4). Figure 5 shows the distribution kinetics of [^{18}F]F$^-$, [^{68}Ga]BPAMD, [^{68}Ga]BPAPD, and [^{68}Ga]BPPED in the heart, kidney, spine and blood (vein). The curves are similar for all compounds. Variations in the curve profiles of the kidney time activity curves seems to be a result of the differing responses of individual rats to anesthesia, and resulting differences in the urine flow between rats.

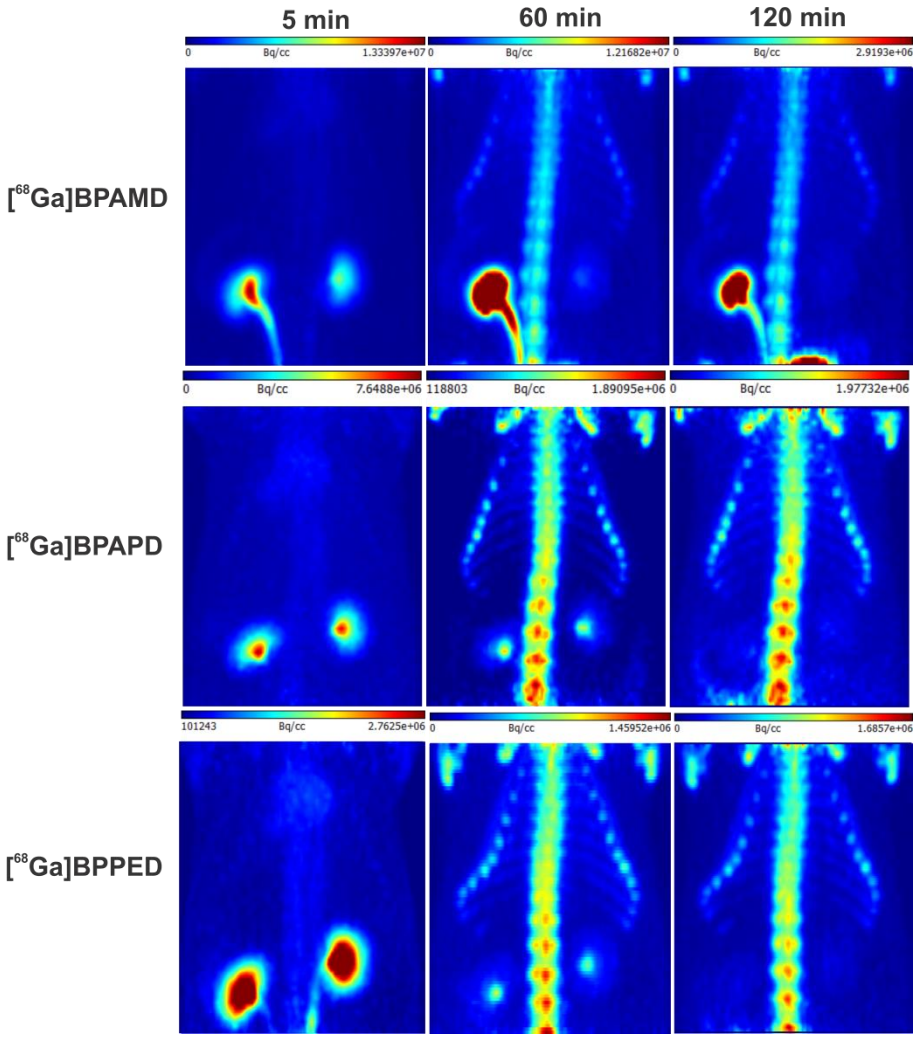

Figure 3. MIP (maximum intensity projection) in the thorax region for [^{68}Ga]BPAMD, [^{68}Ga]BPAPD and [^{68}Ga]BPPED at 5 min, 60 min and 120 min p.i.

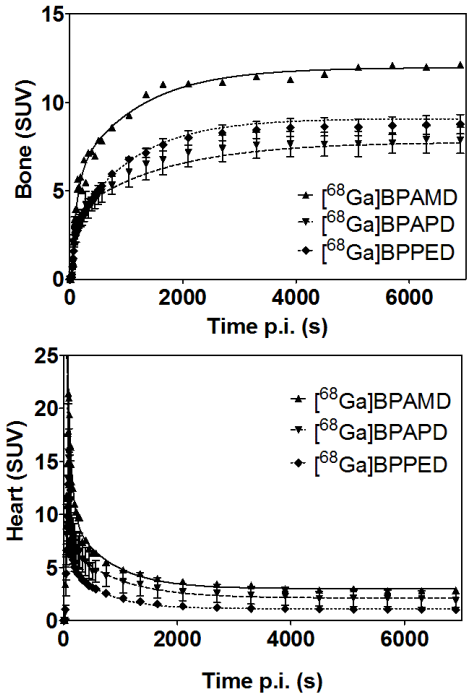

Figure 4. Accumulation of the DOTA functionalised bisphosphonates in the spine (upper) of the rats and clearance from the blood (lower, ROI: over the heart).

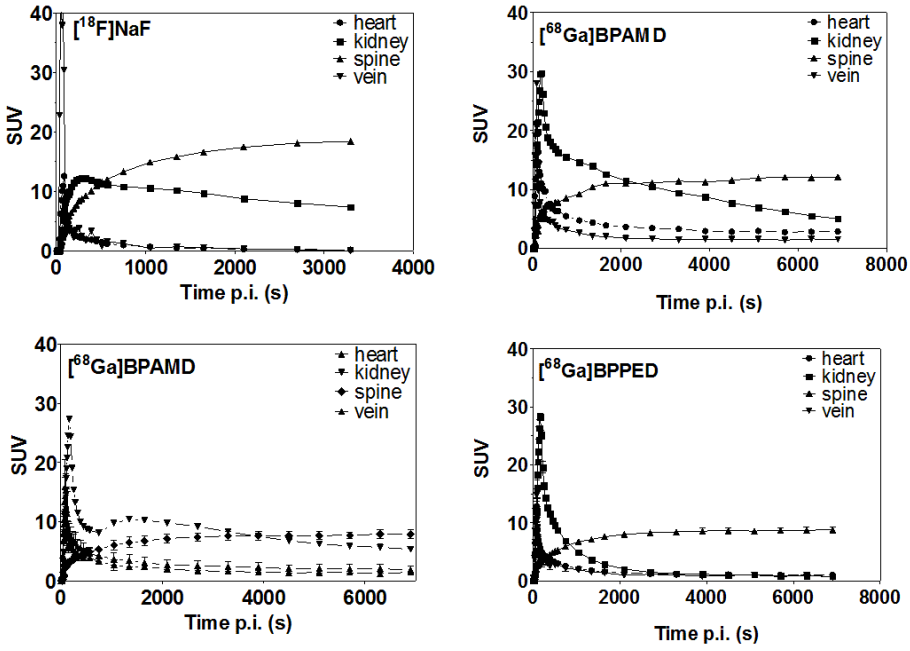

Figure 5. Time activity curves of ^{68}Ga]BPAMD, [^{68}Ga]BPAPD, [^{68}Ga]BPPED and [^{18}F]F^{-} in the heart, kidneys, spine and blood stream.

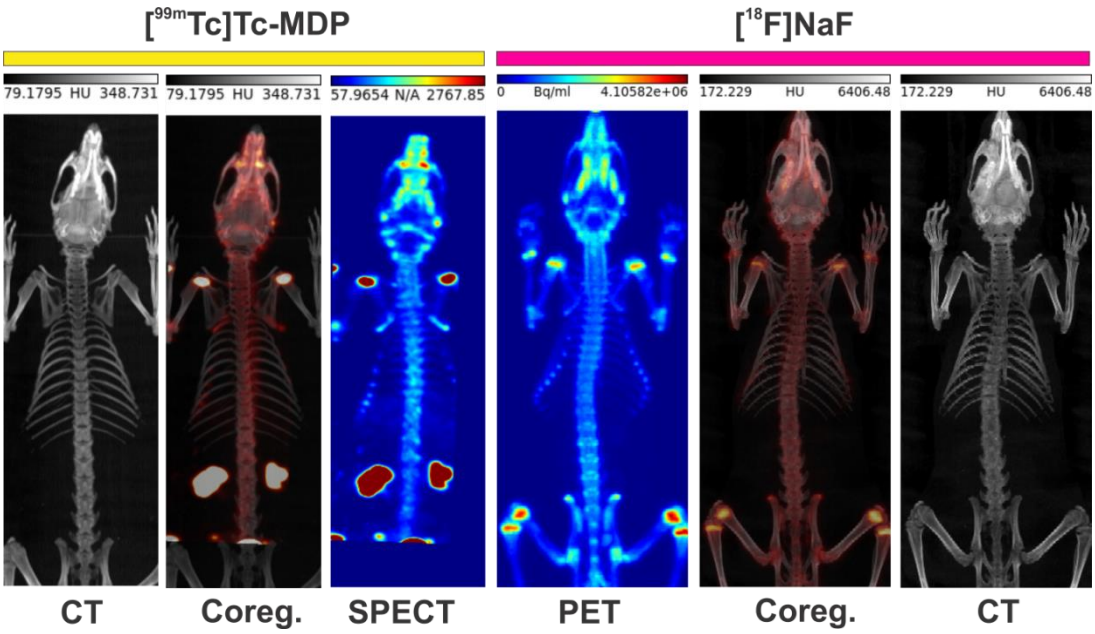

Figure 6. µPET ([^{18}F]F^{-}, MIP, 60 min p.i.), CT (MIP) and SPECT ([^{99m}Tc]MDP, MIP, 120 min p.i.) scans recorded of Wistar rats.

3.4. Metabolite analysis

The metabolism of [^{68}Ga]BPAMD, [^{68}Ga]BPAPD, and [^{68}Ga]BPPED was investigated in arterial blood plasma over one hour. The results are presented in figure 7. All three compounds showed similar degrees of decomposition over time. The half-lives of the parent compounds in the arterial blood plasma were 14.4 min (9.3 to 31.7 min) for [^{68}Ga]BPAMD, 10.2 min (7.4 to 16.5 min) for [^{68}Ga]BPAPD and 20.8 min for (18.1 to 24.4 min) [^{68}Ga]BPPED. At 60 min p.i. only about 10% of the plasma activity belonged to the parent compound. This did not have any effect on the blood cell and proteins binding in the arterial blood, where over the observed time about 4 to 7% were bound to these blood components.

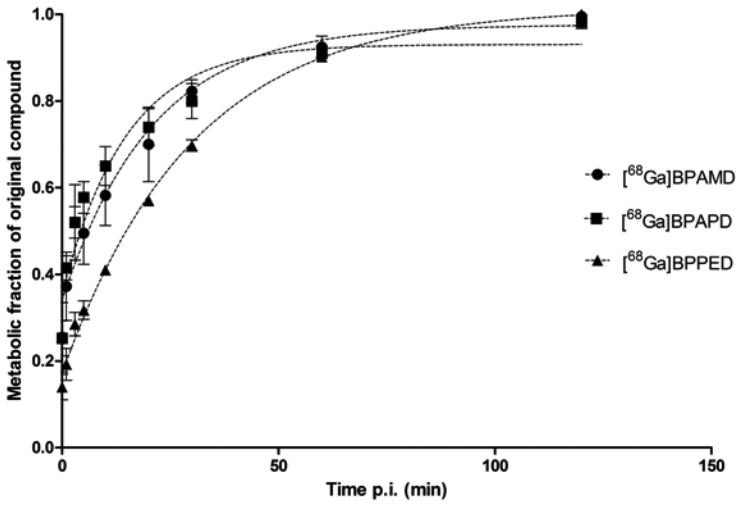

Figure 7. Metabolic fractions of [^{68}Ga]BPAMD, [^{68}Ga]BPAPD and [^{68}Ga]BPPED analysed in arterial blood plasma at 1, 3, 5, 10, 30, 60 and 120 min p.i.

4. Discussion

The three DOTA based bisphosphonates BPAMD, BPAPD and BPPED have been radiolabeled with ^{68}Ga to give tracers of high radiochemical purity. Each of these tracers showed fast and high binding to the surface of healthy bones. [^{68}Ga]BPPED was the most promising DOTA-based derivative with bone accumulation equal to [^{18}F]F^{-} and [^{99m}Tc]MDP, and significantly higher than that of [^{68}Ga]BPAMD and [^{68}Ga]BPAPD. The blood clearance and renal elimination was fast for all compounds investigated. Approximately 90% of the radiolabeled DOTA-bisphosphonates not associated with bone tissue were metabolized within one hour, and eliminated rapidly via the kidneys. These metabolic characteristics produced a very low background from the other organs and tissues. The radiolabeled compounds were not observed in the brain.

The phosphinate conjugated bisphosphonate, [^{68}Ga]BPPED (2.58% ID/g), showed a 20% to 50% higher accumulation in bone than the two amide compounds [^{68}Ga]BPAMD (2.09% ID/g) and [^{68}Ga]BPAPD (1.68% ID/g). Furthermore, [^{68}Ga]BPPED also showed faster clearance from the blood via the renal system. The main structural difference between

BPPED and the other DOTA-bisphosphonates is the presence of a phosphinate group, and it is likely that the different pharmacokinetics observed can be attributed to this feature. It is possible that the presence of the phosphinate provides an additional binding site to hydroxyapatite surfaces, which leads to a higher bone uptake. Furthermore, the acidic phosphinate could be deprotonated and, given its anionic nature, may become involved in ^{68}Ga binding. Regardless of whether the phosphinate oxygen ligates the metal or not, the complex is expected to be more polar (if not have an additional anionic charge) than the other two DOTA-bisphosphonates. This greater polarity may account for the enhanced renal clearance of [^{68}Ga]BPPED.

There was no significant difference in the bone accumulation and blood clearance of labeled BPAMD and BPAPD. Given that these structures only differ in the length of the spacer between the bisphosphonate and DOTA moiety, it is apparent that this has no influence on the pharmacokinetics and bone accumulation of the tracer.

In terms of the ligating moiety, the DOTA-bisphosphonates could be described as hybrids of DOTA and DO3A, both of which have been shown to be effective ligands for the complexation of lanthanide ions [15]. In this respect, these DOTA-bisphosphonates are promising candidates as ^{177}Lu carriers for endoradiotherapy of bone metastases. DOTA-bisphosphonates could potentially be used as theranostic tools for the imaging and treatment of bone metastases [15]. This feature enhances the relevance of DOTA-bisphosphonates and gives them a considerable advantage over both [^{18}F]F$^-$ and [^{99m}Tc]MDP .

In view of a potential application of ^{177}Lu-DOTA-bisphosphonates in therapy, the most important parameters are fast and high binding to the skeleton, combined with a fast blood clearance and non-target tissues (including the kidneys). All of the studied compounds share these parameters, however the best bone uptake and target to background ratio was achieved with [^{68}Ga]BPPED.

^{177}Lu would be ideally suited for the treatment of bone metastases, due to its excellent nuclide parameters: the short β^- range of max. 2 mm does not harm the radiosensitive non-target bone marrow, the non-carrier added production route leads to very high specific activities, and the macrocyclic Lu-DOTA complex is characterized by a high kinetic and

thermodynamic stability. Labeling studies and biodistribution experiments with ^{177}Lu DOTA based bisphosphonates in an animal tumor model will be realized soon.

In summary, all of the studied DOTA-bisphosphonates (BPAMD, BPAPD and BPPED) appear to be potentially useful compounds for radiolabeling and application in the diagnosis and therapy of bone metastases. Further investigations should involve similar evaluations in tumor models, to ascertain the affinity of these DOTA-bisphosphonates for bone metastases.

5. Acknowledgment

We thank Prof. Steinbach for the realization of the animal studies at the Helmholtz-Zentrum Dresden-Rossendorf. We are grateful to Andrea Suhr for developing the metabolite analysis and radiolabeling and to Regina Herrlich for animal handling and biodistribution. We thank Stephan Preusche and Frank Fuechtner for the [^{18}F]fluoride production (all Helmholz-Zentrum Dresden-Rossendorf). Support from Long-Term Research Plan of the Ministry of Education of the Czech Republic (No. MSM0021620857) is acknowledged.

6. References

[1] Greenlee RT, Hill-Harmon MB, Murray T, Thun M. Cancer Statistics 2001 CA. *Cancer J. Clin.* **2001**; 51: 15–36.

[2] Rubens RD. Bone metastases The clinical problem. Eur J Cancer 1998;34:210–3.

[3] Zettinig G, Dudczak R, Leitha T. Nuklearmedizinische Diagnostik der Osteomyelitis. *J. Mineralstoffw.* **2003**; 10: 20–3.

[4] Harmer CL, Burns JE, Sams A, Spittle M. The value of fluorine-18 for scanning bone tumours. *Clin. Radiol.* **1969**; 20: 204–12.

[5] Papapoulos SE. Bisphosphonates: how do they work? *Best. Pract. Res. Cl.* **2008**; 22: 831–47.

[6] Kubíček V, Rudovský J, Kotek J, Hermann P, Vander Elst L, Muller RN, Kolar ZI, Wolterbeek HT, Peters JA, Lukeš I. A Bisphosphonate Monoamide Analogue of DOTA: A Potential Agent for Bone Targeting. *J. Am Chem. Soc.* **2005**; 127: 16477–85.

[7] Fellner M, Baum R, Kubíček V, Hermann P, Lukeš I, Prasad V, Rösch F. PET/CT imaging of osteoblastic bone metastases with ^{68}Ga-bisphosphonates: first human study. *Nucl. Med. Mol. Imag.* **2010**; 37: 834.

[8] Vitha T, Kubíček V, Hermann P, Kolar Z I, Wolterbeek H Th, Peters J A, Lukes I, Complexes of DOTA-Bisphosphonate Conjugates: Probes for Determination of Adsorption Capacity and Affinity Constants of Hydroxyapatite. *Langmuir*, **2008**; 24: 1952-1958.

[9] Zhernosekov KP, Filosofov DV, Baum RP, Aschoff P, Bihl H, Razbash AA, Jahn M, Jennewein M, Rösch F. Processing of generator-produced ^{68}Ga for medicalapplication. *J. Nucl. Med.* **2007**; 48: 1741–8.

[10] Asti M, Pietri G de, Fraternali A, Grassi E, Sghedoni R, Fioroni F, Roesch F, Versari A, Salvo D. Validation of ^{68}Ge/^{68}Ga generator processing by chemical purification for routine clinical application of ^{68}Ga-DOTATOC. *Nuc. Med. Biol.* **2008**; 35: 721–4.

[11] Fellner M, Baum R, Kubicek V, Hermann P, Prasad V, Roesch F, Macrocyclic ^{68}Ga-bisphosphonates for imaging bone diseases. *J. Nucl. Med.* **2010**; 51: 563.

[12] Sontag W. Long-term Behavior of ^{239}Pu, ^{241}Am and ^{233}U in Different Bones of One-year-old Rats: Macrodistribution and Macrodosimetry. *Human Toxicol.* **1984**, 3: 469-483.

[13] Chollet C., Bergmann R., Pietzsch J., Beck-Sickinger AG. Design, Evaluation and Comparison of Ghrelin Receptor Agonists and Inverse Agonists as Suitable Radiotracers for PET Imaging. *Bioconj. Chem.* **2012**; 23: 771−784.

[14] van den Hoff J, Helmholtz-Zentrum Dresden-Rossendorf, Dresden, Germany.

[15] Vitha T, Kubíček V, Hermann P, Elst LV, Muller RN, Kolar ZI, Wolterbeek HT, Breeman WAP, Lukeš I, Peters JA. Lanthanide(III) complexes of bis(phosphonate) monoamide analogues of DOTA: Bone-seeking agents for imaging and therapy. *J. Med. Chem.* **2008**; 51: 677–83.

3.2. Development of a [^{177}Lu]BPAMD labeling Kit and an automated synthesis module for routine bone targeted endoradiotherapy

Development of a [^{177}Lu]BPAMD labeling Kit and an automated synthesis module for routine bone targeted endoradiotherapy

Marian Meckel[1], Alexander Nauth[1], Jan Timpe[1], Konstantin Zhernosekov[2], Ameya D. Puranik[3], Richard P. Baum[3] and Frank Rösch[1*]

[1]*Institute of Nuclear Chemistry, Johannes-Gutenberg-University, Mainz, Germany*

[2]*ITM Isotopen Technologien München AG, Garching, Germany*

[3]*THERANOSTICS Center for Molecular Radiotherapy and Molecular Imaging (PET/CT) ENETS Center of Excellence, Zentralklinik Bad Berka, Germany*

Abstract

Painful bone lesions, both benign and metastatic are often managed using conventional analgesics. However, the treatment response is not immediate, and is often associated with side-effects. Radionuclide therapy is used for pain palliation in bone metastases as well as some benign neoplasms. ´Endoradiotherapy´ has direct impact on the pain producing bone elements, hence, response is significant, with minimal or no side effects.

A new potential compound for endoradiotherapy is [^{177}Lu]BPAMD. It combines a highly affine bisphosphonate, covalently bridged with DOTA through an amide bond, with the low-energy β- emitting therapeutic radiolanthanide ^{177}Lu. For routine chemical application, an automated synthesis of this radiopharmecutical and a Kit type labeling procedure appears to be a basic requirement for its GMP based production. A Kit formulation combining BPAMD, acetate buffer and ethanol resulted in almost quantitative labeling yields. The use of ethanol and ascorbic acid as quenchers prevent radiolysis over 48 h. An automated synthesis unit was designed for the production of therapeutic doses of [^{177}Lu]BPAMD up to 5 GBq. The procedure was successfully applied for patient treatments.

1. Introduction

Management of metastatic bone pain is often a multi-disciplinary concept where nuclear medicine can significantly contribut by applying therapeutic β^- particle emitting radiopharmaceuticals. However, associated side-effects and absence of imaging surrogates of some of these tracers-are challenging. There has been an increasing research in this area for producing an `ideal´ tracer, which could relieve ´pain` symptoms, with minimal toxicity, and provide good physical characteristics for assessing biodistribution. There are several bone targeting radiopharmaceuticals commercially available applying β^- emitting radionuclides, like [^{153}Sm]EDTMP, [^{186}Re]HEDP and $^{89}SrCl_2$ [1]. More recently, the α-particle emitting $^{223}RaCl_2$ was approved in Europe and by the FDA [2].

While EDTMP and HEDP represent non-macrocyclic phosphonate ligands, a new macrocyclic diphosphonate (4-{[(bis(phosphonomethyl))carbamoyl]methyl}-7,10-bis(carboxymethyl)-1,4,7,10-tetraazacyclododec-1-yl)acetic acid (BPAMD**,** Figure 1), showed promising results in the detection of skeletal-related events (SREs) in first human studies, when labeled with the generator derived PET nuclide ^{68}Ga [3]. This compound can further be used as an endoradiotherapeutic agent (Figure 2) by a stable complexation with the beta emitter ^{177}Lu ($t_{1/2}$ = 6.7 d, $E_{\beta max}$ = 0.5 MeV) [4]. The physical characteristics of ^{177}Lu (long half-life and low β-range) are very suitable for the treatment of discriminated bone metastases. Low ranges of the particles emitted are essential for avoiding side effects, like haematotoxicity as induced by irradiation of the red bone marrow. Current production routs of ^{177}Lu by the ^{176}Yb pathway exclude the waste-problematic metastable ^{177m}Lu ($t_{1/2}$ = 160.4 d) and carrier additions [5].

$$^{176}\text{Yb}(n,\gamma)^{177}\text{Yb} \xrightarrow{\beta} {}^{177}\text{Lu}$$

Using [^{68}Ga]BPAMD PET/CT for pre- and post-therapeutic molecular imaging when using [^{177}Lu]BPAMD for ERT, offers a system [*Me]BPAMD which reflects truly a theranostic (see Figure 1 and 2) option [6].

Since bone pain palliation was reported for [^{177}Lu]EDTMP complexes in a phase II study [7]. Therefore, [^{177}Lu]BPAMD is considered a very promising next generation compound for bone targeted endoradiotherapy (ERT). However, for future clinical trials, a Kit type labeling synthesis and an automated labeling module needs to be developed, resulting in high radiochemical yields and suitable for routine preparation. To design the Kit formulation in a way that prevents any upcoming radiolysis in therapeutic dose ranges over a reasonable time scale is also a challenge.

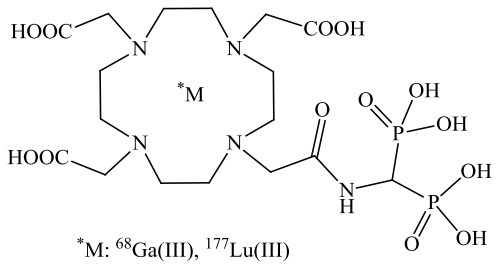

Figure 1. Structure of the macrocyclic bisphosphonate ligand BPAMD and its use as theranostic when labelled with ^{68}Ga (PET/CT) or ^{177}Lu (ERT).

We investigated different Kit compositions varying the ligand concentration, buffer and scavenger amount for labeling with no carrier added (n.c.a.) $^{177}LuCl_3$ with activities up to 5 GBq. Labeling efficiency, [^{177}Lu]BPAMD complex stability, and radiolysis of the different batches were compared.

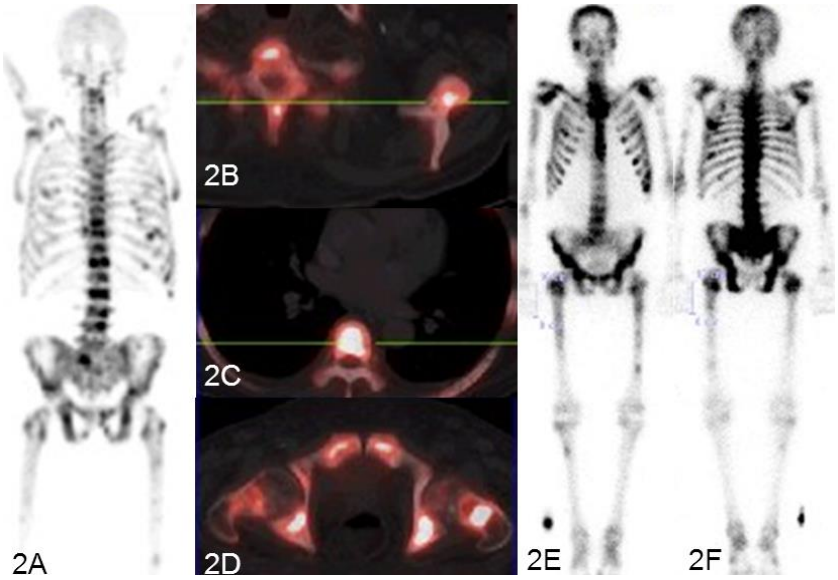

Figure 2. 70-year old male, case of prostate cancer, with rising PSA levels underwent ^{18}F-Fluoride PET/CT. Coronal MIP image (A) showing intense tracer uptake in multiple bones in axial and appendicular skeleton and axial fused PET/CT (B-D) images showing hypermetabolic metastatic lesions in scapula (B), vertebrae (C) and pelvis (D). Patient was treated with 5358 MBq [^{177}Lu]BPAMD. Post therapy images (Ant-E, Post-F) showing intense localization of tracer in the entire skeleton, in concordance with the pre-therapy ^{18}F-Fluoride PET/CT study (A).

2. Materials and methods

2.1. Chemicals

(4-{[(bis(phosphonomethyl))carbamoyl]methyl}-7,10-bis(carboxymethyl)-1,4,7,10-tetraazacyclododec-1-yl) acetic acid (BPAMD) was purchased from ABX (Radeberg, Germany). N.c.a. $^{177}LuCl_3$ in 0.05 M HCl was provided by ITG (Garching, Germany) in a volume of 500 µL containing activities between 3 to 5 GBq. Sodium acetate, sodium ascorbate and ascorbic acid are commercially available by Sigma-Aldrich (Germany) in BioXtra® (≥99.0%) or ReagentPlus® (≥99.0%) grade, as well as ethanol (CHROMASOLV®), water (*Trace*SELECT®) and citrate.

2.2. Kit formulation

The ligand BPAMD as well as sodium acetate, sodium ascorbate and ascorbic acid were dissolved in water with a concentration of 1 mg/mL. Six different concentrations of BPAMD and additives were mixed in a micro reaction vial and lyophilized (Kit #1-6, table 1). Additionally another vial containing 2.5 mg gentisinic acid, without any ascorbate was prepared (Kit #7). Prior the essential labeling process the single Kits were dissolved in water (1 mL per 1 GBq ^{177}Lu) with exceptions for the Kits #4 and #5, which were dissolved in water containing 10% EtOH. Kit #7 was prepared with the lowest amount of 40 µg BPAMD still suitable for an efficient ^{177}Lu labeling. Instead of sodium ascorbate 2.5 mg of gentisinic acid, which is reported as a potent scavenger, was used [8].

Table 1. Compositions of different Kit formulations for [^{177}Lu]BPAMD preparation in 5 mL aqueous solution.

Kit	BPAMD (µg)	NaOAc (mg)	NaOAsc (mg)	HOAsc (mg)	gentisinic acid (mg)	EtOH (%)
#1	100	16	100	-	-	-
#2	250	16	100	-	-	-
#3	100	16	500	-	-	-
#4	100	16	100	-	-	10
#5	250	16	100	-	-	10
#6	100	-	400	100	-	-
#7	40	16	-	-	2.5	-

2.3. Automated synthesis module

Single modular parts of an automated synthesis module of the company Eckert&Ziegler (Berlin, Germany) were combined to form a new device specially designed for the preparation of [^{177}Lu]BPAMD. This unit is a one reactor system that works with over pressure. The control platform of this synthesis unit is shown in figure 3. Here shown is that the unit contains of one Peltier Reaction Modul (**R1**), nine velves (two Stopcock Manifold Modules and one PharmTracer Module, **V1-V9**), six vials (**G1-G6**) and one optional SPE

(solid phase extraction) cartridge (**T1**). The whole system is controlled by the "electrical cabinet" and the program "Modular-Lab" (EZAG, Germany). The reactor has a temperature area from -15 °C up to 150 °C and is cooled with an external heat exchanger. Glass vials (micro reaction vials) common for modular radiosynthesis were purchased from Sigma-Aldrich (Germany). The dissolved BPAMD kit is placed in vial **G1**. Vial **G2** is reserved for the $^{177}LuCl_3$ solution, while **G3** is the product vial and **G4** is the waste vial. The vials **G5** and **G6** are needed for the optional purification step *via* SPE (solid phase extraction). Here **G5** contains pure water as a washing solution and **G6** the eluent solution. The unit is constructed for GMP based synthesis, therefor the reactor, valves and tubes are disposable and can be replaced. Also this unit can be run with pure Helium or Argon instead of a pump. If the synthesis must not be GMP based, it is possible to run a cleaning program and reuse all the disposable parts. It is also possible to run a purification step after the initial labeling reaction. If the purification step is activated the product is trapped on a SPE cartridge (**T1**), washed with 5 mL water in **G5** and eluted into **G3** with the eluent solution in **G6**. In this case the whole reaction takes place in 50 min.

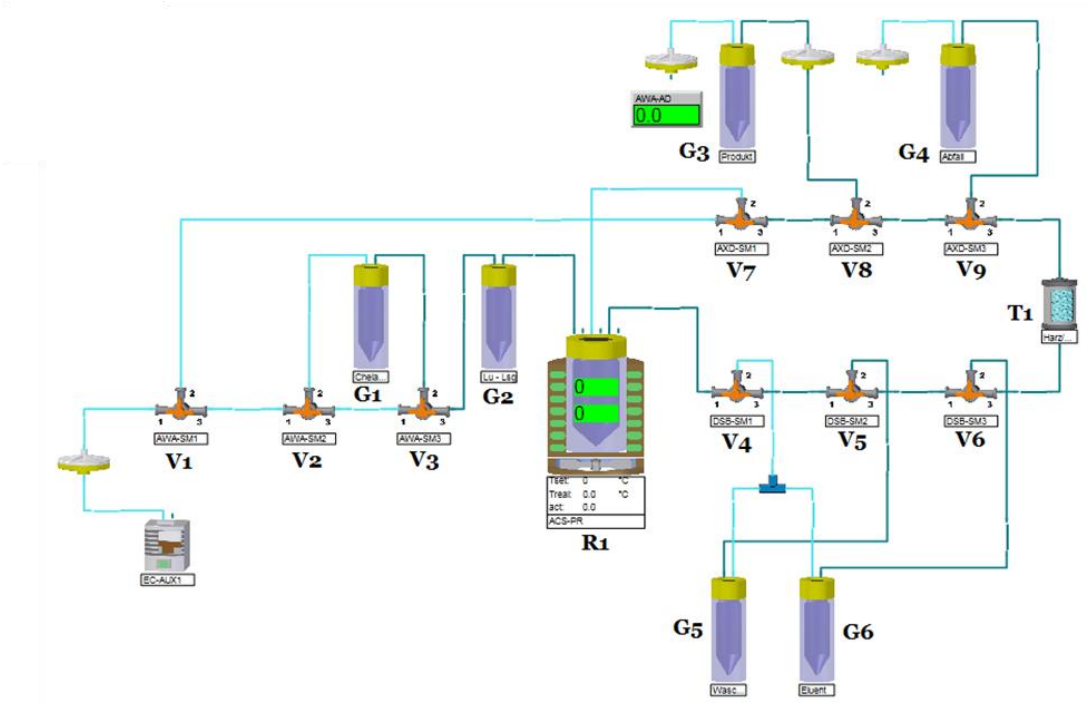

Figure 3. Schematic overview of the module composition out of EZAG-modular compartments. The sketch is shown as presented in the control platform of the synthesis unit in the program: Modular-Lab.

2.4. Automated radiolabeling

Labeling of BPAMD was performed with 3-5 GBq $^{177}LuCl_3$. For this purpose the single Kits, listed in table 1, were dissolved in water or water + 10 % EtOH to a final concentration of 1 mL per 1 GBq ^{177}Lu and placed in the automated synthesis module as well as the $^{177}LuCl_3$ containing vessel (**G2**). The $^{177}LuCl_3$ solution (500 µL in 0.05 M HCl) was transferred by over pressure to the Peltier Reaction Modul (**R1**) followed by the Kit solutions from vial **G1**. The reaction mixture is heated under stirring at 100°C for 30 min. After cooling the whole system, the solution is transferred to the product vial (**G3**). The whole reaction takes place in 36 min. Because of the evaluation of the different Kit formulations in terms of labeling efficiency and complex stability the purification step was always skipped. Radiochemical yields (RCYs) and stability were determined by thin layer chromatography (TLC) (Merck Silica, solvent: 0.1 M sodium citrate pH 4) at the time points 0 h, 1 h , 2 h, 4 h, 24 h, and 48 h after labeling.

2.5. Automated radiolabeling

The stability of the best performing Kits from the above mentioned experiments were further tested, by mixing the product in a 1:8 ratio with human serum and were incubated at 37°C over a period of 48 h. Radio-TLC analysis were done at time points of 0 h, 1 h, 2 h, 4 h, 24 h, and 48 h similar to the radiolysis experiment.

2.6. Serum stability test

The stability of the best performing Kits from the above mentioned experiments were further evaluated regarding the long-term stability of [^{177}Lu]BPAMD. The reaction products were mixed in a 1:8 ratio with human serum and were incubated at 37°C over a period of 48 h. Radio-TLC analysis were done at time points of 0 h, 1 h, 2 h, 4 h, 24 h, and 48 h similar to the radiolysis experiment.

3. Results

The lyophilized Kits presented the content as a white powder and were easily soluble in 3-5 mL water within a minute. Additives of 10%Vol ethanol showed to have no influence on the solubility and were thus added as an additional scavenger. Labeling with n.c.a. ^{177}Lu was almost quantitative (RCY $\geq$ 98 %) within 30 min reaction time for the Kit formulations #2, #5, #6 and #7 (Table 2). The Kit formulations #1 and #4 showed a somewhat less RCY of 97.0 % for Kit #1 and 96.9 % for Kit #4, respectively. Lowest yields of 68.5 % were obtained for Kit #3. The total process time for the preparation of [^{177}Lu]BPAMD in batches up to 5 GBq could be achieved in 36 min and without any need for purification.

Table 2. Synthesis yield and radiolytic stability as percentage of intact [^{177}Lu]BPAMD complexes.

Kit	0 h	1 h	2 h	4 h	24 h	48 h
#1	97.0	96.0	95.0	91.0	86.0	68.0
#2	98.3	98.3	98.3	97.7	97.7	97.7
#3	68.5	92.1	82.2	93.5	89.7	91.7
#4	96.9	98.6	98.5	98.0	93.5	90.2
#5	99.2 (0.1)	99.2	99.0	99.0	98.9 (0.1)	98.8 (0.2)
#6	99.6 (0.6)	99.0	99.0	99.0	99.4 (0.6)	99.3 (0.7)
#7	98.8	98.5	96.4	94.3	77.5	39.0

(S.D.) standard deviation out of a triplicate

While Kit #1 and #7 showed a continuous degradation of the complex with a resulting value of 68.0% and 39.0%, Kit #3 and #4 showed a good but not sufficient stability of 91.7% and 90.2% after 48 h. Optimum complex stability of > 98% was observed for Kit #5 and Kit #6, followed by the Kit composition #2 with 97.7% of intact [^{177}Lu]BPAMD after 48 h, cf. table 2. In table 3 the results from the serum stability test of the [^{177}Lu]BPAMD Ki #6 are listed. No degradation of the [^{177}Lu]BPAMD complex, prepared with Kit #6 was observed in human serum over a period of 48 h.

Table 3. Serum stability of [^{177}Lu]BPAMD prepared with Kit #6. Data are presented as mean percentage of intact complex out of a triplicate.

Kit	0 h	1 h	2 h	4 h	24 h	48 h
#6	99.4 (0.1)	99.2 (0.0)	99.1 (0.1)	99.2 (0.1)	99.0 (0.0)	99.0 (0.1)

(S.D.) standard deviation

4. Discussion

The automated synthesis device was proved to be useful to perform [^{177}Lu]BPAMD preparations up to 5 GBq. Different Kit compositions were tested in terms of RCY and radiolytic stability under GMP like conditions.

a) Amount of BPAMD: In Kit #1 and Kit #2 the amount of precursor was increased from 100 µg to 250 µg BPAMD, whereas the concentration of the ascorbate scavenger was kept constant. Only marginal changes in the RCY were observed, but with slightly better results for Kit #2 with 250 µg BPAMD. Radiolytic stability increased significantly with higher amounts of ligand from 68.0 % for Kit #1 to 97.7 % for Kit #2.

b) Amount of scavenger: Kit #3 differed from Kit #1 in the amount of ascorbate scavenger, while the ligand concentration was kept constant. The increased sodium ascorbate amount of 500 mg resulted in an unsteady labeling yield based on reaction pH of > 6. Nevertheless an increasing stability concerning radiolysis could be observed for higher scavenger amounts resulting in 91.7 % intact [^{177}Lu]BPAMD for Kit #3 compared to 68.0 % for Kit #1 after 48 h.

c) Effect of ethanol: The formulation was kept constant for the Kits #1 and #4, but instead of dissolving the batch in pure water a mixture of water containing 10 %Vol EtOH was used for Kit #4. The ethanol did not influence the solubility of the ingredients, but rather it functioned as an additional radical scavenger. Labeling yields were similar and indeed a higher stability of 90.2 % for the Kit #4 was obtained compared to the 68.0 % for Kit #1 after 48 h, demonstrating that ethanol additions are useful to gain Kit stabilities. Based on these results, Ki #5 was prepared equal to Kit #2, but dissolved in 10 %Vol EtOH as for Kit #4. The formulation of Kit #5 with 250 µg ligand, 100 mg sodium ascorbate and a 10 %Vol of EtOH showed a RCY of 99.2 % and a radiolytic stability of 98.8 % over 48 h.

Finally Kit #6 was prepared similar to Kit #3 containing 100 µg BPAMD, i.e. with a higher specific activity compared to Kit #5 containing 250 µg BPAMD. Instead of sodium ascorbate only, a mixture of sodium ascorbate and ascorbic acid was used to adjust a reaction pH < 6, which results in the best RCY of 99.6 % compared to that of Kit #3. Stability could be maintained over 48 h (99.3 % of the intact complex), similar to that of Kit #5. [^{177}Lu]BPAMD prepared with Kit #6 exhibited also no complex degradation in human serum within 24 h. An additional approach was the reduction of cold BPAMD carrier amounts. Kit #7 exhibited the best specific activity of 125 MBq (^{177}Lu) per 1 µg (BPAMD), but showed also the lowest stability over time.

5. Conclusion

The BPAMD Kit formulation containing a mixture of 100 µg ligand, 400 mg sodium ascorbate and 100 mg ascorbic acid exhibited the best synthesis yields and the best radiolytic stabilities over 48 h, with a specific activity of 50 MBq ^{177}Lu/µg BPAMD. An automated synthesis module for the preparation of [^{177}Lu]BPAMD in scales of up to 5 GBq has been successfully established. The Kit and the automated synthesis unit enable a safe and routine in-house production of the therapeutic tracer [^{177}Lu]BPAMD for the treatment of bone metastases. Additionally the stability over 48 h is an appropriate time scale to even allow the shipment of batches from production facilities ready-to-use to clinical departments. The [^{177}Lu]BPAMD prepared this way selectively accumulates in disseminated bone metastases. Preliminary therapeutic data are promising and will be reported in detail elsewhere.

6. Acknowledgement

We are grateful to ITG (Garching, Germany) for providing ^{177}Lu. The assistance of Dr. Markus Piel and Sabine Höhnemann for the arrangement of the automated synthesis module is greatly acknowledged. This work was supported by a scientific grant of the Wilhelm u. Ingeburg Dinse-Gedächtnis-Stiftung, Hamburg provided to the THERANOSTICS Research Network, ENETS Center of Excellence, Zentralklinik Bad Berka, Germany. The financial support by the Grant of the Max Planck Graduate Center and the COST Action TD1004 is greatly acknowledged.

7. References

[1] L. Bodei, M. Lam, C. Chiesa, G. Flux, B. Brans, A. Chiti, F. Giammarile, EANM procedure guideline for treatment of refractory metastatic bone pain, *Eur J Nucl Med Mol Imaging*, **2008**; 35: 1934-40.

[2] PG. Kluetz, W. Pierce, VE. Maher, H. Zhang, A. Ibrahim, R. Justice, R. Pazdur, Radium Ra-223 dichloride injection: U.S. Food and Drug Administration drug approval summary, *Clin Cancer Res*, **2014**; 20(1): 9-14.

[3] M. Fellner, R. P. Baum, V. Kubíček, P. Hermann, .I Lukeš, V. Prasad, F. Rösch, PET/CT imaging of osteoblastic bone metastases with ^{68}Ga-bisphosphonates: first human study, *Eur J Nucl Med Mol Imaging*, **2010**; 37: 834.

[4] T. Vitha, V. Kubícek, P. Hermann, ZI. Kolar, HT. Wolterbeek, WA. Breeman, I. Lukes, JA. Peters, Lanthanide(III) complexes of bis(phosphonate) monoamide analogues of DOTA: bone-seeking agents for imaging and therapy, *J Med Chem*, **2008**; 51(3): 677-83.

[5] N. A. Lebedev, A. F. Novgorodov, R. Misiak, J. Brockmann, F. Rösch, Radiochemical separation of no-carrier-added ^{177}Lu as produced via the ^{176}Yb(n,γ)^{177}Yb→^{177}Lu process, *Appl Radiat Isot*, **2000**; 53(3): 421-425.

[6] F. Rösch , R. P. Baum, Generator-based PET radiopharmaceuticals for molecular imaging of tumours: On the way to THERANOSTICS. *Dalton Transactions*, **2011**; 40: 6104-6111.

[7] J. Yuan , C. Liu , X. Liu , Y. Wang , D. Kuai , G. Zhang , JJ. Zaknun, Efficacy and safety of ^{177}Lu-EDTMP in bone metastatic pain palliation in breast cancer and hormone refractory prostate cancer: a phase II study, *Clin Nucl Med*, **2013**; 38(2):88-92.

[8] E. de Blois, H. S. Chan, R. de Zanger, M. Konijnenberg, W. A. P. Breeman, Application of single-vial ready-for-use formulation of ^{111}In- or ^{177}Lu-labelled somatostatin analogs, *Applied Radiation and Isotopes*, **2014**; 85: 28–33.

3.3. Gallium(III) complexes of NOTA-bis(phosphonate) conjugates as PET radiotracers for bone imaging

Gallium(III) complexes of NOTA-bis(phosphonate) conjugates as PET radiotracers for bone imaging

Jan Holub[1], Marian Meckel[2], Vojtěch Kubíček[1], Frank Rösch[2] and Petr Hermann[1]

[1] *Department of Inorganic Chemistry, Charles University Prague, The Czech Republic.*

[2] *Institute of Nuclear Chemistry, Johannes-Gutenberg-University Mainz, Germany*

Key words

bis(phosphonate), NOTA derivatives, bone targeting, ^{68}Ga radiopharmaceuticals, phosphinate complexes, macrocyclic complexes, PET imaging, radiotracer biodistribution, *in vivo* imaging, nuclear medicine.

Abstract

Ligands with geminal bis(phosphonic acid) appended to 1,4,7-triazacyclonone-1,4-diacetic acid fragment through acetamide (NOTAM^{BP}) or methylenephosphinate (NO2AP^{BP}) spacers designed for ^{68}Ga were prepared. Ga(III) complexation is much faster for ligand with methylenephosphinate spacer than that with acetamide one, both in chemical (high reactant concentrations) and radiolabeling studies with no-carrier-added ^{68}Ga. For both ligands, formation of the Ga(III) complex was slower than that with NOTA due to the strong *out-of-cage* binding of bis(phosphonate) group. Radiolabelling was efficient and fast only above 60 °C and in a narrow acidity region (pH ~3). At higher temperature, hydrolysis of amide bond of the carboxamide-bis(phosphonate) conjugate was observed during complexation reaction leading to the Ga-NOTA complex. *In vitro* sorption studies confirmed effective binding of the ^{68}Ga complexes to hydroxyapatite being comparable with that for common bis(phosphonate) drugs such as pamindronate. Selective bone uptake was confirmed in healthy rats by biodistribution studies *ex vivo* and by microPET imaging *in vivo*. Bone uptake was very high, with SUV (standardized uptake value) of 6.19±1.27 for [^{68}Ga]NO2AP^{BP}) at 60 min p.i. which is superior to the uptake of ^{68}Ga–DOTA-based bis(phosphonates) and [^{18}F]NaF reported earlier (SUV of 4.63±0.38 and SUV of 4.87±0.32 for [^{68}Ga]DO3AP^{BP} and [^{18}F]NaF, respectively, at 60 min p.i.). Coincidently, accumulation in soft tissue is generally low (e.g. for kidneys SUV of 0.26±0.09 for [^{68}Ga]NO2AP^{BP} at 60 min p.i.), revealing the new ^{68}Ga complexes as ideal tracers for non-invasive, fast and quantitative imaging of calcified tissue and for metastatic lesions using PET or PET/CT.

1. Introduction

Positron emission tomography (PET) is a powerful method for imaging various tissue or physiological states. The choice of the proper PET radionuclide is given by various criteria such as half-life, energy of the emitted positron, production pathway, radiopharmaceuticals preparation and/or means of application. Compared to the most commonly used radioisotopes (^{11}C and ^{18}F) needing on-site production on a cyclotron, various metal radionuclides can conveniently be prepared utilizing a generator – a device containing a parent nuclide that decays with a long half-life to a daughter positron-emitting radionuclide which is periodically eluated off, purified and used. These radionuclide generators are relatively cheap, permanently accessible and easy to handle. One of the most promising generator-produced radionuclides is ^{68}Ga ($t_{½}$ 67.7 min, 89 % positron emission, mean β^+ energy 0.83 MeV) available from commercial ^{68}Ge/^{68}Ga generators (1–7).

However, with only very limited exceptions, most of the metal radioisotopes cannot be applied in a "free" form. The metal radioisotope must be bound in a stable complex to avoid non-specific deposition of the radioisotope in tissues. Ligands used for complexation of the metal ions must ensure very fast and efficient complexation even in highly diluted solutions, sufficient kinetic inertness and thermodynamic stability of the complexes as well as specific accumulation of the formed species in the tissue of interest. The last requirement is commonly fulfilled either by creating a metal-ligand system showing specific interaction with target organs or by adding a biologically relevant targeting vector to the metal-ligand system, thereby turning the "normal" ligand into a "bifunctional" one. Bifunctionality defines the utilization of one of the functional groups of the ligand to covalent attachment of the ligand to the targeting vector while preserving the complexing potency of the remaining structure.

Bone tissue is a prominent target of radionuclide diagnostics and therapeutics as bone metastases represent a very common complication of various types of cancer. Generally, bone targeting is mostly realized via attachment of a germinal bis(phosphonate) moiety to a molecule to be delivered to bone (8–11). Bis(phosphonates) show a high affinity to

hydroxyapatite (HAP). Thus, compounds containing a bis(phosphonate) moiety are efficiently adsorbed on the surface of bones. Consequently, such conjugates have been used to deliver radioisotopes to the calcified tissues (10). Recently, we and others have developed bis(phosphonate)-bearing ligands based on a DOTA-like macrocyclic core (DOTA = 1,4,7,10-tetraazacyclododecane-1,4,7,10-tetraacetic acid, Figure 1) as carriers for metal ions to be delivered to calcified tissue (12–17). The applications include imaging techniques (^{111}In and ^{68}Ga for SPECT and PET imaging, respectively) (13,15,17–19) as well as therapy (^{177}Lu, ^{90}Y) (13,16) or bone metastases pain palliation in human patients (20). The conjugates exhibited a very high affinity to HAP as the bis(phosphonate) moiety is not coordinated to the central metal ion and, thus, remains active for bone targeting (21,22). However, DOTA-like macrocycles are not the best ligands for Ga(III) as incorporation of the ion inside the macrocyclic cavity leads to severe distortion of coordination octahedron around Ga(III) ion (23–26).

Despite high thermodynamic stability and kinetic inertness of the Ga(III) complexes with DOTA-like ligands (27), complexation of no-carrier-added (n.c.a.) ^{68}Ga with these ligands is less efficient and more sensitive to experimental conditions than that of NOTA analogs (NOTA = 1,4,7-triazacyclononane-1,4,7-triacetic acid, Figure 1) (1). Triaza- instead of tetraazamacrocycles have been proved to be more suitable for Ga(III). They form complexes exhibiting much higher thermodynamic stability as well as kinetic inertness (28,29). The size of the coordination cavity imposed by the nine-member macrocyclic ring corresponds very well to the size of the Ga(III) ion. As Ga(III) is small ion and mostly requires octahedral coordination sphere, the NOTA-like ligands provide an optimal size and arrangement of ligand cavity to accommodate trivalent gallium ($\log K_{[Ga\text{-}DOTA]}$ = 26.1, $\log K_{[Ga\text{-}NOTA]}$ =29.6) (27,28). Thus, a number of NOTA-like ligands have been investigated as promising chelators for ^{68}Ga (1,10). Among them (by analogy with the most commonly used ligands in the DOTA-like family, the DOTA-monoamides), NOTA-monoamides appear as an emerging class of ligands due to their easy synthesis and potential easiness of introduction of bifunctionality through amide formation (30–33).

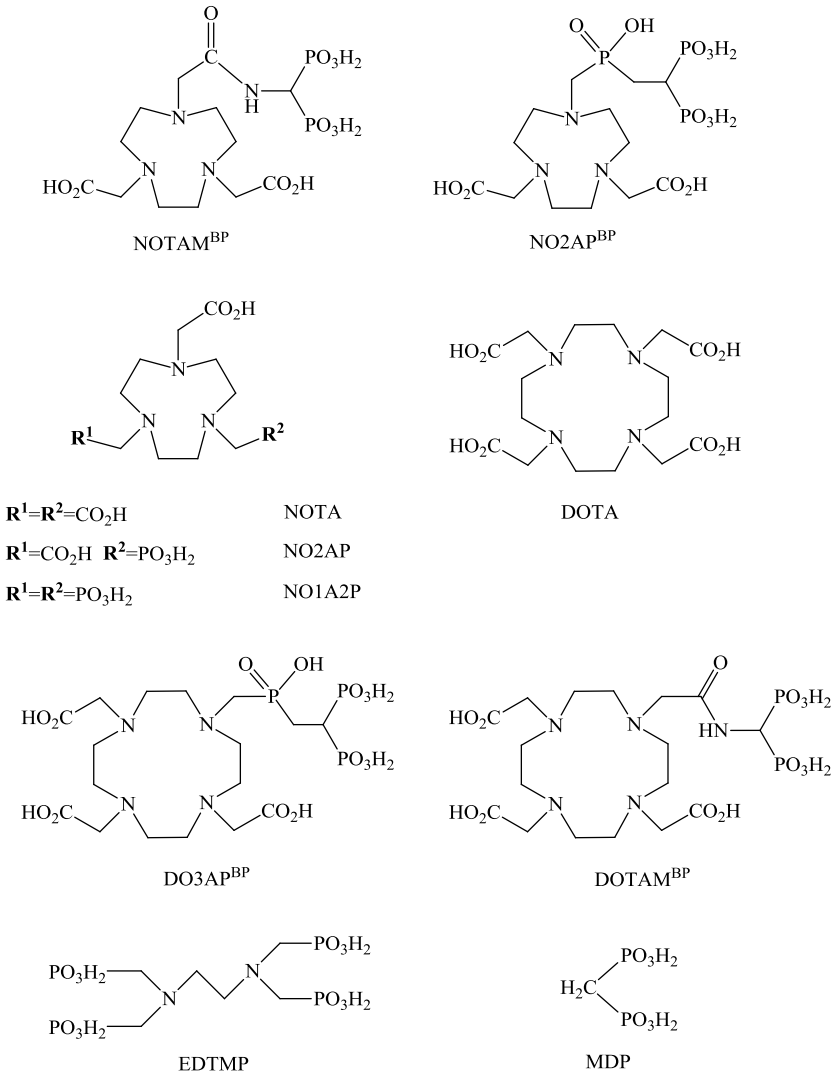

Figure 1. Ligands discussed in this paper.

Imaging of bone lesions is important for location, staging and treatment of several diseases, mainly breast and prostate cancers metastases. Bone scans have been dominated by SPECT imaging with ^{99m}Tc-bis(phosphonate) tracers. However, SPECT resolution and sensitivity is inferior comparing with PET; so, PET tracers should be more convenient. The [^{18}F]NaF tracer has been introduced for bone imaging some time ago. However, ^{18}F is expensive, and its production requires cyclotron and skilled staff. So, cheaper alternative isotopes requiring only relatively simple workup, as e.g. ^{68}Ga produced in long-lived generator, are desired. We have introduced (12–14) bis(phosphonate)-containing macrocyclic ligands, DOTA-

monoamide DOTAM^{BP} and DOTA monophosphinate analog DO3AP^{BP} (Figure 1), which were successfully labelled with ^{68}Ga and used as PET tracers.(18–20,34) However, labelling DOTAM^{BP} and DO3AP^{BP} with ^{68}Ga is not optimal.(19,34) Thus, in order to improve properties of the bone-targeted complexes such as ease labeling and improved bone/soft tissue ratio as well as to get a direct comparison with our previous data on ^{68}Ga-DOTAM^{BP} and ^{68}Ga-DO3AP^{BP}, we decided to study analogous ligands derived from NOTA.

Thus, this paper describes synthesis of the NOTA-like ligands with a bis(phosphonate)-containing side arm (as the bone-targeting group) connected to the metal-binding cage through the acetamide or methylphosphinate pendant arms, NOTAM^{BP} and NO2AP^{BP} (Figure 1). The ligand physicochemical characterization, labeling with ^{68}Ga, *in vitro* binding to HAP, *ex-vivo* biodistribution of the ^{68}Ga-labeled compounds and small animal *in vivo* PET imaging were evaluated. In order to simplify the text, abbreviations as NOTA, Ga-NOTAM^{BP} or Ga-NO2AP^{BP} etc. are used for the ligands/complexes regardless of the in charge/protonation state, except when the distinction is necessary for comprehension.

2. Results and Discussion

2.1. Synthesis

The ligands were synthesized according to Figure 2. A previously described procedure (35) for the benzyl monoprotected macrocycle **2** was modified to a one-pot synthesis and its overall yield was improved. Further reaction with *t*-butyl bromoacetate followed by catalytic hydrogenation resulted in doubly substituted macrocycle **4**. Preparations of compound **4**, commonly used for synthesis of 1,4,7-triazacyclononane-1,4-diacetic acid (NO2A) derivatives, have been known for a long time (36–39); however, the present synthesis was slightly modified, run in much higher scale and resulted in overall yield comparable with the previous ones. The secondary amine of the NO2A diester **4** was used for attachment of geminal bis(phosphonate) moiety *via* the acetamide or methylphosphinate linkers. The

reactions were carried out with the fully esterified reagents due to their better solubility in organic solvents and more efficient chromatographic purification of the intermediates. The acetamide derivative **6** was prepared by alkylation of **4** with the appropriate chloroacetamide **5**. The phosphinate derivative **8** was prepared by Mannich-type reaction using paraformaldehyde and the per(ethyl) bis(phosphono)-phosphinate **7**. Cleavage of the ester protecting groups was performed in two steps. First, *t*-butyl groups were cleaved by action of trifluoroacetic acid and, then, ethyl groups were removed by transesterification with trimethylbromosilane followed by silyl group removal with methanol. The final purification on cation exchange resin yielded NOTAM^{BP} and NO2AP^{BP} in zwitterionic form.

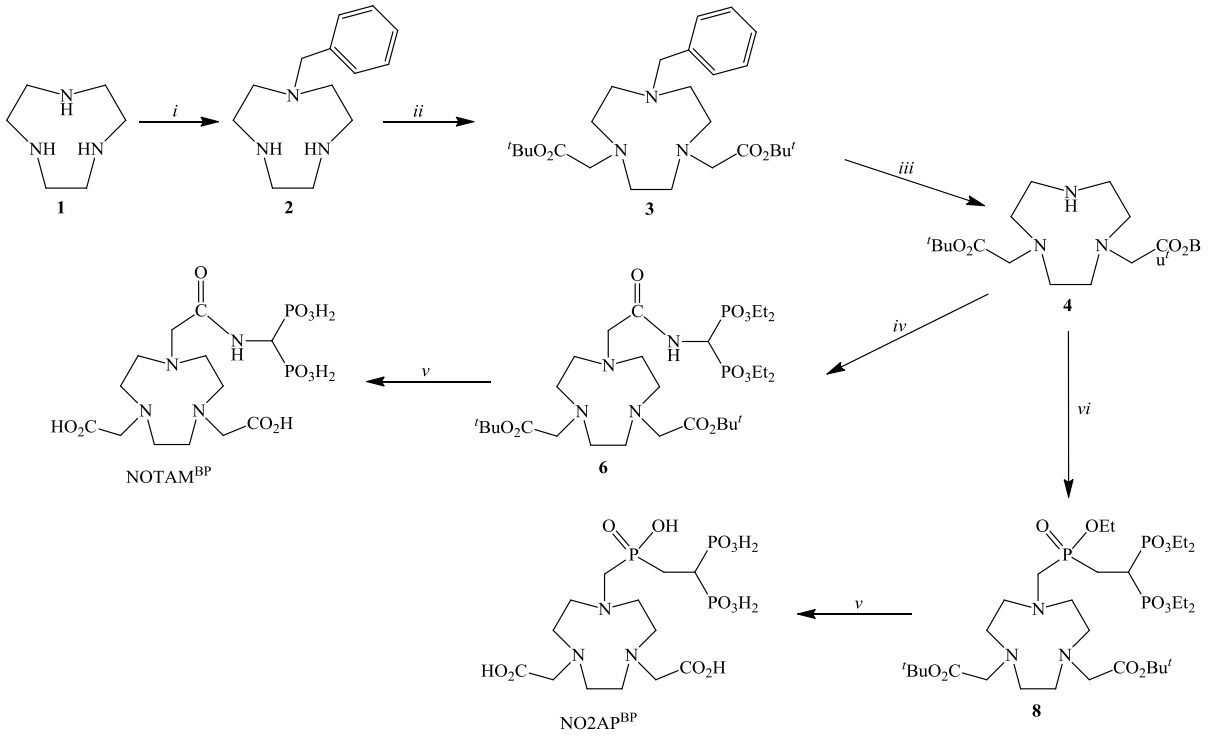

Figure 2. Syntheses of ligands: (*i*) 1. $Me_2NCH(OMe)_2$, dioxan, reflux, 3 h; 2. $BrCH_2Ph$, THF, r.t., overnight; 3. KOH, H_2O/EtOH, reflux, 3 d; 75 %. (*ii*) $BrCH_2CO_2{}^tBu$, K_2CO_3, acetonitrile, r.t., 3 d; 91 %. (*iii*) H_2, Pd/C, EtOH, 50 °C, 12 h; 84 %. (*iv*) $ClCH_2C(O)NH–CH(PO_3Et_2)_2$ (**5**), K_2CO_3, acetonitrile, 50 °C, 3 d; 83 %. (*v*) 1. $CF_3CO_2H/CHCl_3$ 1:1, r.t., 12 h; 2. $BrSiMe_3$, acetonitrile, r.t., 12 h; 80 % (NOTAM^{BP}), 41 % (NO2AP^{BP}). (*vi*) (**7**), $(CH_2O)_n$, acetonitrile, 35 °C, 3 d; 72 %.

2.2. Ga^{3+} complexation

Coordination ability of the title ligands toward Ga(III) was studied due to their intended applications for ^{68}Ga PET imaging. In addition, Fe(III) complexes were prepared as this ion shows similar properties (the same charge and similar ionic radius) as Ga(III) and, thus, can be considered as a surrogate differing just in spectral and magnetic properties.

Dissolving the ligand in a solution containing the equimolar amount of the metal ions leads to significant decrease in pH (pH drops to 1.4–2.0). Addition of strong hydroxide and increase of pH (pH > 2) leads to immediate formation of precipitates. The precipitates are dissolved upon further increase in pH (pH > 4). Most likely, such behavior could be ascribed to a mechanism of complex formation involving several intermediates as it has been suggested for similar macrocyclic ligands (14,28,29). The initial mixing of the reagents leads to immediate coordination of the metal ion to the bis(phosphonate) oxygen atoms and release of protons. It is known that bis(phosphonate) group is able to interact with trivalent metal ions even at very low pH (40,41) and, at pH < 2, the ligands bind the metal ion in a protonated form (with protons bound on macrocyclic amines as well as on the phosphonate groups) forming *out-of-cage* complexes. Such species have overall positive charge and are soluble in water. Increase of pH causes further deprotonation of the bis(phosphonate) group and formation of charge-neutral complexes with low solubility in water. Such solid *out-of-cage* intermediates are expected to be 3-D coordination polymers having metal ions bridged by phosphonate group(s), typical for phosphonate and bis(phosphonate) complexes (40,41). Further pH increase results in dissolution of the precipitates and is associated with the ring amine deprotonation and formation of final *in-cage* macrocyclic complexes where the metal ion is coordinated with three ring nitrogen atoms and three oxygen atoms of carboxylate or acetamide/phosphinate pendants (29,42,43). A similar mechanism involving phosphonate-coordinated *out-of-cage* intermediate has been previously postulated for complexation of lanthanide(III) ions with analogous DOTA-like bis(phosphonate)-bearing ligands as DO3AP^{BP} (12,14). Formation of the *in-cage* complexes was directly confirmed by ^{71}Ga NMR measurements. The Ga-NO2AP^{BP} complex shows a rather broad signal at 158 ppm ($\varpi_{½}$ ~1300 Hz, Figure S1). The quadrupole moment of the ^{71}Ga nucleus leads to a signal broadening if Ga(III) ion is placed in a non-symmetrical coordination environment. The non-

symmetrical charge distribution leads to an extremely broad signal of Ga-NOTAM^{BP} complex centered at ~170 ppm ($\varpi_{½}$ = ~9700 Hz, Figure S1); ^{71}Ga NMR chemical shift of 166 ppm has been observed for other NOTA-monoamide gallium(III) complex (31).

The time course of gallium(III) complexation with the ligand NO2AP^{BP}was studied in details by ^{71}Ga and ^{31}P{^{1}H} NMR. Coordination spheres of the *out-of-cage* intermediates are completely non-symmetrical and, thus, are "invisible" in the ^{71}Ga NMR spectra. Thus, formation of the *in-cage* complex was quantified using an external capillary standard. These experiments were performed with Ga:L 1:1 molar ratio, at pH 2 and 3 (1 M sodium chloroacetate buffer), pH 4 and 5 (1 M sodium acetate buffer). In the presence of the weakly coordinating buffers, the above mentioned precipitation of intermediates was not observed. The results are summarized in Table 1 and Figures 3 and S2. The complexation rates follow the order pH 2 < pH 3 ~ pH 5 < pH 4. As stated above, the complexation can be described as a two-step process. The intermediate *out-of-cage* complex is formed instantly and the metal ion is coordinated only through oxygen atoms of the bis(phosphonate) group and the pendant arms (carboxylate and phosphinate), whereas the macrocyclic amines are protonated. In the rate-determining step, the ring nitrogen atoms lost proton(s) and the metal ion simultaneously moves into the macrocycle cavity; it is, generally, a base-catalyzed process. The mechanism explains the increase in the complexation rate between pH 2 and 3. The complexation at pH 5 might be partially decelerated by presence of acetate anions from the buffer, however at milimolar concentrations used in these experiments, partially protonated bis(phosphonate) anion (41) is much better ligand than acetate and it is known that phosphonate coordination ability is considerably increased with consecutive deprotonation of the group. Thus, the slower complexation at pH 5 is probably caused by more extensive deprotonation of the bis(phosphonate) moiety at higher pH leading to its stronger interaction with the Ga(III) ion and stabilization of the *out-of-cage* complex, or by formation of Ga(III) hydroxido complexes.

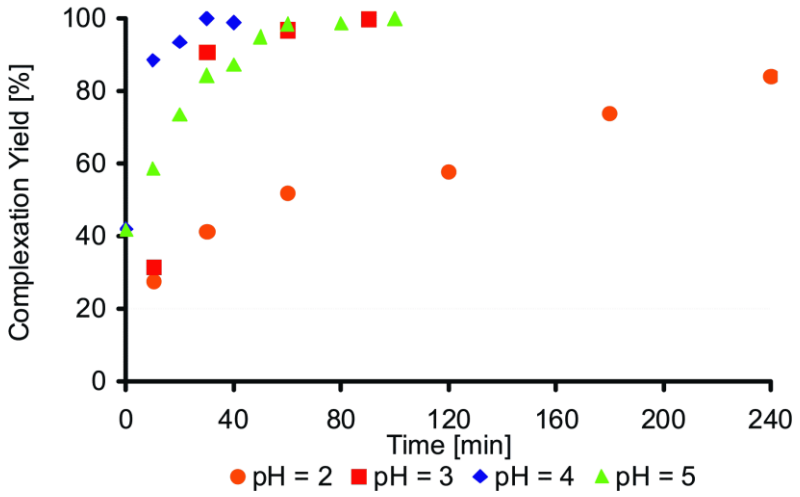

Figure 3. Time course of complexation of Ga(III) with NO2AP^{BP} at different pH (40 °C, molar ratio L : Ga = 1 : 1, c_{Ga} = 0.13 M); dead time for t_0 = 5 min.

Table 1. Half-time ($t_{1/2}$) of the Ga-NO2AP^{BP} complex formation (40 °C, molar ratio L : Ga = 1 : 1, c_{Ga} = 0.13 M).

Ligand	pH	$t_{1/2}$ [min]	95 % complexation [min]
NO2AP^{BP}	5	10	50
	4	<5	20
	3	12	60
	2	65	360
NOTA[a]	3	<2	
	1	270	

[a]25 °C, ref. [28].

In the case of NOTAM^{BP}, the broadening of the ^{71}Ga NMR signal and overlapping of ^{31}P{^{1}H} NMR signals of the product and reaction intermediates disabled precise quantification under the same conditions as those used for the NO2AP^{BP} complexation. However, even after heating at 40 °C for several hours, broad ^{31}P{^{1}H} NMR signals were observed showing that only an *out-of-cage* complex was formed which was stable under these conditions. If the solution was heated at 95 °C (Figures 4 and S3), several signals could be distinguished after several minutes and the spectra indicate that the *in-cage* complex is

fully formed after ~30 min under this conditions. Further heating led only to a decrease of the Ga-NOTAM^{BP} complex signal and increase of that of the aminomethylene-bis(phosphonate) indicating that the Ga-NOTAM^{BP} complex is unstable under this conditions and decomposes to the Ga-NOTA complex (see also below). Some decomposition (i.e. the formation of [Ga(NOTA)]) was observed in the ^{71}Ga NMR spectrum even after 10 min of the reaction (Figure S3).

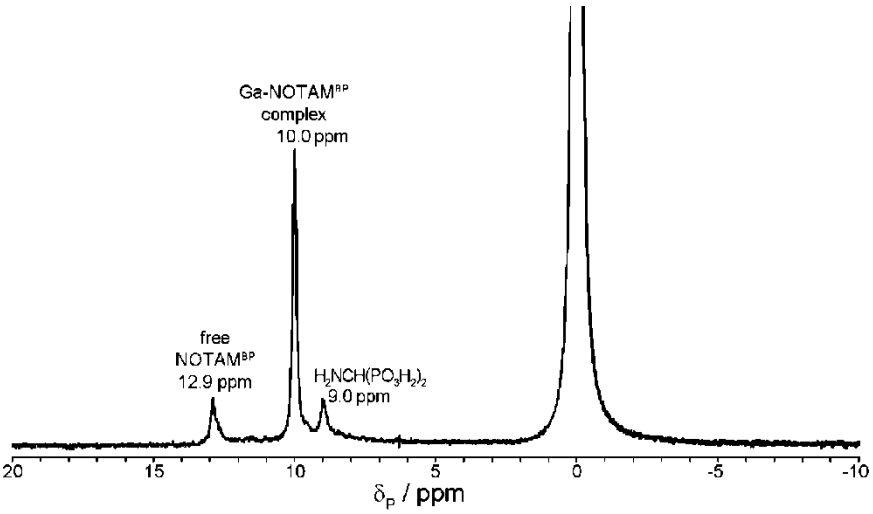

Figure 4. $^{31}P\{^{1}H\}$ NMR spectrum of the reaction mixture after 30 min of reaction of Ga(III) with NOTAM^{BP} at pH 3 and 90 °C (c_{Ga} = 0.13 M, slight molar excess of the ligand; dead time (t_0) approx. 5 min).

The results point to an important role of the spacer connecting the bis(phosphonate) group and the macrocycle. Under all conditions tested, NO2AP^{BP} showed significantly faster gallium(III) complexation than NOTAM^{BP}. Albeit phosphinates are known to be better complexation groups than carboxamides, the pronounced difference in the reaction rate is surprising; the hard and charged phosphinate group as good coordinating group for Ga(III) ion is probably able to assist the ion transfer from the *out-of-cage* species into the *in-cage* complex much better. In addition, basicity of the amine group in the >N–CH_2–P(R)O_2H moiety is significantly lowered (28,44) and, so, deprotonation of the amine group adjacent to the phosphinate is facilitated.

For both ligands, the complexation rates are significantly lower than those reported for NOTA or its phosphinic acid analogues (28,29,45–47). So, presence of a too strongly

complexing hard group such as the bis(phosphonate) one in the proximity of macrocycle could be considered as a rate-decreasing factor in Ga^{3+} complexation reaction. In addition, it has been recently published that presence of three bis(phosphonate) groups in the side chains of a tris(methylenephosphinic acid) NOTA analog completely prevents entering the Ga(III) ion into the macrocyclic cavity and Ga(III) is coordinated only by the phosphonate groups in the *out-of-cage* fashion.(48) Consequently, a number of bis(phosphonate) groups should be balanced to have good bone targeting and, in the same time, efficient *in-cage* complexation.

2.3. Hydrolysis of the amide bond in the Ga-NOTAM^{BP} complex

Single-crystals were formed in time course of Ga(III) complexation with NOTAM^{BP}. According to the X-ray diffraction, these were not crystals of Ga-NOTAM^{BP} but those of the known Ga-NOTA complex (41). It is result of the amide bond hydrolysis in the Ga-NOTAM^{BP} complex (see also Figure 5). Upon complexation, Ga(III) is coordinated through amide oxygen or nitrogen atoms (31). This coordination decreases the electron density on the amide carbon atom and makes it more vulnerable for the solvent nucleophilic attack (it is the same effect as expressed during hydrolysis of peptide bond catalyzed by metalloenzymes).

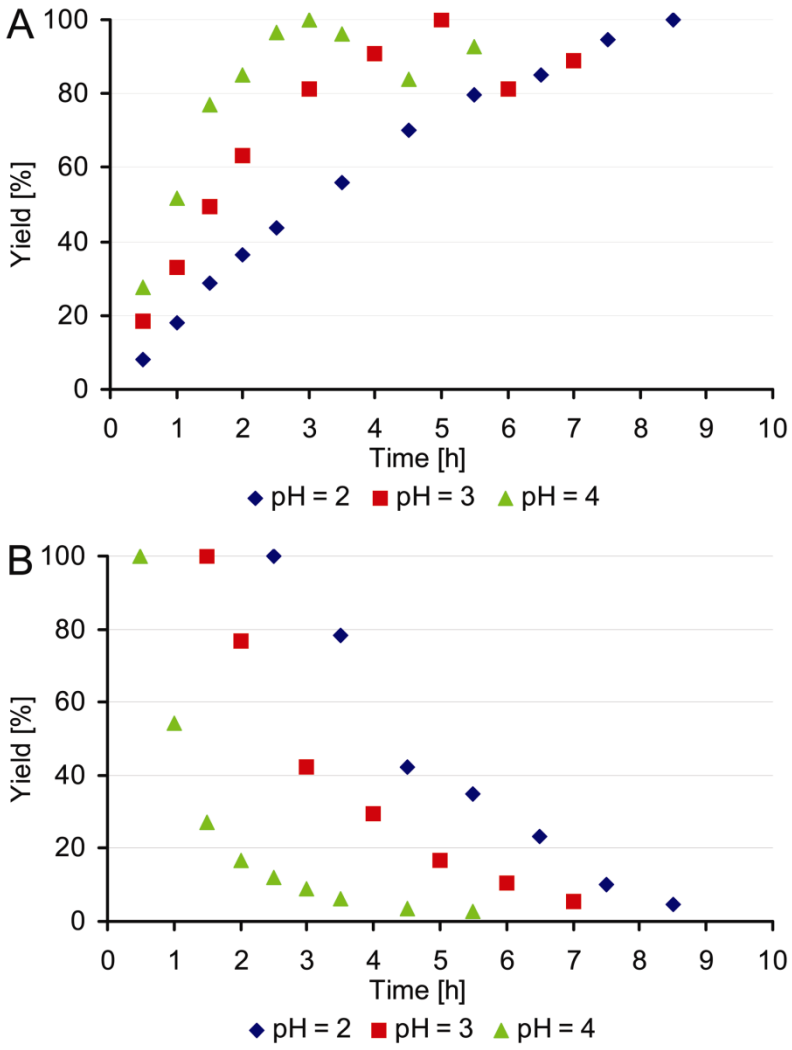

Figure 5. Hydrolysis of amide bond in the Ga-NOTAM^{BP} complex expressed as increasing abundance of the Ga-NOTA complex in ^{71}Ga NMR (**A**) and decreasing abundance of the Ga-NOTAM^{BP} complex in ^{31}P{^{1}H} NMR (**B**) (90 °C, c_{GaL} = 0.13 M). Figures do not have the same *y*-axis absolute scale: precipitation of the Ga-NOTA complex, confirmed by X-ray diffraction, caused decline of the ^{71}Ga NMR signal intensity by the end of the reaction and maximum in the ^{31}P{^{1}H} NMR data refers to a time when the first integration was possible, i.e. after 0.5–2.5 h depending on pH.

As the reaction is important in view of utilization of the ^{68}Ga-labelled ligands in nuclear medicine (see below), the hydrolysis was studied in more detail. It was monitored through an increasing intensity of the sharp Ga-NOTA signal in ^{71}Ga NMR (δ_{Ga} = 170 ppm; $\varpi_{½}$ = 390 Hz) and, in parallel, through increasing intensity of the aminomethyl-bis(phosphonate) signal in ^{31}P{^{1}H} NMR (δ = 8.9 ppm, pH 3), Figure S3. The results show that the hydrolysis is

faster with increasing pH (Figure 5). It indicates a hydroxide-mediated reaction and could be explained as nucleophilic attack of the hydroxide anion on the amide carbon atom of highly polarized carbonyl moiety due to coordination to small trivalent metal ion; thus, the reaction can proceed even in slightly acidic solutions. However, the hydrolysis proceeds with much slower rate than the formation of the *in-cage* complex as only very minor decomposition was observed during 10 min at 90 °C (Figure S3, see also above) under these "chemical" conditions (in this context, "chemical" conditions means milimolar or higher concentrations of the reactants unlike "radiochemical" conditions where the concentrations are many orders of magnitude lower). Thus, the hydrolysis was also checked during the labeling of NOTAM^{BP} with ^{68}Ga and the ^{68}Ga-NOTA complex was also identified *via* radio-HPLC (see below).

It should be noticed that analogous hydrolysis might have been present during studies of Ga(III) complexes with simple NOTA-monoamides where a very broad ^{71}Ga NMR signal of the complexes with a small sharp singlet at 170 ppm (probably attributable to the Ga-NOTA complex) was observed (31).

2.4. Adsorption of iron(III) complexes on hydroxyapatite

To estimate bone targeting efficiency, the most commonly used method is to determine the binding ability of the molecules on hydroxoapatite (HAP) surface. For bis(phosphonate)-containing DOTA derivatives, the long-lived ^{160}Tb metal isotope has been used as a surrogate for lanthanide(III) ions (21). As ^{68}Ga is a short-lived radioisotope, another method was sought. Trivalent iron has properties (charge, size, hardness etc.) similar to those of trivalent gallium and both ions form analogous complexes; thus, Fe(III) was chosen as a surrogate. UV-Vis spectroscopy was used to quantify the sorption ability as the Fe(III) complexes exhibit intensive ligand-to-metal charge transfer (LMCT) band in UV region (Figure S4). The iron(III) complexes of DOTAM^{BP} and DO3AP^{BP} were also prepared and studied for comparison with analogous complexes of DOTA-like ligands already used as ^{68}Ga radiopharmaceuticals (19,20). The adsorption process is usually described by the Langmuir adsorption isotherm

$$\frac{X}{X_{\mathrm{m}}} = \frac{K \times c}{1 + (K \times c)}$$

where K is the analyte (complex) affinity constant for the surface (in $dm^3\ mol^{-1}$), X_m is the maximum sorption capacity of the complex (in mol m^{-2}), c is complex concentration (in mol dm^{-3}) in the solution and X is the specific adsorbed amount of the complex (in mol m^{-2}). Aqueous suspension of HAP was used as a model of bone tissue. The results are shown in Figure S5 and the absorption parameters are summarized in Table 2.

Table 2. Adsorption parameters of the Fe(III) complexes on hydroxyapatite surface (pH 7.5, 25 °C, equilibration time 3 d).

Constant	Complex			
	Fe-NOTAM^{BP}	Fe-NO2AP^{BP}	Fe-DOTAM^{BP}	Fe-DO3AP^{BP}
K / 10^3 ($dm^3\ mol^{-1}$)	31.3 ± 6.1	20.0 ± 3.2	43.7 ± 12.2	207.6 ± 45.3
X_m / 10^{-6} (mol m^{-2})	1.007 ± 0.035	1.271 ± 0.052	0.768 ± 0.019	1.015 ± 0.017

All complexes studied show efficient binding on the HAP surface. Maximum sorption capacities are in the range that corresponds to the formation of monomolecular layer (12). For the complexes of NOTA analogues, maximum sorption capacities are higher than those for the DOTA complexes. This could be explained by the compact shape of the Fe(III) complexes with NOTA derivatives, where all pendant arms are coordinated (49,50). Larger size of the cyclen ring and presence of two uncoordinated pendant arm in the complexes with DOTA-like ligands (51) result in a larger surface area occupied by one molecule of the DOTA complexes. Higher affinity constants found for the complexes with DOTA derivatives indicate, that the uncoordinated pendant arms might be involved in the interaction with the HAP surface; the higher affinity constant for the Fe(III)-DO3AP^{BP} complex can be probably explained by the highest overall charge of among the complexes. Generally, both affinity constants as well as sorption capacities are comparable to those previously reported for

lanthanide(III) complexes with the same DOTA analogs, where all pendant arms are bound to the central metal ion (e.g. K = 250·10^{-3} dm^3 mol^{-1} and X_m = 0.65·10^6 mol m^{-2} for the ^{160}Tb-DO3AP^{BP} complex) (21) as well as to those for simple bis(phosphonates), e.g. for pamidronate (K = 44·10^{-3} dm^3 mol^{-1} and X_m = 1.82·10^6 mol m^{-2}) (21). It indirectly confirms similar accessibility of the distant bis(phosphonate) moiety for bone targeting in all the complexes.

2.5. Radiolabeling with no-carrier-added ^{68}Ga

If ligands are considered as potential radiopharmaceuticals, the efficiency of metal radionuclide incorporation is one of their most important properties and, thus, the title ligands were tested in labeling with n.c.a ^{68}Ga. The ligand-to-^{68}Ga(III) molar ratio was approximated in the order of 10^4 in all experiments (1 MBq ^{68}Ga corresponds to ~0.01 pmol of Ga(III)). The complexation was followed (see an example of the TLC plate in ESI, Figure S6) at various temperatures and solution acidities, and the results are summarized in Figures 6 and 7.

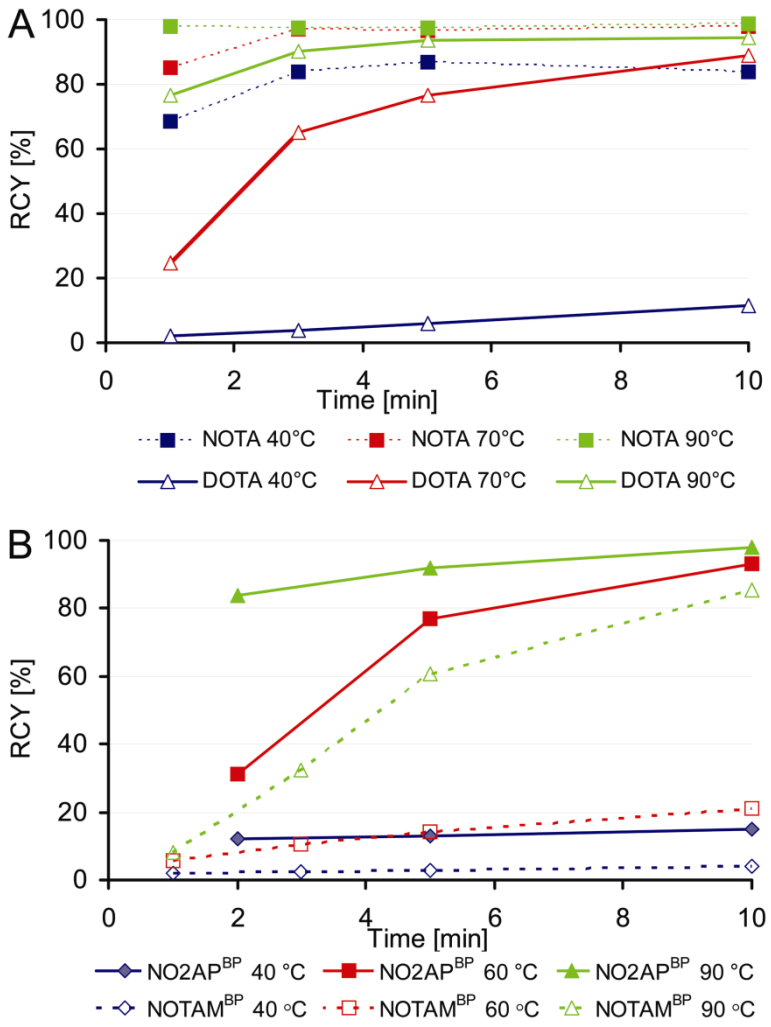

Figure 6. Time course of incorporation of no-carrier-added ^{68}Ga(III) by NOTA and DOTA (**A**, pH 4.0) and the title ligands (**B**, pH 4.2) at various temperatures. Results for NOTAM^{BP} can be influenced by the amide bond hydrolysis (for details, see text).

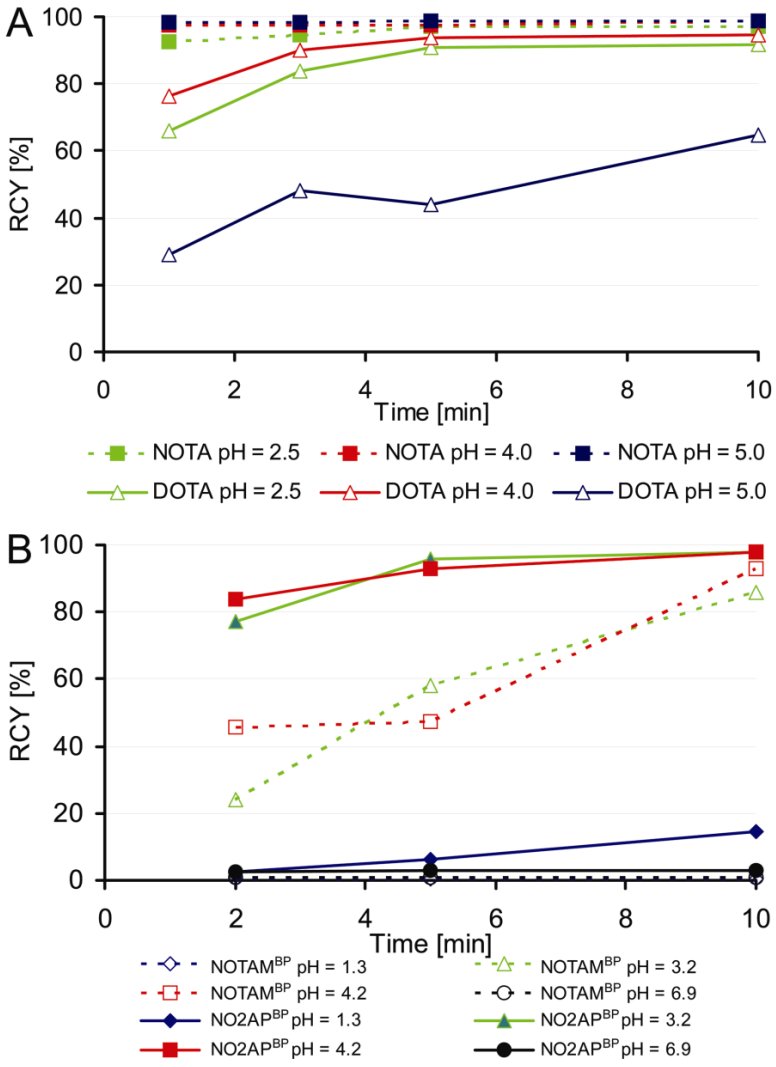

Figure 7. Time course of incorporation of no-carrier-added ^{68}Ga(III) by NOTA and DOTA (**A**) and the title ligands (**B**) at 95 °C and various pH. Results for NOTAM^{BP} can be influenced by the amide bond hydrolysis (for details, see text).

The data show similar trends as those obtained in the NMR experiments (above). For both ligands, fast complexation requires weakly acidic conditions, i.e. pH 3–4. No complexation was observed at pH 1.3 and 6.9 at any temperature. The experiments also confirmed the strong dependence of the complexation rate on the temperature. At pH = 4.2 and at room temperature, no complexation was observed with both ligands. In the case of NO2AP^{BP}, heating to 60 °C is required to reach full complexation in 10 min; at 95 °C ^{68}Ga(III) was quantitatively bound in only 5 min. Temperatures of <60 °C were insufficient for the

radiolabeling with NOTAM^{BP} and reasonable complexation efficiency was reached only at temperature of 95 °C. However, radio-TLC cannot be used for evaluation of hydrolysis of amide bond in the ^{68}Ga-NOTAM^{BP} system (as observed in the NMR experiments, above) as all complexes have the same mobility. To check the decomposition, labelling of NOTAM^{BP} was carried under conditions used in sample preparation for *in-vivo* experiments (pH 4, 90 °C, 15 min) and the reaction mixture was evaluated by HPLC on amine-containing sorbent (Figure S7). Partial decomposition (~20 %) was observed and it probably influenced the sorption and *in-vivo* data (see below). NO2AP^{BP} showed much faster complexation of n.c.a. ^{68}Ga(III) than NOTAM^{BP} under all tested conditions (Figures 6 and 7). This efficient complexation is more pronounced if compared with ^{68}Ga(III) labeling of DO3AP^{BP} where radiochemical yield under more forced conditions was, at the best, approx. 60 %.(34) It has also been shown (under the same conditions) that presence of one or two methylphosphonate arms in NOTA analogs (NO2AP and NO1A2P; for formulae, see Figure 1) accelerates the labeling reaction in comparison with the labeling with NOTA (33). Thus, presence of methylenephosphonic/inic acid pendant arms seems to increase the complexation rate. Radiolabeling of the title ligands with n.c.a. ^{68}Ga is less efficient than that of NOTA; however, NO2AP^{BP} incorporates ^{68}Ga similarly to the unsubstituted DOTA (Figures 6 and 7). Both title ligands are more efficient chelators than DOTAM^{BP} (it needs 20–25 min at 95 °C for 95 % labeling and the best pH is ~5; the same other labelling conditions as for the title ligands) (19). The ^{68}Ga-DOTAM^{BP} complex have been already applied *in vivo* (19,20) and, compared to it, the ^{68}Ga-complexes of the title ligands appear better suited for straight forward labelling adequate to utilization *in vivo* (see below).

2.6. Adsorption of ^{68}Ga-labeled complexes to hydroxoapatite

Binding of complexes labeled with ^{68}Ga to HAP surface was measured at room temperature (Figure 8). The [^{68}Ga]NO2AP^{BP} complex (93.8±4.4 %) is bound much better compared to [^{68}Ga]NOTAM^{BP} complex (38.1±2.6 %), while binding of the [^{68}Ga]NOTA complex (1.5±0.3 %) is negligible under the same conditions. These results are not fully paraleling those of iron(III) complexes obtained under “chemical” equilibrium conditions where no

significant differences were observed. The [^{68}Ga]NOTAM^{BP} might be partially decomposed during complexation decreasing the absorption on HAP. However, the difference is significant and another reason should be present. Because of the short half-life of ^{68}Ga, a short contact time of the complexes with HAP had to be used and full equilibrium could not be reached, unlike during measurements with the Fe(III) complexes (above). Thus, the difference between the experiments might be attributed to the faster absorption kinetics of [^{68}Ga]NO2AP^{BP} complex if compared with [^{68}Ga]NOTAM^{BP} complex; it was observed that the [^{160}Tb]DO3AP^{BP} complex adsorbs on HAP surface very quickly (22). These results are more relevant for *in vivo* conditions. Compounds with slow adsorption kinetics are not suitable for future *in vivo* studies. It is necessary to obtain high binding to the targeted tissue for imaging agents in a short timescale, otherwise long measurement time and high activities are required to develop adequate PET images. However, this experiment showed (Figure 1) no significant difference in HAP adsorption between the [^{68}Ga]NO2AP^{BP}, [^{68}Ga]DO3AP^{BP} and the [^{68}Ga]EDTMP tracers (EDTMP = ethylenediamine-*N,N,N′,N′*-tetrakis(methylenephosphonic acid), Figure 1). [^{68}Ga]NO2AP^{BP} had a binding of 93.8±4.4 % on HAP after 10 min, which is one of the highest rates among ^{68}Ga-labelled macrocyclic bis(phosphonates) (Figure 9). The data in this experiment are well correlating with those of the bone accumulation *in vivo* (in *ex vivo* organ distribution, see below).

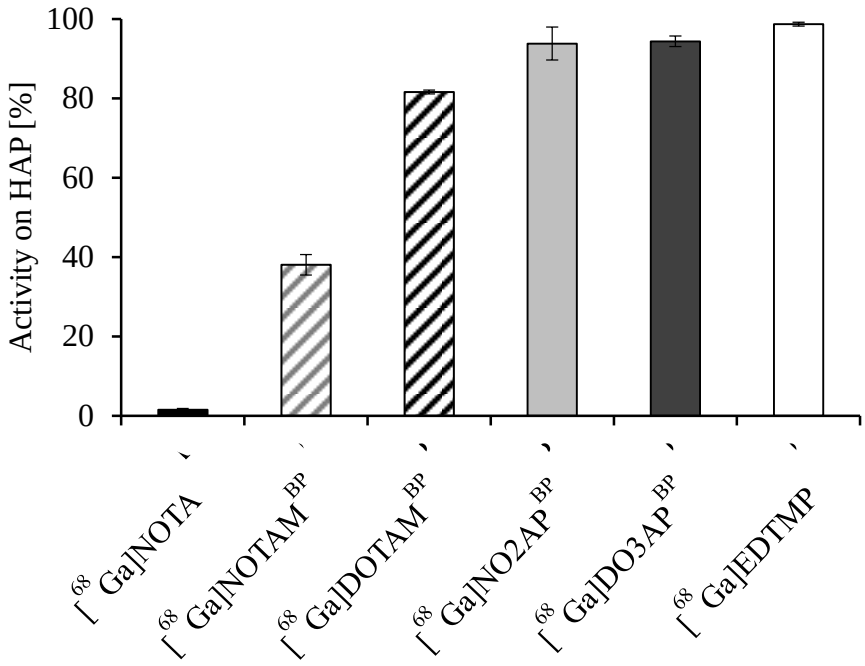

Figure 8. Binding of ^{68}Ga-labeled complexes to hydroxoapatite in isotonic saline (room temperature, 10 min). Data for [^{68}Ga]DOTAM^{BP} (19) and [^{68}Ga]EDTMP (53) were taken from literature (for EDTMP formula, see Figure 1). Results for NOTAM^{BP} can be influenced by the amide bond hydrolysis (for details, see text).

2.7. *In vivo* biodistribution studies

Uptake of the tracers in organism was followed by both μPET and organ dissection. The dissection data (Table 3) clearly shows high uptake of [^{68}Ga]NO2AP^{BP} in bone (femur 4.37 %, 60 min p.i.) and very low uptake in non-target organs like soft tissues. Similar results were observed with of [^{68}Ga]DOTA-based bis(phosphonates) in already published data (19,34). The bone uptake of [^{68}Ga]NO2AP^{BP} on bones (SUV of 6.19±1.27 %ID/g in femur) is clearly superior if compared with the established SPECT, ^{99m}Tc-MDP (MDP = methylene-bis(phosphonic acid), Figure 1), or PET, [^{18}F]NaF, bone tracers and also higher than that of the DOTA-based tracer (Figure 9). Lower uptake of [^{68}Ga]NOTAM^{BP} is in line with the *in vitro* results and can be caused by partial decomposition during labeling (above).

Table 3. *Ex vivo* biodistribution of [^{68}Ga]NOTAM^{BP} and [^{68}Ga]NO3AP^{BP} complexes in healthy male Wistar rats (60 min p.i.). Data are presented as an average from five animals (± S.D.); uptake as % I.D. per gram of tissue (% ID/g).

Organ	Complex	
	[^{68}Ga]NOTAM^{BP}	[^{68}Ga]NOTAM^{BP}
Lung	0.12 ± 0.03	0.04 ± 0.03
Liver	0.05 ± 0.01	0.02 ± 0.01
Spleen	0.04 ± 0.01	0.02 ± 0.01
Kidney	0.45 ± 0.04	0.18 ± 0.07
Muscle	0.03 ± 0.01	0.01 ± 0.00
Heart	0.04 ± 0.01	0.01 ± 0.01
Blood	0.09 ± 0.04	0.02 ± 0.00
Intestine	0.07 ± 0.03	0.03 ± 0.03
Testes	0.04 ± 0.01	0.01 ± 0.00
Femur	1.12 ± 0.36	4.37 ± 0.92

The bone uptake of [^{68}Ga]NO2AP^{BP} is significantly better (Figure 10) than bone uptake of [^{68}Ga]DOTAM^{BP}, the tracer already successfully used in patients, as well as that of its equivalent DOTA-based tracer, [^{68}Ga]DO3AP^{BP}.(19,34) Differences between the *ex-vivo* biodistributions and μPET images (below) might be given by a different age of the animal (see Experimental).

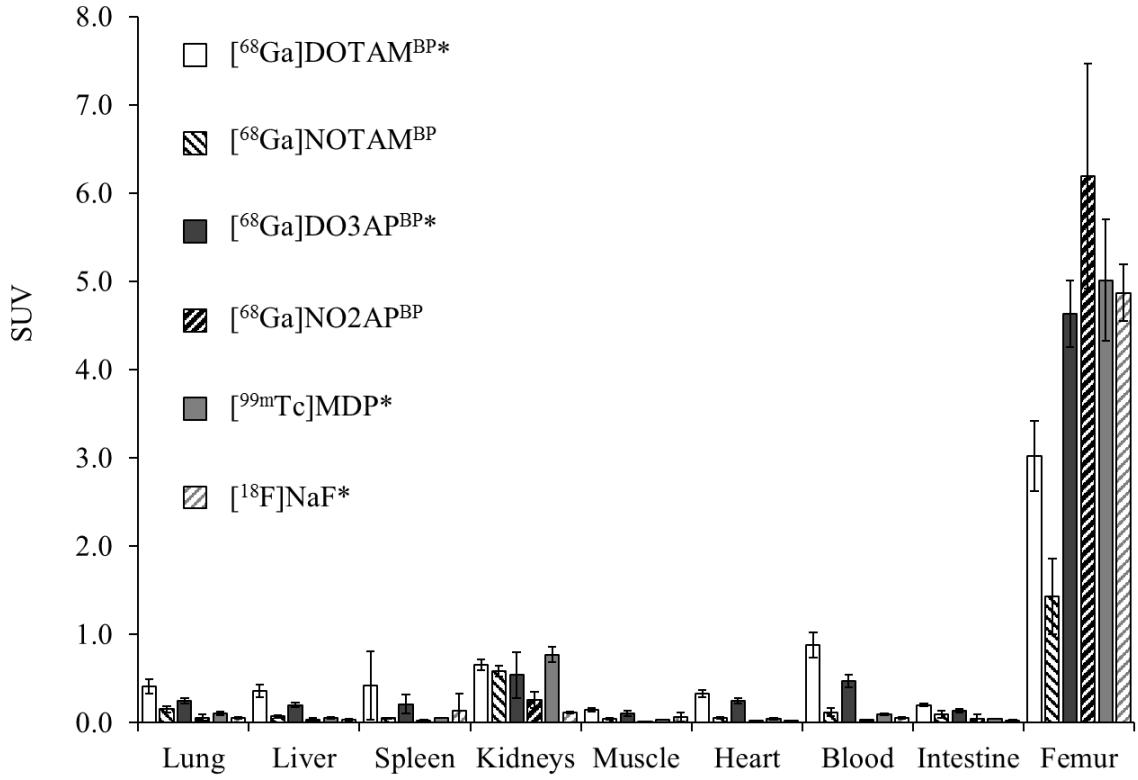

Figure 9. Biodistribution data for different bone-binding ^{68}Ga radiotracers and [^{18}F]NaF in healthy male Wistar rats (n = 5) after 60 min. p.i. *Data for [^{68}Ga]DOTAM^{BP}, [^{68}Ga]DO3AP^{BP}, [^{18}F]NaF and [^{99m}Tc]MDP (for MDP formula, see Figure 1) were taken from literature (19,34). Results for NOTAM^{BP} can be influenced by the amide bond hydrolysis (for details, see text).

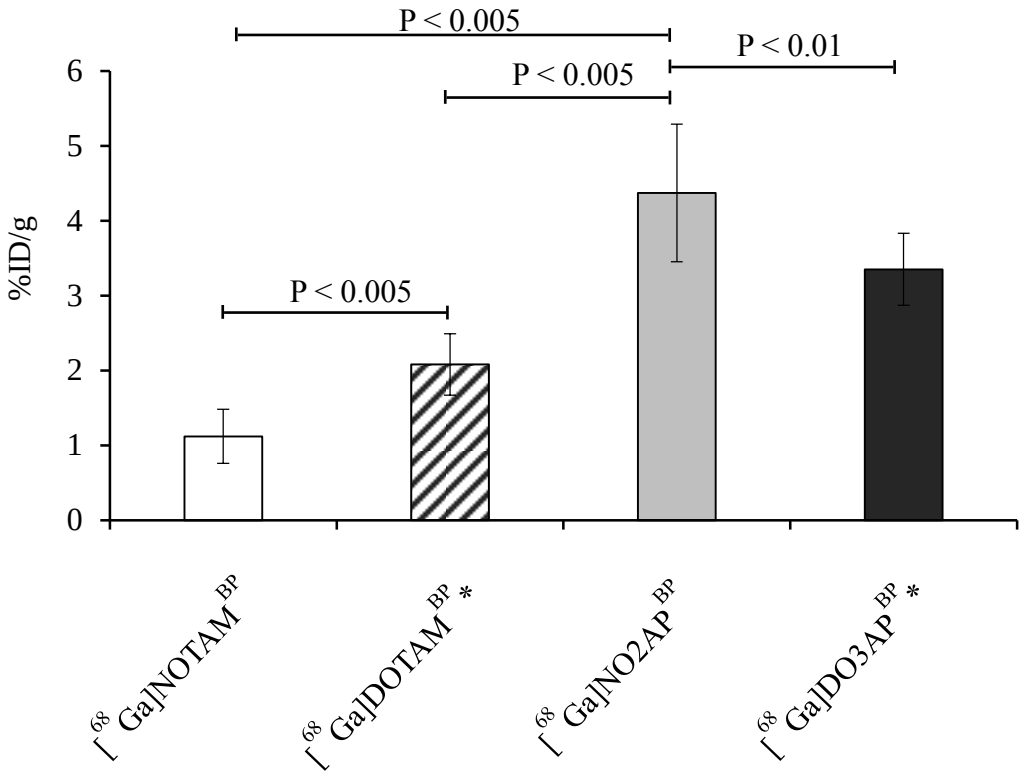

Figure 10. Radioactivity accumulation on femur for [^{68}Ga]NOTAM^{BP}, [^{68}Ga]DOTAM^{BP}, [^{68}Ga]NO2AP^{BP} and [^{68}Ga]DO3AP^{BP} (60 min p.i.). *Data for [^{68}Ga]DOTAM^{BP} and [^{68}Ga]DO3AP^{BP} were taken from literature (19,34). Results for NOTAM^{BP} can be influenced by the amide bond hydrolysis (for details, see text).

To illustrate usefulness of the [^{68}Ga]NO2AP^{BP} as PET tracer, its biodistribution as followed by µPET with two animals. Uptake on bone was observed within few minutes and the labeled compound were cleared out of the blood during 60–120 min via the kidneys and bladder. The µPET images (Figure 11) show a fast clearance of the compound out from the blood. After 5–10 min, only 10–15 % of the injected radiotracer is found in the bloodstream, while a very fast accumulation in the skeleton was observed. Bone images of good quality can be developed at early time points. In Figures 11 and S8, the skeleton is clearly highlighted after only 15 min p.i. In the second animal (Figure 11), the kidneys show a high uptake as the main clearance organ of the [^{68}Ga]NO2AP^{BP} as expressed by SUV values in Figures S9 and S10.

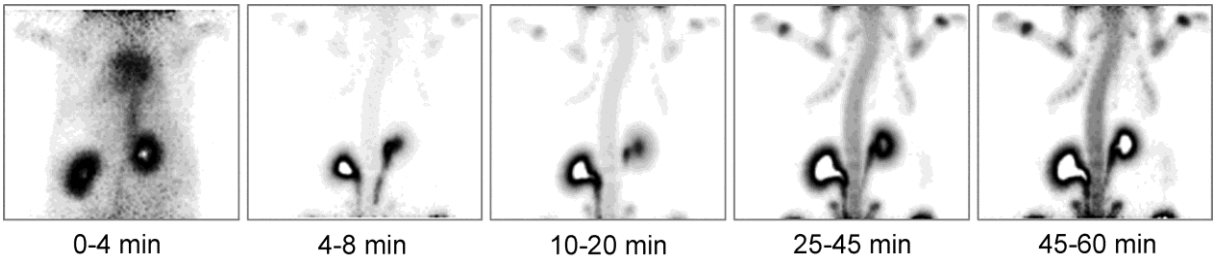

Figure 11. µPET image of the 2nd healthy male Wistar rat at different times after injection of 31 MBq [^{68}Ga]NO2AP^{BP}.

After a fast initial accumulation (up to 50 min. p.i.), the labeled compound is predominantly cleared to the bladder and washed out of the animal *via* the urine. [^{68}Ga]NO2AP^{BP} showed a similar kinetics in both animals with only small differences which could be explained by variation between the animals weight and age. At 60 min p.i., the SUV in the spine was 1.8 for animal no. 1 (536 g, 32 MBq)) and 1.6 for animal no. 2 (346 g, 31 MBq). Uptake of the ^{68}Ga-bis(phosphonate) in bone joints was almost 50 % higher (animal no. 1, SUV in the joint of the scapula and the humerus was 3.1).

3. Conclusions

The new bis(phosphonate)-containing derivatives of NOTA were prepared by scaleable synthesis. They show efficient complexation of trivalent gallium and the phosphinate derivative was shown to bind the metal ion better than the acetamide derivative under any conditions used. The complexation rates of these new ligands were lower than those of NOTA or its phosphinic acid analogues due to presence of phosphonate groups forming rather stable *out-of-cage* complex which is able to compete with formation of the *in-cage* complex. The amide group in the *in-cage* complex is not fully hydrolytically stable due to a strong polarizing effect of the small Ga^{3+} ion after its coordination; thus, ^{68}Ga-NOTAM^{BP} cannot be used in practice. These results indicate that complexes of NOTA-amides can be hydrolytically unstable, unlike complexes of DOTA-amides where analogous hydrolysis has

not been observed. It should be taken into account while designing new ligands for Ga(III) and other highly charged metal ions. Thus, if NOTA skeleton with tri acetate pendants is required, NOTAGA derivatives might be good solution avoiding the hydrolysis problem. The hydrolysis takes place only at high temperature and is rather slow; however, it can occur even during labelling with n.c.a. ^{68}Ga. Radiolabeling with ^{68}Ga was fast at temperatures above 60 °C for the phosphinate and at 90 °C for the acetamide ligand. Biodistribution and μPET studies in healthy male rats showed very quick uptake of the ^{68}Ga-labeled probes on bones and fast elimination of the non-targeted probes through the kidneys. The pharmacokinetics of the new labeled macrocyclic ligands is similar to that of the labeled DOTA-bis(phosphonate) conjugates as well as that of commonly used ^{99m}Tc-bis(phosphonate) radiopharmaceuticals or [^{18}F]NaF but results in a significant higher accumulation of [^{68}Ga]NO2AP^{BP} on bone. [^{68}Ga]NO2AP^{BP} showed a superior adsorption kinetics compared to that of other ^{68}Ga-labeled macrocyclic bis(phosphonates) and a similar affinity HAP as [^{68}Ga]EDTMP; however, [^{68}Ga]EDTMP was reported as an inefficient radiotracer based on its low kinetic and thermodynamic *in vivo* stability (51). Additionally, the new ligands performed in an almost quantitative labeling (RCY more than 98 %) within 10 to 15 min with NO2AP^{BP} being labeled more effectively, while the DOTA-based bis(phosphonates) showed a RCY between 70 % and 85 % and purification steps are necessary before applications. For the routine synthesis in nuclear medicine practice, easy labeling processes and high RCY are essential. These properties and the convenient availability of ^{68}Ga from commercial generators render mainly NO2AP^{BP} as one of the best leading compounds for development of bone-targeted PET probes.

These new ^{68}Ga-based radiotracers bring improvement of a current state-of-art for bone imaging due to much better resolution and sensitivity of PET if compared with SPECT and much lower price of the generator-produced ^{68}Ga radioisotope if compared with cyclotron-produced ^{18}F. Despite that no ^{68}Ge/^{68}Ga generator has been approved, easy operation of the generator and its continuously lowering prizes make the ^{68}Ga-PET based bone scans possibly the most easily implementing PET modality in less developed countries without expensive cyclotrons and skilled staff. Experiments focused on better understanding of biological fate and, finally, directed to a human application of the new probe are under way.

4. Experimental

4.1. General methods

Reagents **5** and **7**, and ligands $DOTAM^{BP}$ and $DO3AP^{BP}$ were synthesized according to published procedures (12,14). The 1,4,7-triazacyclononane (tacn) as free base was purchased from CheMatech (France). The other reactants and solvents were commercially available analytical grade chemicals. Acetonitrile was dried by distillation from P_2O_5. The NMR spectra were recorded using Varian UNITY Inova (400 MHz), Varian VNMRS (300 MHz) or Bruker Avance (600 MHz) spectrometers. The ^{1}H and ^{13}C (at 300 or 600 and 75 or 151 MHz, respectively) NMR shifts were referenced to internal TMS or *t*-BuOH signal, the ^{31}P (121 MHz) and ^{71}Ga (129 MHz) NMR shifts were externally referenced relative to 85 % aq. H_3PO_4 and 0.1 M aq. $Ga(NO_3)_3$, respectively. Homo- and heteronuclear 2D-NMR spectra were used for final characterization of the title ligands. Mass spectra were recorded on Bruker Esquire 3000 spectrometer with ESI as ion source and ion trap as a detector in positive or negative modes. UV-Vis spectra were recorded using Biochrom Lightwave 2 spectrometer. Elemental analyses were performed using an HARAEUS Varian EL III system. TLC analyses of the ligand and intermediates during their synthesis were carried out with silica on aluminium foil (Merck). Radio-TLC analysis was developed with a Canberra Packard Instant Imager. Radioactivity of samples was measured with an Aktivimeter Isomed 2010, MED (Nuklear-Medizintechnik Dresden GmbH). For small animal PET studies, a Siemens microPET Focus 120 was used and the data were reconstructed with the Pmod software (PMOD Technologies Ltd). Radioactivity in tissue samples was determined by using a Wallac WIZARD2 automatic gamma counter (Perkin Elmer, Germany).

4.2. Synthesis of 1-benzyl-1,4,7-triazacyclononane (2)

1,4,7-triazacyclononane (5.0 g, 39.9 mmol) was dissolved in the mixture of 1,4-dioxane (50 ml) and $Me_2NCH(OMe)_2$ (5.52 g, 47.9 mmol). The mixture was refluxed for 3 h, volatiles were evaporated and the residue was re-dissolved in THF (40 ml). Solution of benzylbromide

(8.6 g, 47.9 mmol) in THF (40 ml) was added slowly under vigorous stirring and a yellow precipitate was formed. Then more THF (30 ml) was added and the mixture was stirred overnight. The yellow powder was filtered off and dissolved in a mixture of water (25 ml), EtOH (50 ml) and KOH (12.5 g). The mixture was refluxed for 3 d. Volatiles were evaporated under reduced pressure, the residue was dissolved in water (20 ml) and extracted with chloroform (3×40 ml). The organic fractions containing the product were combined, dried with Na_2SO_4 and solvent was evaporated. The residue was dissolved in aq. HCl (6 M, 20 ml) and the solution was evaporated to dryness. The crude hydrochloride was dissolved in water (10 ml) and it was crystallized by addition of Et_2O (100 ml). The product was filtered off and dried under vacuum to yield white crystals of **2**·2HCl·H_2O (8.5 g, 75 %). NMR (D_2O): ^{1}H δ = 3.07 (C*H*$_2$–NBn, 4H, t, $^3J_{HH}$ 6.0 Hz); 3.25 (C*H*$_2$–CH_2NBn, 4H, t, $^3J_{HH}$ 6.0 Hz; 3.65 (NH–C*H*$_2$C*H*$_2$–NH, 4H, s); 3.95 (N–C*H*$_2$–C$_{ar}$, 2H, s); 7.47 (aryl H, 5H, bm); ^{13}C{^{1}H} δ = 44.8 (*C*H$_2$–CH$_2$NBn, s); 46.1 (NH–*C*H$_2$*C*H$_2$–NH, s); 50.2 (*C*H$_2$–NBn, s); 61.6 (N–*C*H$_2$–C, s); 130.9, 131.4, 132.8, 137.8 (aryl *C*, 4×s). MS(+): 219.9 $[M+H]^+$. Elemental analysis: found (calcd. for $C_{13}H_{21}N_3$·2HCl·H_2O) C 51.1 (50.3); H 8.4 (8.1); N 13.4 (13.5).

4.3. Synthesis of bis(*t*-butyl) 7-benzyl-1,4,7-triazacyclononane-1,4-diacetate (3)

Protected macrocycle **2** (3.0 g, 9.7 mmol) was dissolved in the mixture of dry acetonitrile (100 ml) and K_2CO_3 (5.17 g, 38.8 mmol). Solution of *t*-butyl bromoacetate (3.96 g, 20.4 mmol) in dry acetonitrile (150 ml) was slowly added. The reaction mixture was stirred at room temperature for 3 d, then filtered and evaporated. Product was purified by column chromatography (silica gel, EtOH : 25 % aq. ammonia 20:1). The fractions containing product were combined and evaporated to yield of product **3** (4.2 g, 91 %) in the form of yellowish viscous oil. NMR ($CDCl_3$): ^{1}H δ = 1.40 (C(C*H*$_3$)$_3$, 18H, s); 2.73, 3.10, 3.50, 3.70 (N–C*H*$_2$C*H*$_2$–N, 6H + 2H + 2H +2H; 4×bm); 3.28 (N–C*H*$_2$–CO$_2$, 4H, s); 4.49 (N–C*H*$_2$–C$_{ar}$, 2H, s); 7.34 + 7.66 (aryl H, 3H + 2H, 2×m); ^{13}C{^{1}H} δ = 30.3 (C(*C*H$_3$)$_3$, s); 51.9 + 53.7 + 55.1 (ring C, 3×s); 60.3 (N–*C*H$_2$–CO$_2$, s); 61.6 (N–*C*H$_2$–C, s); 83.9 (*C*(CH$_3$)$_3$, s); 131.3, 131.7, 133.0 (aryl C, 3×s); 172.8 (*C*O$_2$, 2C, s). MS(+): 448.1 $[M+H]^+$.

4.4. Bis(*t*-butyl) 1,4,7-triazacyclononane-1,4-diacetate (4)

Compound **3** (2.1 g, 4.7 mmol) was dissolved in dry ethanol (175 ml). Pd/C catalyst (400 mg) was added and the reaction mixture was stirred overnight at 50 °C under hydrogen atmosphere (atmospheric pressure). Suspension was filtered and filtrate evaporated to dryness. The crude product was purified by column chromatography (silica gel, EtOH : 25 % aq. ammonia 10:1 to elute impurities and 3:2 to eluate the product). The product-containing fractions were combined, evaporated and the residue was co-distilled three times with ethanol to remove traces of ammonia to yield colorless viscous oil that solidified after cooling to room temperature (1.41 g, 84 %). NMR ($CDCl_3$): ^{1}H δ = 1.41 (C(C*H*$_3$)$_3$, 18H, s); 2.81 (N(ac)–C*H*$_2$C*H*$_2$–N(ac), 4H, s); 3.08 (N(ac)–C*H*$_2$CH$_2$–NH, 4H, bm); 3.23 (N(ac)–CH$_2$C*H*$_2$–NH, 4H, bm); 3.39 (N–C*H*$_2$–CO$_2$, 4H, s); ^{13}C{^{1}H} δ = 20.1 (C(*C*H$_3$)$_3$, s); 44.5 (N(ac)–CH$_2$*C*H$_2$–NH, s); 49.0 (N(ac)–*C*H$_2$CH$_2$–NH, s); 51.7 (N(ac)–*C*H$_2$*C*H$_2$–N(ac), s) 56.7 (N–*C*H$_2$–CO$_2$, s); 81.9 (*C*(CH$_3$)$_3$, s); 170.7 (*C*O$_2$, s). MS(+): 358.0 $[M+H]^+$.

4.5. NOTAM^{BP} in ester form (6)

Ester **4** (1.30 g, 3.6 mmol) was dissolved in the mixture of dry acetonitrile (75 ml) and annealed K_2CO_3 (2.60 g). Then, solution of chloroacetamide **5** (2.07 g, 5.4 mmol) in acetonitrile (75 ml) was added. The reaction mixture was stirred at 50 °C for 3 d. Solids were filtered off, filtrate was evaporated and the crude product was purified by column chromatography (silica gel, EtOH to elute impurities, EtOH : 25 % aq. NH_3 50:1 to elute product). Pure product was obtained as yellowish viscous oil (2.1 g, 83 %). NMR ($CDCl_3$): ^{1}H δ = 1.28 (P–OCH$_2$C*H*$_3$, 12H, t, $^3J_{HH}$ 7.2 Hz); 1.39 (C(C*H*$_3$)$_3$, 18H, s); 2.71 (N$_{(ac)}$–C*H*$_2$C*H*$_2$–N$_{(ac)}$, 4H, bm); 2.84 (N$_{(ac)}$–C*H*$_2$C*H*$_2$–N$_{(am)}$, 8H, s); 3.29 (NC*H*$_2$CONH, 2H, s); 3.35 (NC*H*$_2$CO$_2$, 4H, s); 4.14 (P–OC*H*$_2$CH$_3$, 8H, m); 5.06 (NH–C*H*–P, 1H, td, $^2J_{PH}$ 21.2 Hz, $^3J_{HH}$ 7.5 Hz); 8.90 (N*H*, 1H, d, $^3J_{HH}$ 6 Hz);^{13}C{^{1}H} δ = 16.3 (P–OCH$_2$*C*H$_3$, s); 28.1 (C(*C*H$_3$)$_3$, s); 43.6 (NH–*C*H–P, t, $^1J_{PC}$ 148 Hz); 55.3 (N$_{(ac)}$–*C*H$_2$*C*H$_2$–N$_{(ac)}$, s); 56.3 (N$_{(ac)}$–*C*H$_2$*C*H$_2$–N$_{(am)}$, s); 59.2 (N–*C*H$_2$–CO$_2$, s); 60.9 (N–*C*H$_2$–CO$_2$, s); 63.2 (P–O*C*H$_2$CH$_3$, d, $^2J_{PC}$ = 10.0 Hz); 80.7

(*C*(CH_3)$_3$, s); 171.7 (*C*O_2, s); 172.2 (*C*O, s); $^{31}P\{^1H\}$ δ (ppm) 17.2 (s); ^{31}P δ = 17.2 (d, $^2J_{PH}$ 21.2 Hz); MS(+): 701.4 $[M+H]^+$.

4.6. NOTAM^{BP}

Ester **6 (**2.1 g, 3.0 mmol) was dissolved in the mixture of $CHCl_3$ (50 ml) and CF_3CO_2H (50 ml) and stirred in dark at room temperature overnight. Volatiles were evaporated under vacuum and the residue was repeatedly dissolved in CH_2Cl_2 and evaporated. The resulting oil was dissolved in dry acetonitrile (100 ml) and $BrSiMe_3$ (9.8 ml, 60.0 mmol) was added. The mixture was stirred in dark at room temperature overnight. Volatiles were evaporated, the residue was re-dissolved in acetonitrile and evaporated, and then dissolved in 50 % aq. MeOH and evaporated. The residue was dissolved in H_2O (10 ml) and EtOH (100 ml) was added. Crystallization was finished standing in refrigerator overnight. Product was filtered off and dried under vacuum to yield white powder (1.15 g, 80 %). NMR (D_2O, pD 2.9): ^1H δ = 3.34 ($N_{(ac)}$–CH_2CH_2–$N_{(am)}$, 4H, s); 3.38 ($N_{(ac)}$–CH_2CH_2–$N_{(am)}$, 4H, s); 3.46 ($N_{(ac)}$–CH_2CH_2–$N_{(ac)}$, 4H, s); 3.89 (N–CH_2–CO_2, 4H, s); 3.94 (N–CH_2–CO–NH, 2H, s); 4.51 (NH–C*H*–P, t, $^2J_{PH}$ 24.0 Hz); $^{13}C\{^1H\}$ δ = 47.8 (NH–*C*H–P, t, $^1J_{PC}$ 125.6 Hz); 50.3 ($N_{(ac)}$–CH_2CH_2–$N_{(ac)}$, s); 50.5 ($N_{(ac)}$–CH_2CH_2–$N_{(am)}$, s); 50.7 ($N_{(ac)}$–CH_2CH_2–$N_{(am)}$, s); 57.5 (N–CH_2–CO_2, s); 57.9 (N–*C*H_2–CO–NH, s); 169.2 (*C*O–NH, s); 172.5 (*C*O_2, s); $^{31}P\{^1H\}$ δ (ppm) 12.7 (s); ^{31}P δ = 12.7 (CH–*P*, d, $^2J_{HP}$ 24.0 Hz). MS(–): 474.8 $[M–H]^–$. Elemental analysis: found (calcd. for $C_{13}H_{26}N_4P_2O_{11}\cdot 1.5H_2O\cdot 0.4HCl$) C 30.0 (30.1); H 5.3 (5.7); N 10.4 (10.8).

4.7. NO2AP^{BP} in ester form (8)

Ester **4** (1.55 g, 4.3 mmol) was dissolved in the mixture of dry acetonitrile (40 ml) and paraformaldehyde (156 mg, 5.2 mmol). Solution of phosphinate **7** (2.05 g, 5.2 mmol) in acetonitrile (30 ml) was added and the mixture was stirred at 35 °C for 3 d. Volatiles were evaporated and the crude product was purified by column chromatography (silica gel, EtOH to elute impurities, EtOH : 25 % aq. ammonia 50:1 to eluate the product). The product-

containing fractions were combined and evaporated to yield yellowish oil (2.40 g, 72 %). NMR ($CDCl_3$): ^1H δ = 1.31 (P–OCH_2CH_3, 15H, m); 1.46 ($C(CH_3)_3$, 18H, s); 2.00–2.80 (PCH_2, PCH, 5H, m); 2.90–3.20 (ring H, 12H, m); 3.56 (N–CH_2–CO_2, 4H, s); 4.18 (P–OCH_2CH_3, 10H, m); $^{13}C\{^1H\}$ δ = 20.5 (CH–P–O–CH_2–CH_3, s); 26.2 (PCH_2CHP, d, $^1J_{PC}$ 82.9 Hz); 32.3 ($C(CH_3)_3$, s); 34.1 (PCH_2CHP, td, $^1J_{PC}$ 132.1 Hz, $^2J_{PC}$ 26.9 Hz); 58.8, 59.2, 60.6 (N–CH_2CH_2–N, ring C, 3×s); 62.1 (N–CH_2–CO_2, s) 64.1 (NCH_2P, d, $^1J_{PC}$ 95.1 Hz); 67.0 (P–OCH_2CH_3, s); 85.1 ($C(CH_3)_3$, s); 174.9 (CO_2, s) $^{31}P\{^1H\}$ δ = 22.7 (PCH_2CHP, 2P, d, $^3J_{PP}$ 20.8 Hz); 49.2 (PCH_2CHP, 1P, t, $^3J_{PP}$ 20.8 Hz). MS(+): 764.4 $[M+H]^+$.

4.8. NO2AP^{BP}

Ester **8 (**2.40 g, 3.1 mmol) was dissolved in the mixture of $CHCl_3$ (50 ml) and CF_3CO_2H (50 ml) and stirred in dark at room temperature overnight. Volatiles were evaporated under vacuum and the residue was repeatedly dissolved in CH_2Cl_2 and evaporated. The resulting oil was dissolved in dry acetonitrile (100 ml) and $BrSiMe_3$ (9.8 ml, 60.0 mmol) was added. The mixture was stirred in dark at room temperature overnight. Volatiles were evaporated and the residue was re-dissolved in acetonitrile and evaporated, and then dissolved in 50 % aq. MeOH and evaporated. The crude product was purified using strong cation exchanger (Dowex 50, H^+-form). Impurities were eluted with H_2O, product with 10 % aq. pyridine. Pyridine was then removed using strong anion exchanger (Dowex 1, OH^--form). Impurities were eluted with H_2O and EtOH 1:1 mixture, product with H_2O and HCl mixture 1:1. The product-containing fractions were combined and evaporated. The resulting solid was dissolved in H_2O (10 ml) and EtOH (100 ml) was added to induce crystallization. Crystallization was finished on standing in refrigerator overnight. Product was filtered off and dried under vacuum to yield white powder (0.66 g, 41 %). NMR (D_2O, pD 2.9): ^1H δ = 2.26 (PCH_2CHP, 2H, m); 2.46 (PCH_2CHP, 1H, m); 3.42 ($N_{(ac)}$–CH_2CH_2–$N_{(ac)}$, 4H, s); 3.50 ($N_{(ac)}$–CH_2CH_2–$N_{(bp)}$, 4H, s); 3.56 ($N_{(ac)}$–CH_2CH_2–$N_{(bp)}$, 4H, s) 3.79 (NCH_2P, 2H, bs) 3.88 (N–CH_2–CO_2, 4H, s); $^{13}C\{^1H\}$ δ = 28.2 (PCH_2CHP_2, d, $^1J_{PC}$ 93.5 Hz); 34.2 (PCH_2CHP_2, t, $^1J_{PC}$ 117.7 Hz); 50.6 ($N_{(ac)}$–CH_2CH_2–$N_{(bp)}$, s); 51.7 ($N_{(ac)}$–CH_2CH_2–$N_{(ac)}$, s); 52.5 ($N_{(ac)}$–CH_2CH_2–$N_{(bp)}$, s); 56.7 (NCH_2P, d, $^1J_{PC}$ 90.6 Hz); 58.0 (N–CH_2–CO_2, s); 173.3 (CO_2, s);

$^{31}P\{^{1}H\}$ δ = 18.9 (PCH_2CHP, 2P, d, $^{3}J_{PP}$ 24.6 Hz); 33.1 (PCH_2CHP, 1P, t, $^{3}J_{PP}$ 24.6 Hz). MS (–): 509.8 $[M–H]^{-}$. Elemental analysis: found (calcd. for $C_{13}H_{28}N_3P_3O_{13}·0.6HCl$) C 29.4 (29.3); H 5.4 (5.4); N 7.3 (7.9).

4.9. Stock solutions of Fe(III) complexes

Ligand (100 μmol) was dissolved in the aq. $FeCl_3$ solution (90 μmol, 0.9 ml of 0.1 M solution), pH was slowly adjusted to 7 with 0.5 M aq. NaOH (precipitates may appear in this stage) and the solution was stirred at 80 °C for 1 h. Finally, water was added to reach the final volume of 10.0 ml.

4.10. Adsorption experiments

Hydroxyapatite (50 mg; Fluka, catalog No. 55496, 63 $m^2\ g^{-1}$) was suspended in 1 M Tris-HCl buffer (0.30 ml; pH 7.5). Then, stock solution of the Fe(III) complex (10 mM, 0.06 to 0.60 ml) was added and the samples were diluted with water to get final volume of 3.0 ml. The samples were stirred at 25 °C for 3 d. After filtration, concentration of the complex in the supernatant was quantified by UV-Vis spectroscopy. The experimental data obtained at 250, 275 and 300 nm were treated by least-square fitting (Micromath Scientist software package) according to the Langmuir adsorption isotherm.

4.11. $^{31}P\{^{1}H\}$ and ^{71}Ga NMR complexation studies

Solid $NOTAM^{BP}$ (25 mg, 51 μmol) was dissolved in 338 μL of 1 M aq. sodium chloroacetate buffer (experiments at pH 2 and pH 3) or 1 M aq. sodium acetate buffer (experiments at pH 4 and 5) and equivalent amount of Ga(III) (62 μL of 0.812 M solution) was added. For $NO2AP^{BP}$, the amounts were: 25 mg of the solid ligand, 343 μL of buffer and 57 μL of 0.812 M Ga(III) solutions, respectively. Samples were shaken and quickly transferred into a standard 5-mm NMR cuvette and measured immediately (overall dead time was ~5 min) or

left in an oil bath at the appropriate temperature for the given amount of time. Then, they were quickly cooled down to room temperature, NMR spectrum was measured at 25 °C and heating was resumed again if necessary. Quantification was done against ^{31}P or ^{71}Ga NMR standard in the insert tube. The times given in the text are those which the samples had spent at the given temperature.

4.12. Radiolabeling studies

Gallium-68 (150 to 350 MBq) was obtained from a ^{68}Ge/^{68}Ga generator system (Eckert&Ziegler AG, Berlin). For *in vivo* experiments, ^{68}Ga labeling was performed in aq. HEPES buffer solution (pH = 4, 0.125 M, 400 μL) by adding the ^{68}Ga solution (400 μL) obtained by post-processing of the generator eluate *via* the cation exchange method (52); final pH of the solution was pH = 3.75. Then, the ligand (17 nmol, as stock solution with a concentration of 1 mg/ml) was added and the solution was shaken in a heating block for 10 min at 95 °C. After cooling, the pH was adjusted to pH = 7 by adding small amounts of 1 M aq. NaOH solution. Radiochemical yields of the ^{68}Ga-complexes of the title ligands were 95–99 %. For labeling studies under various pH conditions, the labeling was carried out in deionized water (pure for pH = 2) or by adding smaller amounts of the buffer solution (i.e. decreasing buffer capacity of the final solution) to get the appropriate final pH. The radiochemical yields were determined by silica TLC (Merck) using a solvent mixture consisting of 2 parts of A (conc. aq. HCl: acetone: water, 100 μL : 1 ml : 1 ml) and 1 part of B (pure acetylacetone). Activity was measured on a Canberra Packard Instant Imager. Free ^{68}Ga migrates as an acetylacetonate complex with the solvent front. *In-cage* complexes stay on the base line. (^{68}Ga-phosphonates: R_f = 0.0–0.1, ^{68}Ga-acac: R_f = 0.8–0.9; for details, see ESI). The radiochemical yields were also determined by radio-HPLC (Merck-Hitachi-LaChrom, Gabi-Raytest) using a LiChrosphere C18 (CS-Chromatographie, Germany) column. The reaction solution (10 μL) was added to a 50 μL of Deferoxamine (DFO) solution (0.1 mg/ml) in 0.1 M NaAc buffer (pH=4.0). ^{68}Ga labelled bis(phosphonates) showed a weak retention, while [^{68}Ga]DFO showed a R_t of 10 min (Figures S11–S13). The [^{68}Ga]NOTA and [^{68}Ga]DOTA complexes were synthesized with the method described

above by using 10 µg of each chelator. The [^{68}Ga]DO3AP^{BP} was labeled with ^{68}Ga with a different method. DO3AP^{BP} was dissolved in deioinized water with a concentration of 1 mg/ml. This solution (17 µL, i.e. 17 µg DO3AP^{BP}) was added to a 0.25 M ammonium acetate buffer (500 µL, pH = 5). The post-processed ^{68}Ga solution (400 µL) was added and the mixture was shaken in a heating block for 20 min. Labeling at lower pHs was carried out by using less concentrated buffer solutions. Labeling at pH = 1–2 was done by using deionized water as the reaction solvent.

4.13. Evaluation of hydrolysis during radiolabeling

Radiolabeling was done as described above (95 °C, pH 4.5, 15 min) and the solution was analysed by HPLC with Merck-Hitachi Lachrom equipment, Raytest Gabi radiodetector and Nucleosil 100-5 NH_2 phase in 125×4.6-mm column. Elution: 0–30 min 100 % 0.1 M aq. NaH_2PO_4 (pH 4.5), 31–60 min 100 % 0.1 M aq. Na-citrate (pH 4.5) and 60–65 min 100 % 0.1 M aq. NaH_2PO_4 (pH 4.5).

4.14. Binding studies of ^{68}Ga-ligand complexes on hydroxyapatite

HAP (20 mg, Sigma-Aldrich, reagent grade powder) was incubated in isotonic saline (1 ml) for 24 h. The test was performed by the addition of 50 µL of the ^{68}Ga-bis(phosphonates) solution (prepared as given above) to the HAP suspension. After vortexing for 10 s, the suspension was incubated for 10 min at room temperature. The samples were centrifuged and the supernatant was removed. The HAP fraction was washed with isotonic saline (0.5 ml). The ^{68}Ga radioactivity in the combined liquids and that of the HAP fraction were measured in a curiemeter (Aktivimeter Isomed 2010, MED Nuklear-Medizintechnik Dresden GmbH). ^{68}Ga-complex binding to HAP was determined as percent of ^{68}Ga absorbed to HAP (53).

4.15. Animals, feeding, husbandry, and animal preparation

The experiments were conducted according to institutional guidelines and the German animal welfare regulations. The experimental procedure used conforms to the European Convention for the Protection of Vertebrate Animals used for Experimental and other Scientific Purposes (ETS No. 123) and to the Deutsches Tierschutzgesetz. Male Wistar rats (Charles River Laboratories International, Inc) weighing 130 ± 15 g (mean ± SD, n = 10) for *ex vivo* organ distribution, 536 g and 346 g for µPET-imaging (n = 2) were anesthetized with isoflurane. Animals were put in the supine position and placed under a infra-red lamp to maintain body temperature.

4.16. Biodistribution studies

Biodistribution studies were performed in male Wistar rats (120–140 g). Each study group contained 5 rats. The rats were injected intravenously, each with ^{68}Ga-labeled compound in saline (0.5 ml); for [^{68}Ga]NO3AP^{BP} 13.5±5.8 MBq, BW 142±3 g; for [^{68}Ga]NOTAM^{BP}, 10.5±1.9 MBq, BW 128±7 g. Animals were sacrificed at 60 min after injection. Organs and tissues of interest were excised rapidly, weighted, and the radioactivity was determined using a Wallac WIZARD2 automatic gamma counter (Perkin Elmer, Germany). The activity of the tissue samples was decay- and background-corrected.

4.17. Small animal µPET

In vivo small animal µPET imaging of male Wistar rats (350–550 g) was carried out under general anesthesia of the rats that was induced with inhalation of 10 % and maintained with inhalation 6.5 % isoflurane in 30 % oxygen/air. Rats were positioned supine to the scanner (Siemens microPET Focus 120). In the µPET experiments, [^{68}Ga]NO2AP^{BP} (32 MBq for the 1st animal, 536 g and 31 MBq for the 2nd animal, 346 g in isotonic saline (0.5 ml) was administered intravenously using a needle catheter into the tail vein. No correction for partial volume effects was applied. The image volume data were converted to Siemens ECAT7

format for further processing. The image files were then processed using the Pmod software (PMOD Technologies Ltd).

4.18. Statistical analysis.

All data were expressed as mean ± SD. Groups were compared using the t-test. All statistical tests were two tailed, with a *P*-value of less than 0.05 representative for significance, except the comparison of [^{68}Ga]NO2AP^{BP}and [^{68}Ga]EDTMP in the HAP-binding experiment, which showed a *P*-value of $P = 0.052$. No differences were observed for [^{68}Ga]NO2AP^{BP} and [^{68}Ga]DO3AP^{BP} in the HAP-binding experiment ($P = 0.7$); for the values, see SI (Table S1).

5. Acknowledgment

Support from the Grant Agency of the Czech Republic (13-08336S), the Grant Agency of the Charles University in Prague (No. 19310) and the Long-Term Research Plan of the Ministry of Education of the Czech Republic (No. MSM0021620857) is acknowledged. The work was carried out in the framework of COST TD1004 and TD1007 Actions. We are grateful to Nicole Bausbacher and Barbara Biesalski (Mainz Universiy) for performing the animal experiments.

6. References

[1] Rösch F, Riss PJ. The renaissance of the ^{68}Ge/^{68}Ga radionuclide generator initiates new developments in ^{68}Ga radiopharmaceutical chemistry. *Curr. Top. Med. Chem*. **2010**; 10: 1633–1668.

[2] Fani M, André JP, Mäcke HR. ^{68}Ga-PET: A powerful generator-based alternative to cyclotron-based PET radiopharmaceuticals. *Contrast Media Mol. Imaging* **2008**; 3: 53–63.

[3] Wadas TJ, Wong EH, Weisman GR, Anderson CJ. Coordinating radiometals of copper, gallium, indium, yttrium, and zirconium for PET and SPECT imaging of disease. *Chem. Rev.* **2010**; 110: 2858–2902.

[4] Velikyan I. Positron Emitting [^{68}Ga]Ga-Based Imaging Agents: Chemistry and Diversity. *Med. Chem.* **2011**; 7: 345–372.

[5] Breeman WAP, de Blois E, Chan HS, Konijnenberg M, Kwekkeboom DJ, Krenning EP. ^{68}Ga-labeled DOTA-peptides and ^{68}Ga-labeled radiopharmaceuticals for Positron Emission Tomography: Current status of research, clinical applications, and future perspectives. *Semin. Nucl. Med.* **2011**; 41: 314–321.

[6] Bartholomae MD. Recent developments in the design of bifunctional chelators for metal-based radiopharmaceuticals used in Positron Emission Tomography. *Inorg. Chim. Acta* **2012**; 389: 36–51.

[7] Banerjee SR, Pomper MG. Clinical applications of gallium-68. *Appl. Radiat. Isotop.* **2013**; 76: 2–13.

[8] Zhang S, Gangal G, Uludag H. Magic bullets' for bone diseases: progress in rational design of bone-seeking medicinal agents. *Chem. Soc. Rev.* **2007**; 36: 507–531.

[9] Kubíček V, Lukeš I. Bone-seeking probes for optical and magnetic resonance imaging. *Future Med. Chem.* **2010**; 2: 521–531.

[10] Palma E, Correia JDG, Campello MPC, Santos I. Bisphosphonates as radionuclide carriers for imaging or systemic therapy. *Mol. BioSyst.* **2011**; 7: 2950–2966.

[11] Fleisch H. Bisphosphonates in Bone Disease, 4th Ed. Academic Press: London, **2000**.

[12] Kubíček V, Rudovský J, Kotek J, Hermann P, vander Elst L, Muller RN, Kolar ZI, Wolterbeek H T, Peters JA, Lukeš I. A bisphosphonate monoamide analogue of DOTA: A potential agent for bone targeting. *J. Am. Chem. Soc.* **2005**; 127: 16477–16485.

[13] Vitha T, Kubíček V, Hermann P, vander Elst L, Muller RN, Kolar ZI, Wolterbeek HT, Breeman WAP, Lukeš I, Peters JA. Lanthanide(III) complexes of bis(phosphonate) monoamide analogues of DOTA: Bone-seeking agents for imaging and therapy. *J. Med. Chem.* **2008**; *51*: 677–683.

[14] Vitha T, Kubíček V, Kotek J, Hermann P, vander Elst L, Muller RN, Lukeš I, Peters JA. Gd(III) complex of a monophosphinate-bis(phosphonate) DOTA analogue with a high relaxivity. Lanthanide(III) complexes for imaging and radiotherapy of calcified tissues. *Dalton Trans.* **2009**; 3204–3214.

[15] Liu W, Hajibeigi A, Lin M, Rostollan CL, Kovács Z, Öz OK, Sun X. An osteoclast-targeting agent for imaging and therapy of bone metastasis. *Bioorg. Med. Chem. Lett*. **2008**; 18: 4789–4793.

[16] Ogawa K, Kawashima H, Shiba K, Washiyama K, Yoshimoto M, Kiyono Y, Ueda M, Mori H, Saji H. Development of [^{90}Y]DOTA-conjugated bisphosphonate for treatment of painful bone metastases. *Nucl. Med. Biol*. **2009**; 36: 129–135.

[17] Suzuji K, Satake M, Suwada J, Oshikiri S, Ashino H, Dozono H, Hino A, Kasahara H, Minamizawa T. Synthesis and evaluation of a novel ^{68}Ga-chelate-conjugated bisphosphonate as a bone-seeking agent for PET imaging. *Nucl. Med. Biol.* **2011**; 38: 1011–1018.

[18] Fellner M, Baum RP, Kubíček V, Hermann P, Lukeš I, Prasat V, Rösch F. PET/CT imaging of osteoblastic bone metastases with ^{68}Ga-bisphosphonates: first human study. *Eur. J. Nucl. Med. Mol. Imag.* **2010**; 37: 834.

[19] Fellner M, Biesalski B, Bausbacher N, Kubíček V, Hermann P, Rösch F, Thews O. ^{68}Ga-BPAMD: PET-imaging of bone metastases with a generator based positron emitter. *Nucl. Med. Biol.* **2012**; 39: 993–996.

[20] Baum RP, Kulkarni, HR. Theranostics: From molecular imaging using ^{68}Ga labeled tracers and PET/CT to personalized radionuclide therapy - The Bad Berka experience. *Theranostics* **2012**; 2: 437–447.

[21] Vitha T, Kubíček V, Hermann P, Kolar ZI, Wolterbeek HT, Peters JA, Lukeš I. Complexes of DOTA-bisphosphonate conjugates: Probes for determination of adsorption capacity and affinity constants of hydroxyapatite. *Langmuir* **2008**; 24: 1952–1958.

[22] Rill C, Kolar ZI, Kickelbick G, Wolterbeek HT, Peters JA. Kinetics and thermodynamics of adsorption on hydroxyapatite of the [^{160}Tb]terbium complexes of the bone-targeting ligands DOTP and BPPED. *Langmuir* **2009**; 25: 2294–2301.

[23] Heppeler A, Froidevaux S, Mäcke HR, Jermann E, Béhé M, Powell P, Hennig M. Radiometal-labelled macrocyclic chelator-derivatised somatostatin analogue with superb tumour-targeting properties and potential for receptor-mediated internal radiotherapy. *Chem. Eur. J.* **1999**; 5: 1974–1981.

[24] Niu W, Wong EH, Weisman GR, Peng Y, Anderson CJ, Zakharov LN, Golen JA, Rheingold AL. Structural and dynamic studies of zinc, gallium, and cadmium complexes of a dicarboxylate pendant-armed cross-bridged cyclen. *Eur. J. Inorg. Chem*. **2004**; 3310–3315.

[25] Cola NA, Rarig, Jr. RS, Ouellette W, Doyle RP. Synthesis, structure and thermal analysis of the gallium complex of 1,4,7,10-tetraazacyclododecane-*N*,*N'*,*N''*,*N'''*-tetraacetic acid (DOTA). *Polyhedron* **2006**; 25: 3457–3462.

[26] Yang C-T, Li Y, Liu S. Synthesis and structural characterization of complexes of a DO3A-conjugated triphenylphosphonium cation with diagnostically important metal ions. *Inorg. Chem.* **2007**; 46: 8988–8997.

[27] Kubíček V, Havlíčková J, Kotek J, Tircsó G, Hermann P, Tóth É, Lukeš I. Gallium(III) complexes of DOTA and DOTA-monoamide: Kinetic and thermodynamic studies. *Inorg. Chem.* **2010**; 49: 10960–10969.

[28] Šimeček J, Schulz M, Notni J, Plutnar J, Kubíček V, Havlíčková J, Hermann P. Complexation of metal ions with TRAP (1,4,7-TRiazacyclononane Phosphinic Acid) ligands and 1,4,7-triazacyclononane-1,4,7-triacetic acid: Phosphinate-containing ligands as unique chelators for trivalent gallium. *Inorg. Chem.* **2012**; 51: 577–590.

[29] Notni J, Hermann P, Havlíčková J, Kotek J, Kubíček V, Plutnar J, Loktionova N, Riss PJ, Rösch F, Lukeš I. A triazacyclononane-based bifunctional phosphinate ligand for the preparation of multimeric ^{68}Ga tracers for Positron Emission Tomography. *Chem. Eur. J.* **2010**; 16: 7174–7185.

[30] Shetty D, Jeong JM, Ju CH, Kim YJ, Lee J-Y, Lee Y-S, Lee DS, Chung J-K, Lee MC. Synthesis and evaluation of macrocyclic amino acid derivatives for tumor imaging by gallium-68 Positron Emission Tomography. *Bioorg. Med. Chem.* **2010**; 18: 7338–7347.

[31] Shetty D, Choi SY, Jeong JM, Hoigebazar L, Lee Y-S, Lee DS, Chung J-K, Lee MC, Chung YK Formation and characterization of gallium(III) complexes with monoamide derivatives of 1,4,7-triazacyclononane-1,4,7-triacetic acid: A study of the dependency of structure on reaction pH. *Eur. J. Inorg. Chem.* **2010**; 5432–5438.

[32] Hoigebazar L, Jeong JM, Choi SY, Choi JY, Shetty D, Lee Y-S, Lee DS, Chung J-K, Lee MC, Chung YK. Synthesis and characterization of nitroimidazole derivatives for ^{68}Ga-labeling and testing in tumor xenografted mice. *J. Med. Chem.* **2010**; 53: 6378–6385.

[33] de Sá A, Matias ÁA, Prata MIM, Geraldes CFGC, Ferreira PMT, André JP. Gallium labeled NOTA-based conjugates for peptide receptor-mediated medical imaging. *Bioorg. Med. Chem. Lett.* **2010**; 20: 7345–7348.

[34] M. Meckel, M. Fellner, N. Thieme, R. Bergmann, V. Kubicek, F. Rösch, In vivo comparison of DOTA based ^{68}Ga-labelled bisphosphonates for bone imaging in non-tumour models, *Nuclear Medicine and Biology*, **2013**; 40: 823–830.

[35] Blake AJ, Fallis IA, Gould RO, Persons S, Ross SA, Schröder M. Selective derivatisation of azamacrocycles. *J. Chem. Soc., Dalton Trans.* **1996**; 4379–4387.

[36] Huskens J, Sherry AD. Synthesis and characterization of 1,4,7-triazacyclononane derivatives with methylphosphinate and acetate side chains for monitoring free Mg^{II} by ^{31}P and ^{1}H NMR spectroscopy. *J. Am. Chem. Soc.* **1996**; 118: 4396–4404.

[37] Chong H-S, Song HA, Birch N, Le T, Lim S, Ma X. Efficient synthesis and evaluation of bimodal ligand NETA. *Bioorg. Med. Chem. Lett.* **2008**; 18: 3436–3439.

[38] Riss PJ, Kroll C, Nagel V, Rösch F. NODAPA-OH and NODAPA-$(NCS)_n$: Synthesis, ^{68}Ga-radiolabelling and in vitro characterization of novel versatile bifunctional chelators for molecular imaging. *Bioorg. Med. Chem. Lett.* **2008**; 18: 5364–5367.

[39] Shetty D, Choi SY, Jeong JM, Lee JY, Hoigebazar L, Lee Y-S, Lee DS, Chung J-K, Lee MC, Chung YK. Stable aluminium fluoride chelates with triazacyclononane derivatives proved by X-ray crystallography and ^{18}F-labeling study. *Chem. Commun*. **2011**; 47: 9732–9734.

[41] Matczak-Jon E, Videnova-Adrabinska V. Supramolecular chemistry and complexation abilities of diphosphonic acids. *Coord. Chem. Rev*. **2005**; 249: 2458–2488.

[41] Kubíček V, Kotek J, Hermann P, Lukeš I. Aminoalkyl-bis(phosphonates): Their complexation properties in solution and in the solid state. *Eur. J. Inorg. Chem.* **2007**; 333–344.

[42] Broan C, Cox JP, Craig AS, Kataky R, Parker D, Harrison A, Randall AM, Ferguson G. Structure and solution stability of indium and gallium complexes of 1,4,7-triazacyclononanetriacetate and of yttrium complexes of 1,4,7,10-tetraazacyclododecanetetraacetate and related ligands: kinetically stable complexes for use in imaging and radioimmunotherapy. X-Ray molecular structure of the indium and gallium complexes of 1,4,7-triazacyclononane-1,4,7-triacetic acid. *J. Chem. Soc., Perkin Trans. 2* **1991**; 87–99.

[43] André JP, Mäcke HR, Zehnder M, Macko L, Akyel KG. 1,4,7-triazacyclononane-1-succinic acid-4,7-diacetic acid (NODASA): a new bifunctional chelator for radio gallium-labelling of biomolecules. *Chem. Commun.* **1998**; 1301–1302.

[44] Lukeš I, Kotek J, Vojtíšek P, Hermann P. Complexes of tetraazacycles bearing methylphosphinic/phosphonic acid pendant arms with copper(II), zinc(II) and lanthanides(III). A comparison with their acetic acid analogues. *Coord. Chem. Rev.* **2001**; 216&217: 287−312.

[45] Notni J, Šimeček J, Hermann P, Wester H-J. TRAP, a powerful and versatile framework for gallium-68 radiopharmaceuticals. *Chem. Eur. J.* **2011**; 17: 14718–14722.

[46] Šimeček J, Notni J, Zemek O, Hermann P, Wester, H-J. A monoreactive bifunctional triazacyclononane phosphinate chelator with high selectivity for gallium-68. *ChemMedChem* **2012**; 7: 1375–1378.

[47] Šimeček J, Hermann P, Wester, H-J, Notni J. How is ^{68}Ga labeling of macrocyclic chelators influenced by metal ion contaminants in ^{68}Ge/^{68}Ga generator eluates? *ChemMedChem* **2013**; 8: 95–103.

[48] Notni J, Plutnar J, Wester H-J.l Bone-seeking TRAP conjugates: surprising observations and their implications on the development of gallium-68-labeled bisphosphonates. *EJNMMI Res.* **2012**; 2: 13.

[49] Wieghardt K, Bossek U, Chaudhuri P, Herrmann W, Menk BC, Weiss J. 1,4,7-Triazacyclononane-*N*,*N'*,*N''*-triacetate (TCTA), a new hexadentate ligand for divalent and trivalent metal ions. Crystal structures of [Cr^{III}(TCTA)], [Fe^{III}(TCTA)], and Na[Cu^{II}(TCTA)]·2NaBr·8H_2O. *Inorg. Chem.* **1982**; 21: 4308–4314.

[50] Dixon DA, Shang M, Lappin AG. Effects of electronic structure on chiral induction in outer-sphere electron transfer reactions of complexes with the C_3 symmetric ligand, 1,4,7-triazacyclononane-1,4,7-tris[2'(*R*)-2'-propionate]$^{3-}$. *Inorg. Chim. Acta* **1999**; 290: 197–206.

[51] Chang CA, Francesconi LC, Malley MF, Kumar K, Gougoutas JZ, Tweedle MF Synthesis, characterization, and crystal structures of M(DO3A) (M = Fe, Gd) and Na[M(DOTA)] (M = Fe, Y, Gd). *Inorg. Chem.* **1993**; 32: 3501–3508.

[52] Zhernosekov KP, Filosofov DV, Baum RP, Aschoff P, Bihl H, Razbash AA, Jahn M, Jennewein M, Rösch F. Processing of generator-produced ^{68}Ga for medical application. *J. Nucl. Med.* **2007**; 48: 1741–1748.

[53] Fellner M, Riss P, Loktionova N, Zhernosekov KP, Thews O, Geraldes CFGC, Kovács Z, Lukeš I, Rösch F. Comparison of different phosphorus-containing ligands complexing ^{68}Ga for PET-imaging of bone metabolism. *Radiochim. Acta* **2011**; 99: 43–51.

3.4. Bone targeting compounds for PET-imaging and radiotherapy: Bisphosphonate-, pamidronate and zoledronate DOTA conjugates

Bone targeting compounds for PET-imaging and radiotherapy:

Bisphosphonate-, pamidronate and zoledronate DOTA conjugates

Marian Meckel[1], Nicole Bausbacher[2], Barbara Biesalski[3], Vojtěch Kubíček [4], Petr Hermann[4], Matthias Miederer[2] and Frank Rösch[1]

[1]*Institute of Nuclear Chemistry, Johannes-Gutenberg-University Mainz, Germany*

[2]*Department of Nuclear Medicine, University Hospital, Mainz, Germany*

[3]*Institute of Physiology and Pathophysiology, University Medicine Mainz, Germany*

[4]*Department of Inorganic Chemistry, Charles University, Prague, The Czech Republic*

Keywords

hydroxy bisphosphonates, PET, theranostics, bone metastases, ^{68}Ga, ^{177}Lu , DOTA, zoledronic acid

Abstract

Introduction: Bisphosphonates have a high affinity to calcified tissues and are commonly used in the treatment of bone disorder diseases. Conjugates of bisphosphonates with macrocyclic chelators open new possibilities in bone targeted radionuclide imaging and therapy. Endoradiotheraphy with ^{177}Lu-labelled macrocyclic bisphosphonates could have great potential subsequent to PET examinations utilized with ^{68}Ga-labelled analogous in the treatment of painful skeletal metastases.

Methods: Two new DOTA α-OH-bisphosphonates DOTAM^{PAM} and DOTAM^{ZOL} were successfully synthesized, based on the established pharmaceuticals pamidronate and zoledronate, respectively. The ligands were labelled with the PET-nuclide ^{68}Ga, purified and compared in *in vitro* and *in vivo* studies against [^{18}F]NaF and a known DOTA α-H-bisphosphonate conjugate (BPAPD) in healthy Wistar rats.

Results: The new ligands reached a RCY of 80 to 90% in 15 min with post processed ^{68}Ga. After resin purification the purity of all studied bisphosphonates was higher than 98%. The tracers showed low uptake in soft tissue, a fast renal clearance and a high accumulation in bone. The best compound was [^{68}Ga]DOTAM^{ZOL} (SUV_{Femur} = 5.4±0.6) followed by [^{18}F]NaF (SUV_{Femur} = 4.8±0.2), [^{68}Ga]DOTAM^{PAM} (SUV_{Femur} = 4.5±0.2) and [^{68}Ga]BPAPD (SUV_{Femur} = 3.2±0.3). Best blood to bone ratios were obtained for [^{18}F]NaF (97.4) and [^{68}Ga]DOTAM^{ZOL} (11.5).

Conclusion: The ^{68}Ga-labelled DOTA-bisphosphonate compounds showed a promising uptake profile and a similar distribution kinetics. Bone accumulation was highest for [^{68}Ga]DOTAM^{ZOL}, which makes this compound an interesting bone targeting tracer for further studies with ^{177}Lu.

1. Introduction

Radionuclide bone scintigraphy usually applied to localize skeletal lesions from various cancer origins. The findings of the scintigraphy reflect the status of metabolic activity of the bone tissue as a result of tumour invasion. Positron emission tomography (PET) has a high diagnostic sensitivity and specificity for the detection of skeletal metastases [1], when used with the cyclotron produced [^{18}F]NaF [2]. The positron emitter ^{68}Ga has several advantages, which makes it an interesting object in the development of radiopharmaceuticals. First of all it is the cyclotron independent availability based on the ^{68}Ge/^{68}Ga generator system. Secondly it is the principle of the bifunctional chelating agent to design radiometal based pharmaceuticals. Substitution of β^+ by β^- or α-particle emitters in principle leads to a theranostic concept, wherein diagnosis and therapy is combined in one compound. Since bisphosphonates show a high affinity to bone, a number of new DOTA (1,4,7,10-tetraazacyclododecane-1,4,7,10-tetraacetic acid) based bone targeting bisphosphonate molecules were described in the literature [3], including conjugates of alendronic acid [4] (4-aminobutyl-1-hydroxy-1,1-bis[phosphonic acid]) and other α-H-bisphosphonates [5]. Within this class of compounds, first promising human applications were reported for [^{68}Ga]BPAMD. PET studies demonstrating equal quality to [^{18}F]NaF and particularly a higher SUV_{max} in seleceted bone lesions [6].

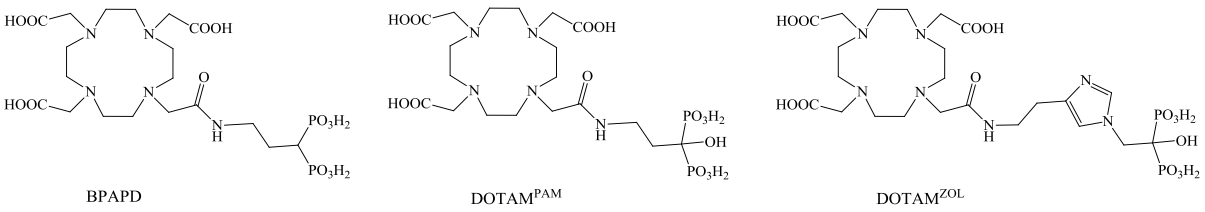

Chart 1. Structure of discussed ligands.

The evolution of modern osteoporosis drugs went from α-H bisphosphonates to α-OH and *N*-heteroaromatic bisphosphonates [7]. Actually the synthesis of DOTA conjugated α-OH-bisphosphonates is more difficult compared to DOTA conjugated α-H-bisphosphonates. The

benefit of DOTA-α-OH-bisphosphonates against DOTA-α-H-bisphosphonates is hypothetical and might be based on the higher affinity of α-OH bisphosphonates to calcified surfaces compared to the α-H bisphosphonates [7]. Consequently we synthesized a pamidronate (3-aminopropyl-1-hydroxy-1,1-bis[phosphonic acid]) and a zoledronate (([1-hydroxy-2-(1H-imidazol-1-yl)-ethylidene]bisphosphonic acid) derivatives as DOTA conjugates, labelled both with ^{68}Ga and compared them in *in vivo* small animal PET and in *ex vivo* organ distribution studies in healthy Wistar rats to the known DOTA-α-H-bisphosphonate of similar structure (BPAPD) and to [^{18}F]NaF (for structures see Chart 1).

2. Results

2.1. Synthesis

Synthesis of BPAPD is published in the literature [8] as well as the synthesis of pamidronate [9]. Compound (**4**) was prepared by a standard method for the synhtesis of hydroxyl-bisphosphonates from carboxylic acids [10]. The cleavage of the amide to from the primary amine was achieved in the same step, based on the strong acidic condition after hydrolysis of the phosphorus trichloride. The imidazole derivative (**3**) was obtained from ω-*N*-acetylhistamine (**1**) after alkylation with benzyl bromoacetate and hydrogenation. Only the 1,4-(H-2 and H-5) imidazole (**2**) was formed during this reaction. A convenient method to discriminate between the 1,4- and the 1,5-alkylation product is described in the literature by the different coupling constants of the aromatic imidazole ring protons [11]. (**2**) showed a coupling constant of $J_{2,5}$ = 1.3 Hz, which is characteristic for the 1,4-product (range from 1.1-1.5 Hz). The final conjugation of the hydroxy-bisphosphonates (DOTAM^{PAM} and DOTAM^{ZOL}) were performed *via* a route described by Ogawa et al [4]. Products were first purified by preparative HPLC workup, and the amounts of DOTA impurities remaining were removed by solid phase extraction (SPE) using a weak anion exchanger resin.

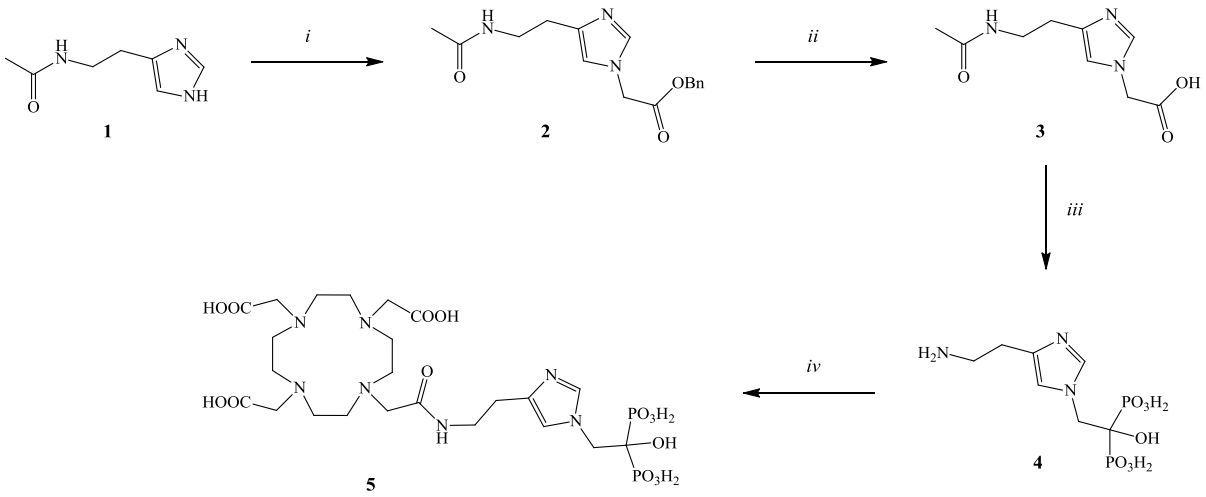

Scheme 1. Synthesis of $DOTAM^{ZOL}$: (***i***) benzyl bromoacetate, DMF, Cs_2CO_3, 0°C, 12 h. (***ii***) H_2, Pd/C, MeOH, RT, 24 h. (***iii***) 1. PCl_3 ,H_3PO_3, $MeSO_3H$, 75°C, 12 h, 2. H_2O, 105°C, 24 h. (***iv***) DOTA-NHS-ester, Na_2CO_3, 40°C, 24 h.

2.2. Radiolabelling with n.c.a. ^{68}Ga and quality control

Labelling with n.c.a. ^{68}Ga was performed in sodium acetate buffer under heating on a thermo shaker for 15 minutes. Radiochemical yields (RCY) of the ^{68}Ga-DOTA-BP complexes were obtained between 80 and 90%. After SPE using again a weak anion exchanger, the labelled compounds were present in 2 mL phosphate buffered saline (PBS) with a radiochemical purity over 98%, ready for injection. Yields and purities were checked by radio-TLC and HPLC (Figure 1). Aliquots of the purified and the reaction solutions were quenched with desferoxamine (DFO). Remaining uncomplexed ^{68}Ga converted into the stable complex [^{68}Ga]DFO, which then could be discriminated effectively on RP-HPLC from the ^{68}Ga-DOTA-BPs.

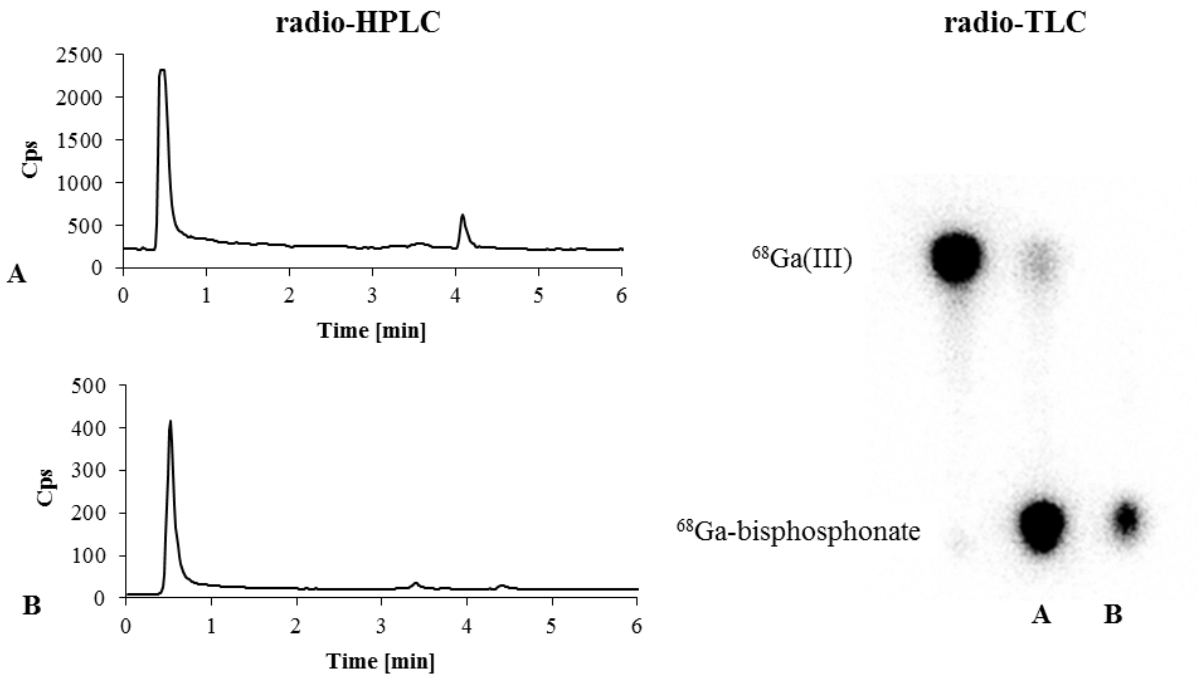

Figure 1. Quality control of [^{68}Ga]DOTAM^{ZOL} by means of cross checked radio-HPLC and radio-TLC, as a representative of ^{68}Ga-labelled bisphosphonates. A: After 15 min reaction time. B: After SPE purification. A(HPLC): R_t([^{68}Ga]DOTAM^{ZOL}) = 0.6 min. (88%), R_t([^{68}Ga]DFO) = 4.1 min. (12%). B(HPLC): R_t([^{68}Ga]DOTAM^{ZOL}) = 0.6 min. (98%). A(TLC): R_f([^{68}Ga]DOTAM^{ZOL}) = 0.1 (85%), R_f([^{68}Ga]citrate) = 0.9 (15%). B(TLC): R_f([^{68}Ga]DOTAM^{ZOL}) = 0.1 (99%). Control (TLC): R_f([^{68}Ga]citrate) = 0.9 (99%).

2.3. Adsorption experiments on apatite

Simple binding experiments on hydroxy apatite (HAP) proved the high affinity of the ^{68}Ga-labelled compounds to calcified surfaces like bone tissue. The hydroxy bisphosphonates [^{68}Ga]DOTAM^{PAM} (91.2±2.7) and [^{68}Ga]DOTAM^{ZOL} (92.7±1.3) showed an identical adsorption in this experiment (Figure 2). Thus binding of the pamidronate and zoledronate conjugates was superior compared to the α-H-bisphosphonate [^{68}Ga]BPAPD (83.0±0.8). [^{68}Ga]DOTA as a control showed almost no binding.

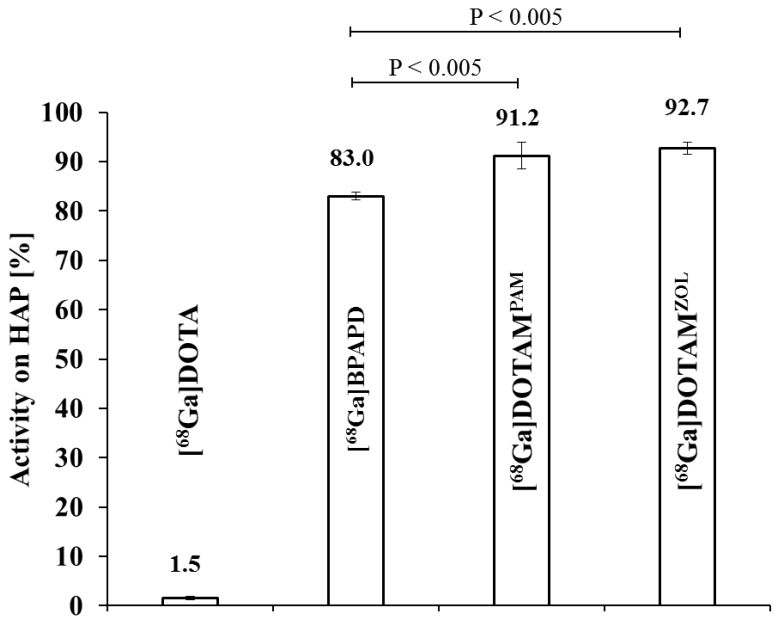

Figure 2. Adsorption efficacies of the three ^{68}Ga-labelled DOTA-BPs on 20 mg HAP after 10 min incubation time, compared to [^{68}Ga]DOTA.

2.4. *Ex vivo* biodistribution

The results of the *ex vivo* organ distribution in healthy Wistar rats of [^{68}Ga]DOTAM^{PAM}, [^{68}Ga]DOTAM^{ZOL}, [^{68}Ga]BPAPD and [^{18}F]NaF are presented in Tables 1 and 2, respectively. All ^{68}Ga-labelled compounds showed high accumulation in bone and low uptake in soft tissue. Compared to the bisphosphonates [^{18}F]NaF showed an slight faster renal clearance and an overall lower concentration of activity in other organs, besides the bone. The bone to blood ratio determined from biodistribution were 3.7 for [^{68}Ga]BPAPD, 7.6 for [^{68}Ga]DOTAM^{PAM}, 11.5 for [^{68}Ga]DOTAM^{ZOL} and 97.4 for [^{18}F]NaF.

Table 1. *Ex vivo* biodistribution of [^{68}Ga]DOTAM^{PAM}, [^{68}Ga]DOTAM^{ZOL}, [^{68}Ga]BPAPD and [^{18}F]NaF in healthy Wistar rats after 60 min. p. i.

organ	[^{68}Ga]DOTAM^{PAM}	[^{68}Ga]DOTAM^{ZOL}	[^{68}Ga]BPAPD[a]	[^{18}F]NaF[a]
Lung	0.53 (0.16)*	0.45 (0.11)*	0.43 (0.08)	0.05 (0.01)
Liver	0.43 (0.04)*‡	0.28 (0.03)*‡	0.37 (0.11)	0.03 (0.01)
Spleen	0.31 (0.04)*‡	0.17 (0.02)*‡	0.23 (0.08)	0.13 (0.20)
Kidneys	0.48 (0.06)*	0.53 (0.04)*	0.56 (0.08)	0.11 (0.01)
Muscle	0.09 (0.02)†	0.08 (0.02)†	0.17 (0.02)	0.06 (0.05)
Heart	0.23 (0.02)*†‡	0.14 (0.04)*†‡	0.32 (0.09)	0.02 (0.01)
Blood	0.60 (0.03)*†	0.47 (0.19)*†	0.86 (0.21)	0.05 (0.01)
Intestine	0.28 (0.12)*	0.14 (0.08)*	0.26 (0.05)	0.02 (0.01)
Femur	4.53 (0.17)†‡	5.40 (0.62)†‡	3.21 (0.29)	4.87 (0.32)

Data are expressed in SUV. Each value represents the mean (S.D.) for five animals.

[a]Data taken from lit. [12].

*P<0.05 vs. [^{18}F]NaF

†P<0.05 vs. [^{68}Ga]BPAPD

‡P<0.05 [^{68}Ga]DOTAM^{PAM} vs. [^{68}Ga]DOTAM^{ZOL}

Table 2. Bone to blood ratios and calculated total activity in the skeleton in healthy Wistar rats, after 60 min. p. i. of [^{68}Ga]DOTAM^{PAM}, [^{68}Ga]DOTAM^{ZOL}, [^{68}Ga]BPAPD and [^{18}F]NaF.

compound	%ID in skeleton (S.D.)	bone to blood ratio (S.D.)
[^{68}Ga]DOTAM^{PAM}	48.4 (4.7)	7.6 (0.6)
[^{68}Ga]DOTAM^{ZOL}	42.7 (5.2)	11.5 (5.9)
[^{68}Ga]BPAPD[a]	38.3 (5.0)	3.7 (1.2)
[^{18}F]NaF[a]	43.7 (1.9)	97.4 (26)

Each value represents the mean for five animals. [a]Data taken from lit. [12].

After 60 minutes the estimated activity in the skeleton was in the range of 40 to 50% of the injected dose (ID) for [^{68}Ga]BPAPD (38.8% ID), [^{68}Ga]DOTAM^{PAM} (48.4% ID) and [^{68}Ga]DOTAM^{ZOL} (42.7% ID), which is comparable to that of [^{18}F]NaF (43.7% ID), cf. table 2.

2.5. *In vivo* biodistribution

Uptake kinetics and images from *in vivo* µPET studies are presented in Figure 2. [^{68}Ga]BPAPD, [^{68}Ga]DOTAM^{PAM} and [^{68}Ga]DOTAM^{ZOL} showed a rapid bone accumulation, reaching a plateau level at 45 minutes and a fast blood elimination. The terminal elimination half-life of [^{68}Ga]DOTAM^{ZOL} is significantly lower compared to [^{68}Ga]BPAPD and [^{68}Ga]DOTAM^{PAM}, cf. table 3. Distribution kinetics as time activity curves, Figure 2 and Figure 3, are very similar for all ^{68}Ga-tracers. Variation in the kidney profile is a result of differing response of the rats to anesthesia and diverging kidney activity. After 60 minutes all ^{68}Ga-labelled bisphosphonates gave clearly visible bone scans of good quality[^{18}F]NaF PET showed in small animals a slight better quality, which is based on the better spatial resolution of the lower β^+-energy of ^{18}F compared to ^{68}Ga. In human PET applications these volume effects are negligible.

Table 3. Pharamcological parameters calculated by a two-compartment model of [^{68}Ga]DOTAM^{PAM}, [^{68}Ga]DOTAM^{ZOL} and [^{68}Ga]BPAPD obtained from µPET experiments in healthy Wistar rats.

Elimination half-lives	[^{68}Ga]BPAPD	[^{68}Ga]DOTAM^{PAM}	[^{68}Ga]DOTAM^{ZOL}
$t_{1/2}(\alpha)$	5 min	4.5 min	5 min
$t_{1/2}(\beta)$	4 h	4.5 h	2.3 h

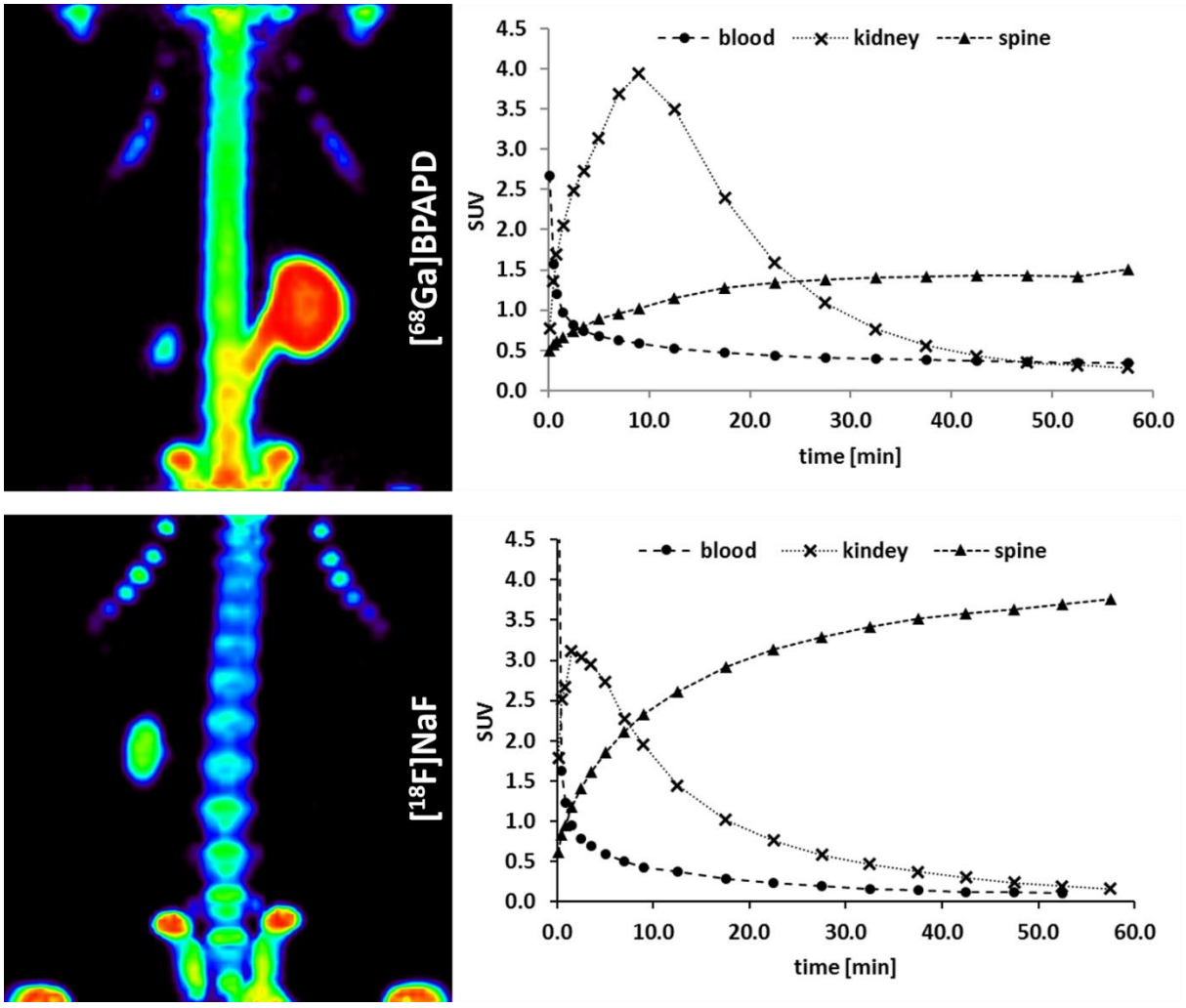

Figure 2. MIP (maximum intensity projection) in the thorax region of Wistar rats after 60 min p.i. and time activity curves (TAC) of [^{68}Ga]BPAPD and [^{18}F]NaF.

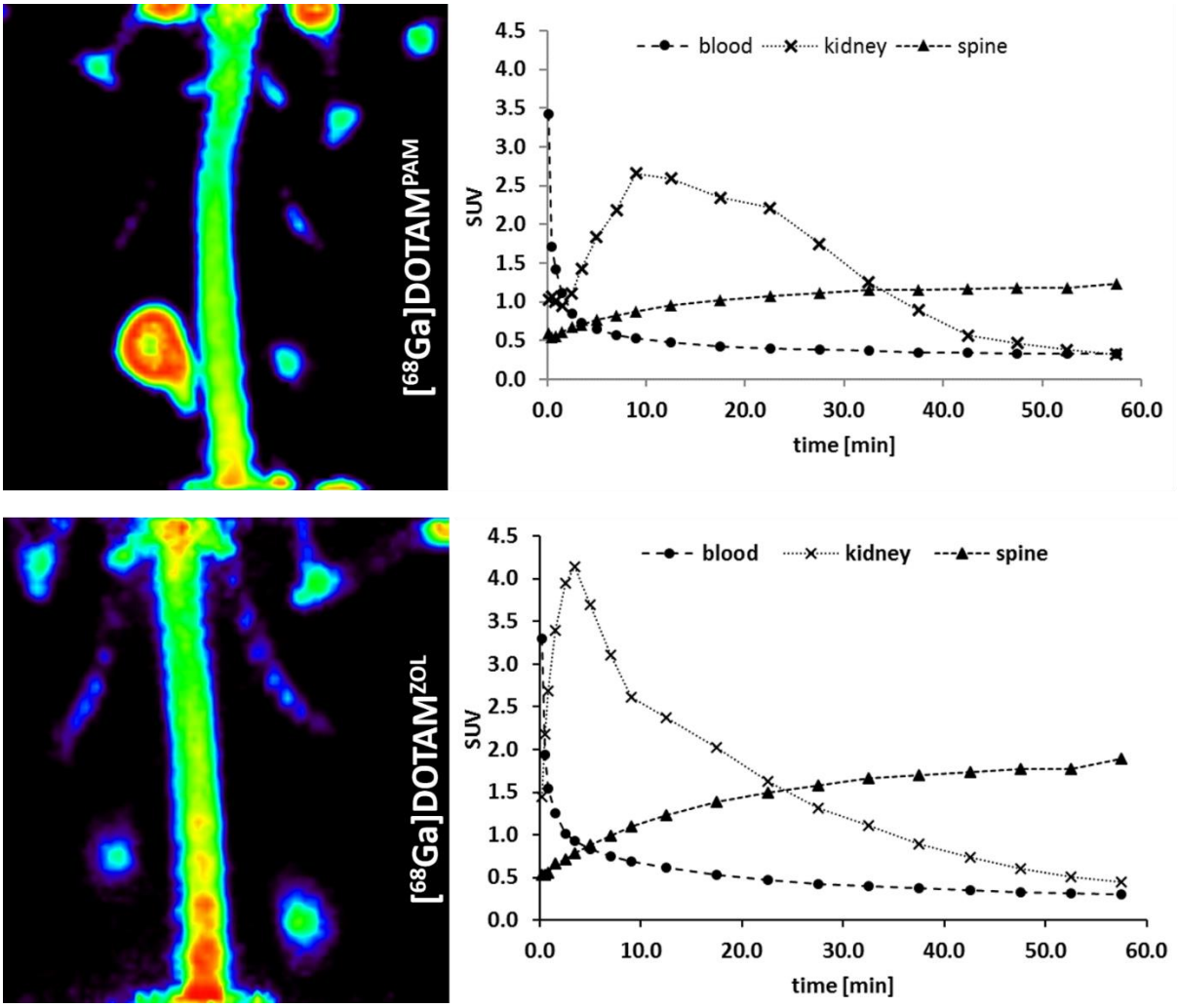

Figure 3. MIP (maximum intensity projection) in the thorax region of Wistar rats after 60 min p.i. and time activity curves (TAC) of [^{68}Ga]DOTAM^{PAM} and [^{68}Ga]DOTAM^{ZOL}.

3. Discussion

The synthetic route for the DOTA-α-OH-bisphosphonate derivatives is distinctly different from that of the compound BPAPD. As a consequence, The α-H-bisphosphonate is definitely in a more easy way to synthesize. Purities and yields are quite higher. The coupling of the primary amine of the pamidronate or imidazole moiety in water *via* the *N*-hydroxysuccinimide ester of DOTA results in lower yields and the formation of problematic side products from ester hydrolysis, which have to be removed. Ogawa et al. [4] separated the [^{90}Y]DOTA-alendronate derivative from [^{90}Y]DOTA after labelling by semipreparative HPLC. A combination of semipreparative HPLC and SPE showed the best purification results after the amide formation. Other groups reported the synthesis of protected alendronate, where the hydroxy bisphosphonate part is esterified by ethyl groups and a tert.butyldimethylsilyl ether [13], leading to a new route for the developing of chelator α-OH-bisphosphonate conjugates [14]. Nevertheless, this reaction seemed to be limited for compounds like alendronate. We were not able to prepare other derivatives with different alkyl or aromatic residues on the geminal hydroxy bisphosphonate, by this synthetic pathway. The rearranged phosphonic acid derivative was the main product [15,16].

Complex formation with n.c.a. ^{68}Ga was comparable for BPAPD, DOTAM^{PAM} or DOTAM^{ZOL} in terms of labelling yields and kinetics. Yields between 80 and 90% were routinely achieved after 15 min. The same strategy to remove DOTA impurities during the synthesis of the precursors showed to be convenient to purify the radio-labelled tracers from uncomplexed ^{68}Ga. The ^{68}Ga-DOTA-BP is trapped via its bisphosphonate moiety on a weak anion exchanger and separated from labelling buffer as well as from free ^{68}Ga. This method is efficient, fast and easy and afterwards the product is present in PBS, suitable for injection after sterile filtration. Adding a small aliquot from the product containing solution to DFO results in an easy HPLC method suitable for working on common C18 columns. The [^{68}Ga]DFO complex differs in retention time to the^{68}Ga-DOTA-BPs. Together with the TLC and the SPE cartridge a useful package of quality control and purification methods could be developed for DOTA conjugated bisphosphonates labelled with ^{68}Ga.

Data from *in vitro* adsorption study indicate a higher affinity towards apatite for the two DOTA-α-OH-BPs compared to the DOTA-α-H-BP. This could be further proofed in *ex vivo* and *in vivo* experiments. The DOTA pamidronate conjugate [^{68}Ga]DOTAM^{PAM} (SUV_{Femur} = 4.5±0.2) showed a higher accumulation in bone compared to the DOTA bisphosphonate conjugate [^{68}Ga]BPAPD (SUV_{Femur} = 3.2±0.3). This proves the expectation that bisphosphonates containing an α-OH group have an enhanced affinity to calcified surfaces, as currently discussed in the literature. This leads to an almost doubled bone to blood ratio of 7.6 for [^{68}Ga]DOTAM^{PAM} to that of 3.7 for [^{68}Ga]BPAPD. According to previous studies nitrogen-containing hydroxy bisphosphonates, especially *N*-heteroaromatic compounds, have an even more enhanced accumulation on bone. Indeed the *N*-heteroaromatic [^{68}Ga]DOTAM^{ZOL} showed the best bone uptake (SUV_{Femur} = 5.4±0.6) and the best bone to blood ratio of 11.5 of all bisphosphonates tested.

The overall skeleton accumulation is very similar for all tracers and it is comparable to that of [^{18}F]NaF, which is in the range of 40 to 50%ID. In rats all DOTA based bisphosphonates showed PET images of good quality, which proof their potential as useful skeletal imaging agents. Bisphosphonates are known to have a long biological half-life in bone. Since DOTA compounds are easy to label with β^-- or α-particle emitters like ^{177}Lu or ^{212}Bi, the tracers discussed in this paper seemed to be excellently suitable for bone targeted radionuclide therapy. Labelling studies, complex stabilities and animal experiments with therapy nuclides will be reported elsewhere.

In conclusion, simple ^{68}Ga-labelled bisphosphonates like BPAPD are easier to synthesize, but show less affinity to bone compared to hydroxy bisphosphonates like [^{68}Ga]DOTAM^{ZOL}. The DOTA conjugated bisphosphonates attained high RCY (80-90%) with ^{68}Ga after 15 min. A fast and easy purification and quality control method could be established. Data from *in vivo* µPET and *ex vivo* biodistribution showed fast blood clearance, low uptake in soft tissue and a high accumulation in the skeleton with [^{68}Ga]DOTAM^{ZOL} as the best leading compound.

4. Experimental

4.1. General methods.

Chemicals and solvents were commercially available in analytical, HPLC or *Trace*SELECT® grade and were purchased by Sigma-Aldrich or Merck KGaA. DOTA-NHS ester (1,4,7,10-Tetraazacyclododecane-1,4,7,10-tetraacetic acid mono(*N*-hydroxysuccinimidyl ester)) was synthesized according to a procedure described in the literature [17] or purchased from Chematech (Dijon, France). Proton nuclear magnetic resonance (^{1}H-NMR) spectra were recorded on a Bruker 300, ^{31}P-NMR were recorded on a Bruker 600. Mass spectra were recorded on Agilent Technologies 6130 Quadrupole LC/MS spectrometer with ESI as ion source in positive or negative modes or on a Finnigan MAT-95 spectrometer with FD as ion source. TLC analyses were carried out with silica on aluminium foil (Merck). Radio-TLC analysis of labelled compounds were performed also with silica on aluminium foil (Merck) and a Canberra Packard Instant Imager. For HPLC and radio-HPLC a Waters-system 1525 with an UV- and a radio-detector (Berthold Technologies, Germany) was used. Radioactivity of samples were measured with an Aktivimeter Isomed 2010, MED (Nuklear-Medizintechnik Dresden GmbH). Radioactivity in tissue samples was determined by using a Wallac WIZARD2 automatic gamma counter (Perkin Elmer, Germany). N.c.a. ^{68}Ga was obtained from a ^{68}Ge/^{68}Ga generator system (Eckert & Ziegler). [^{18}F]NaF was purchased from DKFZ (Deutsches Krebsforschungszentrum, Heidelberg, Germany).

4.2. Synthesis of DOTAM^{PAM}

Pamidronate was synthesized according to a description by Kieczykowski et al [9]. 4.85 g (54.3 mmol) β-alanine was dissolved in 25 mL of methanesulfonic acid. 4.45 g (54.3 mmol) .) phosphorous acid was added and 10 mL (115 mmol) phosphorus trichloride was added slowly under vigorous stirring at75^{o}C. The reaction mixture was kept under argon atmosphere for 12 h at 75^{o}C. After cooling to room temperature 50 g of crushed ice was added under vigorous stirring. The aqueous solution was heated for 12 h under reflux. After

cooling to room temperature conc. aquaous NaOH was added until the formation of a white precipitate was observed. The mixture was stored in a fridge for 5 h to complete precipitation and filtered, washed with cold water and recrystallized from boiling water. Precipitation was initiated by adding EtOH. The white solid (5.3 g, 69 %) was filtered, washed with EtOH and dried in an oven at 60°C. ^{1}H-NMR (D_2O/NaOD, 300 MHz): δ 2.30 (m, 2H), 3.34 (t, J_H = 6.8 Hz, 2H). ^{31}P-NMR (D_2O/NaOD, 162.05 MHz): δ 17.7 (s, 2P). ESI-MS(-): cald 234.07 obsd 234.10 ($M - H^+$), ESI-MS(+): cald 235.07 obsd 258.0 ($M + Na^+$).

DOTAM^{BP} was synthesized according to a description by Ogawa et al [4]. 25 mg (0.11 mmol) pamidronate was dissolved in 1 mL 0.1 M Na_2CO_3 in water. 38 mg (0.05 mmol) DOTA-NHS-ester was dissolved in 0.5 mL deionized water and added to the pamidronate solution. The reaction solution was kept at 40°C on a thermo shaker for 24 h. The pH was checked periodically and small amounts of aqueous Na_2CO_3 were used to keep the pH between 8 and 9. The crude mixture was purified initially by preparative HPLC (Phenomenex Synergy Hydro-RP 80, 10µ, 250 x 30 mm, H_2O + 0.1% TFA). In the second step the crude product was purified further to remove DOTA impurities by solid phase extraction (SPE). An aqueous solution of the compound was passed over a silica NH_2-phase (Merck LiChroprep NH_2). After washing with water/methanol/water the product was eluted with H_2O +2 % TFA. After lyophilisation 4.5 mg (14.5%) of a white solid was obtained. ^{1}H-NMR (D_2O/NaOD, 300 MHz): δ 2.0-2.3 (b, 8H, cyclen-*CH*$_2$), 2.0-2.33 (b, 2H,-*CH*$_2$-), 2.9-3.5 (b, 8H, cyclen-*CH*$_2$), 2.9-3.5 (b, 2H,-*CH*$_2$-), 3.74 (bs, 8H, -*CH*$_2$-CO). ^{31}P-NMR (D_2O/NaOD, 162.05 MHz): δ 18.3 (s, 2P). ESI-MS(+): cald 621.18 obsd 1243.3 ($2M + H^+$), 622.1 ($M + H^+$), 311.6 ($M + 2H^+$).

4.3. Synthesis of DOTAM^{ZOL}

1-(benzyl acetate) 4-(ethyl acetamide)-imidazole (2). 1 g (6.53 mmol) ω-*N*-acetylhistamine (**1**) was dissolved in 50 mL dry DMF. 4.4 g (13 mmol) ceasium carbonate was added. The solution was stirred under Argon atmosphere and ice cooling. 2.2 g (13 mmol) benzyl bromoacetate was dissolved in 50 mL dry DMF and added slowly to the imidazole solution. The mixture was allowed to warm to room temperature and stirred for 12 h. Charcoal was

added and the solids were filtered off. After removing the solvents under reduced pressure, the crude red residue was recrystallized from ethyl acetate to obtain 1.14 g (58%) pale yellow crystals. ^{1}H-NMR ($CDCl_3$, 300 MHz): δ 1.97 (s, 3H, *CH*$_3$-CO), 2.76 (t, J_H = 6.3 Hz, 2H, *CH*$_2$-CH_2), 3.53 (q, J_H = 6.0 Hz, 2H, *CH*$_2$-CH_2), 4.70 (s, 2H, N-*CH*$_2$-CO), 5.22 (s, 2H, Bn-*CH*$_2$-CO), 6.53 (bs, 1H, N*H*), 6.75 (d, J_H = 1.3 Hz, imidazole-*H*), 7.39 (m, 5H, benzyl), 7.44 (d, J_H = 1.3 Hz, 1H, imidazole-*H*).). FD-MS(+): cald 301.14 obsd 302,3 (M + H^+), 603,2 (2M + H^+).

1-(1-hydroxy-ethane-1,1-bis(phosphonic acid)) 4-(ethyl amine)-imidazole (4). 300 mg (1 mmol) of (**2**) was dissolved in 20 mL of dry MeOH. Pd/C (10%w) was added and stirred under hydrogen atmosphere (5 bar) for 12 h. After removing the solvents the hydrogenated product (**3**) was weighted to determine yield (208 mg, 98%). The acid (**3**) was used without further purification in the next step. 1 mL methanesulfonic acid and 164 mg (2 eq.) phosphorous acid was added. The mixture was stirred at 75^{o}C and 300 mg (2.2 eq.) phosphorus trichloride was added slowly under argon atmosphere. After 12 h the reaction mixture was cooled down to room temperature and 2 mL of iced water was added. The aqueous solution was heated for 24 h under reflux. Charcoal was added and the solution was filtered. After cooling to room temperature conc. aquaous NaOH was added until the formation of a white precipitate was observed. The mixture was stored in a fridge overnight to complete precipitation and filtered, washed with cold water and recrystallized from boiling water to obtain 88.6 mg (28%) of a white solid. ^{1}H-NMR (D_2O/NaOD, 300 MHz): δ 2.46 (m, 2H, *CH*$_2$-CH_2), 2.66 (m, 2H, *CH*$_2$-CH_2), 4.28 (m, 2H, N-*CH*$_2$-phosponate), 6.89 (s, 1H, imidazole-*H*), 7.54 (s, 1H, imidazole-*H*). ^{31}P-NMR (D_2O/NaOD, 162.05 MHz): δ 14.4. ESI-MS(+): cald 315.04 obsd 316.05 (M + H^+), 338.04 (M + Na^+).

DOTAM^{ZOL} (5). To 15.75 mg (0.05 mmol) (**4**) in 1 mL water, triethylamine (TEA) was added drop wise until all solids were dissolved. 38 mg (0.05 mmol) DOTA-NHS-ester was dissolved in 0.5 mL water and added to the bisphosphonate solution [4]. The reaction solution was kept at 50^{o}C on a thermo shaker for 24 h. The pH was checked periodically and small amounts of aqueous TEA were used to keep the pH between 8 and 9. The crude mixture was purified initially by preparative HPLC (Phenomenex Synergy Hydro-RP 80, 10µ, 250 x 30 mm, solvent: H_2O + 0.1% TFA). In the second step the crude product was

purified further to remove DOTA impurities by solid phase extraction (SPE). An aqueous solution of the compound was passed over a silica NH_2-phase (Merck LiChroprep NH_2). After washing with water/methanol/water the product was eluted with H_2O + 2% TFA. After lyophilisation 5.6 mg (15.7%) of a white solid was obtained. ^{1}H-NMR (D_2O/NaOD, 300 MHz): δ 2.42 (m, 2H, *CH_2*-CH_2), 2.61 (m, 2H, *CH_2*-CH_2), 2.9-3.5 (b, 16H, cyclen-*CH_2*), 3.75 (bs, 8H, -*CH_2*-CO), 4.55 (m, 2H, N-*CH_2*-phosponate), 7.28 (s, 1H, imidazole-*H*), 8.54 (s, 1H, imidazole-*H*). ^{31}P-NMR (D_2O/NaOD, 162.05 MHz): δ 14.3. ESI-MS(+): cald 701,2 obsd 702.5 ($M + H^+$), 351.1 ($M + 2H^+$).

4.4. Radiolabelling with n.c.a. ^{68}Ga and quality control

N.c.a. ^{68}Ga was obtained in 400 µL acetone/HCl from a ^{68}Ge/^{68}Ga generator system by cationic post processing [18]. The labelling itself was performed by adding 500 µL sodium acetate buffer (0.5 M, pH = 4) and 25 nmol ligand to the ^{68}Ga containing solution. The mixture was heated at 98^{o}C under moderate shaking on a thermo shaker for 15 min. Subsequently the solution was diluted to 5 mL with water and passed over a weak anion exchanger cartridge (25 mg, Merck LiChroprep NH_2). After washing with 1 mL water the purified product was eluted with 2 mL PBS. Radiochemical yields and purities were determined by radio-TLC (Merck silica, solvent: acetone/acetylacetone/HCl, 10/10/1) and radio-HPLC (Merck Chromolite RP-18e 100 x 4.6 mm, gradient: H_2O to acetonitrile). To discriminate between free ^{68}Ga and ^{68}Ga-bisphosphonates a small aliquot of the product solution was incubated for 1 min with a 0.25 M DFO (Desferoxamine) solution. DFO complexes unlabelled ^{68}Ga instantly and shows a longer retention time on RP-18 HPLC (see Figure 1).

4.5. Adsorption experiments on apatite

Hydroxy apatite (HAP) (20 mg, Sigma-Aldrich, reagent grade powder) was incubated in isotonic saline (1 mL) for 24 h. 50 µL of the ^{68}Ga-labelled bisphosphonate solution to the HAP suspension. After vortexing for 10 s, the suspension was incubated for 10 min at room

temperature under moderate shaking on a thermo shaker. The supernatant was removed by centrifugation. The HAP fraction was washed with saline (0.5 mL) and the ^{68}Ga radioactivity in the combined liquids and that of the HAP fraction were measured. ^{68}Ga-complex binding to HAP was determined as percentage of ^{68}Ga absorbed to HAP [19].

4.6. Animal studies

Male Wistar rats were purchased from Charles River Laboratories Inc weighting 140-220 g. The animal experiments were carried out in consensus to institutional guidelines, the German welfare regulations and the *European Convention for the Protection of Vertebrate Animals for Experimental and other Scientific Purposes.*

µPET: Small animal µPET imaging was performed under general anesthesia with isoflurane inhalation. The rats were positioned supine in a Siemens Focus 120 µPET and 15 to 18 MBq of the radio tracers were administrated in 0.5 mL isotonic saline intravenously (i.v.) via the tail vein. Images were reconstructed to OSEM 2D and files were processed using Pmod software (TAC) and Amine software (MIP).

Biodistribution: For each compound five animals were injected with 8 to 10 MBq of the radio tracers in 0.5 mL PBS/isotonic saline via the tail vein. The rats were sacrificed at 60 min p.i. and organs of interest were excised, weighed and the radioactivity was measured decay corrected on a gamma counter. The amount of organ accumulation is expressed in SUV (standard uptake value) by the equitation: SUV = (activity per g tissue)/(injected activity) x body weight. Activity in the skeleton was calculated as percentage of injected dose (%ID) by the following equitation: %ID(skeleton) = femur(%ID/g) x skeleton weight (g). The skeleton weight of the rats were calculated using: skeleton weight = 9.66 + 0.0355 x body weight [12].

4.7. Statistical analysis

All data were expressed as mean ± SD. Groups were compared using the t-test. All statistical tests were two tailed, with a *P*-value of less than 0.05 representative for significance.

5. Acknowledgment

This work was supported by the grant of the Max Planck Graduate Center and the COST Action TD1004. The assistance in the processing of the animal data is greatly acknowledged to Dr. R Bergmann (Helmholtz Zentrum Dresden Rossendorf). The authors are grateful to Dr V Kubicek and P Hermann (both Charles University Prague) for providing the compound BPAPD.

6. References

[1] T. Hamaoka, J. E. Madewell, D. A. Podoloff, G. N. Hortobagyi, N. T. Ueno, bone imaging in metastatic breast cancer, *J Clin Oncol*, **2004**, 22; 2942-2953.

[2] E. Evan-Sapir, U. Metser, E. Mishani, G. Lievshitz H. Lerman, I. Leibovitch, The Detection of Bone Metastases in Patients with High-Risk Prostate Cancer: ^{99m}Tc-MDP Planar Bone Scintigraphy, Single- and Multi-Field-of-View SPECT, ^{18}F-Fluoride PET, and ^{18}F-Fluoride PET/CT, *J Nucl Med*, **2006**; 47: 287–297.

[3] K. Ogawa, H. Saji, Advances in Drug Design of Radiometal-Based Imaging Agents for Bone Disorders, *Int J Mol Imag*,**2011**; 537687.

[4] K. Ogawa, H. Kawashima, K. Shiba, K. Washiyama, Y. Kiyono, M. Ueda, H. Mori, H. Saji, Development of [^{90}Y]DOTA-conjugated bisphosphonate for treatment of painful bone metastases, *Nuclear Medicine and Biology*, **2009**; 36: 129–135.

[5] T. Vitha, V. Kubicek, P. Hermann, Z. I. Kolar, H. Th. Wolterbeek, J. A. Peter, I. Lukes, Complexes of DOTA-Bisphosphonate Conjugates: Probes for Determination of Adsorption Capacity and Affinity Constants of Hydroxyapatite, *Langmuir*, **2008**; 24: 1952-1958.

[6] M. Fellner, R. P. Baum, F. Rösch, PET/CT imaging of osteoblastic bone metastases with ^{68}Ga-bisphosphonates: first human study, *EJNMMI*, **2010**; 37:834.

[7] R. G. G. Russell, N. B. Watts, F. H. Ebetino, M. J. Rogers, Mechanisms of action of bisphosphonates: similarities and differences and their potential influence on clinical efficacy, *Osteoporos Int*, **2008**; 19: 733–759.

[8] T. Vitha, V. Kubicek, P. Hermann, Z. I. Kolar, H. Th. Wolterbeek, J. A. Peter, I. Lukes, Complexes of DOTA-Bisphosphonate Conjugates: Probes for Determination of Adsorption Capacity and Affinity Constants of Hydroxyapatite, *Langmuir*, **2008**; 24: 1952-1958.

[9] G. R. Kieczykowski, R. B. Jobson, D. G. Melillo, D. F. Reinhold, I. Shinkai, Preparation of (4-Amino-1-Hydroxybutylidene)bisphosphonic Acid Sodium Salt, MK-217 (Alendronate Sodium). An Improved Procedure for the Preparation of 1-Hydroxy-1,1-bisphosphonic Acids, *J. Org. Chem.*, **1995**; 60: 8310–8312.

[10] L. Widler, K. A. Jaeggi, M. Glatt, K. Müller, R. Bachmann, U. Ramseier, J. Schmid, G. Schreiber, Y. Seltenmeyer, J. R. Green, Highly Potent Geminal Bisphosphonates. From Pamidronate Disodium (Aredia) to Zoledronic Acid (Zometa), *J. Med. Chem.* **2002**; 45: 3721-3738.

[11] Y. Amino, H. Eto, C. Eguchi, Synthesis of 1,5-disubstituted imidazoles including an imidazole analogue of prostaglandine from 4(5)-hydroxymethylimidazole, *Chem. Pharm. Bull.*, **1989**, 37, 1481-1487.

[12] M. Meckel, M. Fellner, N. Thieme, R. Bergmann, V. Kubicek, F. Rösch, In vivo comparison of DOTA based ^{68}Ga-labelled bisphosphonates for bone imaging in non-tumour models, *Nuclear Medicine and Biology*, **2013**; 40: 823–830.

[13] P. Vachal, J. J. Hale, Z. Lu, E. C. Streckfuss, S. G. Mills, K. Manser, F. Kesisoglou, L. L. Alani, Synthesis and Study of Alendronate Derivatives as Potential Prodrugs of Alendronate Sodium for the Treatment of Low Bone Density and Osteoporosis, *J. Med. Chem.* **2006**: 49; 3060-3063.

[14] K. Suzuki, M. Satake, J. Suwada, S. Oshikiri, H. Kasahara, T. Minamizawa, Synthesis and evaluation of a novel ^{68}Ga-chelate-conjugated bisphosphonate as a bone-seeking agent for PET imaging, *Nuclear Medicine and Biology*, **2011**; 38: 1011–1018.

[15] R. Ruel, J.-P. Bouvier, R. N. Young, Single-Step Preparation of 1-Hydroxybisphosphonates via Addition of Dialkyl Phosphite Potassium Anions to Acid Chlorides, *J. Org. Chem.*, **1995**; 60: 5209-5213.

[16] D. R. Brittelli, A Study of the Reaction of 2-Haloacyl Halides with Trialkyl Phosphites. Synthesis of (2-Substituted acy1)phosphonates, *J. Org. Chem.*, **1985**; 50: 1845-1847.

[17] C. Li, P. T. Winnard Jr., T Takagi, D. Artemov, ZM. Bhujawalla, Multimodal Image-Guided Enzyme/Prodrug Cancer Therapy, *JACS*, **2006**; 128: 15072-15073.

[18] KP. Zhernosekov, DV. Filosofov, R.P. Baum, P. Aschoff, H. Bihl, AA. Razbash, M. Jahn, M. Jennewein, F. Rösch Processing of generator-produced ^{68}Ga for medical application, *J Nucl Med*, **2007**; 48: 1741

[19] M. Fellner, P. Riss, NS. Loktionova, KP. Zhernosekov, O. Thews, F. Rösch, Comparison of different phosphorus-containing ligands complexing ^{68}Ga for PET-imaging of bone metabolism. *Radiochim. Acta*, **2011**; 99: 43–51.

3.5. A DOTA based bisphosphonate with an albumin binding moiety for delayed body clearance in bone targeting radiotherapy

A DOTA based bisphosphonate with an albumin binding moiety for delayed body clearance in bone targeting radiotherapy

Marian Meckel[1], Nicole Bausbacher[2], Barbara Biesalski[3], Vojtěch Kubíček[4], Petr Hermann[4], Matthias Miederer[2], Frank Rösch[1]

[1]*Institute of Nuclear Chemistry, Johannes-Gutenberg-University Mainz, Germany.*

[2]*Department of Nuclear Medicine, University Hospital, Mainz, Germany*

[3]*Institute of Physiology and Pathophysiology, University Medicine Mainz, Germany*

[4]*Department of Inorganic Chemistry, Charles University, Prague, The Czech Republic*

Keywords

Bisphosphonate, PET, theranostics, bone metastases, ^{68}Ga, albumin binder, DOTA.

Abstract

Introduction: Radio-labelled bisphosphonates are commonly used in the diagnosis and therapy of bone metastases. In many cases, blood clearance is fast and only 30 to 50 % of the injected activity is retained in the skeleton, while most of the activity is excreted, predominantly *via* the kidneys and the bladder. In the context of endoradiotherapeutic applications, this would reduce the radioactivity accumulated at the target side. A longer blood circulation may enhance accumulation of bisphosphonate compounds in the bone metastases. A portable Albumin binder was reported to delay the excretion of polar imaging agents. Therefore a chemically modified macrocyclic bisphosphonate derivative with an additional binding entity to human albumin was synthesized and evaluated in relation to the modification of the pharmacokinetics of the bisphosphonate.

Methods: The theranostic bisphosphonate BPAMD ((4-{[bis-(phosphonomethyl)) carbamoyl]methyl}-7,10-bis(carboxymethyl)-1,4,7,10-tetraazacyclododec-1-yl)acetic acid) was compared to the novel albumin binding bisphosphonate DOTAGA(**428**-D-Lys)M^{BP} of similar structure. Both tracers were labelled with the generator derived PET nuclide ^{68}Ga(III) and evaluated in binding studies to artificial bone material as well as to human serum albumin (HSA). The compounds were further compared in *in vivo* µPET and *ex vivo* organ distribution studies in healthy Wistar rats over a time period of 3 h p.i..

Results: Radio-labelling with no carrier added (n.c.a.) ^{68}Ga(III) resulted in initial yields of >80% and in radiochemical purities >98% after solid phase extraction purification. Binding studies revealed a consistent affinity to hydroxyl apatite (HA) of both the albumin binding bisphosphonate (81.3 ± 2.2 %) and the original compound (81.6 ± 0.5 %). [^{68}Ga]DOTAGA(**428**-D-Lys)M^{BP} showed a distinguished binding of 88.1 ± 5.9 % to HSA compared to 28.8 ± 1.1 % for [^{68}Ga]BPAMD, respectively. *In vivo* µPET and *ex vivo* organ distribution studies resulted in significant longer blood concentration levels (SUV_{blood} = 2.59 ± 0.72 and 0.06 ± 0.01, respectively). Skeletal accumulation of the modified compound

resulted in a SUV_{femur} = 4.16 ± 0.62 compared to the original compound of a SUV_{femur} = 4.20 ± 0.20 after 3 h p.i.. Ratios between the high metabolic femur epiphyseal plate to the ordinary bone showed to be more favourable for [^{68}Ga]DOTAGA(**428**-D-Lys)M^{BP} with a ratio of 2.9 compared to 1.9 for [^{68}Ga]BPAMD respectively.

Conclusion: The chemical modification of BPAMD towards an albumin binding bisphosphonate (DOTAGA(**428**-D-Lys)M^{BP}) resulted in a novel compound, which conserves the activity of both functional groups within one and the same molecule. Blood retention was significantly longer for the DOTA bisphosphonate bridged to an albumin binding moiety. The better bioavailability of DOTAGA(**428**-D-Lys)M^{BP} resulted in better ratios between high and low metabolic bone sections. Further studies with longer living PET nuclides like ^{44}Sc(III) or ^{64}Cu(II) as well as dosimetric studies with the therapeutic nuclide ^{177}Lu(III) have to be determined in future to conclude the therapeutic potential of this new class of tracers for the treatment of bone metastases.

1. Introduction

The bone is frequently affected by metastatic invasion of tumour cells in consequence of various cancer diseases. This complication is accompanied by several symptoms like severe pain, spinal cord compression and hyper calcemia. Tumour cell invasion in the skeleton cause a activation of the osteoclasts and osteoblasts, which liberate signal molecules, resulting in a feedback mechanism, which is called the *viscous circle* [1]. Common treatment includes chemotherapy, analgesic medication, hormone respectively bisphosphonate treatment and external radiation therapy.

Another application are bone-seeking radiopharmaceuticals, which showed good results in the last decades in the palliative care. The early approved β-emitters [^{32}P]PO_4^{3-} and $^{89}SrCl_2$ are now replaced by compounds of carrying radionuclides emitting lower β-energy particles like [^{153}Sm]EDTMP and [^{177}Lu]EDTMP, which cause less side effects to the radio sensitive bone marrow. The recently approved α-particle emitting $^{223}RaCl_2$ showed, beside pain relief, an overall longer survival rate of 3 month in prostate cancer patients afflicted by bone metastases [2]. There are several more, rather experimental compounds and nuclides like [^{186}Re]HEDP or [^{117m}Sn]DTPA described in the literature, as well as macrocyclic DOTA-bisphosphonate conjugates like [^{90}Y]DOTA-HBP [2,3]. One of these new compounds is BPAMD (Chart 1). In contrast to the open chain chelating agents like HEDP and ETMP the macrocyclic tetraaza-compound is able to complex the positron emitting PET nuclide ^{68}Ga(III) as well as the therapeutic low energy β-emitter ^{177}Lu(III) [4]. BPAMD showed a high and stable bone association with a fast pharmacokinetic, when labelled with ^{68}Ga(III) or with ^{177}Lu(III) [5]. First ^{68}Ga-PET scans in cancer patients [6] and in a rat tumour model [7] proofed the high potential of this tracer as a useful theranostic agent for the detection and treatment of skeletal metastases [8].

Bisphosphonates are known to have a fast blood clearance and almost half of the injected dose is excreted via the kidneys [9]. In previous studies this effect could be confirmed also for the radiolabelled derivatives, i.e. a fast body elimination of [^{68}Ga]BPAMD and [^{177}Lu]BPAMD. An injected dose of 30-40 % remained exclusively on the bone, while most

of the activity was washed out of the body *via* the urinary system[5,10] and is therefore no longer available for a binding on the target tissue. Nuclear magnetic resonance imaging (MRI) contrast agents like Gd-DTPA (Magnevist) or Gd-DOTA (Dotarem) show a similar fast blood clearance and these compounds are excreted in a short timescale with low retention in the body. Dumelin et al. conjugated MRI and fluorescence agents with an albumin binding entity. The albumin binding moiety induced a relative strong binding (K_d = 3.3 µM) of a Gd-DTPA derivative to human serum proteins. Within this study the blood half-life of [^{177}Lu]DTPA was shifted from $t_{1/2,\alpha}$ = 8.3 min to $t_{1/2,\alpha}$ = 22.3 min for the [^{177}Lu]DTPA-albuminbinding-derivative [11]. Furthermore, it is reported that [$^{67/68}$Ga]DOTA-folate conjugates have an unfavourable tumour to kidney ratio, based on the expression of the Folate receptor in the kidneys as well as in the targeted folate receptor positive tumour tissue [12]. Müller et al. further developed the concept of an albumin binding DOTA-folate conjugate as an ^{177}Lu-endoradiotherapy (ERT) agent with an enhanced tumour to kidney ratio [13]. The same strategy was successful to develop a new ^{18}F-labelled folate conjugate, where kidney uptake was reduced to a quarter compared to previously published folate receptor targeting compounds [14]. The longer blood circulation time of these new tracers resulted in distinct higher accumulation in the target tissue.

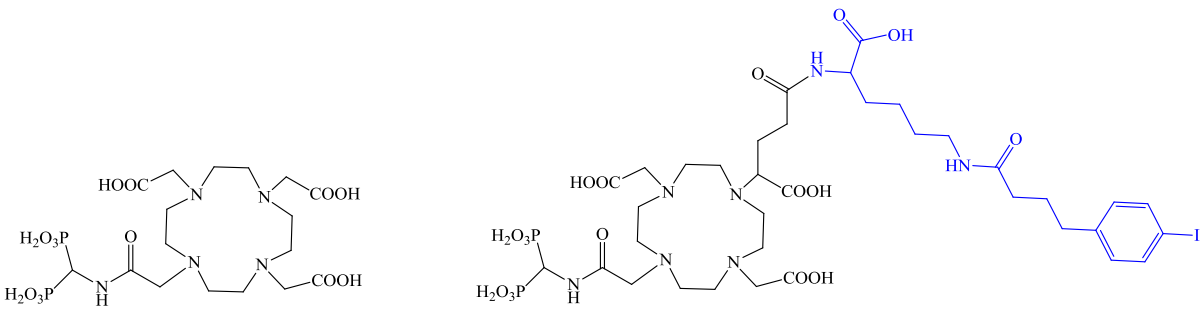

Chart 1. Structure of ligands discussed in this paper.

Since radio labelled bone tracers have a fast washout out of the body, longer blood retention times could first minimize unintended urinary exertion and second, consequently enhance the uptake of the compound on the targeted bone tissue. In addition a better metastases to healthy

bone ratio might be achieved. Furthermore longer blood retention of a radio labelled bisphosphonate may have the same therapeutic effect when a reduced dose is administered, compared to a radio-labelled bisphosphonate, where almost half of the injected dose is excreted within few minutes. For that reason we synthesized the Albumin binding DOTA-bisphosphonate conjugate (Chart 1) DOTAGA(**428**-D-Lys)M^{BP} aiming at a longer blood circulating character. The compound was labelled with ^{68}Ga(III) and compared to [^{68}Ga]BPAMD in *in vitro* essays and in *in vivo* small animal PET and *ex vivo* biodistribution studies.

2. Results

2.1. Synthesis

The compounds tert.Butyl-DO2A (**1**) and α-bromoglutaric acid-1-tertbutyl ester-5-benzyl ester (**2**), which were used to form the seven dentate bifunctional chelator moiety (**3**) in the first reaction step were synthesized according to published procedures[15,16]. Mono alkylation of the macrocycle (**1**) was done under excess conditions of the nucleophile to prevent the formation of the di-alkylated side product. Insertion of the bisphosphonate targeting vector (**4**) was performed in the same way as described in the BPAMD synthesis route published [17] to form a protected bisphosphonate-DOTAGA derivative (**5**). Standard deprotection of the glutaric pendant arm under hydrogenation conditions enables the addition of the albumin binder **428**-D-Lys mediated by HATU in two steps (**6** and **7**) by liquid-phase peptide synthesis. An excess of trimethylsilyl bromide, which is an effective an mild dealkylation reagent for the cleavage of phosphor esters, was used to form the bone affine bisphosphonate pharmacophore. Finally deprotection of the tert.Butyl ester yields the compound DOTAGA(**428**-D-Lys)M^{BP} (**8**).

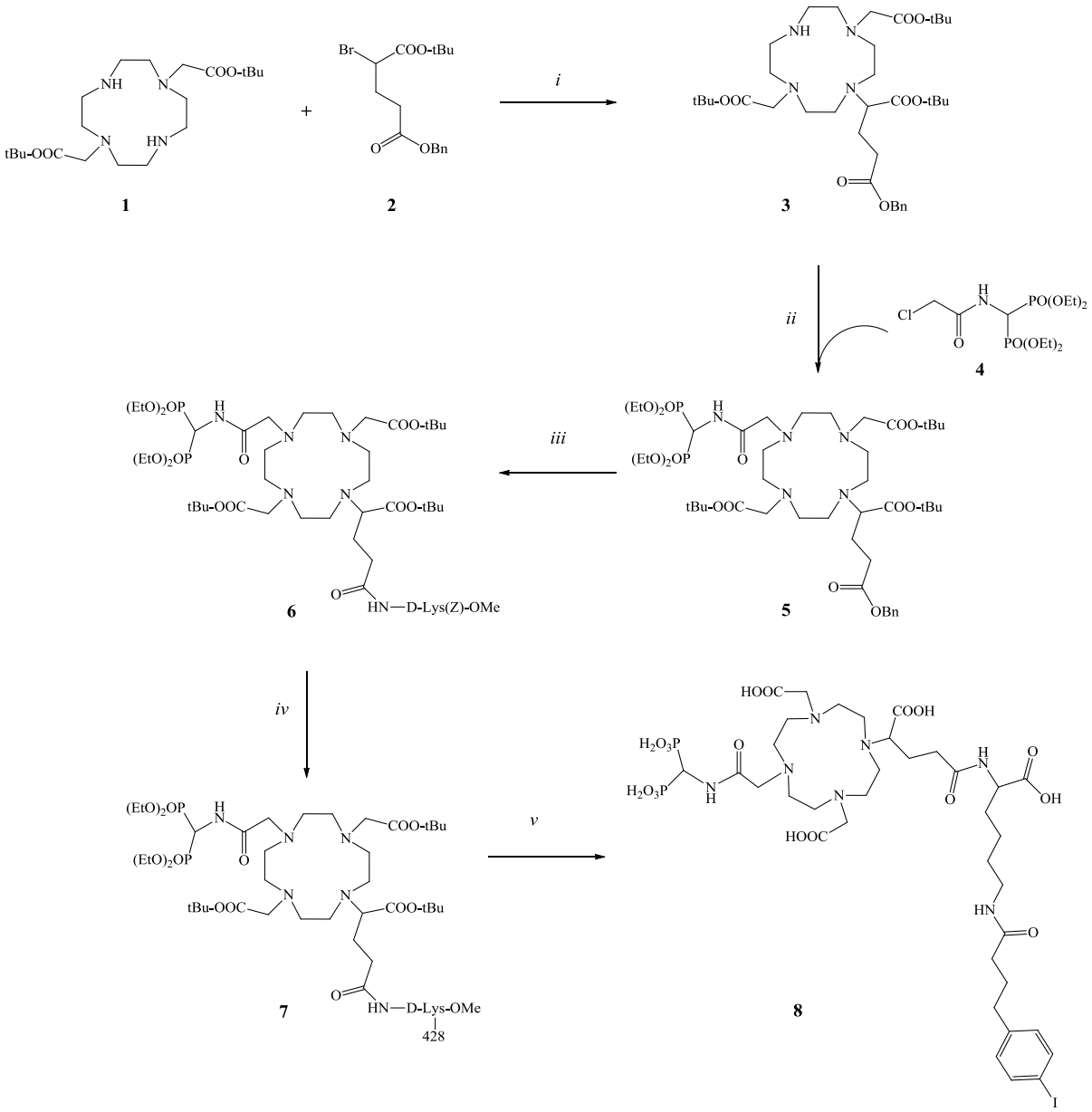

Scheme 1. Synthesis of DOTAGA(**428**-D-Lys)M^{BP}: (*i*) Dichloromethane, RT, 48 h. (*ii*) K_2CO_3, acetonitrile, 40°C, 24 h. (*iii*) 1. H_2, Pd/C, MeOH 2. DIPEA, HATU, DCM, RT, 12 h. (*iv*) 1. H_2, Pd/C, MeOH 2. DIPEA, HATU, NMP, RT, 12 h. (*v*) 1. TFA/DCM, RT, 5 h 2. TMS-Br, DMF, RT, 12 h 3. H_2O, RT, 24 h.

2.2. Radiolabelling with n.c.a. ^{68}Ga and quality control

Radiochemical yields (RCY) for [^{68}Ga]DOTAGA(**428**-D-Lys)M^{BP}, with post processed n.c.a. ^{68}Ga(III) in sodium acetate buffer, were 80 to 90 % after 15 min at 98°C. After cartridge purification the tracer showed a radiochemical purity (RCP) > 98 % as determined by radio-HPLC (fig.1).

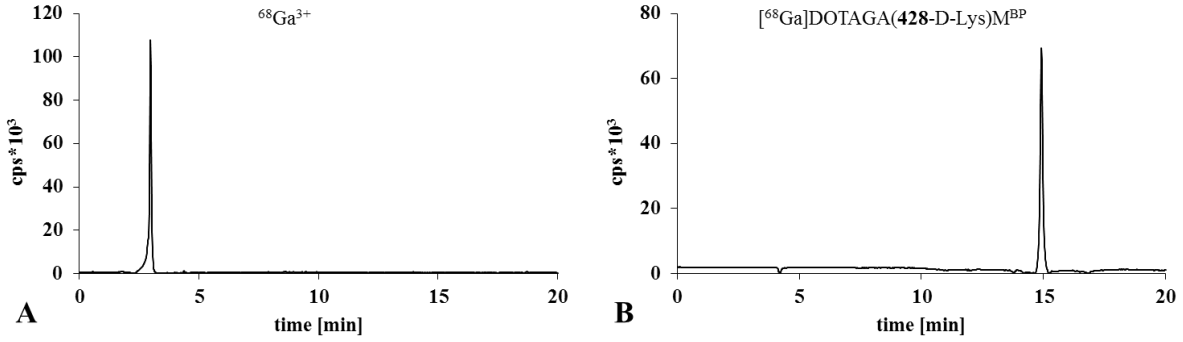

Figure 1. RP-HPLC radiochromatograms of unbound ^{68}Ga (A) and [^{68}Ga]DOTAGA(**428**-D-Lys)M^{BP} after SPE purification (B).

2.3. Adsorption experiments on Apatite

The two ^{68}Ga-labelled bisphosphonate derivatives showed an almost identical binding profile to hydroxy apatite (HA) after 10 min incubation time, while [^{68}Ga]DOTA as a control showed no relevant adsorption on HA. The results are presented in table 1.

Table 1. Adsorption efficiency of ^{68}Ga-labelled macrocycles on 20 mg HA after 10 min. incubation.

	[^{68}Ga]BPAMD	DOTAGA(**428**-D-Lys)M^{BP}	[^{68}Ga]DOTA
% of activity on HA ± SD	81.6 ± 0.5	81.3 ± 2.2	0.8 ± 1.1

Standard deviation (SD)

2.4. Protein binding

Human serum protein binding, determined by ultrafiltration of the two ^{68}Ga-labelled DOTA-conjugated bisphosphonates, indicated a significant ($P < 0.005$) higher binding for [^{68}Ga]DOTAGA(**428**-D-Lys)M^{BP} compared to [^{68}Ga]BPAMD, which is shown in figure 2. Binding of [^{68}Ga]DOTAGA(**428**-D-Lys)M^{BP} to human serum proteins was 88.1 ± 5.9 %, while [^{68}Ga]BPAMD showed a binding of 28.8 ± 1.1 %. Compared to that the retention of [^{68}Ga]DOTAGA(**428**-D-Lys)M^{BP} and [^{68}Ga]BPAMD on the ultrafilter in isotonic saline as a control was 33.3 ± 2.6 % and 15.0 ± 1.7 %, respectively.

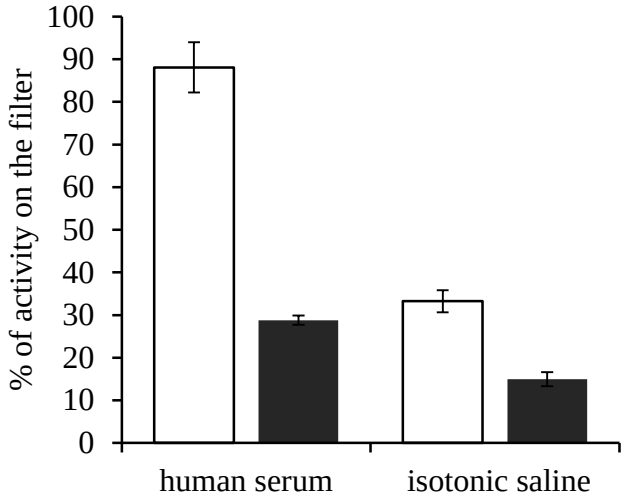

Figure 2. Results of the protein binding experiments for [^{68}Ga]DOTAGA(**428**-D-Lys)M^{BP} (□) and [^{68}Ga]BPAMD (■) determined by ultrafiltration out of a triplicate. Low retention on the filter was observed for both compounds in isotonic saline, in contrast to human serum samples were retention was significant higher for [^{68}Ga]DOTAGA(**428**-D-Lys)M^{BP} compared to [^{68}Ga]BPAMD.

2.5. *Ex vivo* organ distribution

The organ distribution of the ^{68}Ga-labelled compounds in selected tissues at 1 h and 3 h p.i. in healthy male Wistar rats are presented in table 2. [^{68}Ga]BPAMD showed a fast blood clearance (SUV_{blood} = 0.34 ± 0.05) and a high degree of bone accumulation (SUV_{femur} = 3.36 ± 0.81) within 1 h, which is consistent to the µPET results, see below, and matching the literature data [10]. [^{68}Ga]DOTAGA(**428**-D-Lys)M^{BP} showed an overall higher retention in the organism. Radioactivity in soft tissue is higher after 1 h p.i., which could be explained by a significant ($P < 0.001$) higher blood level of the albumin-binder bisphosphonate conjugate (SUV_{blood} = 3.38 ± 0.31) compared to [^{68}Ga]BPAMD (SUV_{blood} = 0.34 ± 0.05). The accumulation on the femur of [^{68}Ga]DOTAGA(**428**-D-Lys)M^{BP} and [^{68}Ga]BPAMD was 2.75 ± 0.46 and 3.36 ± 0.81, respectively, indicating a similar ($P = 0.2$) accumulation on bone within 1 h. [^{68}Ga]BPAMD activity in blood and in soft tissue organs decrease after 3 h compared to 1 h p.i.. SUV of the blood pool was significantly lower with a value of 0.06 ± 0.01 ($P < 0.001$) , while femur accumulation showed a value of 4.20 ± 0.20, which is similar to that of 1 h ($P = 0.09$). Biodistribution of [^{68}Ga]DOTAGA(**428**-D-Lys)M^{BP} after 3 h p.i. showed only minor changes in soft tissue compared to the 1 h values. Significant changes in the uptake profile were observed for blood ($P \leq 0.05$) and femur ($P < 0.005$), with SUV_{blood} = 2.59 ± 0.72 and SUV_{femur} = 4.16 ± 0.62, respectively. No significant differences in femur accumulation of [^{68}Ga]DOTAGA(**428**-D-Lys)M^{BP} and [^{68}Ga]BPAMD ($P = 0.9$) could be observed after 3 h p.i., while the different SUVs in the blood indicating significance ($P < 0.002$).

Table 2. *Ex vivo* organ distribution of [^{68}Ga]BPAMD and [^{68}Ga]DOTAGA(**428**-D-Lys)M^{BP} 60 min and 180 min p.i.

organ	[^{68}Ga]BPAMD		[^{68}Ga]DOTAGA(428-D-Lys)M^{BP}	
	1 h	3 h	1 h	3 h
lung	0.20 ± 0.11	0.16 ± 0.07	1.66 ± 0.12	1.31± 0.19
liver	0.10 ± 0.02	0.06 ± 0.01	0.68 ± 0.18	0.77 ± 0.36
spleen	0.08 ± 0.01	0.04 ± 0.01	0.50 ± 0.05	0.48 ± 0.12
kidneys	0.25 ± 0.04	0.34 ± 0.06	1.06 ± 0.10	0.99 ± 0.21
muscle	0.07 ± 0.02	0.03 ± 0.01	0.63 ± 0.20	0.42 ± 0.06
heart	0.12 ± 0.02	0.04 ± 0.00	1.34 ± 0.36	0.84 ± 0.09
intestine	0.08 ± 0.02	0.08 ± 0.08	0.55 ± 0.13	0.46 ± 0.15
testes	0.07 ± 0.01	0.03 ± 0.00	0.50 ± 0.11	0.65 ± 0.13
blood	0.34 ± 0.05	0.06 ± 0.01	3.38 ± 0.31	2.59 ± 0.72
femur	3.36 ± 0.81	4.20 ± 0.20	2.75 ± 0.46	4.16 ± 0.62

Data presented in mean SUV ± SD of five animals.

Table 3 shows the calculated total retention of [^{68}Ga]BPAMD and [^{68}Ga]DOTAGA(**428**-D-Lys)M^{BP} at 1 h and 3 h p.i. in the blood and the skeleton, respectively. After 1 h 36.3 ± 8.8 %ID of [^{68}Ga]BPAMD and 24.8 ± 3.8 %ID of [^{68}Ga]DOTAGA(**428**-D-Lys)M^{BP} were observed in the skeleton. While the total skeleton activity after 3 h showed no changes for [^{68}Ga]BPAMD (33.7 ± 3.4 %ID) the bone accumulation of [^{68}Ga]DOTAGA(**428**-D-Lys)M^{BP} (32.1 ± 4.0 %ID) increased this over time. The blood level of [^{68}Ga]BPAMD dropped from 2.3 ± 0.3 %ID (1 h) to 0.5 ± 0.1 %ID (3 h). A blood retention of 22.9 ± 2.1 %ID after 1 h was observed for [^{68}Ga]DOTAGA(428-D-Lys)M^{BP}. After 3 h 17.2 ± 5.0 %ID of [^{68}Ga]DOTAGA(428-D-Lys)M^{BP} still remained in the blood pool.

Table 3. Bone and blood accumulation of [^{68}Ga]BPAMD and [^{68}Ga]DOTAGA(**428**-D-Lys)M^{BP} 1 h and 3 h p.i.

	[^{68}Ga]BPAMD		[^{68}Ga]DOTAGA(**428**-D-Lys)M^{BP}	
	1 h	3 h	1 h	3 h
skeleton	36.3 ± 8.8	33.7 ± 3.4	24.8 ± 3.8	32.1 ± 4.0
blood	2.3 ± 0.3	0.5 ± 0.1	22.9 ± 2.1	17.2 ± 5.0

Data presented in mean % of injected dose ± SD of five animals.

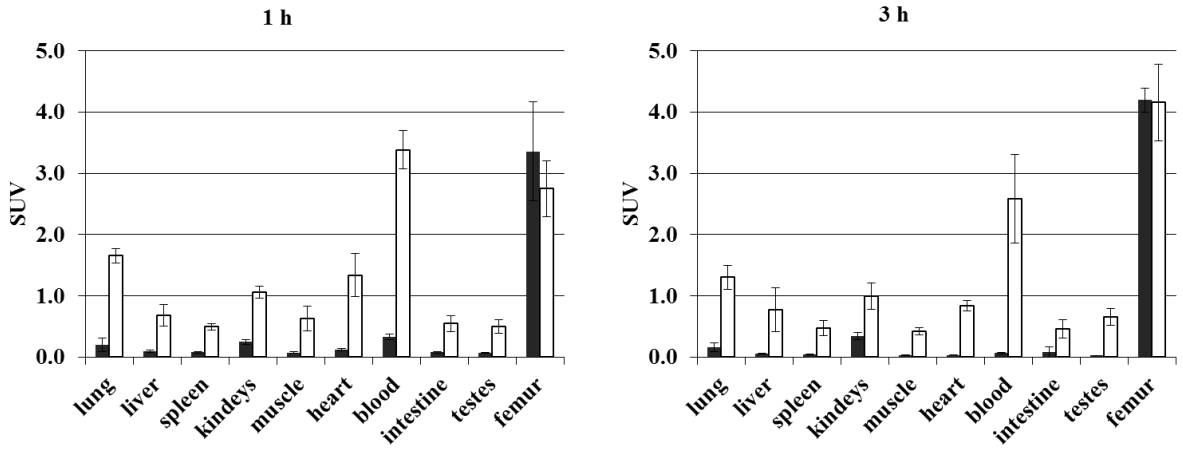

Figure 3. Comparison of the *ex vivo* organ distribution of [^{68}Ga]BPAMD (■) and [^{68}Ga]DOTAGA(**428**-D-Lys)M^{BP} (□) 1 h and 3 h p.i.

2.6. *In vivo* µPET

In vivo µPET scans were conducted over 120 min p.i. for [^{68}Ga]BPAMD and [^{68}Ga]DOTAGA(**428**-D-Lys)M^{BP} in one and the same animal. Images obtained after 120 min p.i. are consistent to the data obtained from *ex vivo* biodistribution experiments. The skeleton is clearly visible in the [^{68}Ga]BPAMD PET scan with a low observed background activity. [^{68}Ga]DOTAGA(**428**-D-Lys)M^{BP} showed bone uptake as well, but with a distinct higher background activity (Figure 4 and 5). The higher background activity is based on the lower blood clearance of the albumin binding bisphosphonate, which is consistent to the results

from *ex vivo* biodistribution. Organs of high perfusion like the heart and the abdominal aorta as well as the branching to the common iliac arteries are visible. No significant uptake in liver was observed for both compounds. The ^{68}Ga-labelled albumin binding bisphosphonate as well as [^{68}Ga]BPAMD were both excreted *via* the kidneys to the bladder. Particularly high accumulation of the radio tracers were found in the joint regions (figure 5), where bone metabolism is enhanced.

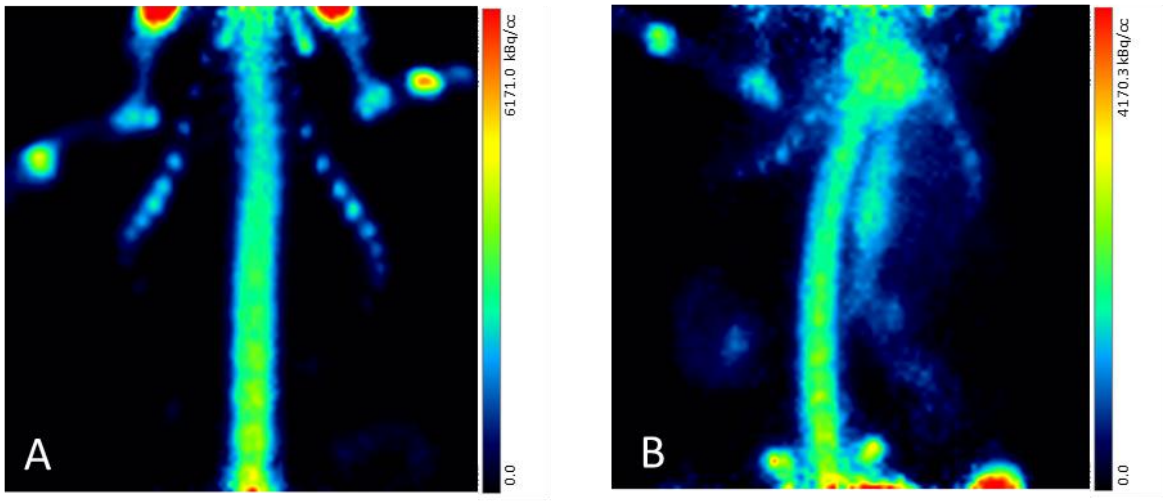

Figure 4. MIP of [^{68}Ga]BPAMD (A) and [^{68}Ga]DOTAGA(**428**-D-Lys)M^{BP} (B) after 120 min p.i. in healthy Wistar rats with the focus on the thorax region.

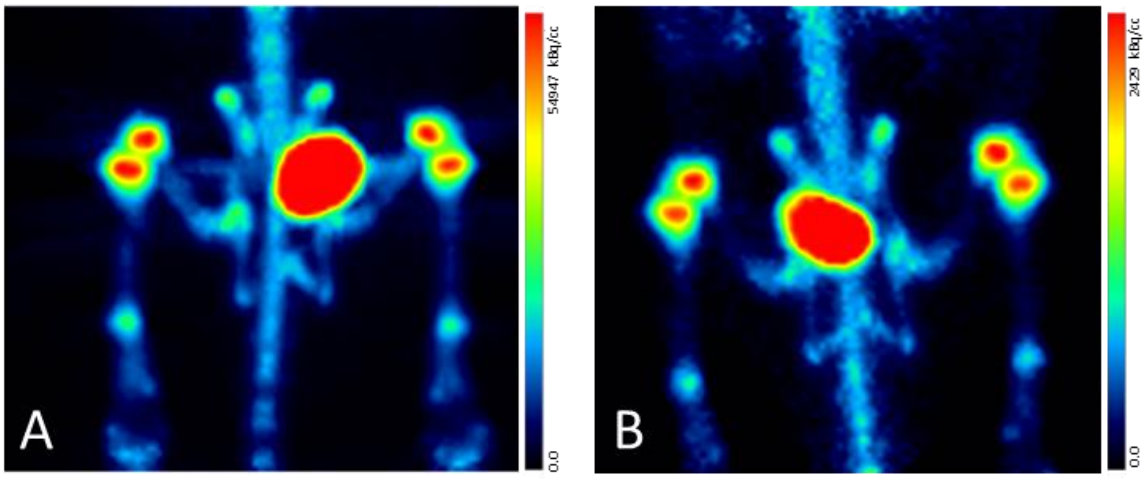

Figure 5. MIP of [^{68}Ga]BPAMD (A) and [^{68}Ga]DOTAGA(**428**-D-Lys)M^{BP} (B) after 120 min p.i. in healthy Wistar rats with the focus on the pelvis region and the articulation between the femur and the tibia.

Time activity curves (TAC) of the *in vivo* µPET data are presented in figures 6 and 7. [^{68}Ga]BPAMD showed a fast uptake kinetics in the spine, reaching a plateau level between 35 and 40 min p.i.. No significant changes in the SUV profile of the spine could be observed for the remaining scan time. The half-life in the blood of [^{68}Ga]BPAMD was $t_{1/2,\alpha}$ = 6.5 min. After 120 min only marginal changes in the uptake profile were monitored, indicating that the body distribution and excretion reaching its kinetic completion. In contrast, no kinetic endpoint could be determined for the TAC of [^{68}Ga]DOTAGA(**428**-D-Lys)M^{BP}, within 120 min scan time. The uptake profile of [^{68}Ga]DOTAGA(**428**-D-Lys)M^{BP} on the spine showed a delay in time. No plateau level was reached after 120 min, rather the accumulation followed a linear progression. Blood retention was obviously improved for [^{68}Ga]DOTAGA(**428**-D-Lys)M^{BP} with a half-life of $t_{1/2,\alpha}$ = 36.7 min.

TAC of [^{68}Ga]BPAMD in the joint region between the femur and the tibia (figure 8) showed the profile of an exponential saturation function as well as in the spine region, but reaches after 120 min a higher plateau level (SUV_{joint} = 4.4; SUV_{spine} = 2.3). The ratio in SUV between the joint of the femur and the tibia to the spine was 1.9, which reveals an almost doubled uptake of the radiotracer. TAC of [^{68}Ga]DOTAGA(**428**-D-Lys)M^{BP} in the joint region and in the spine (figure 6 and 7) showed a lower SUV compared to [^{68}Ga]BPAMD. After 120 min the SUVs in the joint and the spine was 3.2 and 1.1, respectively. The graphs

in figure 6 and 7 indicate no kinetic equilibrium and after 120 min a SUV ratio of 2.9 between the femur and the tibia articulation and the spine was determined, which is an almost threefold higher uptake of [^{68}Ga]DOTAGA(**428**-D-Lys)M^{BP} at the high metabolic bone region.

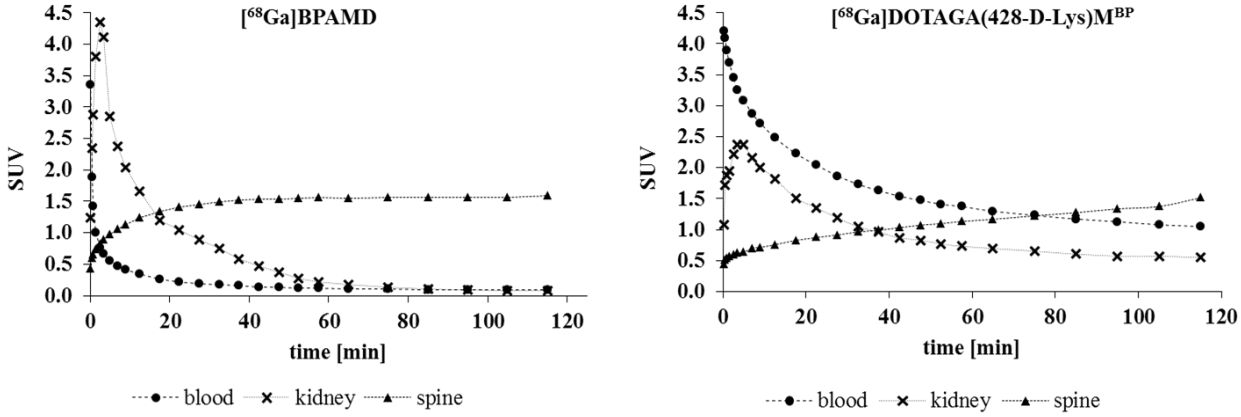

Figure 6. Time activity curves (TAC) determined over 120 min p.i. in selected tissues of [^{68}Ga]BPAMD and [^{68}Ga]DOTAGA(**428**-D-Lys)M^{BP} administered in one and the same animal.

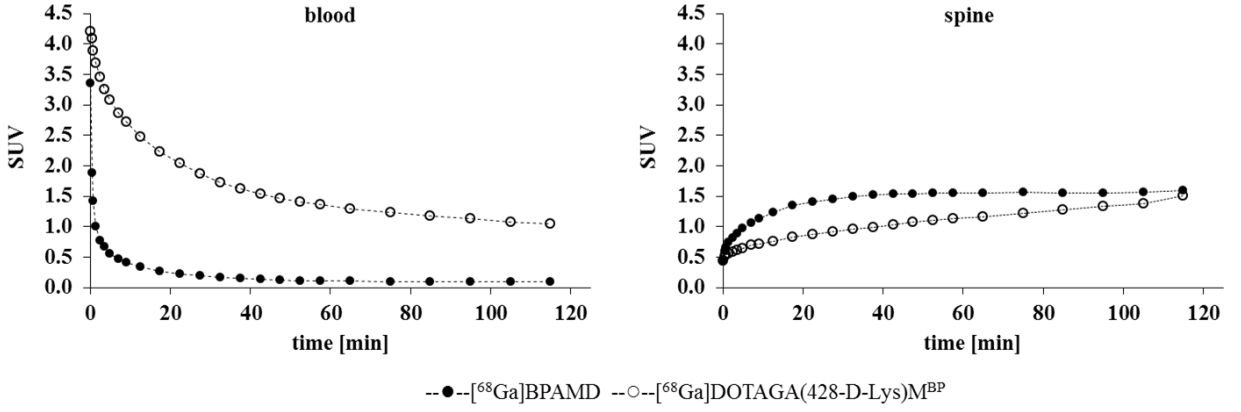

Figure 7. Time activity curves (TAC) determined over 120 min p.i. in the spine and the blood of [^{68}Ga]BPAMD and [^{68}Ga]DOTAGA(**428**-D-Lys)M^{BP} administered in one and the same animal.

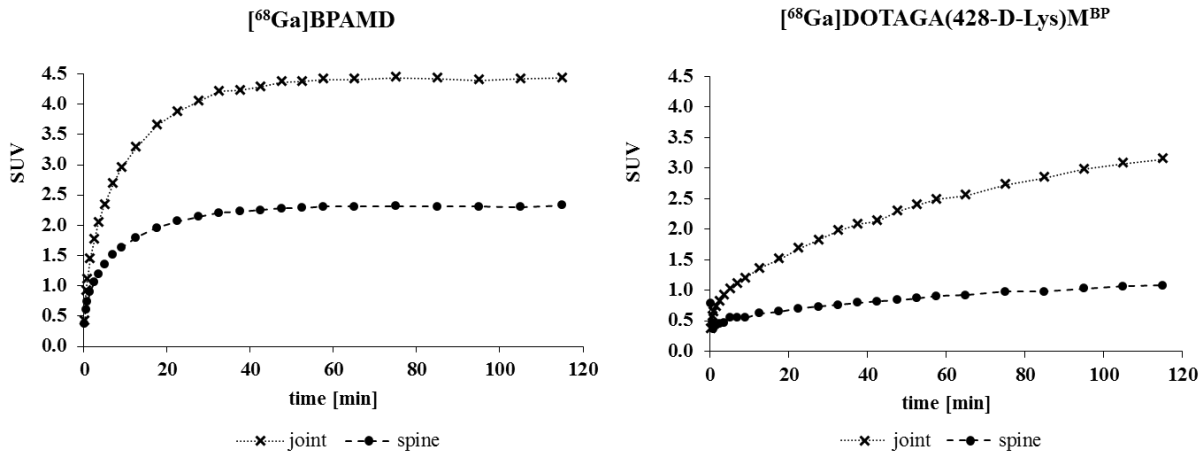

Figure 8. Time activity curves (TAC) determined over 120 min in the joint region between the femur and the tibia of [^{68}Ga]BPAMD and [^{68}Ga]DOTAGA(**428**-D-Lys)M^{BP} administered in one and the same animal.

3. Discussion

We studied the consequences of a chemical modification of the well evaluated radiopharmaceutical BPAMD, with the main purpose to retard the excretion rate of the DOTA-bisphosphonate. The modification includes the BPAMD scaffold by using an asymmetric substitution of DO2A, whereby a DOTAGA like BPAMD-derivative was formed. Contrary to BPAMD it is able to modify the pendant glutaric acid arm of DOTAGA(**428**-D-Lys)M^{BP} with the albumin binding moiety without losing one of the complexation donors to an additional amide bond. Since a potential therapy application with ^{177}Lu, which is the long term goal, was kept in mind the conservation of seven donors had to be ensured. The new compound DOTAGA(**428**-D-Lys)M^{BP} could be synthesized in good yields.

To proof the concept, we decided to label the ligand with the PET nuclide ^{68}Ga and to quantitatively compare the pharmacokinetics of [^{68}Ga]DOTAGA(**428**-D-Lys)M^{BP} with the well evaluated tracer [^{68}Ga]BPAMD in *in vivo* µPET, *ex vivo* organ distribution and in *in vitro* essays. DOTAGA(**428**-D-Lys)M^{BP} can be labelled with n.c.a. ^{68}Ga(III) in high RCY

between 80 and 90 %, within a reaction time of 15 min. The compound was successful purified *via* a C18 solid phase extraction cartridge, providing a RCP > 98%. Furthermore the new ligand showed distinctly retention on C18 HPLC columns, which is contrary to [^{68}Ga]BPAMD where C18 phases are useless, indicating a very increased lipohilicity for DOTAGA(**428**-D-Lys)M^{BP}. The aromatic benzyl group also lead to a better UV-adsorption, enhancing the HPLC analytics of the compound.

No differences in the binding affinity was observed in terms of HA adsorption between [^{68}Ga]DOTAGA(**428**-D-Lys)M^{BP} (81.3 ± 2.2 %) and [^{68}Ga]BPAMD (81.6 ± 0.5 %) , which indicates that the modification of the original BPAMD had no relevant influence on the binding to the biological target. However, the albumin binder conjugate proofed to enhance the binding of the bisphosphonate on human serum proteins, revealed by an ultrafiltration essay. Both results indeed successfully prove that the chemical modification of BPAMD resulted in a compound, which exhibits the functionality of the bisphosphonate and the albumin binder moiety.

Results from *in vivo* and *ex vivo* experiments in healthy rat showed a distinguished longer blood circulation time of [^{68}Ga]DOTAGA(**428**-D-Lys)M^{BP} compared to [^{68}Ga]BPAMD. After 3 h p.i. still 22.9 ± 2.1 % of the injected dose of [^{68}Ga]DOTAGA(**428**-D-Lys)M^{BP} were found in the blood compared to 0.5 ± 0.1 %ID of [^{68}Ga]BPAMD. The blood half-life was enhanced up to $t_{1/2,\alpha}$ = 36.7 min compared to $t_{1/2,\alpha}$ = 6.5 min for [^{68}Ga]BPAMD, deduced from µPET examinations. The data clearly showed the strong effect on the pharmacokinetics by the chemical modification of BPAMD. Uptake on healthy bone was lower for the albumin binder conjugate after the first hour p.i.. However, similar levels of bone accumulation (P = 0.9) were found in the *ex vivo* organ distribution already after 3 h. The affinity to the serum protein decelerated not only the body clearance, but also the skeletal accumulation. The articulations are a region of enhanced bone turnover and the tested tracers showed an increased uptake in these focuses. The uptake ratio between the high metabolic joint region and the ordinary bone might be a hint about how the tracers eventually perform, when evaluated in a metastatic model or patients in expressing disseminated bone metastases. On the one hand, the total uptake in the joint and the ordinary bone is dependent on the affinity of the bisphosphonate to the calcified tissue and on the other hand it is dependent on the

bioavailability of the tracer. [^{68}Ga]BPAMD showed a higher total uptake in the joints as well as in the ordinary bone compared to [^{68}Ga]DOTAGA(**428**-D-Lys)M^{BP}, although the affinity of both tracers to artificial HA is determined to be similar. But In the presence of albumin (35 to 53 g/L in human blood), a competition between the binding to Albumin HSA and bone exists for [^{68}Ga]DOTAGA(**428**-D-Lys)M^{BP} with a slight better affinity to HA tissues, resulting in a long term uptake mechanism but with a decreased initial accumulation. Since the accumulation kinetics of [^{68}Ga]BPAMD showed no relevant changes after 40 min p.i., the uptake ratio between the high metabolic joint region and the ordinary bone is lower (1.9) compared to the ratio of the chemical modified [^{68}Ga]DOTAGA(**428**-D-Lys)M^{BP} (2.9). This shows that tissue compartments with an enhanced rate of turnover benefit from compounds of longer bioavailability.

In conclusion, the chemical modification of BPAMD by means of a bi-substitution mode of the macrocyclic chelate, leads to a DOTAGA bisphosphonate of longer blood circulating time and delayed whole body clearance. In first µPET experiments with a ^{68}Ga-labelled version the ratio between the high metabolic joints and the ordinary bone was better for the albumin binder conjugate compared to the non-modified compound. Overall bone accumulation became comparable already 3 h p.i.. However, the potential of DOTAGA(**428**-D-Lys)M^{BP} as a therapy agent for the treatment of skeletal metastases in combination with therapeutic β^-- emitters has to be further evaluated. The results obtained with ^{68}Ga ($t_{1/2}$ = 1.1 h) are promising, but an overall 3 hours period is a bit short to figure out the total consequences of the chemical modification based on the longer kinetic profile of the new compound. Other PET nuclides with a longer half-life, like ^{44}Sc ($t_{1/2}$ = 4 h) or ^{64}Cu ($t_{1/2}$ = 12.7 h) might be useful for further evaluations. Relating to a potential therapy with a ^{177}Lu analogue PB, comprehensive dosimetric studies are necessary to determine the consequences of the longer blood retention.

4. Experimental

4.1. General methods

All solvents and chemicals were commercially available in analytical, HPLC or *Trace*SELECT® grade and were purchased by Sigma-Aldrich or Merck KgaA. ^{68}Ga was obtained from a ^{68}Ge/^{68}Ga Obninsk generator system (Eckert & Ziegler). Proton nuclear magnetic resonance (^{1}H-NMR) spectra were recorded on a Bruker 300, ^{31}P-NMR were recorded on a Bruker 600. Mass spectra were recorded on Agilent Technologies 6130 Quadrupole LC/MS spectrometer with ESI as ion source in positive or negative modes. TLC and radio-TLC analyses were carried out with silica on aluminium foil (Merck KgaA) and a Canberra Packard Instant Imager as a radiodetector. For HPLC and radio-HPLC a Waters-system 1525 with an UV- and a radio-detector (Berthold Technologies, Germany) was used. Radioactivity of samples were measured with an Aktivimeter Isomed 2010, MED (Nuklear-Medizintechnik Dresden GmbH). Radioactivity in tissue samples was determined by using a Wallac WIZARD2 automatic gamma counter (Perkin Elmer, Germany).

4.2. Synthesis of DOTAGA(428-D-Lys)M^{BP}

1,4,7,10-tetraazacyclododecane-1,7-bis-tert.butyl diacetic acid ester (**tert.butyl-DO2A**) (**1**) and **α-bromoglutaric acid-1-tertbutyl ester-5-benzyl ester** (**2**) were synthesized according to a description published by Riss et al. [15] and Eisenwiener et al.[16]. The synthesis of tetraethyl chloro-acetamidomethyl-bis(phosphonate) (**4**) followed a procedure by Kubicek et al. [17].

Mono alkylation of (**1**) to compound (**3**): To a solution of 0.6 mg (1.69 mmol) (**2**) in 1 mL dichloromethane a solution of 1.0 g (2.5 mmol) tert.butyl-DO2A (**1**) in 3 mL dichloromethane was added slowly under vigorous stirring. The mixture was kept at room temperature for 48 h. After removing the volatiles under reduced pressure, the crude mixture was purified by column chromatography on silica (DCM:MeOH 10:1). The resulting fraction of monosubstituted product (**3**) yielded 0.85 mg (1.25 mmol, 74%) of a yellow solid. R_f

(silica, DCM:MeOH 10:1) = 0.6-0.7.^{1}H-NMR ($CDCl_3$, 300 MHz): δ 7.30-7.41 (m, 5H, benzyl-*H*), 5.10 (s, 2H, benzyl-CH_2-O), 3.40 (t, 1H, N-*CH*-glut.), 3.24-3.36 (m, 4H, N-CH_2-*CO*), 2.68-3.04 (m, 16H, cyclen-CH_2-N), 2.46-2.54 (m, 2H, CH_2-CH_2-CO), 1.88-2.04 (m, 2H, CH_2-CH_2-CH), 1.43 (s, 27H, *t-Bu*). ESI-MS(+): cald 676.9 obsd 678 ($M + H^+$), 339.5 ($M + 2H^+$).

(**5**) was synthesized by dissolving 304 mg (0.45 mmol) (**3**) in 5 mL dry acetonitrile. Potassium carbonate (1.3 mmol) was added and 1.5 eq. (255 mg, 0.67 mmol) of the chloro compound (**4**) was added dropwise over a period of 1 h to the suspension. The reaction mixture was kept at 40°C and under stirring for 24 h. Charcoal was added and the solids were removed by filtration. After evaporation of the solvent, the resulting oil was purified by column chromatography on silica phase ($CHCl_3$:MeOH 10:1), yielding 234 mg (0.23 mmol, 51%) of a yellow oil. R_f (silica, $CHCl_3$:MeOH 10:1) = 0.3-0.4.^{1}H-NMR ($CDCl_3$, 300 MHz): δ 7.31-7.44 (m, 5H, benzyl-*H*), 5.11 (s, 2H, benzyl-CH_2-O), 4.09-4.42 (m, 8H, O-CH_2-CH_3; m, 1H, P-*CH*-P), 3.67-3.78 (q, 1H, N-*CH*-glut.), 3.49 (bs, 6H, N-CH_2-*CO*), 2.01-3.02 (bm, 20H), 1.46 (s, 27H, *t-Bu*), 1.35 (t, 12H, CH_2-CH_3). ESI-MS(+): cald 1019.5 obsd 1020 ($M + H^+$), 510 ($M + 2H^+$).

Reaction of (**5**) to (**6**): 234 mg (0.23 mmol) (**5**) was dissolved in 10 mL methanol and 10%w/w Pd/C was added. The mixture was kept in a pressured vessel for 24 h under hydrogen atmosphere (6 bar). After filtration over celite the volatiles were evaporated to dryness. The crude product (217.6 mg, 96%) was used in the next step without any need for purification. The acid of (**5**) was dissolved in 5 mL dry dichloromethane, followed by an addition of 72.3 mg (0.2 mmol) HATU ((1-[bis(dimethylamino)methylene]-1H-1,2,3-triazolo[4,5-b]pyridinium 3-oxid hexafluorophosphate)) and 65 mg (0.5 mmol) DIPEA (N,N-diisopropylethylamine). The mixture was stirred at room temperature until any solids were dissolved. Subsequently 63.85 mg (0.19 mmol) H-D-Lys(Z)-OMe (Merck KgaA, Germany) was added in small portions and the solution was kept stirring overnight. The reaction mixture was diluted up to 25 mL with dichloromethane and extracted three times with an equivolume of 0.1 M Na_2CO_3, 0.1M NaH_2PO_4 and finally with water. The organic fraction was evaporated to dryness and the crude product was purified by column chromatography on silica ($CHCl_3$:MeOH 10:1). The fractions containing the product were combined and after

removing the solvents 180.6 mg (0,15 mmol, 65%) of a yellow oil was obtained. R_f (silica, $CHCl_3$:MeOH 10:1) = 0.2-0.3.^{1}H-NMR ($CDCl_3$, 300 MHz): δ 7.32-7.40 (m, 5H, benzyl-*H*), 5.10 (s, 2H, benzyl-CH_2-O), 4.41-4.51 (m, 1H, P-*CH*-P) 4.07-4.33 (m, 8H, O-CH_2-CH_3), 3.73 (bs, 6H, N-CH_2-*CO*), 1.64-3-69 (bm, 30H, N-*CH*-glut, cyclen-*H*, glut-*H*, lys-*H*), 1.47 (s, 27H, *t-Bu*), 1.36 (t, 12H, CH_2-CH_3). ESI-MS(+): cald 1206.34 obsd 603,8 ($M + 2H^+$).

Reaction of (**6**) to (**7**): 180.6 mg (0.15 mmol) of (**6**) dissolved in methanol was kept under hydrogen atmosphere with 10%w/w Pd/C for 12 h. After removing the solids and the solvent the resulting colourless oil (151.4 mg, 95%) was used without further purification. 48.7 mg (0.17 mmol) 4-(p-iodophenyl)butyric acid (Sigma-Aldrich) was dissolved in 2 mL N-methyl-2-pyrrolidone (NMP) together with 63.9 mg (0.17 mmol) HATU and 54.26 mg (0.45 mmol) DIPEA. The mixture was incubated at room temperature for 15 min, until it was added to a 2 mL NMP solution containing the amine from (**6**). The reaction mixture was stirred overnight and the solvent was removed in vacuum. The crude residue was dissolved in 20 mL dichloromethane and extracted three times with an equivolume of 0.1 M Na_2CO_3, 0.1 M NaH_2PO_4 and finally with water. After column chromatography on silica ($CHCl_3$:MeOH 20:1) a pale foam of 147.8 mg (0.11 mmol, 73%) was obtained. R_f (silica, $CHCl_3$:MeOH 20:1) = 0.3-0.4. ESI-MS(+): cald 1343.57 obsd 672.8 ($M + 2H^+$).

The final product DOTAGA(**428**-D-Lys)M^{BP} (**8**) was obtained by successive dealkylation of (**7**). 147.8 mg (0.11 mmol) (**7**) was dissolved in a mixture of DCM/TFA 2:3 and stirred for 12 h. After evaporation of the volatiles the remaining TFA was removed by repeated co-evaporation with MeOH. Subsequently, the colourless solid was dissolved in 2 mL DMF and 20 eq. (340 mg) of trimethylsilyl bromide (TMS-Br) was added under argon atmosphere. The reaction mixture was kept at room temperature and by exclusion of light for 12 h, until the volatiles were removed under reduced pressure. Hydrolysis of the TMS-ester was realized by dissolving the crude red oil in methanol. After 12 h the mixture was evaporated to dryness, yielding 101.2 mg (85%) of the crude product which was further purified by semi preparative reversed phase HPLC (Hydrosphere C-18, 5µ, 250 x 10 mm, YMC, Japan) by using a solvent gradient (3 mL/min) of 100% water to 80% acetonitrile. Fractions containing the product were determined by ESI-MS(-) and were combined. After lyophilisation 80 mg (69%) of a white solid was obtained. ^{1}H-NMR (D_2O/NaOD, 300 MHz): δ 7.63 (d, 2H, benzyl-*H*, J_H=8.2

Hz), 7.02 (d, 2H, benzyl-*H*, J_H=8.2 Hz), 3.33 (bs, 6H, N-*CH*$_2$-*CO*), 3.19 (t, 2H, alkyl-*H*), 2.60 (t, 2H, alkyl-*H*) 1.2-2.6 (bm, 32H, cyclen-*H*, alkyl-*H*). ^{31}P-NMR (D_2O/NaOD, 162.05 MHz): δ 14.87 ESI-MS(-): cald 1049.24 obsd 524 (M - $2H^+$).

4.3. Radiolabelling with n.c.a. ^{68}Ga and quality control

50 µg (48 nmol) of DOTAGA(**428**-D-Lys)M^{BP} was dissolved in 500 µL of a 0.5M sodium acetate buffer at pH = 4 and added to n.c.a. ^{68}Ga (300-600 MBq), which was obtained in 400 µL acetone/HCl from a ^{68}Ge/^{68}Ga generator system by cationic post processing [18]. The solution was kept under moderate shaking on a thermo shaker for 15 min at 98°C. Subsequently the solution was diluted up to 2 mL with deionized water and passed over a SPE cartridge (Strata X, Phenomenex). The solid phase was first washed with 3 mL of water followed by the elution of the purified product with 1 mL of an ethanol/water mixture. Aliquot samples were taken for radio HPLC (Hydrosphere C-18, 5µ, 250 x 10 mm, YMC, Japan, solvent A: H_2O B: ACN, 5 mL/min gradient flow) and TLC (silica, solvent: 0.1 M citrate buffer pH = 4) analysis.

[^{68}Ga]BPAMD was prepared by dissolving 20 µg (33 nmol) of BPAMD in 500 µL 0.5M sodium acetate buffer at pH = 4. 400 µL n.c.a. ^{68}Ga solution was added and the reaction kept on a thermo shaker for 15 min at 98°C. The solution was diluted with water up to 5 mL and passed over a SPE cartridge (Isolute NH2, Biotage). The cartridge was washed with 1 mL water followed by the elution of the purified [^{68}Ga]BPAMD with 2 mL phosphate buffered saline (PBS). Aliquot samples were taken for radio-HPLC (MultoKrom 100 C18, 5µ, 250 x 4 mm, CS-Chromatographie, Germany, solvent A: 10 mM tetrabutylammonium citrate pH = 4.5 B: ACN, 1 mL/min gradient) and TLC (silica, solvent: acetone/acetylacetone/HCl, 10:10:1).

4.4. Adsorption experiments on apatite

20 mg of hydroxy apatite (HA) powder (Sigma-Aldrich, Germany) was incubated for 24 h in 1 mL isotonic saline. 50 µL of the ^{68}Ga-labelled bisphosphonate solution (prepared as described above) was added and vortexed for 15 seconds. After 10 minutes the HA was centrifuged at 10 x g and the supernatant was removed. 0.5 mL isotonic saline was added to the Ha fraction, vortexed for 15 seconds and centrifuged again. The supernatant was removed and combined with the first solution. Radioactivity was determined in the combined supernatants and the ^{68}Ga-complex binding to HA was calculated as percent of ^{68}Ga absorbed to HA [4].

4.5. Protein binding assay

Binding to serum proteins of [^{68}Ga]BPAMD and [^{68}Ga]DOTAGA(**428**-D-Lys)M^{BP} was determined by ultrafiltration. 50 µL of each radio tracer was added to 200 µL human serum samples (Sigma-Aldrich, Germany), vortexed and incubated for 1 min. The sample was transferred to a centrifugal device (Nanosep®, 30K, Pall Corporation, USA) containing a filtration membrane which separates proteins from small molecules. As a control the radio tracers were incubated in isotonic saline. The ultrafiltration device was centrifuged for 45 minutes, until 50 µL of isotonic saline was added to wash the filter by an additional 15 minute centrifugation step. Radioactivity was counted in the filter and the filtrate solution and calculated as a fraction of the total activity, which was set to 100% [13].

4.6. Animal studies

The experimental procedure used conforms to the European Convention for the Protection of Vertebrate Animals used for Experimental and other Scientific Purposes (ETS No. 123), and to the Deutsches Tierschutzgesetz (German animal welfare regulations). Male Wistar rats (154 ± 24 g, N = 10, 1 h; 215 ± 18 g, N = 12, 3 h) were purchased from Charles River Laboratories International, Inc. For dynamic *in vivo* µPET studies, the animal was

anesthetized with isoflurane and placed in supine position in the PET scanner (Siemens microPET, Focus 120). An infrared lamp was used to maintain body temperature. 19.8 MBq [^{68}Ga]BPAMD (107 MBq per Kg body weight) and 17.0 MBq [^{68}Ga]DOTAGA(**428**-D-Lys)M^{BP} (92 MBq per Kg body weight) in 0.5 mL isotonic saline were administered intravenously using a needle catheter into the tail vein. The focus of the µPET scanner was adjusted to the thorax region. Each compound was tested in one and the same animal in a time distance of two days. In an additional experiment the focus of the µPET scanner was adjusted to the pelvis region to examine the tracer accumulation in the articulation between the femur and the tibia. The experiment was done in the same animal with in a timescale of two days. 16.3 MBq [^{68}Ga]BPAMD (80 MBq per Kg body weight) and 16.1 MBq [^{68}Ga]DOTAGA(**428**-D-Lys)M^{BP} (79 MBq per Kg body weight) in 0.5 mL isotonic saline were administered intravenously. All images were reconstructed to OSEM2D and processed using Pmod (PMOD Technologies Ltd.) software.

Ex vivo organ distribution was carried out in five animals (160-210 g) per time point and compound. A mean dose of 10 ± 2 MBq of the ^{68}Ga-labelled bisphosphonates in 0.5 mL isotonic saline were injected intravenously in the tail vein. Animals were sacrificed at 1 h and 3 h after injection. The organs of interest were excised, weighted and the radioactivity in the samples were measured decay- and background-corrected on an automated gamma counter. Data were normalized to the body weight (BW) and expressed in SUV, determined by the formula: (activity per g tissue)/(injected activity) × BW. The activity in the skeleton was calculated by using the activity concentration in the femur and the total skeleton weight (calculated as: skeleton weight (g) = 9.66 + 0.0355 × BW (g)) [10]. Blood density was set to 1.05 mg/mL. The blood volume (BV) of the Wistar rats were calculated using the formula: BV (mL) = 0.06 × BW (g) + 0.77 to determine total blood activities of the radio tracers [19].

4.7. Statistical analysis

All data were expressed as mean ± SD. Groups were compared using the t-test. All statistical tests were two tailed, with a P-value of less than 0.05 representative for significance.

5. Acknowledgment

This study was supported by the grant of the Max Planck Graduate Center Mainz.

6. References

[1] K. N. Weilbaecher, T. A. Guise, L. K. McCauley, Cancer to bone: a fatal attraction, *Nature Reviews: Cancer*, **2011**; 11: 411.

[2] O. Sartor, P. Hoskin, Ø. S. Bruland, Targeted radio-nuclide therapy of skeletal metastases, *Cancer Treatment Reviews*, **2013**; 39: 18–26.

[3] K. Ogawa, H. Kawashima, K. Shiba, H. Sajib, Development of [^{90}Y]DOTA-conjugated bisphosphonate for treatment of painful bone metastases, *Nucl. Med. and Biol.*, **2009**; 36: 129–135.

[4] M. Fellner, P. Riss, N. Loktionova, K. Zhernosekov, O. Thews, C. F. G. C. Geraldes, Z. Kovacs, I. Lukes, F. Rösch, Comparison of different phosphorus-containing ligands complexing ^{68}Ga for PET-imaging of bone metabolism, *Radiochim. Acta*, **2011**; 99: 43–51.

[5] T. Vitha, V. Kubícek, P. Hermann, Z. I. Kolar, H. T. Wolterbeek, W.A.P. Breeman, I. Lukeš, J. A. Peters, Lanthanide(III) Complexes of Bis(phosphonate) Monoamide Analogues of DOTA: Bone-Seeking Agents for Imaging and Therapy, *J. Med. Chem*. **2008**; 51: 677–683.

[6] M. Fellner, R. P. Baum, V. Kubíček, P. Hermann, I. Lukeš, V. Prasad, F. Rösch, PET/CT imaging of osteoblastic bone metastas with ^{68}Ga-bisphosphonates: first human study, *Eur. J. Nucl. Med. Mol. Imaging*, **2010**; 37: 834.

[7] M. Fellner, B. Biesalski, N. Bausbacher, V. Kubícek, P. Hermann, F. Rösch, O. Thews, ^{68}Ga-BPAMD: PET-imaging of bone metastases with a generator based positron emitter, Nuclear Medicine and Biology, **2012**; 39: 993–999.

[8] F. Rösch, R. P. Baum, Generator-based PET radiopharmaceuticals for molecular imaging of tumours: on the way to THERANOSTICS, *Dalton Transactions*, **2011**; 40: 6104.

[9] R. Bartl, B. Frisch, E. von Tresckow, C. Bartl, *Bisphosphonates in Medical Practice*, Springer-Verlag Berlin Heidelberg **2007**, pp. 43-46.

[10] M. Meckel, M. Fellner, R. Bergmann, F. Rösch, In vivo comparison of DOTA based ^{68}Ga-labelled bisphosphonates for bone imaging in non-tumour models, *Nucl. Med. and Biol.*, **2013**; 40: 823–830.

[11] C. E. Dumelin, S. Trüssel, F. Buller, E. Trachsel, D. Neri, J. Scheuermann, A portable albumin binder from a DNA-encoded chemical library, *Angew. Chem. Int. Ed.* **2008**; 47: 3196 –3201.

[12] M. Fani, X. Wang, G. Nicolas, C. Medina, I. Raynal, M. Port , H.R. Maecke, Development of new folate-based PET radiotracers: preclinical evaluation of ^{68}Ga-DOTA-folate conjugates. *Eur. J. Nucl. Med. Mol. Imaging*. **2011**; 38: 108-19.

[13] C. Müller, H. Struthers, C. Winiger, K. Zhernosekov, R. Schibli, DOTA conjugate with an albumin-binding entity enables the first folic acid-targeted ^{177}Lu-radionuclide tumor therapy in mice. *J. Nucl. Med.*, **2013**; 54: 124-31.

[14] C. R. Fischer, V. Groehn, J. Reber, R. Schibli, S. M. Ametamey, C. Müller, Improved PET Imaging of Tumors in Mice Using a Novel ^{18}F-Folate Conjugate with an Albumin-Binding Entity, *Mol. Imaging. Biol.*, **2013**; 15: 649-654.

[15] P. J. Riss, C. Burchardt, F. Rösch, A methodical ^{68}Ga-labelling study of DO2A-(butyl-L-tyrosine) 2 with cation-exchanger post-processed ^{68}Ga: practical aspects of radiolabelling, *CMMI*, **2011**; 6: 492-498.

[16] K.-P. Eisenwiener, P. Powell, H. R. Maecke, A Convenient Synthesis of Novel Bifunctional Prochelators for Coupling to Bioactive Peptides for Radiometal Labelling, *Bioorg. & Med. Chem. Lett.*, **2000**; 10: 2133-2135.

[17] V. Kubicek, J. Rudovský, J. Kotek, P. Hermann, L. Van der Elst, R. N. Muller, Z. I. Kolar, H. T. Wolterbeek, J. A. Peters, I. Lukeš, A Bisphosphonate Monoamide Analogue of DOTA: A Potential Agent for Bone Targeting, *JACS*. **2005**, 127, 16477-16485.

[18] K. Zhernosekov, D. V. Filosofov, R.P. Baum, P. Aschoff , H. Bihl, A. A. Razbash, M. Jahn, M. Jennewein, F. Rösch, Processing of generator-produced ^{68}Ga for medical application, *J. Nucl. Med.*, **2007**; 48: 1741.

[19] H. B. Lee, M. D. Blaufox, Blood volume in the rat, *J. Nucl. Med.*, **1985**; 26: 72-6

.

3.6. ^{177}Lu labelled macrocyclic bisphosphonates for targeting disseminated in cancer treatment.

^{177}Lu labelled macrocyclic bisphosphonates for targeting disseminated in cancer treatment

Ralf Bergmann[1], Marian Meckel[2], Andrea Suhl[1], Jens Pietzsch[1], Vojtech Kubicek[3], Jörg Steinbach[1], Petr Hermann[3] and Frank Rösch[2]

[1]*Institute of Radiopharmacy, Helmholtz-Zentrum Dresden-Rossendorf, Germany*

[2]*Institute of Nuclear Chemistry, University Mainz, Germany.*

[3]*Department of Inorganic Chemistry, Charles University Prague, The Czech Republic.*

.

Keywords

Bisphosphonate, bone metastases, ^{177}Lu, DO2A, DOTA, organ distribution, theranostics.

Abstract

General: Metastatic bone lesion is a common syndrome of many cancer diseases in an advanced state. The major symptom is severe pain, spinal cord compression and pathological fracture, associated with an obvious morbidity. Common treatments including systemic application of bisphosphonate drugs aim on pain reduction and on improving the quality of life of the patient. Particularly patients with multiple metastatic lesions benefit from bone-targeting therapeutic radiopharmaceuticals. Agents utilizing beta-emitting radionuclides in routine clinical praxis are, for example, [^{89}Sr]$SrCl_2$ and [^{153}Sm]EDTMP. No carrier added (n.c.a.) ^{177}Lu is remarkably suitable for an application in this scope.

Methods: Five DOTA and DO2A based bisphosphonates, including including monomeric and dimeric structures and one NO2A derivative, were synthesized and labelled with n.c.a. ^{177}Lu. Radio-TLC and HPLC methods for quality control were successful established. Their stability and binding to hydroxyapatite were measured *in vitro*. *Ex vivo* biodistribution experiments and dynamic *in vivo* SPECT/CT measurements were performed in healthy rat for 1 hour time points. Data on %ID/g or SUV for femur, blood and soft tissue organs were analysed and compared with [^{177}Lu]citrate.

Results: Radiolabeling yields for ^{177}Lu-DOTA and NO2A monomeric bisphosphonate complexes was >98% within 15 minutes. The dimeric macrocyclic bisphophosphonates showed a decelerated labelling kinetic reaching a plateau after 30 min of a RCY = 60 to 90 %. All ^{177}Lu-bisphosphonate complexes showed exclusively accumulation in the skeleton. Blood clearance and renal elimination were fast ($t_{1/2\alpha,blood}$ = 5-10 min) After 60 min SUV data in the femur ranged from 3.34 to 5.67. The bone/blood ratios were between 3.6 and 135.6, correspondingly. ^{177}Lu-bisphosphonate dimers showed a slightly higher bone accumulation (SUV_{femur} = 4.48 ± 0.38 for [^{177}Lu]DO2A(P^{BP})$_2$; SUV_{femur} = 5.41 ± 0.46 for [^{177}Lu]DOTA(M^{BP})$_2$) but a decreased blood clearanced (SUV_{blood} = 1.25 ± 0.09 for [^{177}Lu]DO2A(P^{BP})$_2$; SUV_{blood} = 1.43 ± 0.32 for [^{177}Lu]DOTA(M^{BP})$_2$), after 60 min. In

conclusion, ^{177}Lu-complexes of macrocyclic bisphosphonates might be become therapy options for skeletal metastases.

1. Introduction

The treatment of cancer is one of the most important challenge of mankind. In the year 2012 worldwide 8.2 million people died in consequence of this disease, while 32.6 million are living with cancer [1]. Quite often the bones are afflicted by invasive primary tumours. These bone metastases occur for example in 65 % to 80 % of patients with breast and prostate cancer [2]. The fatal consequences are various, including bone fractures, hypercalcaemia, spinal cord and nerve-compression and severe bone pain syndromes [2,3]. The overall prediction for a cure is poor and the common therapy tends, in the present, to a palliative care. Since skeletal metastases disturb the close metabolic balance between the activity of osteoblasts and osteoclasts, bone seeking radiopharmaceuticals showed promising results in the last decades both for diagnosis and therapy [3]. The mechanism of the therapy effect is the synergy of an enhanced accumulation of osteotropic agents on the metastatic lesion and the energy deposit by particle radiation (β^-, inner conversion or α-particles). One of the earliest therapeutic concepts was the administration of $^{89}SrCl_2$ as a calcium mimetic [4]. While ^{89}Sr showed unfavourable nuclear properties in the such as β-energy and half-life (β_{max} = 1.5 MeV, $t_{1/2}$ = 50.d d) [5], new radiopharmaceuticals, like [^{153}Sm]Sm-EDTMP were utilized. More radionuclides are under consideration such as IC-transforming ^{117m}Sn. Recently, α-emitting [^{223}Ra]$RaCl_2$ was introduced [3].

The potential of lanthanide radionuclides for bone targeting was recognized early [6]. Skeletal ^{177}Lu-images were obtained with the Anger camera already in the 60´s [7]. The γ-photons of 113 keV (6.4%) and 208 keV (11.4%) [8] from the ^{177}Lu decay are a pleasant side effect for the usage in Single Photon Computed Tomography (SPECT), whereas today the focus of ^{177}Lu-compounds is mainly on the therapeutic benefit of the β^--emission. ^{177}Lu-labelled somatostatine analogs are successfully used in the treatment of neuroendrocrine

tumours in the peptide receptor radionuclide therapy (PRRT) [9]. The ideal nuclide properties of a half-life of 6.7 d and the maximum β-energy of 0.497 MeV [8] together with the carrier free production route, makes ^{177}Lu an interesting candidate in the treatment of skeletal metastases.

In the early times of radiopharmacy it was discovered already that the addition of chelating agents alters the biological distribution of lanthanides from primary liver up-take to almost exclusively bone accumulation [7]. "Bone seeking" polycarboxy-polyphosphates like EDTMP (ethylenediamine tetra(methylene phosphonic acid)) showed promising first results [10,11]. Due to their low stability with lanthanide ions (log$K$ = 14.4) [12] a high EDTMP concentration in the blood pool is necessary for a stable complexation *in vivo*, which consequently creates a high amount of carrier [13]. As opposed to these open chain, macrocyclic chelators, like DOTA (1,4,7,10-tetraazacyclododecane N,N',N'',N'''-tetra-acetic acid) show a very strong thermodynamic and kinetic stability (log$K$ = 25.4) with lanthanides[14,15]. Even equimolar metal to DOTA ratios show well complexation and *in vivo* stability results. Initial experiments with phosphonic acid derivatives (DOTP) of DOTA complexed with ^{177}Lu showed sufficient bone accumulation and low uptake in soft tissue [16].

Theranostic concepts, which in one compound combine imaging and therapy modalities, come more and more into the focus also in nuclear medicine. An ideal chelator based PET (positron emission thomography) nuclide is the generator derived ^{68}Ga. In contrary to the ^{177}Lu outcomes, [^{68}Ga]EDTMP and [^{68}Ga]DOTP showed only disappointing results [17,18]. The first compound, which yielded excellent ^{68}Ga-PET was the DOTA-based bisphosphonate BPAMD (for formula see Chart 1) [19,20]. [^{68}Ga]BPAMD-PET/CT showed uptake values on disseminated bone metastases as high as ^{18}F-fluoride, sometimes even superior [21]. Recently, the NOTA-derivative [^{68}Ga]NO2AP^{BP} was identified to show even improved imaging quality [22]. The current question is, whether analogue macrocyclic bisphosphonate ligands can directly converted from ^{68}Ga complexes to ^{177}Lu analogues, i.e. retaining organ uptake and pharmacology profiles known from Ga(III) structures, or whether an alternative ligand chemistry is needed to match the coordination features of Lu(III).

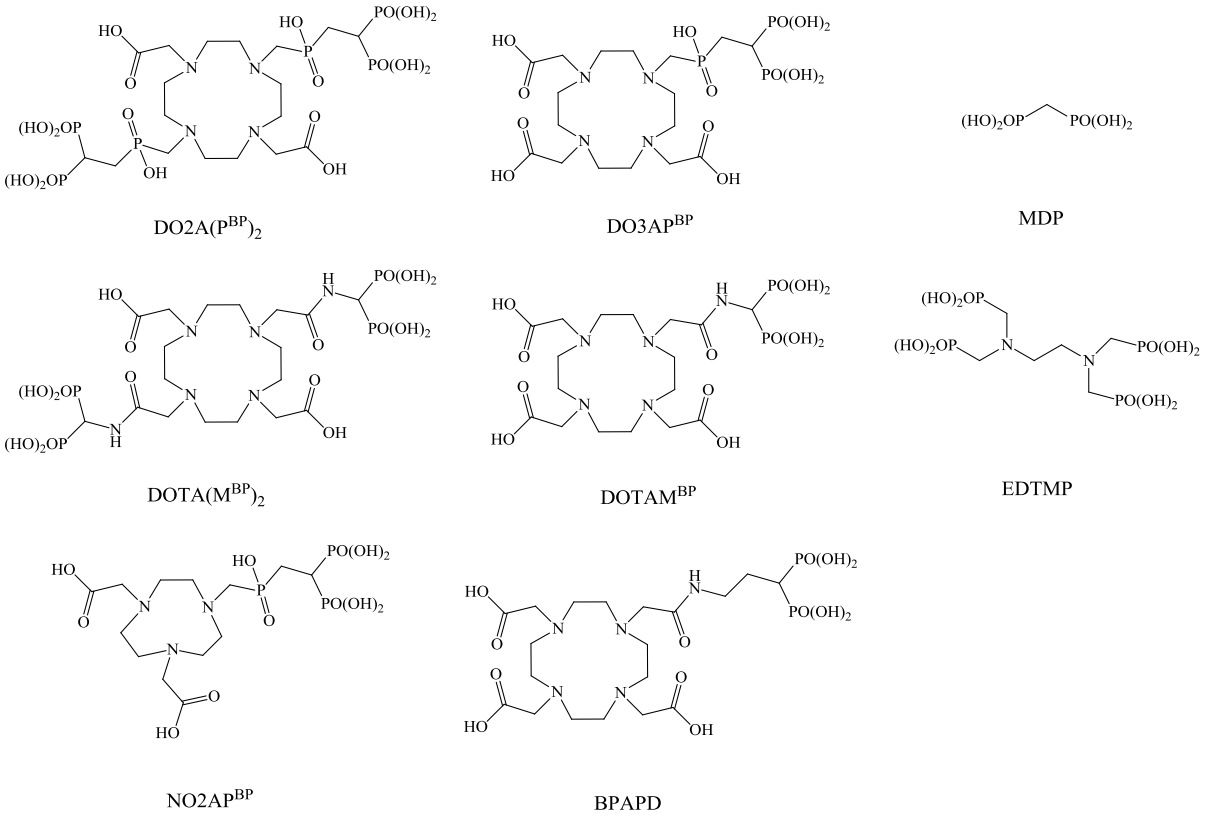

Chart 1. Structure of ligands discussed in this paper.

Currently, several new macrocyclic bisphosphonates are intensely discussed in the literature as candidates for complex formation with ^{177}Lu and ^{90}Y and subsequent "bone seeking" parameters, including hydroxy bisphosphonates [23] and phosphinates (Chart 1) [24]. In this paper the biodistribution and bone accumulation of various macrocyclic bisphosphonates, including two dimeric DOTA and one NO2A (1,4,7-triazacyclononane-1,4-diacetic acid) compounds (Chart 1) were studied in a healthy rat model. The ligand synthesis, in particular the synthesis of the new dimeric bisphosphonates DO2A(P^{BP})$_2$ and DOTA(M^{BP})$_2$ as well as labelling, radio-analytics with ^{177}Lu are reported. All the ^{177}Lu species were investigated in healthy rats in *in vivo* small animal SPECT and *ex vivo* organ distribution (1 h p.i.) studies and SUV data were determined (n=4) of the interested organs.

2. Experimental

Chemicals: Chemicals and solvents were commercially available in analytical or HPLC grade and were purchased from Sigma-Aldrich or Merck KGaA

Analytics: Proton nuclear magnetic resonance (^{1}H-NMR) spectra were recorded on a Bruker 300, ^{31}P-NMR were recorded on a Bruker 600. NMR shifts were referenced to internal TMS or externally referenced to 85 % aq. H_3PO_4 signal. Mass spectra were recorded on Agilent Technologies 6130 Quadrupole LC/MS spectrometer with ESI as ion source in positive or negative modes. TLC analyses of the ligand and intermediates during their synthesis were carried out with silica on aluminium foil (Merck).

Radio-TLC analysis of labelled compounds were carried out with silica on aluminium foil (Merck) or RP18 on alumina and a Canberra Packard Instant Imager. Radio-HPLC was performed on a Hewlett Packard Series 1100 with a Raytest (Radeberg, Germany) Ramona radiodetector. Radioactivity of samples was measured with an Aktivimeter Isomed 2010, MED (Nuklear-Medizintechnik Dresden GmbH).

Radionuclides: N.c.a. ^{177}Lu was produced via the ^{176}Yb-based neutron capture pathway provided by ITG (Garching, Germany) as $LuCl_3$ in 0.05 M HCl [25].

2.1. Synthesis of the dimeric bisphosphonates DOTA(M^{BP})$_2$ and DO2A(P^{BP})$_2$

1,4,7,10-tetraazacyclododecane-1,7-bis-tert.butyl diacetic acid ester (**tert.Butyl-DO2A**) [26], tetraethyl chloro-acetamidomethyl-bis(phosphonate) (**1**), tetraethyl{[(ethoxyhydrophosphoryl)methyl]methylene} bis(phosphonate) (**4**) and the compounds DOTAM^{BP}, DO3AP^{BP}, DOTAM^{EBP} and NO2AP^{BP} were synthesized according to the published literature [22,27,28].

DOTA(M^{BP})$_2$ in ester form (**2**): Tert.Butyl-DO2A (200 mg, 0.5 mmol) was dissolved in 50 mL dry acetonitrile. Potassium carbonate (10 eq., 5 mmol, 691 mg) was added and the

mixture was heated to 40°C. tetraethyl chloro-acetamidomethyl-bis(phosphonate) (**1**) (5 eq., 2.5 mmol, 948 mg) was dissolved in 25 mL dry acetonitrile and added drop wise to the DO2A solution. The reaction mixture was kept at 40°C for 24 h under stirring and Argon atmosphere. Activated charcoal was added, the solution was filtered and the solvent was removed under reduced pressure. The crude product was purified by column chromatography (silica phase using a solvent mixture of NH_4OH:MeOH:EA (1:4:15). R_f = 0.2-0.4) resulting in a yellow oil (308.5 mg, 57%). ^{1}H-NMR ($CDCl_3$, 300 MHz): δ 1.37 (m, 24H, CH_2-*CH_3*), 1.46 (s, 18H, *t-Bu*), 2.6-3.0 (bs, 8H, cyclen- *CH_2*-N), 3.1-3.5 (bs, 8H, cyclen- *CH_2*-N), 3.5 (s, 8H, N-*CH_2*-CO), 4.23 (m, 8H, *CH_2*-CH_3), ^{31}P-NMR ($CDCl_3$, 162.05 MHz): δ 7.78 (s, 2P). ESI-MS(+): cald 1086.49 obsd 1087.50 ($M + H^+$), 1109.48 ($M + Na^+$).

DOTA(M^{BP})$_2$ (**3**): The protected compound (**2**) (308.5 mg, 0.29 mmol) was dissolved in dry dichloromethane and Trimethylsilylbromide (20 eq., 6 mmol, 920 mg) was added at room temperature under argon atmosphere. The reaction mixture was stirred overnight and volatiles were removed under reduced pressure. The resulting red oil was dissolved in methanol and stirred for 5 h until the solvent was removed. The residue was kept under high vacuum to remove volatiles until no change in weight was observed. Subsequent a 2:1 mixture of TFA/DCM was added and the mixture was stirred overnight under argon atmosphere. After removing the solvents under reduced pressure the crude compound was purified two times by recrystallization from boiling water. The precipitating white solid was filtered, washed with ethanol and dried in vacuum with a yield of 140 mg (64%). ^{1}H-NMR (D_2O/NaOD, 300 MHz): δ 2.84 (bs, 8H, cyclen-*CH_2*-N), 2.92 (bs, 8H, cyclen-*CH_2*-N), 3.37 (bs, 4H, N-*CH_2*-CO), 3.64 (bs, 4H, N-*CH_2*-CO), 4.38 (t, 2H, P-*CH*-P, $^2J_{PH}$=18.22 Hz). ^{31}P-NMR (H_2O/NaOD, 162.05 MHz): δ 13.5. ESI-MS(–): cald 750.42 obsd 749.21 ($M - H^+$), 374.10 ($M - 2H^+$).

DO2A(P^{BP})$_2$ in ester form (**5**): To a solution of bisphosphonate (**4**) (2.4 g, 6 mmol) in 70 mL dry toluene 601 mg tert.Butyl-DO2A (0.25 eq., 1.5 mmol) and 180 mg (1 eq., 6 mmol) paraformaldehyde was added. The reaction solution was stirred under reflux for 24 h. The solvent was removed under reduced pressure and the residue was purified by column chromatography (silica gel, NH_4OH:MeOH:EA (1:4:15). R_f = 0.2-0.3) resulting in 625 mg

(35%) of a pale yellow oil. ^{31}P-NMR ($CDCl_3$, 162.05 MHz): δ 22.3 (m, 4P), 36.3 (m, 2P). ESI-MS(+): cald 1212.52 obsd 1213.51 ($M + H^+$), 1236.53 ($M + Na^+$).

DO2A(P^{BP})$_2$ (**6**): The protected bisphosphonate (**5**) (625 mg, 0.52 mmol) was dissolved in 50 mL 6 M aqueous HCl and kept at a temperature of 100°C for 24 h. The solvent was evaporated under reduced pressure and the excess of HCl was removed by repetitive co-evaporation from deionized water. The crude product was passed over a strong cation exchanger (Dowex 50, H^+-form) and the aqueous solution was dried by lyophilisation. The white solid was further purified by recrystallization from boiling water. Precipitation was initiated by adding small volumes of ethanol. The white solid (337 mg, 79%) was filtered, washed with ethanol and dried in vacuum. ^{1}H-NMR (D_2O/NaOD, 300 MHz): δ 2.56 (m, 4H –*CH$_2$*–CH), 3.1 (bs, 8H, cyclen-*CH$_2$*-N), 3.3 (bs, 8H, cyclen-*CH$_2$*-N), 3.4 (bs, 4H, N-*CH$_2$*-P) 3.5 (m, 2H, P-*CH*-P) 3.7 (bs, 4H, N-*CH$_2$*-CO). ^{31}P-NMR (D_2O/NaOD, 162.05 MHz): δ 22.01 (s, 4P), 43.50 (s, 2P). ESI-MS(–): cald 820.08 obsd 819.04 ($M - H^+$), 409.00 ($M - 2H^+$).

2.2. Radiolabelling with n.c.a. ^{177}Lu and quality control

Labelling of bisphosphonates with n.c.a. ^{177}Lu was performed in 0.1 M sodium acetate buffer at pH = 4, by adding 4 volume equivalents of buffer to a solution of $^{177}LuCl_3$ in 0.05 M HCl. A 10 molar excess, based on ^{177}Lu concentration, of bisphosphonate containing chelator was added and the solution was kept on a thermo shaker at 98ºC up to 30 minutes. [^{177}Lu]citrate was prepared by adding 100 µL $^{177}LuCl_3$ in 0.05 M HCl to 100 µL of 0.25 M citrate buffer. Radiochemical yields (RCY) were determined by radio-HPLC (Zorbax 300SB-C18, 9.4 x 250 mm 5µ, solvent: 100 mM tetraethylammonium phosphate pH=2.24, 1 mL/min isocratic flow) and were cross-checked by two radio-TLC methods (silica, solvent: 0.1 M citrate buffer pH 4 and RP18 on alumina, solvent: 100 mM tetraethylammonium phosphate pH=2.24 + 20% ACN).

2.3. Animal studies

The experiments were realized corresponding to the german animal welfare regulations, institutional guidelines and with the permission of the local animal research committee at the Landesdirektion Dresden. All experimental procedures are following the guidelines of the *European Convention for the Protection of Vertebrate Animals used for Experimental and other Scientific Purposes (ETS No. 123)*. Male Wistar rats weighing157.69 ± 17.10 g (mean ± SD, N = 35), were purchased from Unilever (HsdCpb:WU, Harlan Winkelmann, Borchen, Germany). Anaesthetization was initiated and maintained by desflurane and animals were put in the supine position and placed on a heating pad to maintain body temperature. A needle catheter was used for administration of the tracers in the tail vein. A second catheter was introduced into the right femoral artery for the extraction of blood samples for metabolite analysis, which was routinely done during SPECT/CT measurements.

2.4. *Ex vivo* organ distribution

The male Wistar rats received a short term anaesthetization by desfluran inhalation and a mean activity of 2.36 ± 0.27 MBq/kg of the ^{177}Lu labelled tracers in isotonic saline were injected in a volume of. 0.5 mL in the tail vein, with the following specific details: [^{177}Lu]citrate: 2.56 ± 0.07 MBq/kg, 128.58 body-weight (BW, g), n = 4 (g); [^{177}Lu]BPAMD: 2.33 ± 0.11 MBq/kg, 159.41 BW (g), n = 4 (g); [^{177}Lu]BPAPD: 2.58 ± 0.24 MBq/kg, 156.38 BW (g), n = 4 (g); [^{177}Lu]BPPED: 2.27 ± 0.25 MBq/kg, 153.43 BW (g), n = 4 (g); [^{177}Lu]NO2AP^{BP}: 2.52 ± 0.25 MBq/kg, 173.82 BW (g), n = 4 (g); [^{177}Lu]DOTA(M^{BP})$_2$: 1.80 ± 0.10 MBq/kg, 181.64 BW (g), n = 4 (g); [^{177}Lu]DO2A(P^{BP})$_2$: 2.46 ± 0.15 MBq/kg, 150.60 BW (g), n = 4 (g). Animals were sacrificed after 60 min p.i. and organs of interest were excised rapidly, weighted and the ^{177}Lu activity was determined with a Wallac WIZARD automatic gamma counter (PerkinElmer, Germany) and were decay corrected. The distribution data is expressed in %ID/g tissue or is normalized to the BW as SUV (standard uptake value), which was calculated with the formula: SUV = (activity per g tissue)/(injected activity) × BW. The skeleton weight was calculated using: skeleton weight = 9.66 + 0.0355 ×

BW and the total activity associated with the skeleton was calculated by using the activity concentration in the femur and the total skeleton weight [29].

2.5. Metabolite Analysis and *in vivo* stability

Arterial blood plasma samples were taken during SPECT/CT examinations after 1, 3, 5, 10, 20, 30, 60 and 120 min. p.i. and the *in vivo* metabolism of [^{177}Lu]BPAMD, [^{177}Lu]BPAPD, [^{177}Lu]BPPED, [^{177}Lu]NO2AP^{BP}, [^{177}Lu]DOTA(M^{BP})$_2$ and [^{177}Lu]DO2A(P^{BP})$_2$ was analyzed. Plasma was separated by centrifugation (3 min, 11000 g) followed by precipitation of the plasma proteins with ice-cold methanol (1.5 parts per 1 part plasma) and centrifugation (3 min, 11000 g). The supernatants were analyzed by radio-TLC and HPLC using the above mentioned methods for quality control. Additionally urine samples were treated in the same way prior radio-TLC and radio-HPLC analysis.

2.6. SPECT/CT

Tracer accumulation *in vivo* was monitored with a nanoScan® SPECT (Mediso Medical Imaging Systems, Budapest, Hungary) scanner. CT images were obtained with a nanoScan® PET/CT (Mediso Medical Imaging, Budapest Hungary) scanner. Rats were prone and head first positioned. The animals were anesthetized by 5% desflurane inhalation.

2.8. Statistical analysis

The statistical analyses was performed by using GraphPad Prism (V5.02 for Windows, GraphPad Software, San Diego California USA, www.graphpad.com). Data are expressed as an average ± standard deviation (S.D.). Two tailed students t-test was usually done to compare groups of data.

3. Results

3.1. Synthesis

The pendant arms (**1**) and (**4**) were prepared as described in literature procedures (see *experimental* part) in good yields. Alkylation of DO2A was done by a nucleophilic substitution (**2**) or by a mannich like reaction (**5**), followed by a two-step cleavage (**3**) of the protection groups, by using trimethylsilyl bromide as a mild and efficient de-esterification agent of ethyl protected bisphosphonates and trifluoroacetic acid for the *t*-butylesters of the carboxylic acid arms. 6 M aqueous HCl was used to de-protect the phosphinate compound (**6**) (Scheme 1). The final dimeric bisphosphonates DOTA(M^{BP})$_2$ (**3**) and DO2A(P^{BP})$_2$ (**6**) were obtained in moderate yields after resin and recrystallization purification.

Scheme 1. Synthesis of DOTA(M^{BP})$_2$ and DO2A(P^{BP})$_2$

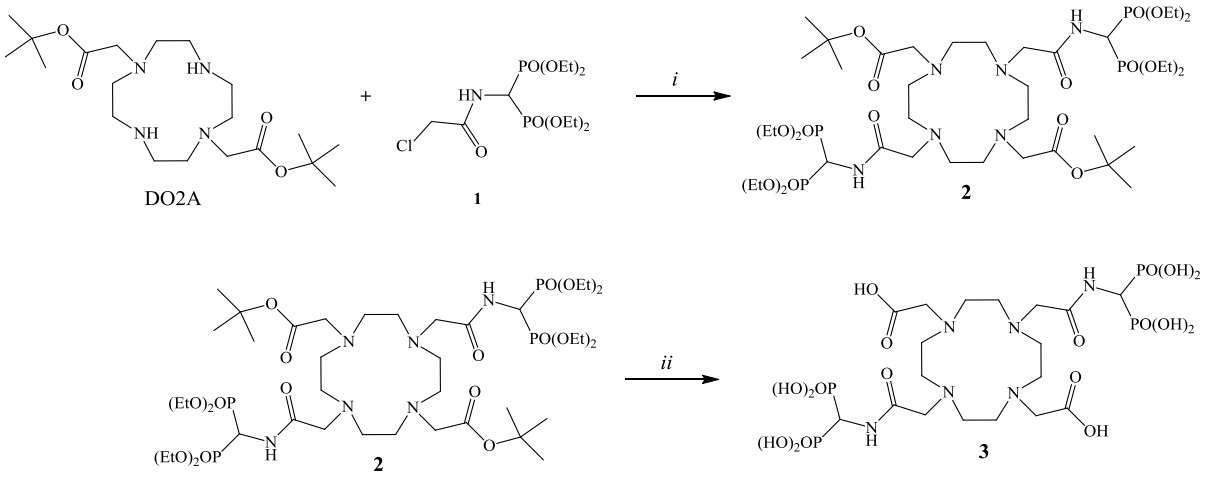

i) K_2CO_3, acetonitrile, 40°C *ii*) 1. TMS-Br, DCM, RT; 2. MeOH; 3. TFA/DCM, RT.

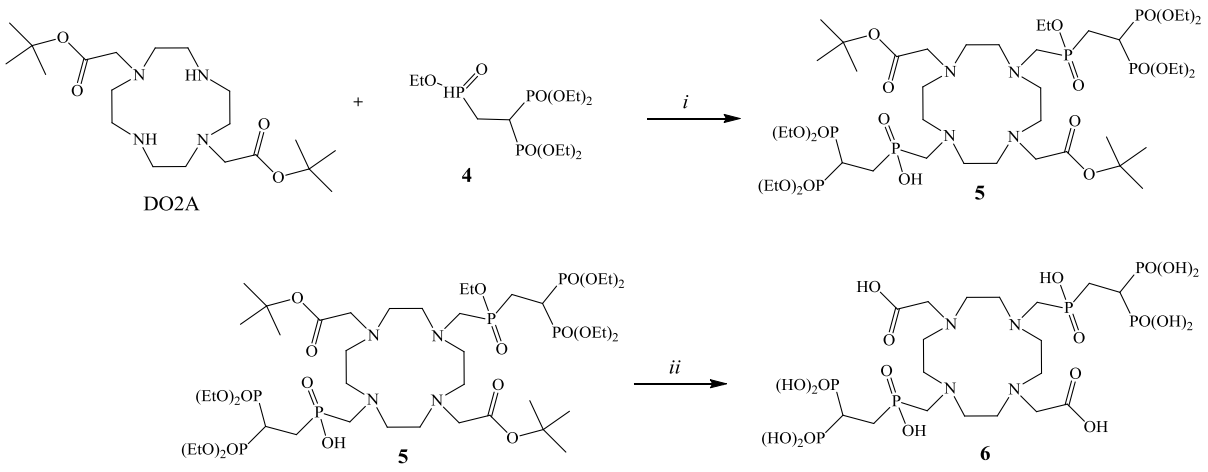

i) Toluene, H_2CO, reflux *ii*) 6 M HCl.

3.2. Radiolabelling with n.c.a. ^{177}Lu and quality control

The DOTA, DO2A and NO2A conjugated bisphosphonates were successfully labelled with n.c.a. ^{177}Lu(III). Yields and purities were controlled by radio-TLC and HPLC (Figure 1) All bisphosphonates showed a very fast complexation kinetic. Since DOTA derivatives show a very excellent complexation ability with lanthanides, a radiochemical yield (RCY) of more than 98% was obtained for the abovementioned compounds within 30 minutes. Even the NO2A based bisphosphonate NO2AP^{BP} showed an excellent labelling efficiency. Complexation occurred fast and quantitative (RCY > 99%).

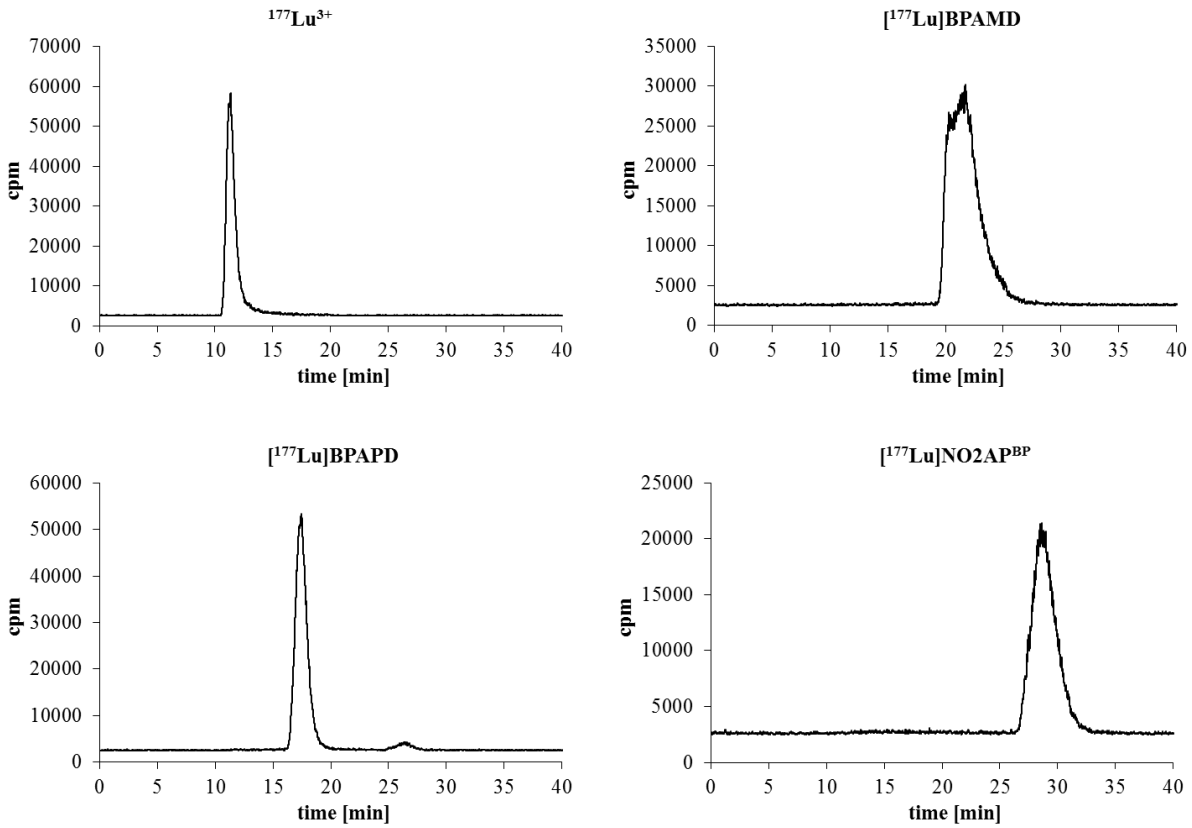

Figure 1. Radio-HPLC chromatograms of [^{177}Lu]BPAMD, [^{177}Lu]BPAPD and [^{177}Lu]NO2AP^{BP} as a representative for ^{177}Lu-labelled bisphosphonates in comparison to $^{177}Lu^{3+}$.

3.3. Biodistribution

The ^{177}Lu-labelled bisphosphonates showed a similar organ distribution with a predominant accumulation in the skeleton, cf. table 1 and 2. Besides the bone an appreciable amount of activity was found in the kidneys, which is reasonable according to the compounds renal clearance. Considerable liver accumulation was only observed for [^{177}Lu]citrate and [^{177}Lu]DOTA(M^{BP})$_2$ with SUVs of 1.04 ± 0.09 and 0.69 ± 0.36, respectively. After 60 min p.i. the SUV in the femur for the monomeric DOTA conjugates was 4.84 ± 0.44 for [^{177}Lu]BPAMD, 4.05 ± 0.36 for [^{177}Lu]BPAPD and 5.67 ± 0.10 for [^{177}Lu]BPPED. The SUV for the dimeric bisphosphonate compounds was 4.48 ± 0.38 for [^{177}Lu]DO2A(P^{BP})$_2$ and 5.41 ± 0.46 for [^{177}Lu]DOTA(M^{BP})$_2$ in the femur. [^{177}Lu]NO2AP^{BP} showed a femur SUV of

3.34 ± 0.38 and [^{177}Lu]citrate showed a SUV of 4.12 ± 0.38 after 60 min p.i., respectively. SUVs in blood, liver and kidney showed the strongest variations between the tested compounds. Highest blood levels were determined for the dimeric compound [^{177}Lu]DOTA(M^{BP})$_2$ with a SUV of 1.43 ± 0.32 after 60 min p.i. Lowest blood SUV of 0.04 ± 0.01 was obtained for [^{177}Lu]BPAMD and [^{177}Lu]BPAPD. The SUV in the liver was highest for [^{177}Lu]citrate with a value of 1.04 ± 0.09, contrary to the bisphosphonates which showed a consistently low liver accumulation, with a SUV of 0.04 ± 0.01 for [^{177}Lu]BPAMD for example. Activity accumulation in the kidneys was lowest for [^{177}Lu]BPAMD and [^{177}Lu]BPAPD with SUVs of 0.35 ± 0.06 and 0.39 ± 0.06, respectively. Highest kidney concentrations were found for the dimeric bisphosphonates [^{177}Lu]DO2A(P^{BP})$_2$ and [^{177}Lu]DOTA(M^{BP})$_2$ as well as for [^{177}Lu]citrate with SUVs of 1.66 ± 0.40, 1.41 ± 0.16 and 1.41 ± 0.11, respectively. The highest SUV determined for [^{177}Lu]citrate was found in the harderian glands with a value of 9.62 ± 5.62, which is more than the doubled uptake value compared to the femur after 60 min p.i.. Contrast to that all the tested bisphosphonates showed obviously lower SUVs in the harderian glands with SUVs between 0.04 and 0.46.

Table 1. Biodistribution of radioactivity after 5 min p.i. of ^{177}Lu-complexes in Wistar rats.

organ	[^{177}Lu]citrate		[^{177}Lu]BPAMD		[^{177}Lu]BPAPD		[^{177}Lu]BPPED		[^{177}Lu]NO2AP^{BP}		[^{177}Lu]DO2A(P^{BP})$_2$		[^{177}Lu]DOTA(M^{BP})$_2$	
	mean	SD	mean	SD	mean	SD	mean	SD	mean	SD	mean	SD	mean	SD
blood	n.d.	n.d.	0.90	0.42	0.84	0.07	1.30	0.20	2.08	2.83	3.35	0.33	3.98	0.40
brain	n.d.	n.d.	0.04	0.01	0.05	0.02	0.04	0.01	0.04	0.01	0.09	0.01	0.13	0.03
pancreas	n.d.	n.d.	0.31	0.14	1.60	1.18	0.37	0.12	0.27	0.08	0.73	0.15	0.68	0.14
spleen	n.d.	n.d.	0.37	0.35	1.27	0.94	0.39	0.05	0.23	0.03	0.60	0.13	0.78	0.10
adrenal gland	n.d.	n.d.	0.40	0.13	0.55	0.17	0.70	0.41	0.60	0.42	1.23	0.19	1.07	0.19
kidneys	n.d.	n.d.	4.53	4.01	3.61	1.81	3.09	0.48	3.08	1.14	2.87	0.29	3.10	0.54
adipose tissue	n.d.	n.d.	0.42	0.19	1.80	0.78	0.24	0.07	0.53	0.14	1.52	0.50	0.55	0.13
muscle	n.d.	n.d.	0.19	0.08	0.78	0.70	0.24	0.03	0.21	0.05	0.49	0.30	0.49	0.11
heart	n.d.	n.d.	0.36	0.14	0.36	0.04	0.52	0.10	0.31	0.06	1.34	0.17	1.45	0.30
lung	n.d.	n.d.	0.61	0.24	0.61	0.07	0.75	0.08	0.50	0.05	1.87	0.41	2.04	0.32
thymus	n.d.	n.d.	0.29	0.11	0.30	0.06	0.38	0.08	0.22	0.04	0.76	0.09	0.93	0.14
thyroid	n.d.	n.d.	0.79	0.13	0.77	0.11	0.71	0.29	0.87	0.34	1.13	0.23	1.75	0.85
harderian gland	n.d.	n.d.	0.36	0.13	0.37	0.10	0.40	0.12	0.35	0.08	0.95	0.23	1.12	0.16
liver	n.d.	n.d.	0.26	0.11	0.39	0.08	0.48	0.12	0.29	0.12	1.07	0.15	1.13	0.39
testes	n.d.	n.d.	0.25	0.07	0.28	0.03	0.36	0.01	0.32	0.05	0.24	0.02	0.30	0.03
femur	n.d.	n.d.	3.36	0.63	3.43	0.44	4.16	0.35	2.67	0.04	2.11	0.22	2.31	0.15

Data are expressed in SUV. Each value represents the mean (S.D.) for four animal. Data not determined (n.d.).

Table 2. Biodistribution of radioactivity after 60 min p.i. of ^{177}Lu-complexes in Wistar rats.

organ	[^{177}Lu]citrate		[^{177}Lu]BPAMD		[^{177}Lu]BPAPD		[^{177}Lu]BPPED		[^{177}Lu]NO2AP^{BP}		[^{177}Lu]DO2A(P^{BP})$_2$		[^{177}Lu]DOTA(M^{BP})$_2$	
	mean	SD	mean	SD	mean	SD	mean	SD	mean	SD	mean	SD	mean	SD
blood	0.22	0.11	0.04	0.01	0.04	0.00	0.06	0.01	0.07	0.02	1.25	0.09	1.43	0.32
brain	0.06	0.01	0.01	0.00	0.01	0.00	0.01	0.01	0.01	0.01	0.04	0.01	0.05	0.01
pancreas	0.50	0.05	0.04	0.02	0.04	0.02	0.03	0.01	0.06	0.01	0.31	0.05	0.30	0.07
spleen	0.70	0.12	0.07	0.06	0.05	0.01	0.14	0.04	0.05	0.01	0.31	0.03	0.52	0.25
adrenal gland	0.62	0.05	0.04	0.04	0.09	0.06	0.08	0.12	0.11	0.05	0.49	0.09	0.52	0.20
kidneys	1.41	0.11	0.35	0.06	0.39	0.06	0.38	0.04	0.47	0.07	1.66	0.40	1.41	0.16
adipose tissue	0.35	0.03	0.04	0.02	0.06	0.02	0.02	0.01	0.09	0.03	0.55	0.12	0.29	0.16
muscle	0.35	0.02	0.02	0.01	0.03	0.02	0.02	0.00	0.02	0.01	0.15	0.01	0.24	0.06
heart	0.87	0.10	0.02	0.01	0.03	0.00	0.04	0.01	0.04	0.01	0.54	0.10	0.63	0.12
lung	1.13	0.13	0.07	0.01	0.06	0.00	0.08	0.02	0.07	0.01	0.89	0.12	0.89	0.13
thymus	0.53	0.09	0.08	0.04	0.06	0.02	0.03	0.01	0.06	0.01	0.39	0.05	0.37	0.10
thyroid	0.89	0.18	0.57	0.06	0.44	0.21	0.62	0.44	0.21	0.06	1.00	0.27	0.85	0.12
harderian gland	9.62	5.62	0.04	0.01	0.11	0.11	0.16	0.08	0.06	0.01	0.42	0.05	0.46	0.09
liver	1.04	0.09	0.04	0.01	0.04	0.01	0.13	0.01	0.04	0.00	0.52	0.11	0.69	0.36
testes	0.42	0.03	0.03	0.01	0.02	0.01	0.03	0.00	0.03	0.01	0.28	0.03	0.33	0.04
femur	4.12	0.31	4.84	0.44	4.05	0.36	5.67	0.10	3.34	0.28	4.48	0.38	5.41	0.46

Data are expressed in SUV. Each value represents the mean (S.D.) for four animal.

The bone to soft tissue ratios are presented in table 3 and 4. Ratio between bone and blood was 3.6 for [^{177}Lu]DO2A(P^{BP})$_2$, 3.8 for [^{177}Lu]DOTA(M^{BP})$_2$, 18.7 for [^{177}Lu]citrate, 45.8 for [^{177}Lu]NO2AP^{BP}, 92.9 for [^{177}Lu]BPPED, 95.1 for [^{177}Lu]BPAPD and 135.6 for [^{177}Lu]BPAMD after 60 min p.i., respectively. The best bone to muscle ratio was observed for [^{177}Lu]BPPED (355.8) followed by [^{177}Lu]BPAMD (251.7). [^{177}Lu]BPPED showed as well the best bone to kidney ratio of 14.9 followed by 14.0 for [^{177}Lu]BPAMD again. The best bone to liver ratio was determined for [^{177}Lu]BPAMD (127.5) followed by [^{177}Lu]BPAPD (105.4), while the lowest ratio was obtained for [^{177}Lu]citrate (4.0). The total skeleton retention was calculated as following, starting with the lowest value of 30.5 ± 1.1 %ID for [^{177}Lu]NO2AP^{BP}, 39.4 ± 2.5 %ID for [^{177}Lu]BPAPD, 44.6 ± 3.2 %ID for [^{177}Lu]DO2A(P^{BP})$_2$, 45.7 ± 6.2 %ID for [^{177}Lu]citrate, 46.7 ± 5.3 %ID for [^{177}Lu]BPAMD, 48.2 ± 4.1 %ID for [^{177}Lu]DOTA(M^{BP})$_2$ and 56.3 ± 6.7 %ID for [^{177}Lu]BPPED.

Table 3. Ratios between bone and soft tissue after 5 min p.i. of ^{177}Lu-complexes in Wistar rats.

bone/organ	[^{177}Lu]citrate	[^{177}Lu]BPAMD	[^{177}Lu]BPAPD	[^{177}Lu]BPPED	[^{177}Lu]NO2AP^{BP}	[^{177}Lu]DO2A(P^{BP})$_2$	[^{177}Lu]DOTA(M^{BP})$_2$
blood	n.d.	3.7	4.1	3.2	1.3	0.6	0.6
brain	n.d.	83.9	68.5	104.0	66.8	23.4	17.7
pancreas	n.d.	10.8	2.1	11.2	9.9	2.9	3.4
spleen	n.d.	9.1	2.7	10.7	11.6	3.5	3.0
adrenal gland	n.d.	8.4	6.2	5.9	4.5	1.7	2.2
kidneys	n.d.	0.7	0.9	1.3	0.9	0.7	0.7
adipose tissue	n.d.	8.0	1.9	17.3	5.0	1.4	4.2
muscle	n.d.	17.7	4.4	17.3	12.7	4.3	4.7
heart	n.d.	9.3	9.5	8.0	8.6	1.6	1.6
lung	n.d.	5.5	5.6	5.5	5.3	1.1	1.1
thymus	n.d.	11.6	11.4	10.9	12.1	2.8	2.5
thyroid	n.d.	4.2	4.4	5.9	3.1	1.9	1.3
harderian gland	n.d.	9.3	9.3	10.4	7.6	2.2	2.1
liver	n.d.	12.9	8.8	8.7	9.2	2.0	2.0
testes	n.d.	13.4	12.2	11.6	8.3	8.8	7.7

Table 4. Ratios between bone and soft tissue after 60 min p.i. of ^{177}Lu-complexes in Wistar rats.

bone/organ	[^{177}Lu]citrate	[^{177}Lu]BPAMD	[^{177}Lu]BPAPD	[^{177}Lu]BPPED	[^{177}Lu]NO2AP^{BP}	[^{177}Lu]DO2A(P^{BP})$_2$	[^{177}Lu]DOTA(M^{BP})$_2$
blood	18.7	135.6	95.1	92.9	45.8	3.6	3.8
brain	65.4	613.4	513.9	419.9	254.3	111.5	104.0
pancreas	8.2	136.4	104.9	181.6	56.7	14.5	18.0
spleen	5.8	68.2	85.7	41.0	66.0	14.2	10.4
adrenal gland	6.6	109.6	45.8	72.5	31.4	9.1	10.4
kidneys	2.9	14.0	10.3	14.9	7.1	2.7	3.8
adipose tissue	11.8	134.5	70.7	269.7	37.2	8.2	18.4
muscle	11.8	251.7	158.7	355.8	141.4	29.8	22.9
heart	4.7	210.1	158.7	141.1	89.0	8.2	8.6
lung	3.7	69.1	62.6	67.5	46.8	5.1	6.1
thymus	7.7	58.6	70.7	212.0	59.0	11.6	14.4
thyroid	4.7	8.5	9.2	9.1	15.6	4.5	6.3
harderian gland	0.4	118.8	35.8	36.4	85.6	10.6	11.7
liver	4.0	127.5	105.4	42.3	87.0	8.6	7.8
testes	9.9	179.1	199.7	185.1	113.5	15.8	16.2

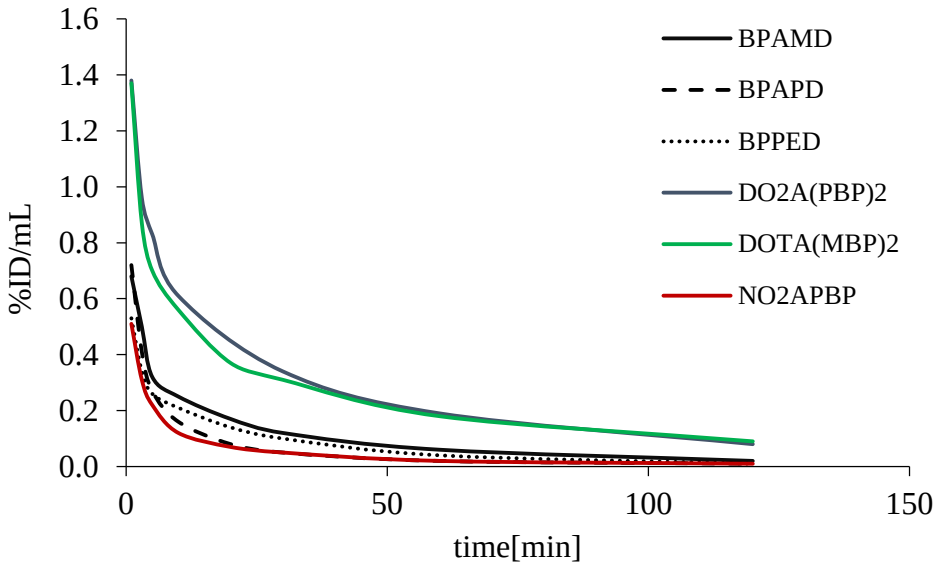

Figure 4. Blood concentration curves of different ^{177}Lu labelled bisphosphonates.

3.4. Metabolite Analysis and *in vivo* stability

Radio-HPLC and TLC analysis of blood samples showed no evidence of any metabolization of the compounds [^{177}Lu]NO2AP^{BP}, [^{177}Lu]BPAMD, [^{177}Lu]BPAPD and [^{177}Lu]BPPED within a period of 120 min. The above mentioned compounds were found to be intact in the urine and the serum probes as revealed by radio-HPLC and TLC. No traces of unknown ^{177}Lu species or compounds were observed. The elimination half-lives were determined from blood samples and summarized in table 5.

Table 5. Elimination half-lives of the ^{177}Lu-labelled bisphosphonates calculated by a two comparatement model.

	[^{177}Lu]BPAMD	[^{177}Lu]BPAPD	[^{177}Lu]BPPED	[^{177}Lu]NO2AP^{BP}	[^{177}Lu]DO2A(P^{BP})$_2$	[^{177}Lu]DOTA(M^{BP})$_2$
$t_{1/2}(\alpha)$	8.5 min	6.5 min	9.0 min	12.3 min	12.6 min	9.5 min
$t_{1/2}(\beta)$	76.2 min	93.8 min	63.0 min	93.8 min	100.5 min	120.0 min

3.5. SPECT/CT

Images obtained from SPECT showed that the therapeutic ^{177}Lu-labelled bisphosphonates exclusively accumulated in the skeleton with a high target to background ratio, cf. figure 5. After 60 min no considerable fractions of ^{177}Lu activity was found in other organs, which is consistent to the data gathered from the *ex vivo* organ distribution. An obviously concentration of activity was present in the epiphyseal gap as well as in other articulations.

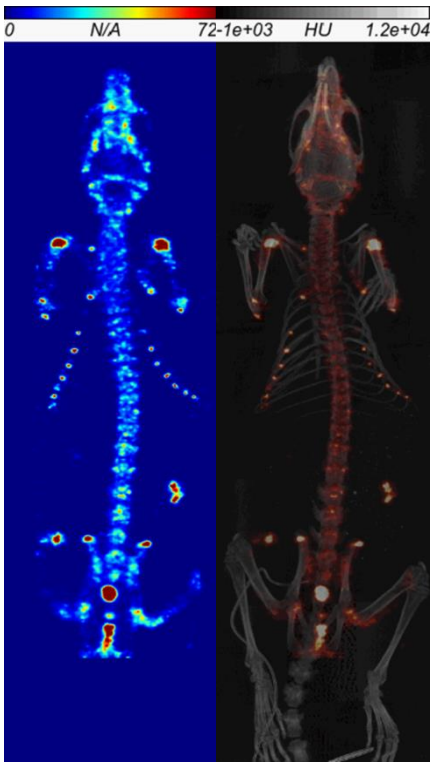

Figure 5. [^{177}Lu]BPAMD SPECT image (left) and SPECT/CT fusion image (right) developed in a healthy Wistar rat 60 min p.i., as a representing example for ^{177}Lu-labelled bisphosphonates.

4. Discussion

The DOTA based monomeric bisphosphonates BPAMD, BPAPD, BPPED have been successfully radiolabeled with the therapeutic β^--emitter ^{177}Lu(III) in excellent yields over 98 % as well as the NO2A based bisphosphonate NO2AP^{BP} and the dimeric compounds DOTA(M^{BP})$_2$ and DO2A(P^{BP})$_2$. All tracers tested showed a distinguished high accumulation on the bone surface, eminently in the epiphyseal plate. High uptakes were observed for the dimeric compound [^{177}Lu]DOTA(M^{BP})$_2$ (SUV_{femur} = 5.41 ± 0.41). All bisphosphonates underwent a renal body clearance and the blood elimination was very fast especially for the monomeric compounds. No brain or notable liver uptake was observed. The compounds were found to be intact in the urine and blood.

The characteristic accumulation specific in the growth plate of the skeleton shows that the compounds uptake profile is subject to the bone turnover. For that reason the described compounds in this manuscript should be well suited for a targeted ^{177}Lu therapy to osteoblastic bone metastases, in which they should preferred accumulate. An important factor for a therapeutic application is the target to background ratio (TBR) and a fast excretion of non-target bond activity. A good TBR and a fast blood and body clearance reduces the radiation dose of the non-targeted tissue and thus will reduce toxic side effects and enhances the therapeutic efficiency and tolerance.

Although the dimeric compounds [^{177}Lu]DOTA(M^{BP})$_2$ and [^{177}Lu]DO2A(P^{BP})$_2$ showed the highest bone accumulation, their TBR was lowest, beside [^{177}Lu]citrate. The additional bisphosphonate moiety might to have a stronger bone binding effect. Albeit the blood levels of these compounds were significantly higher after 60 min (SUV_{blood}{[^{177}Lu]DOTA(M^{BP})$_2$} = 1.43 ± 0.32; SUV_{blood}{[^{177}Lu]DO2A(P^{BP})$_2$} = 1.25 ± 0.09) compared to the monomeric bisphosphonates (SUV_{blood}{[^{177}Lu]BPAMD} = 0.04 ± 0.01; SUV_{blood}{[^{177}Lu]NO2AP^{BP}} = 0.07 ± 0.02). It might be the case that these higher blood concentration are the reason for the enhanced skeletal accumulation. Because of the fast blood and renal clearance of the monomeric bisphosphonates the time scale for target accumulation is shortened compared to the dimeric compounds. The reason for the decreased clearance of the dimeres is yet not clear

and it might be an effect of the higher negative charge of these compounds or may be influenced by serum protein binding. The data from *ex vivo* organ distribution of the dimeric bisphosphonates are also not matching with [^{177}Lu]citrate. Liver uptake, blood values and the accumulation in the harderian glands as well as in the femur are significantly different. If a therapeutic approach of bone metastases benefits from the higher skeleton accumulation of the dimeric bisphosphonates has yet to be evaluated in future in a dosimetry study, considering the lower TBR and the higher blood levels.

The lowest skeleton uptake was observed for the NO2A phosphinate linked bisphosphonate [^{177}Lu]NO2AP^{BP} (SUV_{femur}{[^{177}Lu]NO2AP^{BP}} = 3.34 ± 0.28, 60 min p.i.). Contrary to the results with ^{177}Lu(III) it was reported previously, that [^{68}Ga]NO2AP^{BP} showed an excellent bone binding with a brilliant TBR [22], remarkably suitable as an PET imaging agent. However it is known that lanthanides require seven dentate chelators like DOTA-derivates and the NO2A-phosphinate offer only six. Since the bisphosphonate moiety is able to complex divalent metal ions like Ca^{2+} it might be the case that some parts of the phosphonate groups function as additional donors to the ^{177}Lu-NO2AP complex. A partly loss of the functional bisphosphonate moiety due to stabilizing the ^{177}Lu(III) complex might reduce the binding potential of the bisphosphonate group to the bone and thus reduces the affinity of the [^{177}Lu]NO2AP^{BP} compound to the target tissue in contrast to the ^{68}Ga(III) complex.

Highest bone accumulation of tested tracers was observed for [^{177}Lu]BPPED with a SUV of 5.67 ± 0.10 in the femur after 60 min. with a TBR of the muscle and blood of 355.8 and 92.3, respectively. Excellent bone accumulation (SUV = 4.84 ± 0.44) as well as superb TBRs were observed also for [^{177}Lu]BPAMD, with TBR values of 127.5 to the liver and 135.6 to the blood, which was the highest for all tested compounds. [^{177}Lu]BPAMD revealed a very fast blood clearance and renal excretion.

Within this study BPAMD revealed its great potential as a palliative bone targeting agent to treat skeleton metastases with ^{177}Lu(III). Contrary to other actual discussed tracers like EDTMP, BPAMD proved to be an efficient ^{68}Ga-PET imaging agent for bone metastasis [21]. Neither ^{177}Lu/^{153}Sm-EDTMP nor $^{223}RaCl_2$ offer this *theranostic* approach. Patients would benefit greatly from a specific [^{177}Lu]BPAMD dose application, calculated from the

patients individual uptake profile previously determined by [^{68}Ga]BPAMD PET examinations.

5. Acknowledgment

The authors are grateful to Jan Holub and Petr Hermann for providing the bisphosphonate compounds BPAMD, BPAPD, DO3AP^{BP} and NO2AP^{BP}. The n.c.a. ^{177}Lu was provided from ITG, Germany. Financial support from the *THERANOSTICS Center for Molecular Radiotherapy and Molecular Imaging ENETS*, Bad Berka (Germany) is particularly acknowledged. This study was supported by the grant of the Max Planck Graduate Center Mainz.

6. References

[1] GLOBOCAN 2012: Estimated Cancer Incidence, Mortality and Prevalence Worldwide 2012. *World Health Organization*.

[2] K. N. Weilbaecher, T. A. Guise, L. K. McCauley, Cancer to bone: a fatal attraction, *Nature Reviews|Cancer,* **2011**; 11: 411-425.

[3] O. Sartor, P. Hoskin, Ø. S. Bruland, Targeted radio-nuclide therapy of skeletal metastases, *Cancer Treatment Reviews*, **2013**; 39: 18–26.

[4] J. Kutzner, W. Grimm, K. Hahn, Palliative radiotherapy with Strontium-89 in case of extended formation of skeleton metastases, *Strahlentherapie*, **1978**; 154:317-22.

[5] S. Zenda, Y Nakagami, M. Toshima, S. Arahira, M. Kawashima, Y. Matsumoto, H. Kinoshita, M. Satake, T. Akimoto, Strontium-89 (Sr-89) chloride in the treatment of various cancer patients with multiple bone metastases, *Int J Clin Oncol*, **2013.**

[6] P. W. Durbin, C. W. Asing, M. E. Johnston, The metabolism of the lanthanons in the rat. II. Time studies of the tissue deposition of intravenously administered radioisotopes. USAEC Report, **1956**: ORINS-12; 171.

[7] R. E. O'Mara, Rare earth nuclides as potential agents for skeletal imaging, *J Nucl Med*, **1968**; 10: 49-51.

[8] Lutetium-177: Handling Precautions, **2010**, Perkin-Elmer Inc. www.perkinelmer.com

[9] D. Campana, G. Capurso, S. Partelli, F. Nori, M. Falconi, P. Tomassetti, Radiolabelled somatostatin analogue treatment in gastroenteropancreatic neuroendocrine tumours: factors associated with response and suggestions for therapeutic sequence. *EJMMI*, **2013**; 40(8):1197-205.

[10] J. Yuan, C. Liu, X. Liu, Y. Wang, D. Kuai, G. Zhang, J. J. Zaknun, Efficacy and safety of ^{177}Lu-EDTMP in bone metastatic pain palliation in breast cancer and hormone refractory prostate cancer: a phase II study, *Clin Nucl Med*., **2013**; 38: 88-92.

[11] S. Chakraborty, T. Das, P. R. Unni, H. D. Sarma, G. Samuel, S. Banerjee, M. Venkatesh, N. Ramamoorthy, M. R. Pillai, ^{177}Lu labelled polyaminophosphonates as potential agents for bone pain palliation, *Nucl Med Comm*, **2002**; 23: 67-74.

[12] N. V. Jarvis, J. M. Wagener, G. E. Jackson, Metal-ion speciation in blood plasma as a tool for elucidating the in vivo behaviour of radiopharmaceuticals containing ^{153}Sm and ^{166}Ho, *J. Chem. Soc. Dalton Trans*., **1995**; 1411-1415.

[13] B. J. Beyer, R. Offord, G. Künzi, Y. Aleksandrova, U. Ravn, S. Jahn, J. Barker, O. Tengblad, M. Lindroos, The Influence of EDTMP-Concentration on the Biodistribution of Radio-Lanthanides and 225-Ac in Tumor-Bearing Mice, *Nucl Med & Biol*,**1997**; 24: 367-372.

[14] J. Byegård, M. Skarnemark, M. Skålberg, The stability of some metal EDTA, DTPA and DOTA complexes: Application as tracers in groundwater studies, *J Radioanal & Nucl Chem*, **1999**; 241: 281-290.

[15] L Smentek, Lanthanides caged by the organic chelates; structural properties, *J Phys: Condens Matter*, **2011**; 23: 143202.

[16] S. Chakrabotry, T. Das, H. D. Sarma, M. Venkatesh, S. Banerjee, Comparative studies of ^{177}Lu–EDTMP and ^{177}Lu–DOTMP as potential agents for palliative radiotherapy of bone metastasis, *Applied Radiation and Isotopes*, **2008**; 66: 1196–1205.

[17] M. Mitterhauser, S. Toegel, W. Wadsak, R. R. Lanzenberger, L. K. Mien, C. Kutner, T. Wanek, R. Dudczak, K. Kletter, Pre vivo, ex vivo and in vivo evaluations of [^{68}Ga]-EDTMP, *Nucl Med & Biol*, **2007** ; 34: 391–397.

[18] M. Fellner, P. Riss, NS. Loktionova, KP. Zhernosekov, O. Thews, F. Rösch, Comparison of different phosphorus-containing ligands complexing ^{68}Ga for PET-imaging of bone metabolism. *Radiochim. Acta*, **2011**; 99: 43–51.

[19] M. Fellner, B. Biesalski, N. Bausbacher, V. Kubícek, P. Hermann, F. Rösch, O. Thews, ^{68}Ga-BPAMD: PET-imaging of bone metastases with a generator based positron emitter, *Nucl. Med. Biol*., **2012**; 39: 993–999.

[20] T. Vitha, V. Kubícek, P. Hermann, Z. I. Kolar, H. T. Wolterbeek, W.A.P. Breeman, I. Lukeš, J. A. Peters, Lanthanide(III) Complexes of Bis(phosphonate) Monoamide Analogues of DOTA: Bone-Seeking Agents for Imaging and Therapy, *J. Med. Chem*. **2008**; 51: 677–683.

[21] M. Fellner, R. P. Baum, V. Kubíček, P. Hermann, I. Lukeš , V. Prasad, F. Rösch, PET/CT imaging of osteoblastic bone metastases with ^{68}Ga-bisphosphonates: first human study, *Eur. J. Nucl. Med. Mol. Imaging*, **2010**; 37: 834.

[22] J. Holub, M. Meckel, V. Kubicek, F. Rösch, P. Hermann, Gallium(III) complexes of NOTA-bis(phosphonate) conjugates as radiotracers for bone imaging, *CMMI*, **2014,** may 6

[23] K. Ogawa, K. Takai, H. Kanabara, T. Kiwada, Y. Kitamura, K. Shiba, A. Odani, Preparation and evaluation of a radiogallium complex-conjugated bisphosphonate as a bone scintigraphy agent, *Nucl Med & Biol*, **2011**; 38: 631–636.

[24] T. Vitha, V. Kubicek, P. Hermann, Z. I. Kolar, H. Th. Wolterbeek, J. A. Peter, I. Lukes, Complexes of DOTA-Bisphosphonate Conjugates: Probes for Determination of Adsorption Capacity and Affinity Constants of Hydroxyapatite, *Langmuir*, **2008**; 24: 1952-1958.

[25] N. A. Lebedev , A. F. Novgorodov, R. Misiak, J. Brockmann, F. Rösch, Radiochemical separation of no-carrier-added ^{177}Lu as produced via the ^{176}Yb(n,γ)^{177}Yb®^{177}Lu process, *Appl Radiat Isot*, **2000**; 53: 421-425.

[26] P. J. Riss, C. Burchardt, F. Rösch, A methodical ^{68}Ga-labelling study of DO2A-(butyl-L-tyrosine) 2 with cation-exchanger post-processed ^{68}Ga: practical aspects of radiolabelling, *CMMI*, **2011**; 6: 492–498.

[27] V. Kubıcek, J. Rudovsky, J . Kotek, P. Hermann, L. Vander Elst, R. N. Muller, Z. I. Kolar, H. T. Wolterbeek, J. A. Peters, I. Lukes, A Bisphosphonate Monoamide Analogue of DOTA: A Potential Agent for Bone Targeting, *J. Am. Chem. Soc*., **2005**; 127: 16477-16485.

[28] T. Vitha, V. Kubicek, J. Kotek, P. Hermann, L. Vander Elst, R. N. Muller, I. Lukes J. A. Peters, Gd(III) complex of a monophosphinate-bis(phosphonate) DOTA analogue with a high relaxivity; Lanthanide(III) complexes for imaging and radiotherapy of calcified tissues, *Dalton Trans*., **2009**, 3204–3214.

[29] W. Sontag, Long-term Behavior of ^{239}Pu, ^{241}Am and ^{233}U in Different Bones of One-year-old Rats: Macrodistribution and Macrodosimetry. *Human Toxicol*, **1984**; 3: 69-483.

3.7.1. Supplementary Results I: *Ex vivo* organ distribution studies of the α-particle emitting calcium mimetic $^{223}RaCl_2$ (Xofigo®) in healthy Wistar rats.

1. Introduction

After the discovery of radioactivity a strange cult about radioactive rays in general and particular in radium emerged in these early days of nuclear sciences. The people as well as the scientists believed to have an ultimate form of elixir to cure any kind of diseases or other forms of malaises. Mineral waters and a plenty number of every days objects were added with radium in odd ways to prevent the bearer from any kind of healthy misfortune, until the toxic effects of radium isotopes circularized as first reported by physicians, who treated necrosis of the jaws in painters of luminous watch-dials [1].

Radium itself is an earth alkaline element and therefore it behaves as a calcium analog. Incorporated radium isotopes undergo the calcium metabolism in the human body and thus large fractions are accumulated in the skeleton with quite a long biological half-life [2,3]. The same metabolic mechanism was used with isotopes of strontium to treat skeletal metastases. The β-particle emitter ^{89}Sr, when injected as $^{89}SrCl_2$, accumulates in high metabolic osseous tumor sites to attain pain relief [4]. ^{89}Sr has a relatively long physical half-life of 50.5 days, considered to its usage as an endotherapeutic agent. The maximum energy of the β-particles emitted is 1.46 MeV [5]. Due to this high β-energy, the decay of ^{89}Sr inflicts the radio sensitive bone marrow with a high dose fraction and yet showed no benefit in survival rates against external radiation [4,6]. Contrary the range of α-particles is very short and is accompanied with a very high energy deposit in the surrounding tissue and conceptually should not affect the bone marrow [4].

The high linear energy transfer (LET) of α-particles and the short range of only few cell diameters inflict an intense damage of the DNA. Especially DNA double strand breaks

caused by α-irradiation initiate the apoptosis mechanism in cells. First results in cell and animal studies revealed the high potential of the targeted α-particle therapy (TAT) [7,8]. The only α-particle emitter approved for endo-radiotherapy is $^{223}RaCl_2$ for the treatment of castrate resistant prostate cancer metastasized in the bone [4]. ^{223}Ra has a moderate long half-life of 11.4 days and the daughter nuclides in the decay chain convert quickly to the stable lead isotope ^{207}Pb, cf. figure 1.

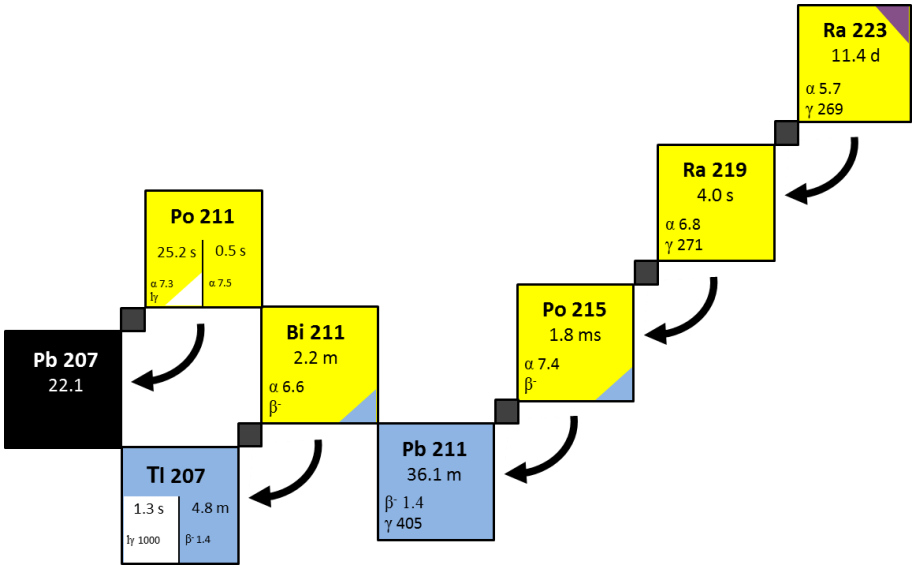

Figure 1. Decay chain from ^{223}Ra to the stable isotope ^{207}Pb.

First data in castrate resistant prostate cancer patients with proven skeletal metastases revealed a significant pain relief and a drop of PSA (prostate specific antigen) and ALP (alkaline phosphatase) levels [9]. The short ranged α-irradiation destroys the tumor cells nearby the bone surface as well as the osteotropic cells of the tumor lesion and thus decreases the bone turnover and reduces further skeletal related events with an overall benefit according to the survival rate [10]. In a randomized patient study $^{223}RaCl_2$ offered a significant longer overall survival rate in metastatic prostate cancer patients of 2.8 month against placebo [10,11]. Unfortunately, $^{223}RaCl_2$ showed also some problematic side effects related especially to the red bone marrow, which is may be caused by the ´hard´ β-emission of the daughter nuclides in the decay chain. Dosimetric studies estimate a dose of 16 Gy

absorbed by the bone endosteum and 1.5 Gy by the red bone marrow after a cycle of six injections of 21 MBq $^{223}RaCl_2$ [12]. Since ^{223}Ra behaves as a calcium mimetic it undergoes the same excretion route as Ca^{2+}-ions in the human body, which is mainly the guts. Szintigraphic images of patients treated with ^{223}Ra showed therefor mainly the intestine, cf. figure 2.

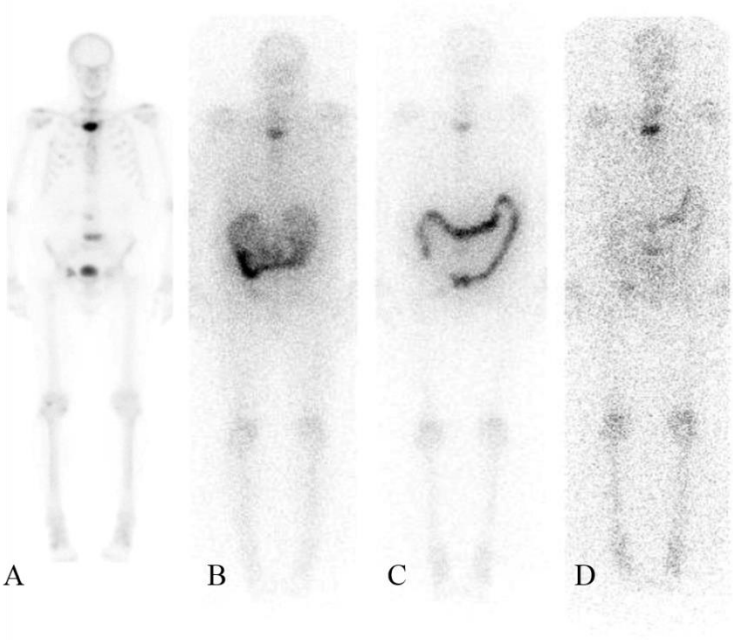

Figure 2. Szintigraphic images of patient developed with [^{99}Tc]MDP (A) and $^{223}RaCl_2$ on day 0 (B), day 2 (C) and day 6 (D) p.i [4].

Also the liver, the colon and the intestine receive a significant dose of radiation by $^{223}RaCl_2$, whereby the dose of the colon and the intestine was calculated based on the β-emission of the daughter nuclides from the ^{223}Ra decay chain only [12]. However, the authors of this study assumed that the emitted α-particles are self-absorbed by the colon and intestine content and thus the emitted α-particles were excluded from the dose calculations of the intestine and colon [12]. The side effects of an α-therapy of bone metastases with $^{223}RaCl_2$ are mainly the hematological toxicity and diarrhoe [13]. To reduce these effects a treatment with $^{223}RaCl_2$ is divided into six applications of 0.05 MBq/kg contrary to the standard radioparmaceutical for

the palliative treatment of bone metastases [^{153}Sm]EDTMP, where only one application is needed to obtain pain relief.

Another concept of treating painful bone metastases are ^{177}Lu(III) labelled DOTA conjugated bisphosphonates. Compounds like [^{177}Lu]BPAMD proved in animal studies to have a high bone accumulation and a fast body clearance via the kidneys [14]. ^{177}Lu is a therapeutic emitter of low energetic β^--particles and commonly used in the ERT. Furthermore, BPAMD offers the opportunity as an imaging agent, in combination with the positron emitter ^{68}Ga(III). This *theranostic* concept allows for a patient specific dose calculation of [^{177}Lu]BPAMD concerning the patients individual tracer uptake profile. [^{177}Lu]BPAMD therapy of osseous metastases is now offered in some hospitals with promising results and therefore the different pharmacokinetics of $^{223}RaCl_2$ and [^{177}Lu]BPAMD have to be described in terms of bone accumulation, excretion route and target to background ratio in a healthy animal model [15].

2. Materials and Methods

$^{223}RaCl_2$ (Xofigo®) was purchased from Bayer HealthCare (Germany). Male Wistar rats weighting 205 ± 19 g were obtained from Charles River Laboratories International, Inc. The animal studies were done according to the guidelines of the European Convention for the Protection of Vertebrate Animals used for Experimental and other Scientific Purposes (ETS No. 123), and to the Deutsches Tierschutzgesetz (German animal welfare regulations). In mean 9.5 ± 0.6 kBq and 51.0 ± 2.7 kBq were injected in tail vein in each rat, after 1 h and 24 h the rats were sacrificed at the and organs of interest were harvested. Radioactivity of samples were measured with a γ-spectrometer (MUCHA, raytest Isotopenmessgeräte GmbH, Germany) previously calibrated with a ^{223}Ra standard. Data are calculated in SUV (standard uptake value) by the formula: (activity per g tissue)/(injected activity) × BW. The skeleton weights of the rats were calculated by the formula: skeleton weight = 9.66 + 0.0355 × BW. The total skeleton accumulation of $^{223}RaCl_2$ was calculated by the activity concentration in

the femur and the total skeleton weight. Data of the organ distribution of the ^{177}Lu-labelled bisphosphonates and the experimental process is described elsewhere (this manuscript: 3.6).

3. Results

Activity accumulation in the excised tissue samples are shown in table 1. The results validate that $^{223}RaCl_2$ strongly retains in the bones. After 1 h p.i. a SUV in the femur of 7.04 ± 3.02 was observed and the total activity in the skeleton was found to be 56 ± 22 %ID. Beside the calcified tissues significant concentrations of ^{223}Ra were determined in the kidneys (SUV = 3.01 ± 0.97) followed by the intestine (SUV = 2.87 ± 0.82), respectively. ^{223}Ra accumulation on the femur was still present after 24 h with a SUV of 5.93 ± 0.14. Total skeleton retention was calculated after 24 h to be 52 ± 3 %ID. Activity concentrations in other organs were significantly lower after 24 h. The SUV in the kidneys and the intestine decreased to 0.10 ± 0.03 and 0.07 ± 0.01, respectively. The lowest activity observed was in muscle and heart samples with SUVs of 0.01 ± 0.01.

Table 1. *Ex vivo* organ distribution of $^{223}RaCl_2$ in healthy Wistar rats at different time points.

organ	1 h p.i.	24 h p.i.
lung	0.53 ± 0.33	0.05 ± 0.03
liver	0.26 ± 0.12	0.03 ± 0.03
spleen	0.19 ± 0.10	0.02 ± 0.02
kindeys	3.01 ± 0.97	0.10 ± 0.03
muscle	0.10 ± 0.06	0.01 ± 0.01
heart	0.17 ± 0.04	0.01 ± 0.01
blood	0.29 ± 0.09	0.02 ± 0.01
intestine	2.87 ± 0.82	0.07 ± 0.01
testes	0.11 ± 0.04	0.04 ± 0.01
femur	7.04 ± 3.02	5.93 ± 0.14

Data are expressed in mean SUV ± S.D. (standard deviation) out of three animals.

Activity ratios between bone and soft tissues after 1 h and 24 h p.i. are presented in table 2, respectively. Highest target to background ratio (TBR) was observed for muscle tissue after 1 h and 24 h, with TBR of 72 and 558. The lowest TBR of 2.3 and 2.4 was determined for the kidneys and the intestine after 1 h p.i. Ratios after 24 h p.i. of the TBR for the kidneys and the intestine increased to 58 and 82. The bone to blood ration was found to be 25 after 1 h p.i. and 272 after 24 h p.i.

Table 2. Ratios between bone and soft tissue 1 h and 24 h p.i. of $^{223}RaCl_2$ in healthy Wistar rats.

bone / organ	1 h p.i.	24 h p.i.
lung	13 ± 13	128 ± 74
liver	28 ± 25	215 ± 215
spleen	38 ± 37	306 ± 289
kindeys	2 ± 2	58 ± 17
muscle	72 ± 72	558 ± 364
heart	41 ± 28	531 ± 524
blood	25 ± 18	272 ± 180
intestine	2 ± 2	82 ± 10
testes	63 ± 51	386 ± 296

4. Discussion

The data obtained from *ex vivo* organ distribution in male healthy Wistar rats showed a strong retention of $^{223}RaCl_2$ in the skeleton, the intestine and the kidneys. However, kidney accumulation is not reported in humans and excreted ^{223}Ra activity is only found in the faeces. Significant ^{223}Ra accumulation is reported for the spleen (12.4 %ID/g, after 60 min.) in mice with only a slow decrease over time contrary to the data in dogs and rats, where no relevant spleen uptake was observed [16]. The distribution data of ^{223}Ra are consistent to the literature in healthy Wistar rats. After 24 h ^{223}Ra was exclusively present in the skeleton. It is

reported that ^{223}Ra inflicts the red bone marrow, with a reduction in blood levels and effects a strong toxicity [16,17]. However it is not clear, if this is mainly caused by the hard β-fraction of the daughter nuclides ^{212}Pb and ^{207}Tl or by secondary conversation effects, like X-ray or γ-emissions. Discussible in this term is may be the low bone to blood ratio (24.6) during the first hours after injection.

Although bisphosphonates have a high affinity to calcified tissues, the skeletal accumulation of [^{177}Lu]BPAMD (SUV_{femur} = 4.8 ± 0.4) was lower than $^{223}RaCl_2$ (SUV_{femur} = 7.0 ± 3.0), but not significant (P = 0.34), cf. figure 1. The %ID retained in the skeleton was calculated to be 48 ± 4 for [^{177}Lu]BPAMD and 56 ± 22 for $^{223}RaCl_2$, respectively.

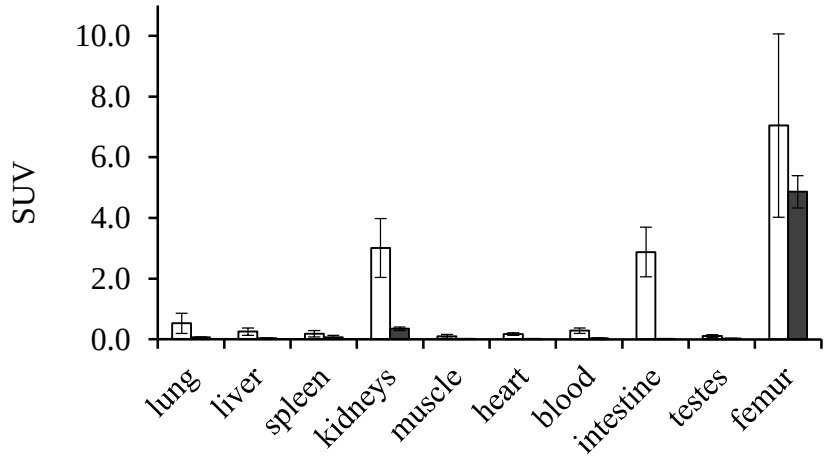

Figure 1. *Ex vivo* organ distribution of $^{223}RaCl_2$ (□) and [^{177}Lu]BPAMD (■) 60 min p.i.

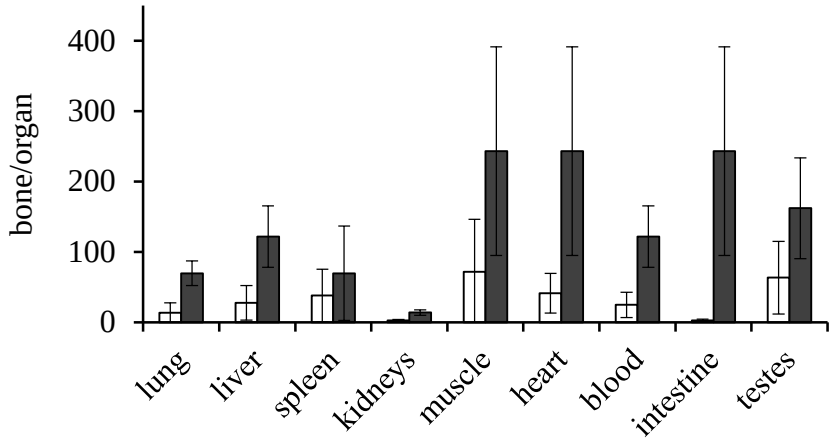

Figure 2. Ratios between bone and soft tissue of $^{223}RaCl_2$ (□) and [^{177}Lu]BPAMD (■) 60 min p.i.

The higher body retention of $^{223}RaCl_2$ can be explained by the resorption of $^{223}Ra^{2+}$ in the intestine and kidneys similar to Ca^{2+}-ions, while [^{177}Lu]BPAMD showed a fast renal elimination to the bladder. The missing resorption pathway of bisphosphonates in the kidneys and the intestine result in distinctly higher target to background ratios for [^{177}Lu]BPAMD, even though the bone uptake is slightly lower, cf. figure 2. In contrast to $^{223}RaCl_2$, [^{177}Lu]BPAMD showed an excellent target to background ratio even in the first minutes. The bone to blood ratios of [^{177}Lu]BPAMD was 4 after 5 min p.i. and 136 after 60 min. p.i., which is more than 550% higher compared to $^{223}RaCl_2$ after 60 min.

Consequently, [^{177}Lu]BPAMD showed a superior body distribution in terms of TBR, blood clearance and excretion rate and should thus be better tolerable. Whether [^{177}Lu]BPAMD attains pain relief and an overall longer survival rate in cancer patients as reported for $^{223}RaCl_2$ needs to be revealed in future patient studies. Indeed bone targeting compounds like [^{153}Sm]EDTMP, $^{223}RaCl_2$ or $^{89}SrCl_2$ cannot offer a pre-therapeutic diagnosis strategy, where the patients individual uptake profile conducts to a personalized dose calculation. Only macrocyclic bisphosphonates like BPAMD provide this opportunity as ^{177}Lu(III) and ^{68}Ga(III) ligands. Furthermore, these compounds are also suitable as possible carriers for other α-particle emitting therapy nuclides, such as $^{212/213}$Bi(III) and ^{225}Ac(III). A treatment of bone metastases with ^{225}Ac(III) in combination with [^{68}Ga]/[^{177}Lu]BPAMD would combine the benefits of the α-radiation therapy known from $^{223}RaCl_2$ with the superior excretion route

and target to background ratio of macrocyclic bisphosphonates. On account of this the complex formation and stability as well as the organ distribution in an animal model of ^{225}Ac- or $^{212/213}$Bi-bisphosphonates should be investigated in future.

5. References

[1] H. A. Colwell, S. Russ, Radium as a pharmaceutical poison, *The Lancet*, **1932**; 220: 221-223.

[2] M. Domenici, M. Laborde, Radium fixes on the skeleton, *Journal of the Franklin Institute*. **1914**, 177; 4: 467.

[3] F. E. Hoecker, P. G. Hoofe, Structural Differences in Bone Matrix Associated with Metabolized Radium, *Radiology*. **1949**; 52: 856-65.

[4] O. Sartor, P. Hoskin, Ø. S. Bruland Targeted radio-nuclide therapy of skeletal metastases, *Cancer Treatment Reviews*, **2013**; 39: 18–26.

[5] Metastron® (Strontium-89 Chloride Injection), SMS.2PA, GE Healthcare, **2006.**

[6] Radiation Dose to Patients from Radiopharmaceuticals, *ICRP*,53, Vol. 18, No. 1-4, 171, Pergamon Press, **1988**.

[7] F. Graf, J. Fahrer, S. Maus, A. Morgenstern, F. Bruchertseifer, S. Venkatachalam, C. Fottner, M. M.Weber, J. Huelsenbeck, M. Schreckenberger, B. Kaina, M. Miederer, DNA double strand breaks as predictor of efficacy of the alpha-particle emitter Ac-225 and the electron emitter Lu-177 for somatostatin receptor targeted radiotherapy, *PLoS One*, **2014**; 9: 2.

[8] J. P. Norenberg, B. J. Krenning, I. R.H.M. Koning, D. F. Kusewitt, T. K. Nayak1, T. L. Anderson, M. de Jong, K. Garmestani, M. W. Brechbiel, L. K. Kvols, ^{213}Bi-[DOTA^{0},Tyr^{3}]Octreotide Peptide Receptor Radionuclide Therapy of Pancreatic Tumors in a Preclinical Animal Model, *Clin Cancer Res*, **2006**;12: 897-903.

[9] G. Cook Jr, CC. Parker, S. Chua , B. Johnson, AK. Aksnes, VJ. Lewington, ^{18}F-fluoride PET: changes in uptake as a method to assess response in bone metastases from castrate-resistant prostate cancer patients treated with ^{223}Ra-chloride (Alpharadin), *EJNMMI*, **2011**; 1: 4.

[10] CC. Parker, S. Pascoe, A. Chodacki, JM. O'Sullivan, JR. Germá, CG. O'Bryan-Tear, T. Haider, P. Hoskin, A randomized, double-blind, dose-finding, multicenter, phase 2 study of radium chloride (Ra-223) in patients with bone metastases and castration-resistant prostate cancer, *Eur Urol.* **2013**; 63(2): 189-97.

[11] PG. Kluetz, W. Pierce, VE. Maher, H. Zhang, S. Tang, P. Song, Q. Liu, MT. Haber, EE. Leutzinger, A. Al-Hakim, W. Chen, T. Palmby, E. Alebachew, A. Sridhara, A. Ibrahim, R. Justice, R. Pazdur, Radium Ra-223 dichloride injection: U.S. Food and Drug Administration drug approval summary, *Clin Cancer Res*, **2014**; 20(1): 9-14.

[12] M. Lassmann, D. Nosske, Dosimetry of ^{223}Ra-chloride: dose to normal organs and tissues, *EJNMMI*, **2013**; 40: 207–212.

[13] J. A. Carrasquillo, J. A. O Donoghue, N. Pandit-Taskar, J. L. Humm ,D. E. Rathkopf, H. I. Scher, M. J. Morris, Phase I pharmacokinetic and biodistribution study with escalating doses of ^{223}Ra-dichloride in men with castration-resistant metastatic prostate cancer, *EJNMMI*, **2013**; 40: 1384–1393.

[14] Vitha T, Kubíček V, Hermann P, Elst LV, Muller RN, Kolar ZI, Wolterbeek HT, Breeman WAP, Lukeš I, Peters JA. Lanthanide(III) complexes of bis(phosphonate) monoamide analogues of DOTA: Bone-seeking agents for imaging and therapy. *J. Med. Chem.* **2008**; 51: 677–83.

[15] R. P. Baum, H. R. Kulkarni, THERANOSTICS: From Molecular Imaging Using Ga-68 Labeled Tracers and PET/CT to Personalized Radionuclide Therapy - The Bad Berka Experience, *Theranostics*, **2012**; 2(5): 437-447.

[16] J. K. Leighton, PHARMACOLOGY REVIEW(S): APPLICATION NUMBER: 203971Orig1s000, U.S. Food and Drug Administration, **2013**, http://www.fda.gov

[17] P. W. Durbin, C. W. Asling, N. Jeung, M. H. Williams, J. Post, M. E. Johnston, J. G. Hamilton, The Metabolism and Toxicity of Ra-223 in Rats, Lawrence Berkeley National Laboratory, California, UCRL-81B9, U. S. Atomic Energy Commission, **1958**.

3.7.2. Supplementary Results II: Synthesis and metal chelate stability studies of DOTA bisphosphonates with the α-particle emitter ^{225}Ac(III).

1. Introduction

Alpha particle emitting radionuclides were discussed in the radiopharmaceutical research for cancer treatment, since they are uniquely suited for the targeted endoradiotherapy (ERT). While commonly used β-particle emitters in the ERT have an energy range of few keVs, the energy range of α-particles are in scales of MeV [1]. Therefor the benefit of α-particle emitters is the short range of the α-particle emission paired with a high energy deposit in the targeted tissue. The range of the α-particles in tissue is approximately one to only a few cell diameters, whereby energies of 3 to 8 MeV were delivered in a linear profile. Thus a higher therapeutic efficiency of α-particle emitters compared to β-particle emitters is not only postulated, but also shown in cell and animal studies [2,3]. The main isotopes which come into question in the targeted α-particle therapy (TAT) are ^{225}Ac, ^{211}At, $^{212/213}$Bi, ^{212}Pb, ^{223}Th and ^{223}Ra [1]. The TAT is only a subdomain of the ERT and it stays mostly in the pre-clinical phase, due to its continual unsolved problems in terms of nuclide availability, costs and labelling chemistry. Another problem depicts the daughter nuclides of the initial therapy isotope. It is rarely the case that the decay of the α-particle emitter used in the TAT ends up in a stable isotope in only one conversion step, rather the most TAT nuclides follow a decay chain, including several additional α- and β- emissions until they reach the stable end-nuclide. It is to be assumed that after the initial α-conversion the tight macrocyclic complex dissociates and the daughter nuclide is released. The recoil energy as well as the re-coordination of the electron shell of the decay product after an α-conversion is usually stronger than the energy release by complexation [1]. Therefor TAT nuclides with a short decay chain, or rather very short half-lives of the daughter nuclides are preferable. Though promising candidates with good relations to that criteria, like $^{212/213}$Bi lack in their short half-life of only 45 and 60 min and the usage of the halogen ^{211}At ($t_{1/2}$ = 7.2 h) is related with a

difficult chemistry and *in vivo* stability [1]. ^{225}Ac(III) has been considered as a TAT nuclide, due to its half-life of 10 days, suitable for radioimmuno therapy and the relatively short half-lives of the daughter nuclides, cf figure 1 [4,5].

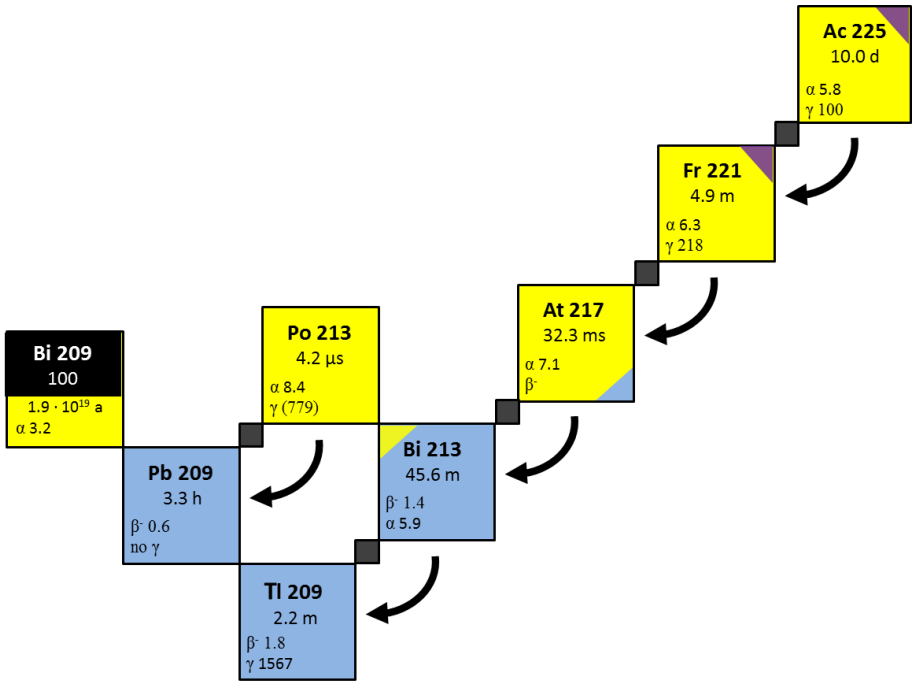

Figure 1. Decay chain from ^{225}Ac to the stable isotope ^{209}Bi.

Actually the best way to form stable Ac(III) complexes is not well documented. The number of coordination sites and the radius of the macrocyclic cavity seem to be an important factor for stable actinide complexation and the question of the best ligand is not yet clear today, due to the fact that no stable Ac(III) isotopes exist, which makes investigations of the character of Ac(III) complexes quite difficult [1,5,6]. In the literature several macrocycles as well as open chain ligands, like CHX´-DTPA (N-[(R)-2-amino-3-(p-isothiocyanato-phenyl) propyl]-trans-(*S*,*S*)-cyclohexane-1,2-diamine-N,N,N',N",N"-pentaacetic acid) are discussed in terms of complexation efficiency and *in vivo* stability. DOTA (1,4,7,10-tetraazacyclododecane-1,4,7,10-tetraacetic acid) derivatives and HEHA (1,4,7,10,13,16-hexaazacyclohexadecane-1,4,7,10,13,16-hexaacetic acid) seem to be the most promising candidates [5,7].

Actually the α-particle emitting ^{223}Ra is approved by the FDA and the EMA for treatment of painful skeletal metastases. Radium itself as an alkaline earth metal functions as a calcium mimetic and it naturally accumulates in the bones. It is known and verified in rat studies (this manuscript: Supplementary Results I) that the main excretion route of ^{223}Ra is the intestinal way. Since DOTA conjugated bisphosphonates showed promising results in the treatment of bone metastases with the β-particle emitter ^{177}Lu, patients may benefit from a TAT in combination with compounds like BPAMD and DO3AP^{BP}, cf chart 1.

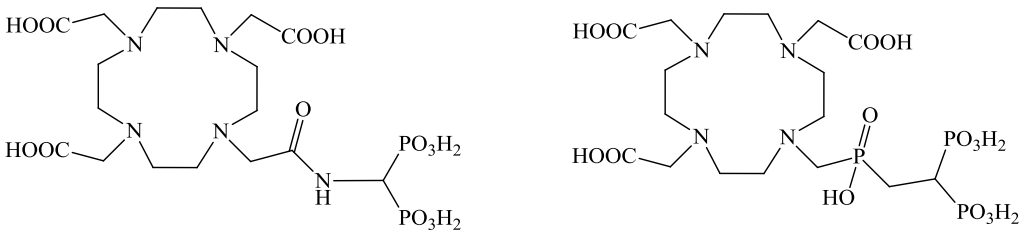

BPAMD DO3AP^{BP}

Chart 1. Structure of macrocyclic bisphosphonates for potential ^{225}Ac(III) comlexation.

Because of the better pharmacokinetics in terms of bone to soft tissue ratios and body excretion (this manuscript: Supplementary Results I) these macrocyclic bisphosphonates should be further investigated as promising candidates for an ^{225}Ac(III) TAT. Therefore it is necessary to reveal the labeling efficiencies as well as the complex stabilities in different medias of these ligands with ^{225}Ac(III), to outline the future prospects of this concept.

2. Materials and Methods

2.1. General methods

Solvents and chemicals were commercially available in analytical, HPLC or *Trace*SELECT® grade and were purchased from Sigma-Aldrich. Radio-TLC analyses were carried out with silica on aluminium foil (Merck KgaA) and a Raytest RITA (Raytest Isotopenmessgeräte GmbH, Germany) radiodetector. Radioactivity of samples were measured with an Aktivimeter Isomed 2010, MED (Nuklear-Medizintechnik Dresden GmbH). ^{225}Ac(III) was obtained from ITM AG (Garching, Germany) as actinium nitrate in a concentration of 60 MBq in 100 µL 6 M HNO_3.

2.2. Radiolabelling with ^{225}Ac(III)

The 100 µL ^{225}Ac(III) stock solution was diluted with 5.9 mL *Trace*SELECT® grade water to obtain a total volume of 6 mL with a final ^{225}Ac(III) concentration of 6 MBq/mL in 0.1 M HNO_3. 15 µg of the ligand was dissolved in 500 µL of a 0.1 M sodium acetate solution (pH = 7.8) and ~1 MBq (150-200 µL) of the diluted ^{225}Ac(III) stock solution was added, which results in a final pH of 5.5-6.0. The solution was kept on a thermo shaker for 30 min at 98°C under moderate shaking and samples were taken regularly for TLC analysis. The TLC were developed in 0.1 M citrate buffer (pH 4) and radioactivity was analyzed 24 h post developing to wait for the decay equilibrium.

2.3. Stability studies in different mediums

100 µL of the ^{225}Ac labelled DOTA bisphosphonates, like prepared above were added to 500 µL of different mediums (0.1 M DTPA pH = 7.2, 0.1 M NaOAc pH = 5.5, human serum probes). The solutions were kept at room temperature and samples were taken regularly for TLC analysis. The TLC were developed in 0.1 M citrate buffer (pH 4) and radioactivity was analyzed 24 h post developing to wait for the decay equilibrium.

3. Results

Complexation of ^{225}Ac(III) with BPAMD and DO3AP^{BP} occurred within 30 min reaction time. Whereas the 8-dentate ligand DO3AP^{BP} showed not only a slight faster kinetic, but also a higher radiochemical yield (RCY), which was quantitative (RCY > 99%) compared to BPAMD, which showed a RCY ≥ 97.8 %, cf figure 2 and 3. The [^{225}Ac]BPAMD complex showed in 0.1 M sodium acetate buffer at pH = 5.5 a slight decomposition over time, resulting in a loss of intact complexes of approximately 60 % at day 6. In contrast to [^{225}Ac]DO3AP^{BP}, which showed at the same conditions a loss of intact complexes of only 4 % at day 6. In human serum probes (pH ~7.4) decomplexation of the ^{225}Ac-labelled bisphosphonates occurred slowly over time and close to 72 % of [^{225}Ac]BPAMD and close to 80 % of [^{225}Ac]DO3AP^{BP} was found to be intact after 7 days. Both complexes showed very low stabilities in the trans-chelating experiment with 0.1 M DTPA (pH = 7.2). After 5 days only [^{225}Ac]DTPA was present.

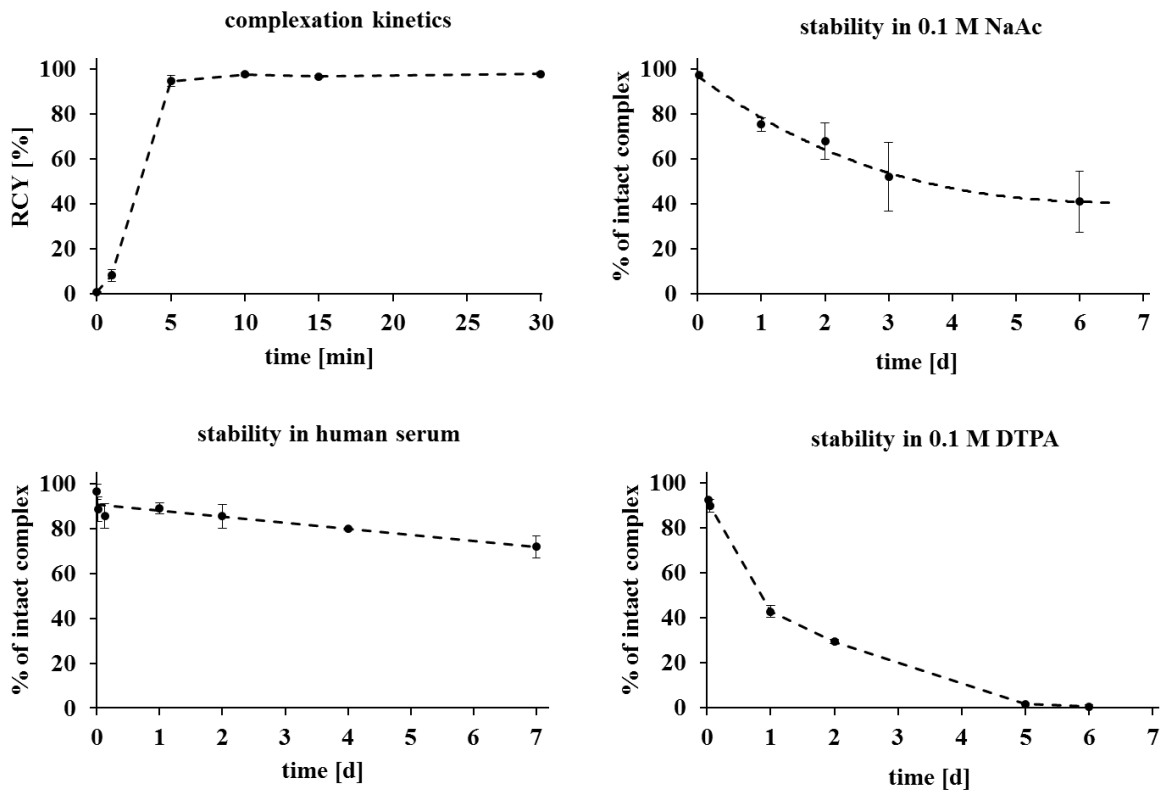

Figure 2. Complexation kinetic in 0.1 M sodium acetate pH 5.5 and complex stabilities in different mediums of [^{225}Ac]BPAMD out of a triplicate.

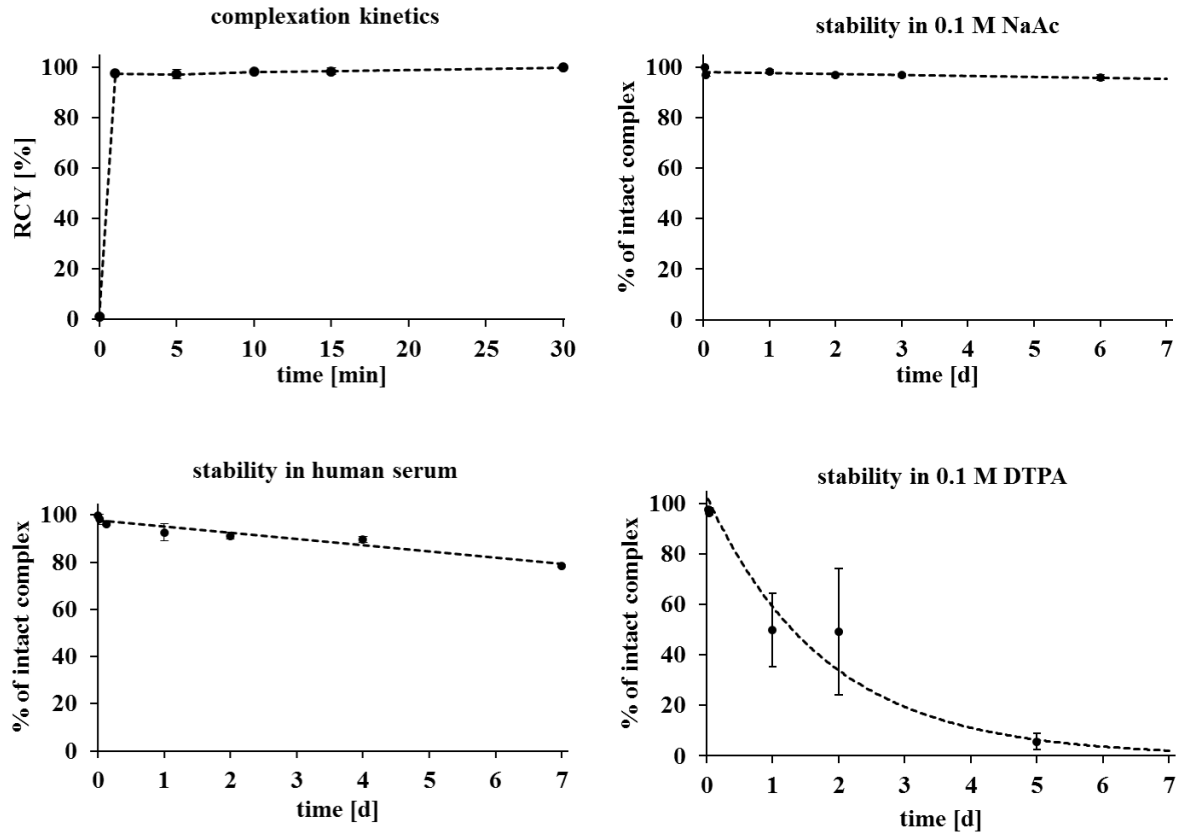

Figure 3. Complexation kinetic in 0.1 M sodium acetate pH 5.5 and complex stabilities in different mediums of [^{225}Ac]DO3AP^{BP} out of a triplicate.

4. Discussion

A major criterion, which assessed the targeted α-particle therapy for future prospects is the stability of the ^{225}Ac-complexes in the body. Since uncomplexed or weakly complexed ^{225}Ac species accumulate in the liver with a high toxicity, a stable chelating of the ligand with ^{225}Ac(III) is explicitly essential [8]. Just this question, related to the stability of different chelators, is yet to be discussed in the literature [1,6,9] and only few clinical trials with ^{225}Ac-labelled compounds are published [4]. It is reported that DOTA derivatives show adequate labelling efficiencies and stabilities with ^{225}Ac(III) [2,5], elsewhere the most

favorable *in vivo* stability of ^{225}Ac(III) complexes showed [^{225}Ac]HEHA (,4,7,10,13,16-hexaazacyclohexadecane-N,N′,N″,N‴,N⁗,N⁗′-hexaacetic acid) [6].

Thus the 7-dentate ligand BPAMD and the 8-dentate ligand DO3AP^{BP} showed both excellent complexation kinetics with ^{225}Ac(III), with a slight better RCY for [^{225}Ac]DO3AP^{BP} (RCY > 99%) within this study. The [^{225}Ac]BPAMD complex dissociates slowly over time (60 % within 6 days) in 0.1 M sodium acetate (pH = 5.5) in contrast to [^{225}Ac]DO3AP^{BP} were only marginal decomposition (4 % within 6 days) was observed. Since the kinetic inertness of complexes of macrocyclic ligands is usually determined in acidic medias [10,11] the results in the slight acidic acetate buffer (pH = 5.5) indicate that the [^{225}Ac]BPAMD complex show a distinctly lower kinetic stability in contrast to [^{225}Ac]DO3AP^{BP}. It might be the case, that ^{225}Ac is released by radiolysis. Even low ^{225}Ac activities of few MBqs can cause strong oxidation processes [2]. The results should be verified in future experiments with the addition of scavengers, like ascorbic acid.

Both compounds showed no inertness against transchelating with the 8-dentate and open chain chelator DTPA. Complex dissociation kinetics of [^{225}Ac]BPAMD and [^{225}Ac]DO3AP^{BP} in this experiment was found to be similar. The results are consistent to assumptions in the literature, which pronounced that more than 8 donors are necessary for a kinetically stable actinide complexation. Within this study the kinetic inertness of the ^{225}Ac-labeled bisphosphonates increased from the 7-dentate BPAMD to the 8-dentate DO3AP^{BP}. In addition it is discussed in the literature that DOTA derivatives have a to small macrocyclic cavity for a stable ´in cage´ complexation of Ac(III), due to its larger ionic radius of ~1.14 Å in contrast to ~0.9 Å for the better fitted lanthanides [6]. The results from the transchelating experiment with the open chain ligand DTPA might sustain these assumptions. However both ligands showed a low and similar dissociation rate in human serum samples with ^{225}Ac. The pH in serum is around 7.4 and this higher pH seemed to have stabilizing effects to the formed complexes. The results are consistent to the literature, where it is described a similar stability in human serum for DOTA conjugates [5].

Thus the stability of [^{225}Ac]BPAMD and [^{225}Ac]DO3AP^{BP} should better be further investigated *in vivo* in an animal model, with regards to increasing radioactivity

concentrations in the liver over time. It might be the case that once the compound is attached to the bone surface the released daughter nuclides just as released ^{225}Ac are adsorbed instantly on the bone as well and thus the accumulation in critical organs like the liver might to be kept in a low concentration. Additionally new bisphosphonate conjugates to chelators like HEHA should be synthesized in future concerning to the better assumed *in vivo* stability of [^{225}Ac]HEHA complexes.

As a conclusion, TAT in combination with macrocyclic bisphosphonates might be a strong advantage in the treatment of bone metastases contrary to the therapy with $^{223}RaCl_2$. The better pharmacokinetics of the radio-bisphosphonates, in terms of body clearance might be reduce the critical toxic sight effects of a ^{223}Ra-therapy by keeping a high radiation dose to tumor sites. The complex stability of ^{225}Ac-labelled bisphosphonates is indeed an important hurdle, which is to be overcome in future.

5. References

[1] Y. S. Kim, M. W. Brechbiel, An overview of targeted alpha therapy, *Tumor Biol.* **2012**; 33: 573–590.

[2] M. Miederer, D. A. Scheinberg, M. R. McDevitt, Realizing the potential of the Actinium-225 radionuclide generator in targeted alpha particle therapy applications, *Advanced Drug Delivery Reviews*, **2008** ; 60: 1371–1382.

[3] F. Graf, J. Fahrer, S. Maus, A. Morgenstern, F. Bruchertseifer, S. Venkatachalam, C. Fottner, M. M.Weber, J. Huelsenbeck, M. Schreckenberger, B. Kaina, M. Miederer, DNA double strand breaks as predictor of efficacy of the alpha-particle emitter Ac-225 and the electron emitter Lu-177 for somatostatin receptor targeted radiotherapy, *PLoS One*, **2014**; 9: 2.

[4] K. E. Baidoo, K. Yong, M. W. Brechbiel, Molecular Pathways: Targeted a-Particle Radiation Therapy, *Clin Cancer Res*, **2013**; 19(3): 530-537.

[5] M.R. McDevitt, D. Ma, J. Simon, R.K. Frank, D.A. Scheinberg, Design and synthesis of ^{225}Ac radioimmunopharmaceuticals, *Applied Radiation and Isotopes*, **2002**; 57: 841–847.

[6] K. A. Deal, I. A. Davis, S. Mirzadeh, S. J. Kennel, M.W. Brechbiel, Improved in Vivo Stability of Actinium-225 Macrocyclic Complexes, *J. Med. Chem*., **1999**; 42: 2988-2992.

[7] I. A. Davis, K. A. Glowienka, R. A. Boll, K. A. Deal, M. W. Brechbiel, M. Stabin, P. N. Bochsler, S. Mirzadeh, S. J. Kennel, Comparison of ^{225}Actinium Chelates: Tissue Distribution and Radiotoxicity, *Nucl Med & Biol*, **1999**; 26: 581–589.

[8] G. J. Beyer, R. Offord, G. Künzi, Yu. Aleksandrova, U. Ravn, S. Jahn, J. Barker, O. Tengblad, M. Lindroos, ISOLDE Collaboration, The Influence of EDTMP-Concentration on the Biodistribution of Radio-Lanthanides and 225-Ac in Tumor-Bearing Mice, *Nucl Med & Biol*, **1997**; 24: 367-372.

[9] I. A. Davis, K. A. Glowienka, R. A. Boll, K. A. Deal, M. W. Brechbiel, M. Stabin, P. N. Bochsler, S. Mirzadeh, S. J. Kennel, Comparison of ^{225}Actinium Chelates: Tissue Distribution and Radiotoxicity, *Nucl Med & Biol*, **1999**; 26: 581–589.

[10] P. Táborský, I. Svobodová, ,P. Lubal, Z. Hnatejko, S. Lis, P. Hermann, Formation and dissociation kinetics of Eu(III) complexes with H_5do3ap and similar dota-like ligands, *Polyhedron*, **2007**; 26: 4119-4130.

[11] E. Toth , E. Brucher , I. Lazar , I. Toth, Kinetics of Formation and Dissociation of Lanthanide(III)-DOTA Complexes, *Inorg. Chem.*, **1994**; 33: 4070–4076.

4 Summary, Conclusion and Future Perspective

Since bone metastases still preserve as an untreatable infirmity worldwide with an increasing number of cases, the medical research is enforced to focus on novel concepts and developments in the recent decade. New discovered molecular biological pathways routed to the emerging of artificial antibodies and specific targeting agents, which aim on a substantially improved tumor management. Among these novel concepts, radiopharmaceuticals appear to have a leading position and particularly macrocyclic bisphosphonates are to be highlighted.

Within this present work the novel macrocyclic bisphosphonate concept was further developed, not only in terms of practice by a kit-type application, but also in terms of more modern compounds and experimental nuclide capabilities. These new compounds were successfully synthesized and evaluated in an healthy animal model with the diagnostic PET-nuclide ^{68}Ga(III) and the therapy nuclide ^{177}Lu(III). Furthermore, the concept was rudimental extended to the targeted α-particle therapy by implying the nuclide ^{225}Ac(III). A milestone in the progress of the work were the first human studies in cancer patients with the most promising compounds [^{68}Ga]NO2AP^{BP} and [^{68}Ga]/ [^{177}Lu]DOTAM^{ZOL}, which finally leaded to an initial clinical trial in collaboration with international hospitals. The outcomes of the single segments of the project are discussed as follows.

One task aimed on the development of a kit-type application of [^{177}Lu]BPAMD. The radiopharmaceutical was evaluated by Fellner et al. in previous work and was first administered in prostate cancer patients suffering from bone metastases in collaboration with the Zentralklinik Bad Berka. The first results appeared to be promising, but an important hurdle had to be overcome to introduce [^{177}Lu]BPAMD in routine clinical practice. A [^{177}Lu]BPAMD-kit is a distinct need for a GMP conform production of the radiopharmaceutical and the kit composition was evaluated in terms of a high labelling efficiency and complex stability. Within this work the kit development was successfully completed and the kit complies all scheduled requirements in terms of radiochemical yields

and radiolytic stabilities. The kit will be produced in future by a collaborating company and opens the implementation of future clinical trials, which have set to reveal the potential of the [^{177}Lu]BPAMD therapy.

A further task was the development of improved targeting structures to enhance the bone affinity of new macrocyclic bisphosphonate derivatives. With an increased bone accumulation the target to background ratio should also be further augmented and hence this would strengthen the diagnostic and therapeutic efficiency. The improvements should be achieved by two different concepts.

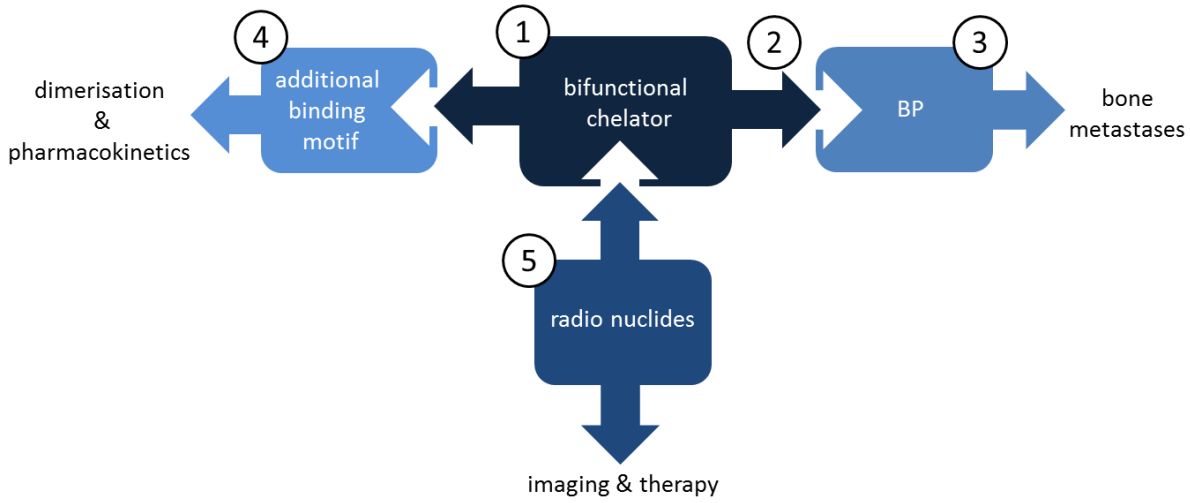

Figure. 4.1. Schematic overview of the BPAMD modification sites based on the bifunctional chelator concept of radiopharmaceutical.

① The development of the NOTA derivatives resulted in a class of bisphosphonates with perfect tracer characteristics for ^{68}Ga(III). The compound NO2AP^{BP} showed not only excellent labelling abilities with ^{68}Ga(III), but also an outstanding target to background ratio combined with a high bone accumulation. The compound was easy and robust to label and no purification steps were necessary. The *in vivo* results in an animal model were such auspicious, that the compound was chosen for an initial study in a prostate cancer patient, who was suffering from bone metastases. The compound [^{68}Ga]NO2AP^{BP} confirmed the outcomes in the patient from the animal testing and convinced with a brilliant imaging

quality. The NOTA based bisphosphonate [^{68}Ga]NO2AP^{BP} was compared against [^{18}F]NaF and the results of the first patient are depicted in figure 4.2.

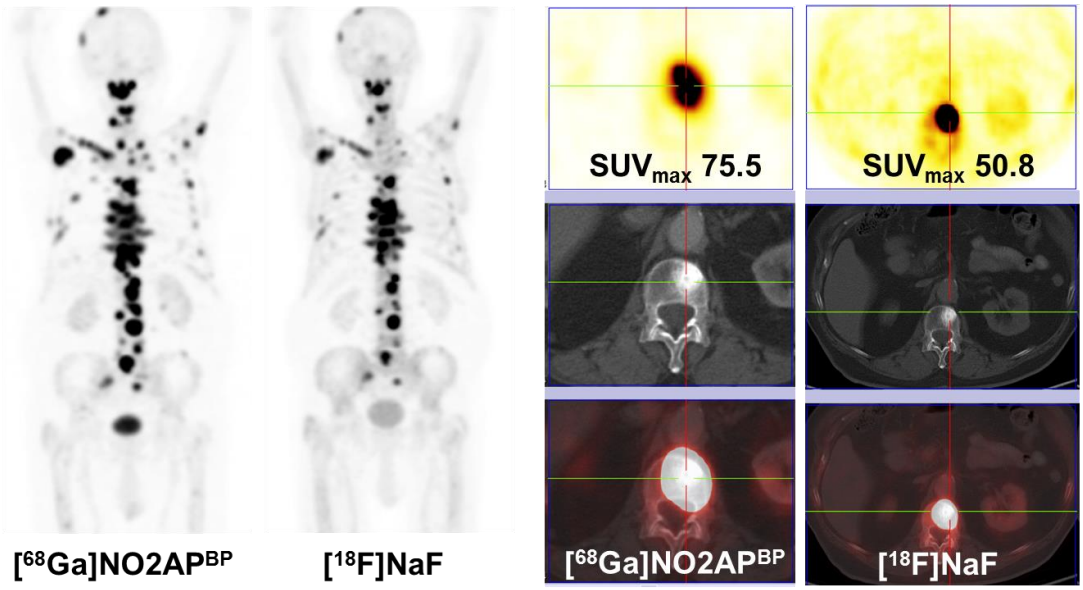

Figure 4.2. First patient study of [^{68}Ga]NO2AP^{BP} in a male prostate cancer patient. Left: Whole body scintigraphy of [^{68}Ga]NO2AP^{BP} vs. [^{18}F]NaF. Right: PET, CT and PET/CT slices of the L4 vertebra of [^{68}Ga]NO2AP^{BP} vs. [^{18}F]NaF. Acquisitions were obtained after 60 min p.i. developed with 161 MBq [^{68}Ga]NO2AP^{BP} and 252 MBq [^{18}F]NaF (Prof. R. P. Baum, Zentralklinik Bad Berka, Germany).

The novel tracer [^{68}Ga]NO2AP^{BP} showed a high uptake in the metastatic lesions combined with a high contrast to the healthy bone. The blood clearance was quite fast and images could be obtained after 60 min p.i.. In the L4 vertebra a SUV_{max} of 75.5 was determined compared to a SUV_{max} of 50.8 in the previous [^{18}F]NaF scan. Subsequent to the first promising human study the tracer was chosen to undergo a phase I clinical trial in collaboration with the All India Institute of Medical Sciences (AIIMS) in New Delhi, India. In this study the compound [^{68}Ga]NO2AP^{BP} will be compared against the common diagnostic tracers [^{18}F]NaF and [^{99m}Tc]MDP in female breast cancer and male prostate cancer patients. The study will focus on the quantity of the detected bone lesions by the different tracers. Preliminary results from the first 12 patients are summarized in table 4.1.

Table 4.1. Bone lesion score of breast cancer patients. Examinations were performed by [^{68}Ga]NO2AP^{BP}-PET, [^{18}F]NaF-PET and [^{99m}Tc]MDP-SPECT and compared against each other, respectively (Data were obtained in collaboration with AIIMS, New Delhi, India).

Nr.	age	no. of lesions [^{68}Ga]NO2AP^{BP}	no. of lesions [^{18}F]NaF	no. of lesions [^{99m}Tc]MDP	disconcordance ^{18}F vs. ^{68}Ga	disconcordance ^{18}F vs. ^{99m}Tc
1	55	6	10	4	4	6
2	38	30	32	29	2	3
3	40	22	23	12	1	11
4	40	11	12	10	1	2
5	65	1	1	1	0	0
6	50	4	4	2	0	2
7	45	1	1	1	0	0
8	35	2	2	2	0	0
9	36	4	5	-	1	-
10	60	3	3	2	0	1
11	30	4	3	3	1	0
12	45	8	8	5	0	3

The diagnostic efficiency of the novel ^{68}Ga-tracer showed to have a high concordance with the current gold standard [^{18}F]NaF and showed to be superior against [^{99m}Tc]MDP. An example of the images from the preliminary clinical study is illustrated in figure 4.2. Since ^{68}Ga is derived from a generator system, similar to ^{99m}Tc, the new tracer NO2AP^{BP} offers now hospitals or small nuclear medical practices a convenient opportunity to perform high qualitative skeletal PET scans without any expansive cyclotron infrastructure. The evaluation of the PET tracer is actually ongoing and first results will be published soon.

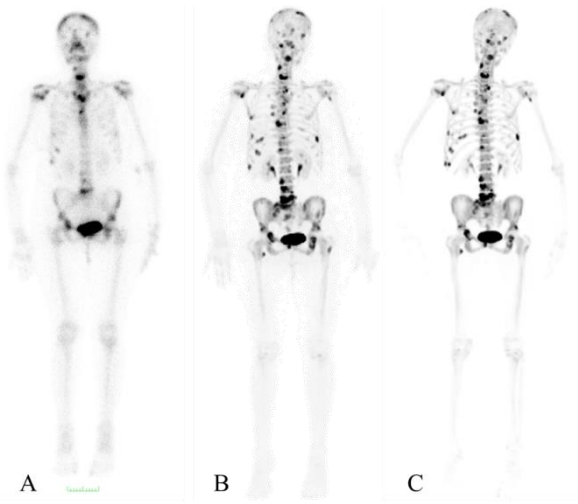

Figure 4.3. Whole body images of a female breast cancer patient suffering from bone metastases. A: Common [^{99m}Tc]MDP skeletszintigraphy. B: [^{68}Ga]NO2AP^{BP} PET scan developed with 140 MBq. C: [^{18}F]NaF PET scan. The images are examples out of the ongoing patient study in collaboration of the All India Institute of Medical Sciences, New Delhi, India by Prof. C. S. Bal.

② The link between the bisphosphonate targeting moiety and the chelator showed to have a remarkable influence on the bone binding and the pharmacokinetics. Contrary to compounds containing an amide bond, the phosphinate conjugates have a slightly higher skeletal retention and faster blood elimination. A further advantage is the additional donor group, provided by the phosphinates. This comes into effect positively, when nuclides are used, which need more than 7-dentate chelators. Further tracer designs should take account of that.

③ Excellent outcomes could be achieved with the modern bisphosphonate conjugates. On the one hand the synthesis of the new DOTA α-OH-bisphosphonates could be successfully accomplished. The pharmacophore of the highly potent osteoporosis drugs zoledronate and pamidronate were successfully conjugated to the DOTA macrocycle and labelled with ^{68}Ga(III) and ^{177}Lu(III). On the other hand these new derivatives showed a significant enhanced bone affinity and thus an improved target to background ratio as revealed from *in vivo* studies. The results are very promising and it might be the case that these next generation compounds replace the DOTA α-H-bisphosphonates, but further patient examinations with the hydroxyl bisphosphonates are necessary to ascertain their true potential in clinical practice.

④ One of them aimed on raising the quantities of the targeting vectors per molecule. Such dimerisations or multimerisations showed promising results in the past with other radiopharmaceutical agents, like RGDs, and it might be the case that an additional bisphosphonate moiety on the chelator backbone may enhance the blood excretion and adsorption kinetics on the bone surface. Within this project two dimeric compounds DOTA(M^{BP})2 and DO2A(P^{BP})$_2$ were successfully synthesized and compared to the corresponding monomers BPAMD and DO3AP^{BP}. In contrast to the mono-substituted macrocycles, the dimers were not able to complex ^{68}Ga(III) effectively and thus they are not suitable as PET imaging agents. The reason behind the low complexation-ability might be the additional bisphosphonate entity. Since it is known that bisphosphonates are good ligands for divalent and trivalent metal ions, the two bisphosphonate moieties tend to form relatively strong ´out of cage´ complexes with radio metal cations and thus compete with the rigid complexation of the macrocyclic cavity. This effect could also be observed for the ^{177}Lu(III) labelled dimers, but merely in a weakened form resulting in significant higher radiochemical yields. The better complexation-ability with the therapy nuclide ^{177}Lu(III) opened the possibility for a comprehensive animal study by SPECT and *ex vivo* organdistribution. Within this study no significant improvements of the skeletal uptake could be observed for the dimers compared to the monomeric bisphosphonates. On the contrary, the blood and organ clearance of the ^{177}Lu-labelled dimers was obviously decelerated, which resulted in lower target to background ratios. The reason therefor remained unclear, but it might be the case that the character of the ^{177}Lu-bisphosphonate-dimer complexes are rather similar to open chain complexes than rigid macrocyclic complexes. As a consequence, ^{177}Lu might be released in the body and thus would reduce the target to background ratio. The results from the *in vivo* experiments strengthen this assumption, since the data of the dimers take a position between the corresponding monomers and the [^{177}Lu]citrate control. Finally, the concept of increasing the quantities of the targeting vectors per molecule did not result in any improvements, but other approaches were successful.

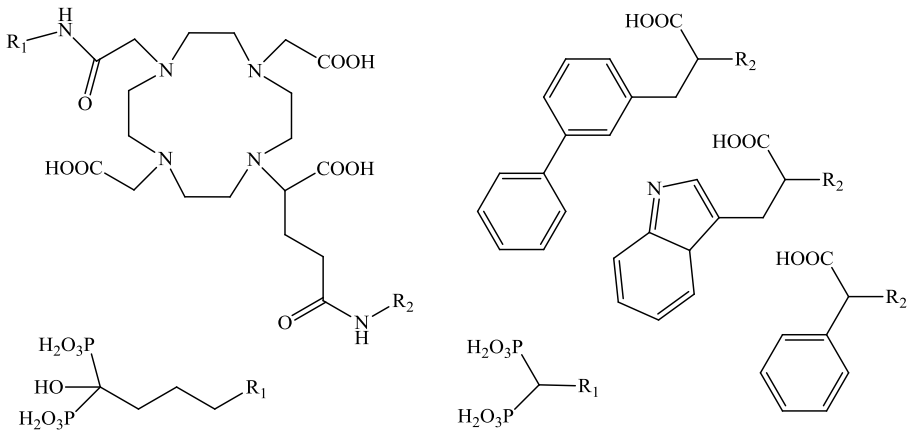

Figure 4.4. Asymmetric substituted DO2A derivatives with an albumin binding entity and a bisphosphonate targeting vector. The targeting structure R_1 may consist of a hydroxyl bisphosphonate or a simple bisphosphonate. R_2 represents different lipophilic substitutions with a possible weakened albumin affinity.

The chemical modification of the well-established tracer BPAMD with an albumin-binding motif leaded to a bone targeting tracer with a decelerated body excretion. Since the body clearance is usually very fast for the bisphosphonate tracers, the most of the injected activity is not retained in the skeleton and excreted out of the body. The albumin binding entity shows a strong affinity to serum albumin and thus slowed down the excretion and bone accumulation kinetic. The blood pool functions as a reservoir for the tracer. As a consequence, the total skeletal retention was enhanced and furthermore the ratio between the high metabolic foci and the areas of normal bone turnover was strongly improved. It is to mention that this novel concept focusses more on the ^{177}Lu-therapy than on the ^{68}Ga-imaging, because of the higher tracer blood levels during the first hours the imaging quality is greatly influenced. The tracer was initially evaluated with ^{68}Ga and hence the total consequences of the chemical modification are yet not fully clear, first ^{177}Lu examinations will reveal the total potential and will follow.

Nevertheless, the improvement of the pharmacological structure based on the albumin binding motif can further be aimed. The conjugates may contain of an improved targeting vector, for example an α-OH-bisphosphonate, and a less potent albumin binding moiety, like it is outlined in figure 4.4. Such structures might also result in increased blood retentions, but a in a faster skeletal binding, which reach its kinetic endpoint earlier. Although the total consequences in terms of dose calculations of critical organs by the albumin binder conjugate

is not fully clarified, a less strong blood retention combined with an improved targeting moiety might be favorable.

⑤ The usage of the bone targeting bisphosphonates in combination with the targeted α-particle therapy may be further advancemet. The α-particle emitter $^{223}RaCl_2$ was approved for therapy of skeletal metastases and showed good results in terms of pain relief and an overall longer survival rate, but it showed significant side effects, which are mainly based on the intestinal excretion route. Since the macrocyclic bisphosphonates are excreted via the kidneys, these side effects should be avoided or reduced. The first experiments with the α-particle emitter ^{225}Ac were promising, but the stable complexation of actinides is still an unanswered question. New compounds based on the eventually better fitted macrocycle HEHA may enhance the complex stability and examples of hypothetical derivatives are sketched in figure 4.5. It might also be the case that the 7-dentate ligand DO3AP^{BP} is suitable for a stable *in vivo* complexation of ^{225}Ac, but finally these assumptions have to be disclosed in future.

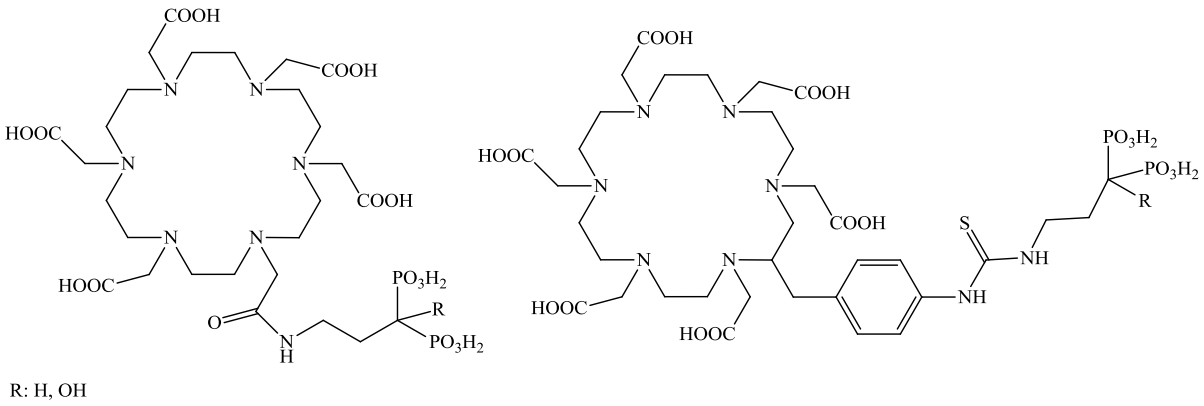

Figure 4.5. Macrocyclic bisphosphonates based on the chelator HEHA as potential high stable $^{225}Ac(III)$ carriers for the targeted α-therapy.

dies. The beginning trials with the PET tracer [^{68}Ga]NO2AP^{BP} seem to be very promising and the [^{177}Lu]BPAMD labelling kit will expand the application of [^{177}Lu]BPAMD to other

users, resulting in comprehensive phase I and II clinical trials. In the long term, the advanced α-OH-bisphosphonate derivatives will replace the first generation compounds and thus makes initial patient studies and kit formulations a necessary goal in future.

In conclusion, the potential of bisphosphonates conjugated with a macrocyclic chelate is very promising in nuclear medicine. The concept offers twice an option, compared to currently available techniques. With the generator derived PET nuclide ^{68}Ga(III) a high qualitative skeletal examination is possible, followed by a subsequent therapy option with ^{177}Lu(III). Since the therapy and the diagnosis can be realized with one and the same precursor molecule, DOTA-based bisphosphonates function as true theranostics and patients would benefit strongly from individual therapy dose calculations carried out by preceded ^{68}G-PET scans. This concept might be a next step towards personalized medicine in cancer treatment. Maybe the results out of this work will be another small leap in the global fight against cancer, a disease that tantalizes mankind from the early beginning [1].

3.1. References

[1] C. Prates, S. Sousa, C. Oliveira, S. Ikram, Prostate metastatic bone cancer in an Egyptian Ptolemaic mummy, a proposed radiological diagnosis, *International Journal of Paleopathology*, **2011**; 1: 98–103.